THE FIRST STEP TOWARDS THE DEVELOPMENT OF AN ELECTROPHORETIC PRION DETECTOR

A Thesis Submitted to the College of Graduate Studies and Research
in Partial Fulfillment of the Requirements for the
Degree of Doctor of Philosophy
in the Department of Biochemistry
University of Saskatchewan
Saskatoon

By

Claudia Avis Madampage

PERMISSION TO USE

In presenting this thesis in partial fulfillment of the requirements for a postgraduate degree from the University of Saskatchewan, I agree that the Libraries of this University may make it freely available for inspection. I further agree that permission for copying of this thesis in any manner, in whole or in part, for scholarly purposes may be granted by the professor who supervised my thesis work, or in his absence, by the Head of the Department or the Dean of the College in which my thesis work was done. It is understood that any copying or publication or use of this thesis or parts thereof for financial gain shall not be allowed without my written permission. It is also understood that due recognition shall be given to me and to the University of Saskatchewan in any scholarly use which may be made of any materials in my thesis.

Requests for permission to copy or make other use of material in this thesis in whole or in part should be addressed to:

Head of the Department of Biochemistry
University of Saskatchewan
Saskatoon, Saskatchewan S7N 0W0

ABSTRACT

In nanopore analysis, peptides and proteins can be detected by the change in current when single molecules interact with an α-hemolysin pore embedded in a lipid membrane. Studies into the effects of fluorenylmethoxycarbonyl (Fmoc), acetylation or proline modification to negatively charged α-helical peptides showed that Fmoc peptides give more translocations than acetylated peptides. The addition of a proline in the middle of an acetylated peptide further reduces the number of translocations compared to Fmoc. The effect of peptide conformation on translocation or intercalation was studied with small α-helical and β-sheet hairpins. The capped β-hairpin increased translocations compared to the uncapped. The Fmoc-α-helical hairpin, containing a disulfide link, displayed both bumping and translocations whereas in the unlinked peptide the proportion of translocations was greater.

Prion diseases arise from the misfolding and aggregation of the normal cellular prion protein. Nanopore analysis of prion peptides with α-helical and β-strand sequences show changes to the event parameters that help distinguish them. The interaction of bovine prion protein (bPrP), with α-hemolysin showed both bumping (type-I) and intercalation/translocation (type-II) events. There are several lines of evidence that indicate these type-II events with a blockade current of -65 pA for bPrP, represent translocations. Nanopore analysis showed that about 37% events were translocations. The interaction of metal ions with bPrP showed that Cu(II) or Zn(II) reduced translocations. Surprisingly, Mn(II) caused an increase in translocation events to about 64%.

Complex formation between antibodies and prion peptides and proteins can be detected by nanopore analysis. The PrP/antibody complex is too large to translocate whereas the event parameters for unbound molecules are unchanged. In principle, a nanopore can detect a single molecule; thus, this work represents the first step towards the development of a prion detector. The nanopore will provide the sensitivity and the antibodies will provide the specificity to distinguish between PrP^{C} and PrP^{Sc}. Also, the prion N- and C-terminal signal peptides interact with bPrP changing the event parameters, relating to a new mechanism. Finally, the folding intermediates of bPrP at 0.86 M Gdn-HCl suggests that the protein unfolds and then refolds into a different conformation with event parameters similar to those of bPrP.

PUBLISHED WORKS

Madampage, C.A., Andrievskaia, O., and Lee, J.S. (2010). Nanopore detection of antibody prion interactions. Analytical Biochemistry *396*, 36-41.

Stefureac, R.I., **Madampage, C.A**., Andrievskaia, O., and Lee, J.S. (2010). Nanopore analysis of the interaction of metal ions with prion proteins and peptides. Biochem. Cell Biol. *88*, 347-358.

Meng, H., Detillieux, D., Baran, C., Krasniqi, B., Christensen, C., **Madampage, C**., Stefureac, R.I., and Lee, J.S. (2010). Nanopore analysis of tethered peptides. J Pept Sci *16*, 701-708.

ACKNOWLEDGEMENTS

I would like to take this opportunity to sincerely thank my supervisor Professor Jeremy S. Lee for giving me the chance to complete my graduate degree in an exciting new field of research work, such as nanopore analysis. Your passion for science, innovation and research makes laboratory work so much more interesting and exciting. In addition, you are such a wonderful teacher and person to work with, that I would highly recommend any new student interested in persuing graduate studies in biochemistry to join your lab.

A very special thank you to my advisory and examination committee: Dr. Bill Roesler, Dr. Stan Moore, Dr. Ramji Khandelwal, Dr. Peter Howard (Dept. of Immunology), and Dr. Ron Geyer for all their advice, support and help throughout my program.

I would also like to thank all my friends in the lab (past and present): Dr. Michael Dinsmore, Dr. Sergy Nohkrin, Radu Stefureac, Besnik Krasniqi, Chris Christensen, Chris Baran, Omid Tavassoly and Meena Kumari for being such wonderful colleagues. A special thank you to the biochemistry student lab: Dr. Tricia Ulmer, Moreen Sinclair, James Talbot and Cindy Farar for being such wonderful friends and also helping me with any equipment I needed throughout my program. Additionally, working as a teaching assistant with all of you was very rewarding.

Finally, I would like to thank the Department of Biochemistry, especially Margret Ross and Lori Lisitza for all their assistance throughout my program. Financial support was from the Department of Biochemistry, the College of Medicine, the College of Graduate Studies and Research, Saskatchewan Agriculture, and Natural Science and Engineering Research Council of Canada (NSERC).

DEDICATION

To my late mother, Valerie Gertrude Muller. Thank you for showing me the path to live life to the fullest by respecting and sharing with all around me. You were always so supportive towards my academic work, and I dedicate this thesis to you. Words cannot express my gratitude to you. You always loved the music of Jim Reeves, so my wish is: "*May you walk with sunlight shining and a blue bird in every tree*". May you rest in peace.

To my loving father, Anthony Russel Muller. Thank you for all your support and understanding during the most difficult time in my life. You were always there to pray for me.

To my loving husband, Upul Madampage and son Navod Christopher Madampage. Upul, thank you so much for the love and support you gave me throughout the years. You have always been there to lend a hand in what ever I did.

Navod, thank you for taking - in so much stress during my academic studies. You add spice to my life with all your funny thoughts about everything around you, including science. Your comments on my research work have been overwhelming. I love you very very much.

TABLE OF CONTENTS

LIST OF TABLES

LIST OF FIGURES

LIST OF ABBREVIATIONS

Ach	acetylcholine
BSE	bovine spongiform encephalopathy
CD	circular dichroism
CDI	conformational-dependent immunoassay
CHES	2-[*N*-cyclohexylamino]ethanesulfonic acid
CJD	Creutzfeldt-Jakob disease
CWD	chronic wasting disease
d_c	channel diameter
d_s	diameter of a spherical particle
DLS	dynamic light scattering
DNA	deoxyribonucleic acid
EDTA	ethylenediaminetetraacetic acid
FFI	fatal familial insomnia
Fmoc	N-(9-fluorenyl) methoxycarbonyl
FSE	Feline spongiform encephalopathie
GSS	Gerstmann-Sträussler-Scheinker syndrome
i_c	open channel current
K_B	Boltzmann constant
$l_{c'}$	channel length after correction due to the "end effect"
ms	millisecond
mV	millivolt
NMR	nuclear magnetic resonance
pH	negative logarithm of the hydrogen ion concentration
pA	picoamperes
R_H	hydrodynamic radius
RNA	ribonucleic acid
S (d_c,d_s)	correction factor
T	temperature in degrees Kelvin
TFA	trifluoroacetic acid
ThT	thioflavin T

TME	transmissible mink encephalopathy
TSE	transmissible spongiform encephalopathie
Tris	tris(hydroxymethyl)aminomethane
UV	ultraviolet
wt	wild-type prefix
Δi_c	pulse height
π	3.14159
η	viscosity of the solvent
α HL	α-hemolysin

1.0 INTRODUCTION

The first attempts made by Wallace Henry Coulter to patent his invention the "Coulter principle" was turned down by attorneys who believed "you cannot patent a hole" (Graham, 2003). Today the Coulter-counter (Beckman Instruments, Inc., Fullerton, CA) is the most essential and common analytical tool used in medical laboratories around the world for counting and sizing particles in sample testing. Nanopore analysis uses the same sensing principle as Coulter-counters, except that the small aperture in the counter is replaced with a nanoscale channel (Bayley and Martin, 2000). Today, nanopore analysis is a useful tool for the study of single molecules.

In nanopore analysis, individual molecules can be detected by the change in ionic current when they interact with a nanopore (Kasianowicz *et al*., 1996). Nanoscale channels are of two types. The first are natural protein pore toxins such as α-hemolysin and the second type are synthetic nanoscale pores manufactured on inorganic material such as silicon nitride, silicon dioxide, and organic material. The initial work included the analysis of DNA and RNA by David Deamer and Daniel Branton (Deamer and Branton, 2002). Subsequently, the detection of peptides, proteins, enzymes, organic polymers, and many other small molecules followed. Recently an engineered α-hemolysin channel with a covalently lodged adapter was able to discriminate all four DNA bases with 99% accuracy (Clarke *et al*., 2009). This achievement suggests that sequencing of DNA with single nanopores will be possible in the future (Deamer and Akeson, 2000; Marziali and Akeson, 2001; Clarke *et al*., 2009). In another vein, nanopore analysis of peptides and proteins in Jeremy Lee's laboratory has demonstrated the ability to detect conformational changes due to interactions with the α-hemolysin pore (Sutherland *et al*., 2004b; Stefureac *et al*., 2006, 2008; Stefureac and Lee, 2008).

In principle, a nanopore can detect a single molecule; thus, this method may be useful to identify and quantify infectious particles present in very low concentrations in biological samples. Prion diseases are infectious, neurodegenerative disorders caused by a change in protein conformation (Prusiner, 1982). The disease has a long incubation period in addition to having a very low amount of infective molecules in the blood during the pre-symptomatic period. It has been estimated that only 60,000 infectious molecules are present in 100 µl of rodent blood. This number is much lower in humans and cattle (Soto, 2004). Nanopore detection of prion proteins could be useful to develop an electrophoretic prion detector.

Therefore the introduction of this thesis will focus on the development of the nanopore technique, types of pores, and the large spectrum of molecules analyzed using nanopore analytics. To integrate the development of an electrophoretic prion detector, an introduction on prions including the present methods used in prion diagnostics will also be discussed.

1.1 Single-molecule analysis using nanopores

1.1.1 Origin of single-channel current recording

The Coulter-counter patented in 1953 by W.H. Coulter opened the door to an exciting new area of research, the analysis of nanoscale particles (Coulter, 1953). The simplicity in method and operation of this counter made it tremendously popular as a device used to count and size small particles present in various scientific fields. The Coulter-counter (Beckman Coulter, Fullerton, CA) is routinely used in medical laboratories around the world, mainly for blood cell, spermatozoa, and platelet counts and more recently in the areas of human immunodeficiency virus (HIV) transmission from mother to child and also to assess the number of cell nuclei in cancer cell lines (Ramon *et a*l., 1999; Hwa *et al*., 1999; Bhat and Gartel, 2008; Mehta *et al*., 2009). The Coulter-counter consists of two chambers filled with electrolyte solution connected by an aperture of 20 μm to 2 mm (Coulter, 1953; Bayley and Martin, 2000). The addition of electrodes to each chamber with an applied potential across the chamber (Figure 1.1a) drives an ionic current through the aperture (Henriquez *et al*., 2004). When a particle having a size on the order of the aperture diameter enters the channel, it reduces the magnitude of the ionic current (Henriquez *et al*., 2004). During the residence time of the particle in the aperture, the aperture resistance increases. This increase in aperture resistance corresponds to an increase in transaperture voltage drop (Bayley and Martin, 2000). Coulter-counter results may be easily presented with a plot of current *vs*. time (Figure 1.1b), for a string of ionic current pulses (Henriquez *et al*., 2004).

The pulse height relates to molecular size and the width of the current pulse measured as time may under some conditions determine the charge carried by the molecule (DeBlois and Bean, 1970; Sun and Crooks, 2000; Henriquez *et al*., 2004). The surface charge of a molecule can be determined if the geometry and chemical characteristics of the channel are well defined. The number of particles can be reasonably calculated using the frequency of the current pulses

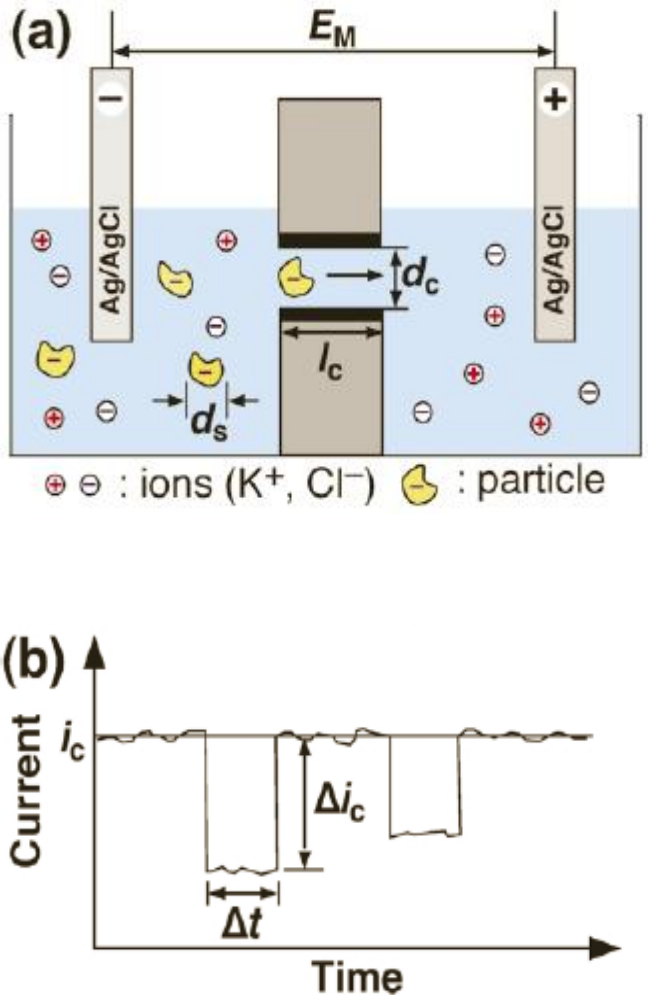

Figure 1.1 The general experimental set up of a Coulter-counter. (a) Schematic diagram of an electric field-driven Coulter-counter consisting of two chambers filled with electrolyte solution, divided by an insulating membrane that contains a single channel. When an appropriate potential is applied across the membrane, an ionic current is driven through the channel. (b) Typical Coulter-counter data which is recorded as a series of current pulses (Δic) and represented in a plot of current *vs*. time. (Reprinted by permission from Henrquez *et al*., 2004. Copyright 2004 Royal Society of Chemistry).

in an experiment. The pulse height depends mainly on the volume of electrolyte displaced when the molecule interacts with the aperture. An increase in solution resistance is observed but is quickly reversed when the molecule traverses the aperture (Henriquez *et al*., 2004). Coulter-counters can be used to analyze very low concentrations of analyte as only one particle enters the sensing zone at any given time. In the early years these counters could only size particles between 2% to 40% of aperture diameter, meaning that below 2%, the signals were overcome by electronic noise and above 40% they blocked the aperture (McCave and Syvitski, 2007). The mathematical relationship between particle size and ionic current is shown as:

$$\Delta i_c / i_c = S(d_c,d_s) \,.\, d_s^3 / l_c.d_c^2 \qquad \text{Equation 1.1}$$

where Δi_c is the pulse height, i_c is the open channel current, d_s is the diameter of a spherical particle, d_c is the channel diameter, S (d_c,d_s) is the correction factor that depends on d_s and d_c, and l_c is the channel width. The channel length, $l_{c'}$ is calculated after the correction due to the "end effect" ($l_{c'} = l_c + 0.8\ d_c)^3$ (Henriquez *et al*., 2004). This equation can be very useful when analyzing smaller molecules using very small apertures (DeBlois and Bean, 1970; Henriquez *et al*., 2004).

The principle of voltage clamping was first developed by K.S. Cole in the 1950's (Cole, 1965). Following this, an introductory study involving the measure of membrane potentials was first published in 1972 (Katz and Miledi, 1972). This group analyzed the membrane noise caused due to drug-receptor interactions. They investigated the neurotransmitter, acetylcholine (ACh), which is released by neurons and is an essential factor for signaling between neurons and muscle, at neuromuscular junctions (Picciotto *et al*., 2002). ACh once released, binds to the acetylcholine receptor located on the endplate of muscle fibers, which then responds by opening the ligand-gated sodium ion channels (Martyn *et al*., 2009). These experiments were conducted using micro-electrodes on regions of frog sartorius muscle fiber in response to the application of ACh (Katz and Miledi, 1972). A significant drawback in these experiments was that when single channels open or close the discrete changes in conductance were not properly measured due to excessive background noise. The study of the flow of ions across membranes which is facilitated by ion channels, transporters, pumps, co-transporters/exchangers, and electrogenic transporters paved the way for single-channel current measurements (Hille, 1992). Hladky and Haydon were able to record the opening and closing of channels formed by gramicidin A (peptide antibiotic) on planar bilayers (Hladky and Haydon, 1970). The first

successful recording of single-channel currents on intact biological membranes was established by Erwin Neher and Bert Sakman using membrane regions of denervated frog muscle fibers (Neher and Sakmann, 1976). These experiments were conducted by limiting the membrane area to a small patch and thereby decreasing background membrane noise. This method was improved and is known as the "patch clamp" technique which is widely used in the field of electrophysiology (Hamil *et al*., 1981; Neher and Sakmann, 1992).

Ion channels, a subset of proteins which span the lipid bilayer membranes, include several bacterial toxins and outer membrane proteins (Gouaux, 1997; Sansom, 1999). These proteins regulate the flow of ions by a mechanism known as gating (opening and closing of the channel) due to external factors such as voltage, hormones, neurotransmitters, Ca^{+2}, and phosphorylation (Molleman, 2008). The gating mechanisms are caused by a change in protein conformation of the channel (Franco-Obregón and Lansman, 2002; Grosman, 2003; Wan *et al*., 2004). Nanopore analyses measures current changes using the same principle as Coulter-counters which represent resistive-pulse sensing (Howorka and Siwy, 2009a). By contrast, nanopore analytics use artificial membranes to reconstitute pores as compared to biological ion channels which measure the gating of many channels in cell membranes (Montal and Mueller, 1972). Also the ionic current changes recorded in nanopore analysis are due to molecules interacting with the pore via steric or electrostatic effects. In biological ion channels, analytes specifically bind the channel and cause conformational changes in the protein channel which then changes the magnitude of the ionic current (Bezrukov and Kasianowicz, 1997; Nestorovich *et al*., 2002).

1.1.2 The principle of single-molecule detection with nanopores

Single-molecule nanopore detection is a simple technique for the analysis of individual molecules using the same principle as Coulter-counters. In Coulter-counters, particles are counted and sized (Coulter, 1953). Nanopore analysis uses the same sensing principle (Figure 1.2) and records molecular movement through a channel as short modulations of electrical conductance (Bayley and Martin, 2000; Marziali and Akeson, 2001; Deamer and Branton, 2002; Howorka and Siwy, 2009b). This simple technique comprises a biological, inorganic or polymeric membrane with a single nanopore inserted into it. The nanoscale channel could be a biological toxin or a solid-state pore. The nanoscale channel connects the two chambers filled

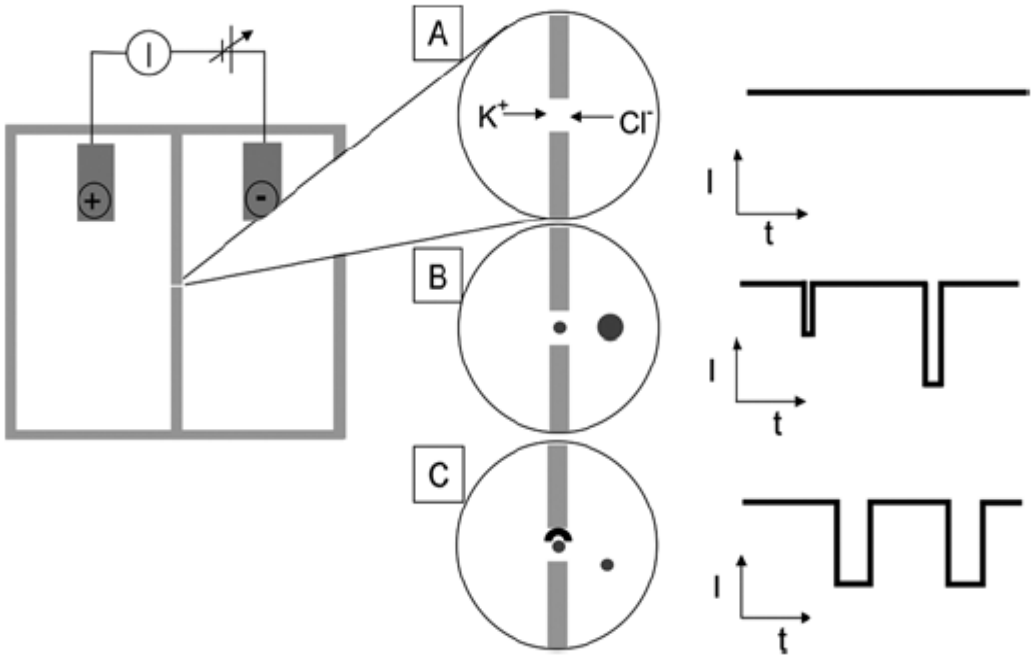

Figure 1.2 The principle of nanopore recording. (A) Schematic diagram showing the applied potential drives a constant flow of ionic current (KCl) through a single-channel. (B) Shows molecules that interact and pass through the pore cause temporary current blockades which are quickly reversed when the molecule traverses the channel. (C) Shows current fluctuations caused by the reversible binding of analytes to specifically engineered binding sites on the channel. I and t represent blockade current and duration respectively. (Reprinted by permission from Howorka and Siwy, 2009b. Copyright 2009 Springer Science + Business Media, LLC).

with electrolyte solution. An electrode is immersed in each chamber and connects a potentiostat that sets a transmembrane potential which drives an ionic current through the nanopore (Howorka and Siwy, 2009b). Most channels conduct constant open pore currents (Figure 1.2A) and when molecules are added to one chamber they traverse the pore leading to transient conductance blockades (Figure 1.2B). If specific binding sites in relation to the analyte are engineered on the pore, these current modulations are reflected with constant channel blocks (Figure 1.2C).

The most attractive benefit in using this method is that the molecules being analyzed are label free and need not be immobilized on a solid surface. Most other single-molecule methods including *in vitro* fluorescence, fluorescent probes, atomic force microscopy, optical traps, and magnetic traps need analytes labeled and immobilized (Selvin and Ha, 2008). Due to its simplicity, nanopore analysis offers a relatively cheap and less complex pathway to analyze single molecules. Another attractive feature is that nanopores are usually blank pores that do not bind analytes, but artificially engineered pores can be designed to bind specific analytes for experimental purposes (Kasianowicz *et al*., 1999; Wu *et al*., 2007). Nanopore analytics can be used to study a variety of features including chemical, physical, electrostatic and kinetic properties in a wide range of molecules. Among bacterial toxins, the α-hemolysin (αHL) pore is currently the most popular biological channel for nanopore analysis (Song *et al*., 1996). Today, the most common biological nanopore apparatus (Figure 1.3) consist of a single αHL channel inserted in a planar lipid membrane of diphytanoyl phosphatidylcholine (DPhPC: $C_{48}H_{96}NO_8P$) (Akeson *et al*., 1999a, b; Meller *et al*., 2001). The chambers are filled with 1 M KCl, and a steady voltage is applied across the membrane. The αHL channel has a steady open pore current of 120 pA at a voltage of 120 mV (Deamer and Branton, 2002). The conductance is monitored by an Axopatch 200B amplifier (Axon Instruments, Union city, CA) using Ag-AgCl electrodes. When single-molecules interact with the αHL channel, translocation is driven by an electric field across the channel (Meller *et al*., 2001).

For example, it has been possible to detect and characterize single stranded ribonucleic acid (RNA) and deoxyribonucleic acid (DNA) through αHL pores (Kasianowicz *et al*., 1996; Akeson *et al*, 1999a, b; Henrickson *et al*., 2000). Furthermore, homopolymers containing cytosine (C) and adenosine (A) show different blockade patterns suggesting that sequencing of DNA with single nanopores will be possible in the future (Deamer and Akeson, 2000; Marziali

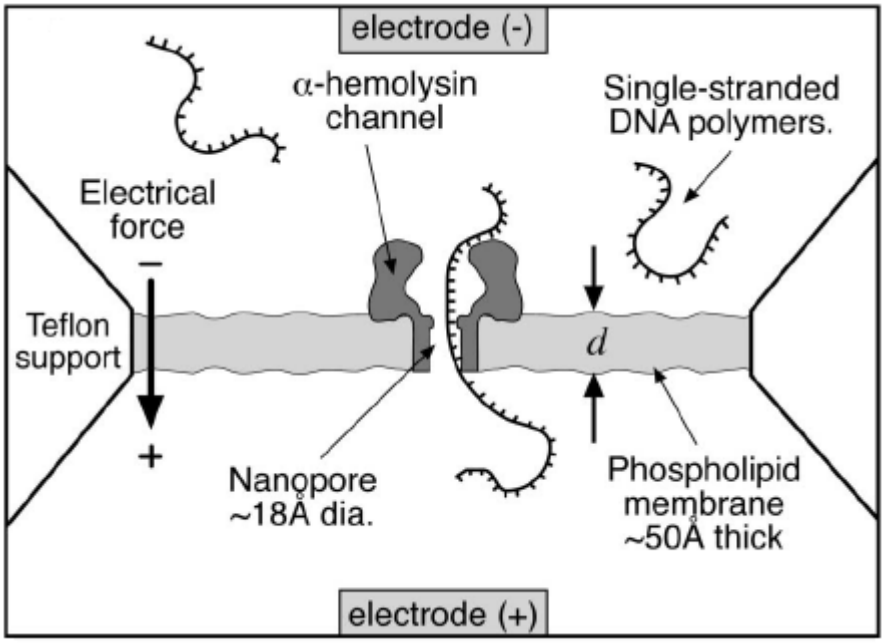

Figure 1.3 A common biological nanopore apparatus. Diphytanoyl phosphatidylcholine ($C_{48}H_{96}NO_8P$) is painted across the teflon support to separate two chambers. Each chamber is filled with KCl buffer. A single αHL pore is inserted into the planar lipid bilayer and a transmembrane potential causes a constant flow of ionic current through the single αHL channel. Nanopore analysis of negatively charged single stranded DNA molecules is added and they are electrically driven through the pore. (Reprinted by permission from Meller *et al.*, 2001. Copyright 2001 American Physical Society).

and Akeson, 2001; Clarke *et al*., 2009). Nanopores have also been used to detect the translocation of charged polypeptides (Movileanu *et al*., 2005; Stefureac *et al*., 2006). Chemically modified αHL pores have been used to detect the binding of tetravalent lectin and study the kinetics of protein-ligand interaction (Howorka *et al*., 2004). Furthermore, the investigation of full-length proteins in the presence and absence of a denaturing agent has been successfully accomplished using an αHL channel. The maltose binding protein (MBP) does not translocate in the absence of guanidinium chloride (Gdn-HCl), but in presence of concentrations greater than 0.8 M Gdn-HCl, the protein starts to unfold and displays well defined current blockades (Oukhaled *et al*., 2007).

1.1.3 Pores

1.1.3.1 Biological pore-forming toxins

The most widely used molecular-scale nanopore toxin, α-Hemolysin (αHL), has also proven to be the most successful pore for the initial groundbreaking work for single-molecule analysis of nucleic acids (Song *et al*., 1996; Kasianowicz *et al*., 1996; Akeson *et al*., 1999a; Meller *et a*l., 2000; Deamer and Branton, 2002; Lin *et al*., 2010). α-Hemolysin secreted by *staphylococcus aureus* is a self-assembling 232 kDa β-barrel pore-forming toxin (βPFT) that forms transmembrane channels (Aksimentiev and Schulten, 2005). A 293 residue long polypeptide monomer assembles to form a mushroom-shaped, heptameric pore consisting of a 14 stranded β-barrel stem (Bhakdi *et al*., 1981; Füssle *et al*., 1981; Song *et al*., 1996). α-Hemolysin causes a number of human diseases which involve cell lysis and hemolytic activity by the leakage of ions, water, and low molecular weight molecules. The toxin can insert into cells such as human blood monocytes or platelets (May *et al*., 1996; Menestrina *et al*., 2001). The conductance of αHL has a linear dependence with solution conductivity and suggests a water-filled channel (Menestrina, 1986). The single channel conductance of αHL in 1 M KCl is ~ 0.8 nS at 22ºC (Wong *et al*., 2006). The αHL channel contains a hydrophilic interior and a hydrophobic exterior and the conductance of the αHL channel increases with decreasing pH (Kasianowicz and Bezrukov, 1995; Song *et al*., 1996). The αHL pore remains as an open channel in concentrated KCl solutions which is very advantageous for biosensing (Menestrina, 1986; Korchev *et al*., 1995a; Bashford *et al*., 1996).

The crystal structure of αHL was solved in 1996 (Song *et al*., 1996). The external dimensions of αHL are 100 Å in height and 100 Å in diameter (Figure 1.4) (Song *et al*., 1996). The mushroom-shaped pore consists of a cap concealing a vestibule which is connected to the β-barrel stem of approximately 50 Å in height and a diameter of 15 Å at its narrowest constriction (Figure 1.4A). The vestibule which lies entirely outside the membrane spans from 14 Å to 46 Å in diameter and the β-barrel stem forms the transmembrane domain which inserts into the lipid bilayer (Figure 1.4B) (Song *et al*., 1996). Figure 1.4C depicts the dimensions of the αHL channel: the cap has a 26 Å diameter at the *cis* entrance, 36 Å in the internal cavity, 15 Å at the inner constriction, containing a ring of lysine and glutamate residues, and 22 Å at the *trans* entrance of the stem (Deamer and Branton, 2002). The suitability of αHL for single-molecule analysis is due to several features. First, it forms ionic channels with a well-defined conductance in neutral and negatively-charged membranes at a wide range of pH (Menestrina, 1986). Second, the assembly of αHL is temperature dependent and is stable up to 50ºC while the transmembrane pore remains open without gating from 15ºC to 50ºC (Belmonte *et al*., 1987; Meller *et al*., 2000). Third, αHL channels form spontaneously in biological or synthetic lipid bilayers giving a unitary conductance which can only fluctuate under low salt concentrations (Korchev *et al*., 1995a, b). This is advantageous for the analysis of molecules that can cause changes in the current blockade. Wild-type αHL (wt-αHL) is considered a blank pore that lacks any intrinsic ability to bind analytes. However genetically engineered pores can be designed to bind specific analytes and αHL has an added benefit due to its homo-heptameric assembly. This means that a single mutation in one subunit can be multiplied seven fold when the pore assembles (Bayley, 1999; Kasianowicz *et al*., 1999; Clark *et al*., 2009; Banerjee *et al*., 2010).

Aerolysin, secreted from the gram-negative bacteria *Aeromonas hydrophila*, was identified in 1974 and is a human pathogen that causes gastroenteritis, deep wound infection and meningitis (Bernheimer and Avigad, 1974; Chakraborty *et al*., 1987). Though the channel-forming toxin aerolysin was known to form ion channels in planar lipid bilayers in voltage-clamped experiments, its use in single-molecule detection was only recently confirmed with the analysis of the translocation of negatively charged helical peptides (Wilmsen *et al*., 1991, 1992; Stefureac *et al*., 2006). The interaction of aerolysin with erythrocyte-membranes is mediated by specific binding to a glycoprotein receptor followed by the formation of channels and selective permeabilization of small ions, such as potassium and calcium (Howard and Buckley,

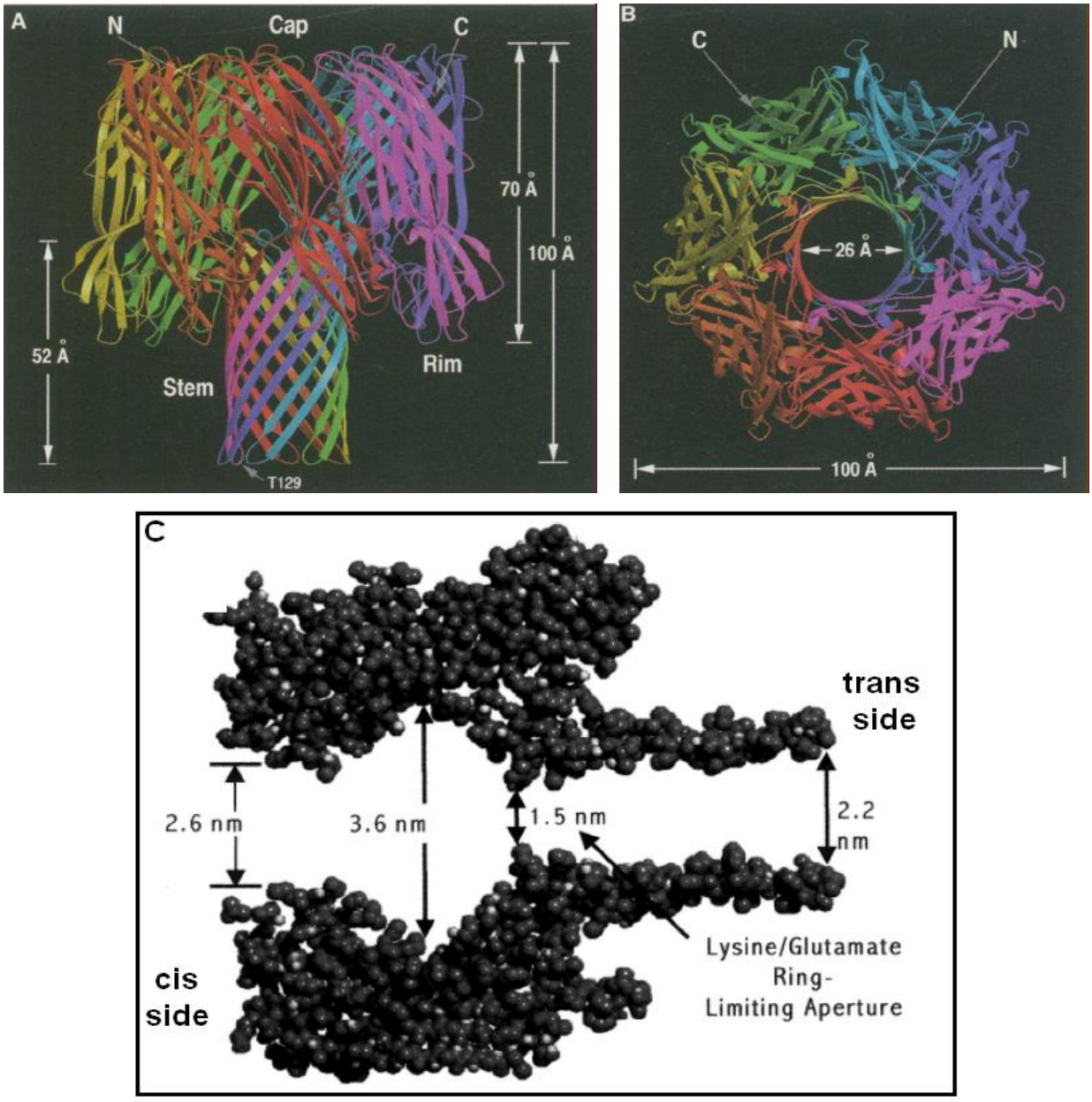

Figure 1.4 Representation of the heptameric α-hemolysin pore using ribbon diagrams and a general configuration of the pore. (A) Shows the side view approximately parallel to the membrane and (B) shows the top view. The seven monomers that form the heptameric channel are represented in different colors. (c) Shows a cross section of the α-hemolysin pore, using general configurations for nanopore analysis, where 10 Ångstroms (Å) = 1 nm. PDB ID: 7AHL. (Reprinted by permission from Song *et al*., 1996. Copyright 1996 AAAS; Deamer and Branton, 2002. Copyright 2002 ACS).

1982; Abrami *et al*., 2000). The protein was purified in 1981 and is secreted as an inactive precursor proaerolysin, having a molecular weight of 52 kDa (Buckley *et al*., 1981; van der Goot *et al*., 1993). The precursor is activated by a proteolytic nicking of ~ 25 amino acids from the carboxy terminus (Howard and Buckley, 1985; van der Goot *et al*., 1992, 1994a, b). The gene coding aerolysin designated as *aerA* has been cloned, expressed, and sequenced with most of the sequence being unrelated to the αHL toxin (Chakraborty *et al*., 1986; Howard and Buckly, 1986; Howard *et al*., 1987). The activated aerolysin binds to cell surface receptors via glycosylphosphatidyl inositol (GPI) anchors and oligomerizes into heptameric rings that insert holes in the membrane (Garland and Buckley, 1988; Parker et *al*., 1994; Fivaz *et al*., 1999). Oligomerization of aerolysin decreases with increasing pH and the rate of channel formation is effective between a pH range of 6.5 to 8.5 (Buckley *et al*., 1995). The transmembrane region of aerolysin has a β-barrel configuration and the turn of the β-hairpin composed of five hydrophobic residues drives membrane insertion of the oligomerized channel (Lacovache *et al*., 2006).

The proaerolysin dimer has a crystal structure (2.8 Å resolution) that adopts a hydrophobic environment between monomer-monomer interfaces (Parker *et al*., 1994). Based on this crystal structure, an electron micrograph model of the aerolysin channel was described (Figure 1.5). The model of the aerolysin oligomer presents a wheel-like structure which lies entirely outside the membrane and a stem like central cylindrical section which presumably inserts into the lipid bilayer to form channels very similar in size as those of αHL (Figure1.5b and Figure 1.5d) (Parker *et al*., 1994). The wheel-like cap does not contain a vestibule as in αHL, but has a well defined diameter of 140 Å and is 30-40 Å thick (Figure 1.5a and Figure 1.5c). The central cylindrical transmembrane channel has a diameter of approximately 17 Å and is 70 Å in height (Wilmsen *et al*., 1992; Parker *et al*., 1994). In voltage-clamp experiments, aerolysin maintained a homogeneous ionic current and the channels remained open between -70 mV to +70 mV. The channels switch between open and closed states in a voltage-dependent manner regardless of polarity outside the previously mentioned voltage range. At a constant membrane voltage of +50 mV, the open pore current of one aerolysin channel was 21 pA with a conductance of 420 pS (Wilmsen *et al*., 1990, 1991).

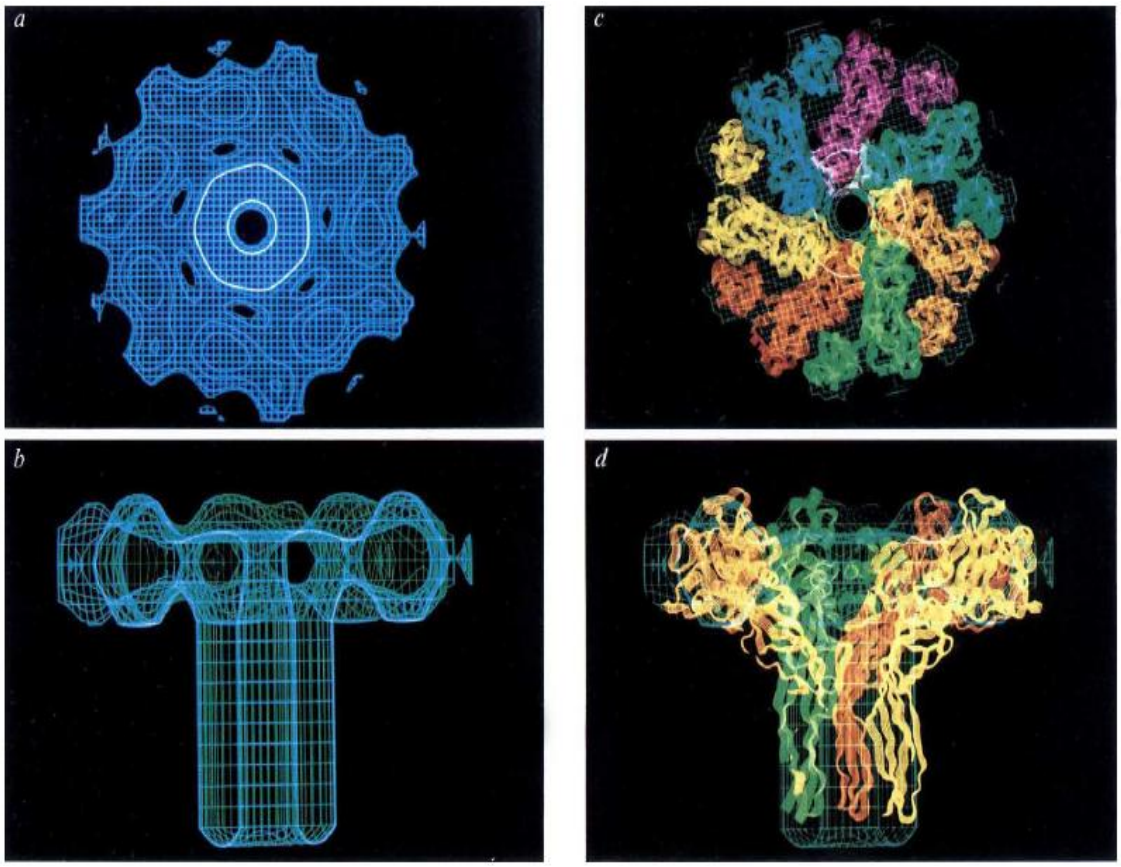

Figure 1.5 Image of the heptameric aerolysin channel derived from electron microscopy. (a) Shows the electron microscopy of the channel when viewed down onto the membrane surface. (b) Shows a side view of the channel from electron microscopy. (c) & (d) Show a top view and a side view of the channel, respectively, with the seven monomers that form the heptameric channel represented in a different color. PDB ID: 1PRE. (Reprinted by permission from Parker *et al*., 1994. Copyright 1994 Nature Publishing Group).

MspA is the major porin in *Mycobacterium smegmatis* (Trias and Benz, 1994). *Mycobacterium* porin A has been purified, cloned, and sequenced with data showing that MspA is a channel-forming protein with properties different from those of gram-negative bacteria (Niederweis *et al*., 1999). MspA is the main channel-forming protein that maintains the hydrophilic pathway and mediates the diffusion of hydrophilic nutrients in *Mycobacterium smegmatis* (Stahl *et al*., 2001; Niederweis, 2003). The X-ray structure of MspA reveals a homooctameric goblet-like monomeric association with a single channel having an approximately 1 nm wide constriction at the limiting aperture (Figure 1.6). Each subunit which forms the octamer in MspA consists of a 134-residue globular domain which builds the thick rim of the goblet and a 50-residue loop that forms the stem of the channel. MspA contains two consecutive β-barrels having a width of 37 Å which form a ribbon around the porin. The β-barrels are composed of nonpolar outer surfaces. The external dimensions of MspA are 96 Å in height and up to 88 Å in diameter (Figure 1.6A). The channel's internal diameter varies between 10 to 48 Å (Figure 1.6B) (Faller *et al*., 2004). MspA oriented with the mouth of the goblet on the *cis* compartment and the stem embedded in a lipid bilayer has a single channel conductance of 4.9 nS in 1 M KCl at 20ºC with a positive voltage of 60 mV applied to the *trans* compartment. Above an applied voltage of 60 mV, MspA demonstrates frequent and spontaneous blockades (Butler *et al*., 2008). The constricted region of MspA contains three negatively charged residues of aspartic acid which prevent the translocation of single stranded DNA (ssDNA). The replacement of these three residues with asparagines allowed the translocation of ssDNA through MspA and also permitted all four DNA nucleotides to be distinguished (Derrington *et al*., 2010). MspA may prove to be an important pore for nanopore DNA sequencing in the future.

Gram-negative bacteria contain a number of channels known as porins in their outer membrane that assist in the passage of ions and nutrients for cell survival. Some of the major outer membrane proteins (Omp) from *Escherichia coli* include OmpF, OmpC, and PhoE that are all trimers and allow the free diffusion of small (<600 Da) molecules (Conlan *et al*., 2000; Conlan and Bayley, 2003). OmpG is also an outer membrane porin obtained from *Escherichia coli*, but is monomeric in structure (Fajaro *et al*., 1998). OmpG forms a 14 stranded β-barrel (β1–β14) with seven extracellular loops (L1-L7) and short periplasmic turns (Yildiz *et al*., 2006). Early studies using proteoliposome swelling assays that measure the pore forming

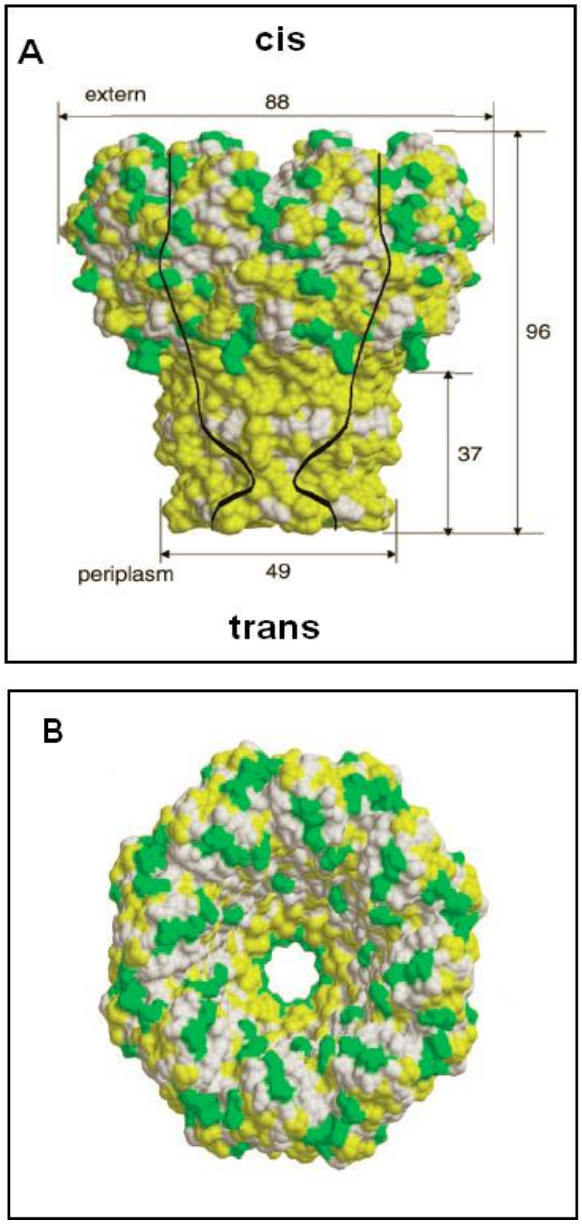

Figure 1.6 Structure of MspA. (A) Shows the channel lining in black which reveals a goblet like shape. The dimensions are given in Ångstroms (Å). (B) Shows the top view, from the external compartment. Green represents polar and yellow represents nonpolar amino acid residues. PDB ID: 1UUN. (Reprinted by permission from Faller *et al*., 2004. Copyright 2004 AAAS).

activity showed that OmpG forms large channels with a diameter of approximately 20 Å (Fajardo *et al*., 1998). The crystal structure for the monomeric porin OmpG was solved in 2006 and has its largest diameter of 20-22 Å at the periplasmic exit (Figure 1.7A) (Subbarao and van den Berg, 2006). The constriction of this channel is mainly established due to the side chains of the residues that line the wall of the barrel pointing inwards and not due to the surface loops protruding inwards (Figure 1.7B). The approximately circular shaped OmpG has a diameter of ~13 Å at the constriction zone and is much larger than other porins (Subbarao and van den Berg, 2006). The conductance of OmpG in 1 M KCl is ~ 0.8 nS and is similar to the conductance of a αHL channel (Wong *et al*., 2006; Conlan *et al*., 2000). The OmpG channel closure occurs at pH values below 7 and voltages above ±100 mV, suggesting that it has a gating mechanism which is voltage-dependent and pH-dependent (Conlan *et al*., 2000; Conlan and Bayley, 2003). The monomeric structure of OmpG and its orientation in planar lipid bilayers to form channels like αHL may show future prospects as a biosensor (Chen *et al*., 2008a, b). However, due to the spontaneous gating of wild-type OmpG, site-directed mutagenesis was performed on the pore resulting in a 95% reduction in gating activity. This variant form of OmpG was introduced with two modifications. Firstly, the flexibility of the L6 loop was reduced by the addition of a disulfide bond between β-strands 12 and 13. Secondly, the deletion of residue D215 caused an increase in hydrogen bonding between β11 and β12. Then a cyclodextrin molecular adopter was fitted to the mutated OmpG, which could be used to detect adenosine diphosphate (ADP) (Chen *et al*., 2008b).

There are many other biological nanopores that are rarely used in biosensing, but may serve as important channels for future applications (Majd *et al*., 2010). Gramicidin A secreted by the bacterium *Bacillus brevis* is a channel forming peptide with a molecular weight of 1.9 kDa (Hladky and Haydon, 1970; Stankovic *et al*., 1989). Gramicidin A spontaneously inserts into lipid bilayers and forms an amino terminal-to-amino terminal helical dimeric channel that conducts ionic current (Wallace, 1986; Woolley and Wallace, 1992). The use of Gramicidin A as a biosensor was first demonstrated by Cornell and co-workers by linking antibodies to this channel (Cornell *et al*., 1997). The lipid bi-layer containing gramicidin A (attached to antibody) was tethered to a gold electrode. When an antigen binds the antibody, gramicidin A no longer conducts (Cornell *et al*., 1997). In another study, the pore formed by *Bacillus anthracis* PA_{63} protein, forms a heptameric ion channel in planer lipid bilayers (Nablo *et al*.,

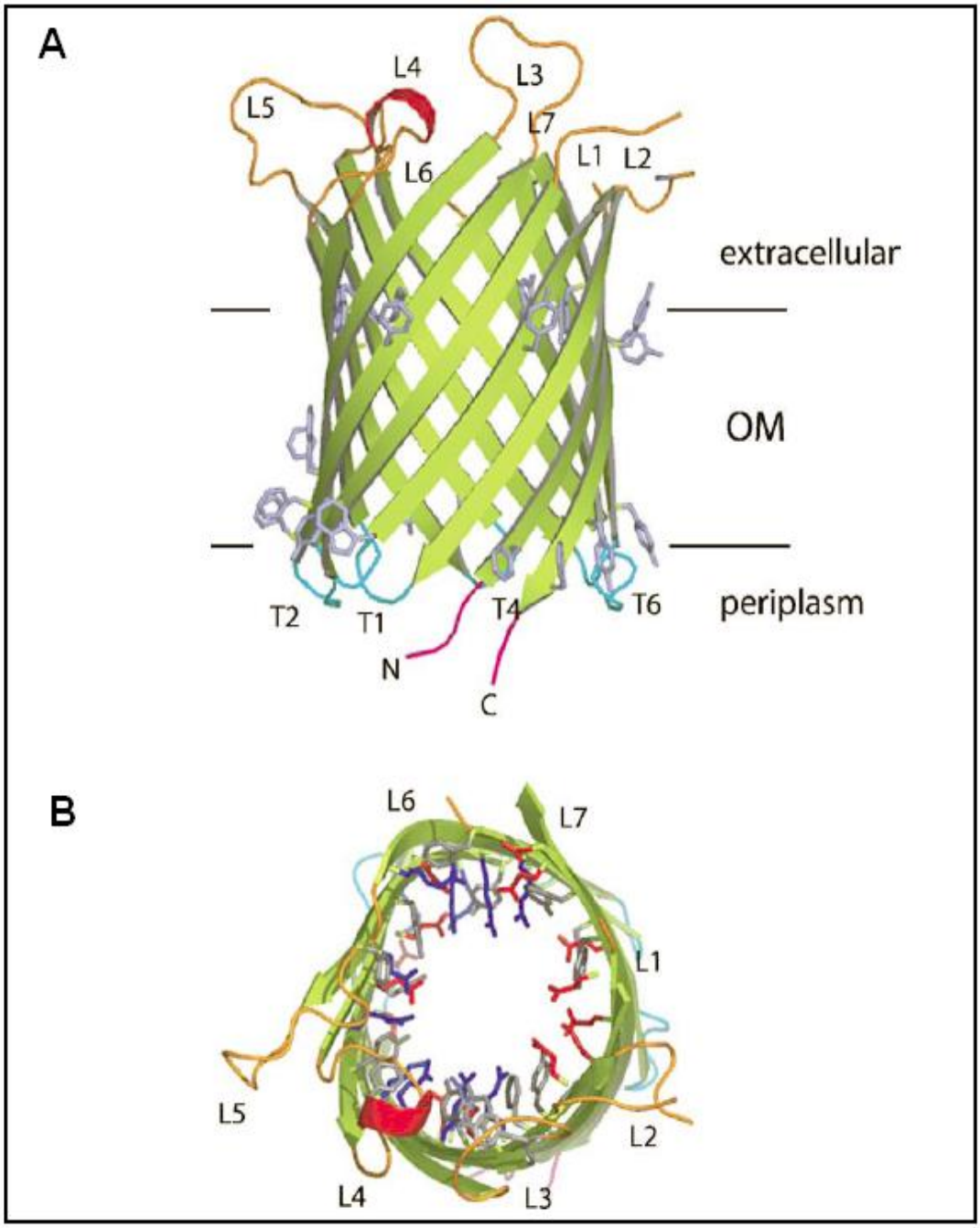

Figure 1.7 Structure of OmpG. (A) Shows OmpG viewed from the plane of the membrane and (B) shows a top view. Loops L1 to L7 are shown in orange strings. PDB ID: 2F1C. (Reprinted by permission from Subbarao and van den Berg, 2006. Copyright 2006 Elsevier Ltd).

2008). The limiting diameter of PA_{63} is < 2 nm and features a much narrower channel than αHL (Nablo *et al*., 2008). A single channel of PA_{63} displays an ionic current of ~ 4 pA at +50 mV. The introduction of the lethal factor (LF) protein completely blocked this channel current (Halverson *et al*., 2005). In the future, the detection of low level toxins for anthrax in animal blood may be possible (Halverson *et al*., 2005). Furthermore, the maltoporin trimer was subjected to a single-channel study in the presence of differently sized maltodextrins (Kullman *et al*., 2002). It was shown that only one molecule of maltohexose is required to completely block one pore in the maltoporin trimer (Kullman *et al*., 2002). Finally, alamethicin and melittin which form helix bundles in planer lipid bilayers have also been used in single-channel experiments but will probably have limited applications (Majd *et al* ., 2010).

1.1.3.2 Genetically engineered protein pores

Engineered protein pores are extremely useful for specific tasks in nanopore analysis. The most widely engineered pore is αHL, while others such as MspA and OmpG pores have also been subjected to mutation (Chen *et al*., 2008b; Derrington *et al*., 2010). Variant αHL pores were synthesized by replacing five glycine residues (residue 130-134) with histidine residues in an effort to detect divalent metal ions. The addition of 100 μM of Zn(II) caused current blockades in this mutant (Walker *et al*., 1994; Kasianowicz *et al*.,1999). Similarly, a cluster of imidazole side chains was introduced within the lumen of αHL by replacing residues 123, 125, 133, and 135 with histidines serving as binding sites for Zn(II), Co(II), and other divalent metal ions (Braha *et al*., 1997). Bayley and co-workers also designed several other mutants of αHL that caused Zn(II) induced current blockades which varied with divalent cation concentration (Bayley, 1999; Kasianowicz *et al*., 1999).

Wild-type αHL was also subjected to site directed mutagenesis, where a single oligonucleotide was covalently attached to a cysteine residue within the lumen of the pore, to form a "DNA-nanopore" complex (Howorka *et al*., 2001a, b). Following the addition of ssDNA which binds the tethered DNA, changes in ionic current blockades were observed (Howorka *et al*., 2001a, b). Engineered αHL pores have also been used to try and develop a method for DNA sequencing. For example, a mutant αHL, $(M113R)_7$ fitted with a cyclodextrin adapter near the constriction of the pore, was able to recognize all four DNA bases with distinct

levels of current blockades (Astier *et al*., 2006). In another approach, single stranded DNA (ssDNA) was immobilized within an engineered αHL pore that contained substituted residues E111N and K147N (Stoddart *et al*., 2009, 2010). The capture of this ssDNA was through an applied potential and translocation was hindered due to a biotin tag at the 3' terminus of the DNA that in turn formed a complex with streptavidin. The recognition of all four DNA bases in this immobilized ssDNA strand was possible using this variant pore (Stoddart *et al*., 2009, 2010). In a further attempt to sequence DNA using nanopores, Bayley and co-workers used an engineered form of αHL that contained substituted residues at M113R/N139Q/L135C (Figure 1.8a) (Clarke *et al*., 2009). This substituted channel also contained a covalently attached cyclodextrin adapter at position 135 that was able to discriminate all four DNA base pairs with 99% accuracy (Figure 1.8b) (Clarke *et al*., 2009). Furthermore, recently the translocation of double stranded DNA (dsDNA) at pH 11.7 was investigated using an engineered αHL pore at residue M113R, where arginine would remain protonated under alkaline conditions (Maglia *et al*., 2009). The strand separation of dsDNA at pH 11.7 promoted translocation of DNA through this mutated pore (Maglia *et al*., 2009).

Two variants of the MspA pore, M1MspA (D90N/D91N/D93N) and M2MspA (D90N/D91N/D93N/D118R/D134R/E139K) were investigated with electrophoretically driven ssDNA (Butler *et al*., 2008). The rate of ssDNA blocking was ~ 20 times faster for M2MspA than M1MspA, which was due to the additional exchange of negatively-charged to positively-charged residues at D118R/D134R/E139K (Butler *et al*., 2008).

In a different approach, protein-ligand interactions were investigated in the presence of a lectin (class of sugar binding proteins) using a αHL pore modified with cysteine residues that were tethered to a natural ligand disaccharide (Howorka *et al*., 2004). Lectin caused reversible binding to this tethered ligand-receptor which produced transient current blockades (Howorka *et al*., 2004). In addition, the kinetics of peptide-protein channel interactions have also been investigated using engineered αHL pores (Zhao *et al*., 2009). Two variants of αHL, M113F and M113F/K147N/T145F, were investigated in an effort to evaluate the effect of protein channel architecture on peptide translocation (Zhao *et al*., 2009). The results indicated that stronger binding affinities between the peptide and protein pore correlates with an increase in aromatic binding sites within the pore (Zhao *et al*., 2009).

In another vein, the αHL pore has also been engineered to detect second messengers

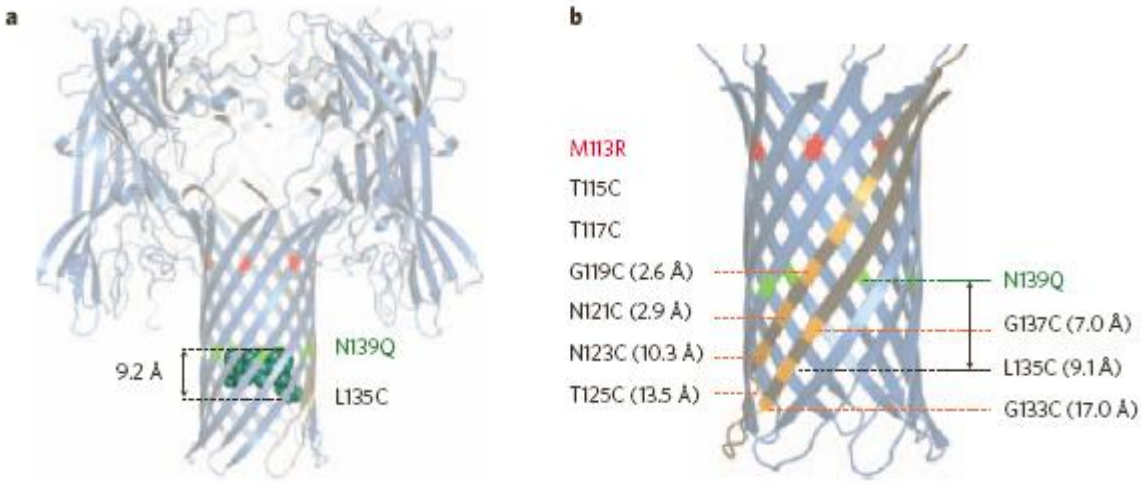

Figure 1.8 Structure of the mutated αHL pore. (a) Shows cyclodextrin attached at position 135 and 139. (b) Shows a close-up of the β-barrel with mutated residues. Substituted residues are stated in single amino acid codes (for example: L135C denotes Lys- 135 replaced by Cys). (Reprinted by permission from Clarke *et al*., 2009. Copyright 2009 Nature Publishing Group).

such as inositol 1,4,5 trisphosphate (IP3) (Cheley *et al*., 2002). Engineered αHL with substituted residues at M113R and T145R containing a ring of 14 arginine residues near the constriction area of the pore permitted the detection of IP3 at nanomolar concentrations (Cheley *et al*., 2002). In another study, engineered pores were also used to distinguish small chiral molecules of ibuprofen and thalidomide (Kang *et al*., 2006). For this purpose, a β-cyclodextrin adapter lodged into an engineered αHL pore that contained substituted residues M113F and K147N produced a distinct current signal for each bound molecule (Kang *et al*., 2006). A similar strategy has also been used for the stochastic sensing of terrorist agents such as trinitrotoluene (TNT), organophosphorus nerve gas, organic arsenicals, and mustard gas using engineered αHL pores (Liu *et al*., 2010). α-Hemolysin variants M113F and M113F/K147N were incorporated with a β-cyclodextrin adaptor and used for the detection of TNT and organophosphorus nerve gases, respectively (Guan *et a*l., 2005). Finally, the addition of a cysteine residue at position 117 allowed the monitoring of organic arsenicals and mustard gas through covalent interactions (Wu and Bayley, 2008; Wang *et al*., 2009).

1.1.4 Protein pores in planar lipid membranes

One of the main problems with biological nanopores is that they have to be first inserted into a planar lipid bilayer in contrast to solid-state nanopores which are generated on synthetic membranes. The main concern is the stability of the lipid bilayer into which the biological pore is inserted. For single-molecule analysis, first an artificial lipid bilayer is made across an ~ 100 μm diameter orifice made from teflon having a thickness of 25 μm. Smaller apertures ranging from 20 μm to 150 μm have also been used for these experiments (Kasianowicz *et al*., 1996; Akeson *et al*., 1999b; Braha *et al*., 2000; Meller *et al*., 2000; Sutherland *et al*., 2004a). The pore is then added to the chamber holding the planer lipid bilayer filled with an electrolyte solution. Random pore insertion into the lipid bilayer occurs within a short time. However, the time taken for single-channel insertion as well as multiple pore insertions that cause membrane rupture are the main drawbacks in this method. Flushing out excess protein pores is one approach that helps reduce multiple channel insertions. On the other hand, single-channel insertions can be enhanced by using a mechanical probe coated with pores fitted on an agarose gel that helps to insert a single pore (Holden and Bayley, 2005). Another method involves the use of a sharp glass tip, dipped into a bacterial colony expressing membrane proteins which is

then driven into an artificial lipid bilayer using a micromanipulator (Holden *et al*., 2006). Also, polymerisable phospholipids, such as 1-palmitoyl-2-10,12 tricosadiynoyl-sn-glycero-3-phosphoethanolamine (PTPE), enhance membrane stability after channel insertion due to the formation of lipid cross-links (Shenoy *et al*., 2005). Other methods for membrane stability include the use of 100 to 400 nm diameter wide glass nanopipettes coated with 3-cyanopropyldimethylchlorosilane which link the membrane through the hydrophobic tail of the lipid (Atanasov *et al*., 2005, 2006; White *et al*., 2007).

1.1.5 Solid-state pores

The possibility of longer recording hours and conducting experiments within a wide range of pH and temperatures has recently made the use of synthetic nanopores popular for single-molecule analysis. Charles Martin's laboratory was the first to develop synthetic membranes made from polycarbonate filters that contained monodispersed Au nanotubes with internal diameters of less than 1 nm (Jirage *et al*., 1997). Further development using reversible electromodulation methods on the inner wall of this Au nanotube permitted the transport of neutral molecules (Lee and Martin, 2002). The fabrication of 5 nm diameter solid-state pores on silicon nitride (Si_3N_4) membranes using ion-beam sculpture capable of identifying a 500 base pair dsDNA molecule was first developed in 2001 (Li *et al*., 2001, 2003). The technique using argon ion-beam sputtering is a two stage process. First, a bowl-shaped cavity or a single hole of ~ 0.1 µm is made on a Si_3N_4 membrane using reactive ion etching (RIE) or a focused ion beam (FIB) (Li *et al*., 2001). RIE is a process that incorporates an electron beam focused onto a Si_3N_4 membrane that uses a chemically reactive etch of CHF_3/O_2 to remove material from Si_3N_4 (Ralls *et al*., 1989). FIB uses a focused beam of gallium ions that can be directed on to a membrane to create a hole (Nagoshi *et al*., 2009). At the end of the first step, an argon ion-beam is used to remove material from a Si_3N_4 membrane with a cavity (Li *et al*., 2001). Second, a feed-back controlled argon ion-beam is then used to laterally deposit material onto the pore until the desired pore size is reached (Figure 1.9a) (Li *et al*., 2001).

Dekker and co-workers used silicon oxide (SiO_2) to manufacture single pores with diameters between 20 nm and 200 nm (Figure 1.9b) (Dekker, 2007). SiO_2 layered on both sides of a free standing silicon membrane is first subjected to electron beam lithography and RIE to form squares up to 500 nm in dimension (Dekker, 2007). Finally, anisotropic KOH

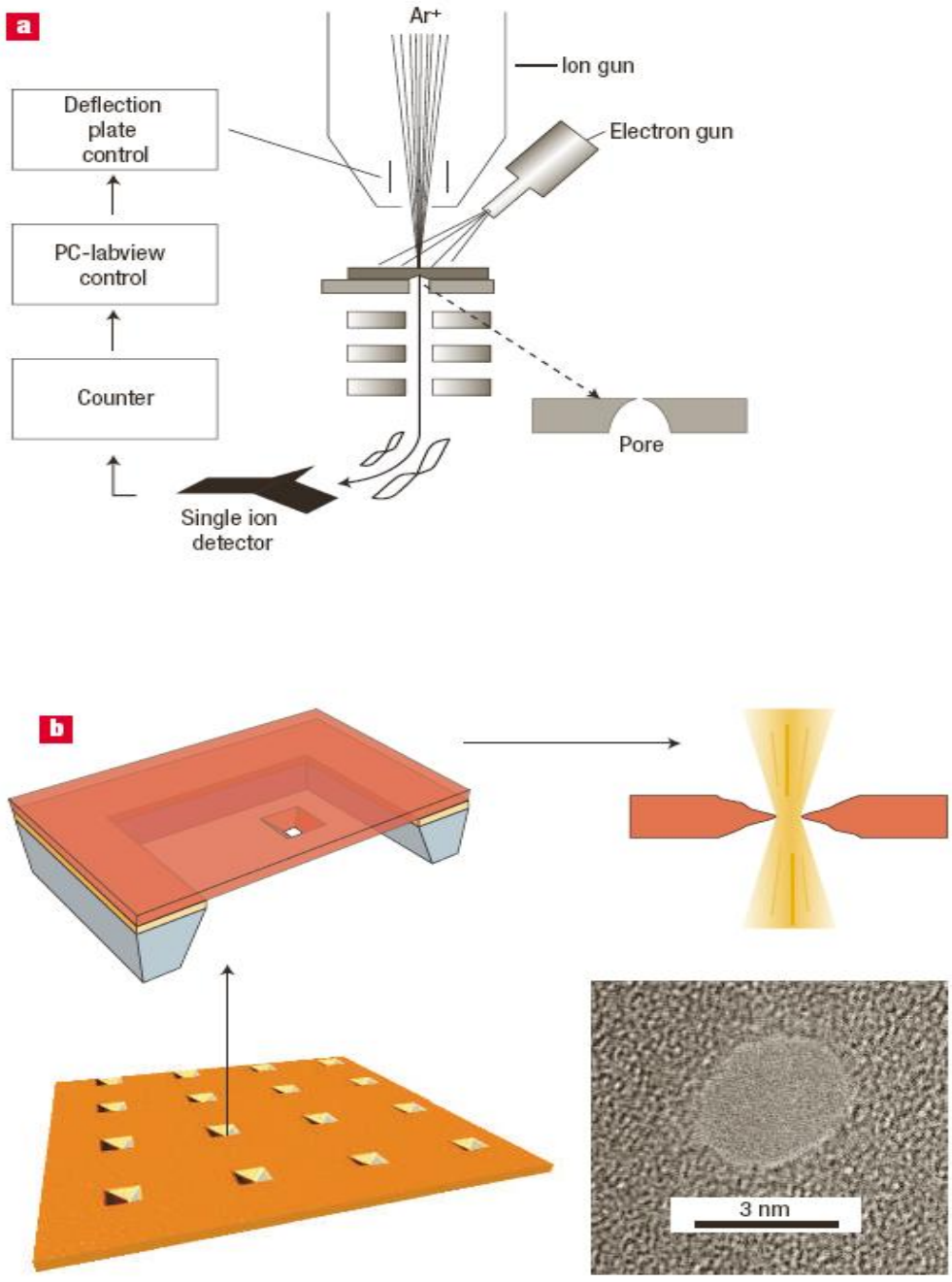

Figure 1.9 Methods used in the fabrication of solid-state nanopores. (a) Shows the use of ion-beam sputtering and feed-back controlled ion-beam sculpting used on Si_3N_4 membranes as shown in Li *et al*., 2001. (b) Shows the method of transmission electron microscope (TEM) used on SiO_2 membranes to develop 3 nm diameter pores. (Reprinted by permission from Dekker, 2007. Copyright 2007 Nature Publishing Group).

wet etching is used to make pyramid-shaped holes. Anisotropic wet etching is a process used to etch along preferred crystallographic directions and is mainly used to attack silicon which then produces an anisotropic V-etched shaped side wall (Bachman, 1999; Holly and Hingerl, 2006). To fine tune the desired pore size, the pore is shrunk using a transmission electron microscope (TEM) with a 300 kV electron beam (Storm *et al*., 2003; Dekker, 2007).

The advantage of using solid-state pores at high pH values is clearly shown in the analysis of denatured dsDNA to ssDNA at pH values above 11.6 using a 4 nm diameter Si_3N_4 pore (Fologeo *et al*., 2005). Translocation of DNA was mostly as single strands (Fologeo *et al*., 2005). Nanopores are also manufactured by the track-etching technique, which first irradiates the membrane with heavy ions such as Xe, Pb, Au and U, followed by subsequent chemical etching. Polymer films such as polyethylene, terephthalate (PET), polyimide (PI) and polycarbonate (PC) are some of the widely used membranes. Generally, chemical etching for PET uses 9M aqueous NaOH at room temperature and sodium hypochlorite (NaOCl) at 50ºC (Siwy *et al*., 2003; Howorka and Siwy 2009b).

A further modification in making solid-state pores was the development of conically shaped nanopores. Ionic current and the resulting transmembrane voltage drop are concentrated near the tip of the sensing zone which is advantageous for single-molecule sensing (Harrell *et al*., 2006). Gold-plated conical nanopores have been used as a biosensor for the detection of protein antibody complexes (Siwy *et al*., 2005). More modifications to conical nanopores prepared in PET include the coating of a thin film of Au which is sandwiched between two Ti adhesion layers and insulated with SiO_2. The Au layer functions as a "gate electrode" because it is connected to a generator while the membrane voltage is applied. The change in the transport of ions at the entrance of this conical nanopore is thought to be due to the concentration depletion that is induced by the metal gate (Kalman *et al*., 2009).

It has also been possible to chemically modify Si_3N_4 based solid-state pores to enhance single-molecule detection. For example, the deposition of aluminium oxide (Al_2O_3) onto the inner walls of the pore reduced the electrical noise and increased the DNA capture rate (Venkatesan *et al*., 2009). Another modification included the deposition of Ti/Au on the inner walls of the pore to form metalized pores which subsequently demonstrated the translocation of λ DNA that interacted with the metallic pore (Wei *et al*., 2010). More recently, a solid-state pore made from Al_2O_3 with surface properties that help in the reduction of velocity in DNA

translocations was developed by Bashir and co-workers (Venkatesan *et al*., 2009, 2010). Finally, the incorporation of solid-state pores with nanopore force spectroscopy helped detect the capture and dissociation of molecular complexes (Tabard-cossa *et al*., 2009). For this purpose, a 3 nm diameter Si_3N_4 pore was put under constant applied forces between 400-900 mV to determine the bond lifetime spectrum of the biotin-neutravidin complex. The long ionic current blockades suggest that a stable complex is formed between biotin and neutravidin. These ionic blockades are diminished when the complex dissociates (Tabard-cossa *et al*., 2009).

1.2 Detection of individual molecules

1.2.1 Nanopore analysis of nucleic acids

1.2.1.1 DNA

Deamer and co-workers reported the first data on the translocation of nucleic acids through αHL pores, where the duration of the current blockades was proportional to polymer length and inversely proportional to the applied voltage (Kasianowicz *et al*., 1996). DNA polymers were analyzed to examine the effects of temperature and secondary structure on the process of translocation. A translocation duration of 120 µsec and 330 µsec was recorded for $(dC)_{100}$ and $(dA)_{100}$ at 22ºC, which increased to 200 µsec and 650 µsec, respectively, when the temperature was decreased to 15ºC, providing clear discrimination between $(dC)_{100}$ and $(dA)_{100}$. Pyrimidine polymers, $(dC)_{100}$ and $(dCdT)_{50}$ also showed a 50% difference in translocation duration values at 15ºC, thus indicating that low temperature enhances sensitivity (Kasianowicz *et al*., 1996). In another study, an increase in temperature reduced the translocation duration of DNA polymers, $(dA)_{100,}$ $(dC)_{100}$, $(dA)_{50}(dC)_{50}$, $(dAdC)_{50}$, $(dC)_{50}(dT)_{50}$, and $(dCdT)_{50}$ (Meller *et al*., 2000). At lower temperatures, such as 5ºC, poly$(dA)_{100}$ forms an extensively stacked structure which then transforms into a random coil when the temperature is increased to 50ºC. A decrease in translocation duration is seen with increased temperature which corresponds to translocations that are temperature dependent in relation to secondary structure formation (Meller *et al*., 2000: Deamer and Branton, 2002). In nanopore analysis, the capture and translocation of DNA strands are electrophoretically driven by the voltage applied across the membrane, provided the voltage drives anions from that side into the pore (Henrickson *et al* 2000; Meller and Branton, 2002; Nakane *et al*., 2002). Also, the use of engineered αHL pores by site-directed mutagenesis, which increased the positive charges inside

the pore, showed a 10 fold increase in the translocation frequency as compared to wt-αHL (Maglia *et al*., 2008). Studies of a captured ssDNA inside the αHL pore suggest a strong dependency on strand orientation. For example, the 3'-end DNA entry into the pore produces a larger current blockade as compared to the 5'-end threading into the pore (Mathe *et al*., 2005).

Further studies on DNA hairpins with varying compositions (number of base pairs in the stem, number of base mismatches, and varying loop length) show that the stem of the hairpin has to first unzip to translocate as an extended strand (Vercoutere *et al*., 2001). In another study, the discrimination of hairpins based on the number of base pairs and individual nucleotides at the terminal ends were also possible (DeGuzman *et al*., 2006). In a different approach, the unzipping of dsDNA and the identification of mismatched DNA pairs can also be analyzed with αHL pores (Sutherland *et al*., 2004a). In this study, a 50-base Guide strand that contained a 10-base probe was hybridized with a 10-base target sequence that contained up to 3 mismatches. Complementary dsDNA took a significantly longer time to pass through compared to the dsDNA that contained up to 2 mismatches. The dsDNA having 3 mismatches was indistinguishable from the Guide strand (Sutherland *et al*., 2004a).

Solid-state pores manufactured with various materials as mentioned earlier have also been used for sensing DNA and RNA (Li *et al*., 2001, 2003; Storm *et al*., 2003; Chang *et al*., 2004; Heng *et al*., 2004; Wanunu *et al*., 2008). Using Si_3N_4 pores, the translocation time for a dsDNA molecule decreased exponentially with increasing voltage (Wanunu *et al*., 2008). Also, the translocation of DNA through a solid-state pore would experience a hydrodynamic drag force, opposite to its electrical driving force giving a power law ($\tau \approx L^{\alpha}$) dependency, where the exponent α, is 1.27, L is DNA length, and τ is translocation dwell time that are correlated (Storm *et al*., 2005a,b; Wanunu *et al*., 2008; Howorka and Siwy, 2009a). Recently, Dekker and co-workers demonstrated the use of optical tweezers with solid-state nanopores in measuring the force acting on a single DNA molecule bound to a streptavidin/biotin complex (Keyser *et al*., 2006a, b). This method can also be used to slow or even stop the translocation of a DNA molecule by manipulating the opposing force exerted from the optical tweezer (Keyser *et al*., 2006a, b). Finally, the development of a single-molecule nanopore sequencing method for DNA would be an attractive option due to low cost and label-free analysis (Marziali and Akeson 2001; Branton *et al*., 2008; Stoddart *et al*., 2009, 2010).

1.2.1.2 RNA

Homopolymers of RNA, polycytidylic acid (poly C)**,** polyadenylic acid (poly A), and polyuridylic acid (poly U) can be distinguished from each other using translocation data through an αHL pore (Akeson *et al*., 1999b). Poly C translocates with a 95% current blockade and a blockade duration of 2 μs/base while poly A recorded a 85% current blockade and 20 μs/base blockade duration. Though cytosine is a smaller base than adenine, the percentage increase in current blockade for poly C is because poly C forms a single-stranded helix having a diameter of 1.34 nm, which can then easily translocate and produce a higher ionic current blockade with the 1.5 nm diameter αHL channel, as compared to the 2.1 nm diameter helix formed by poly A which translocates only when partially unwound (Akeson *et al*., 1999b). Also, the translocation of an $A_{30}C_{70}Gp$ copolymer demonstrates that the thinner oligo C helix first threads into the pore as the leader, while the oligo A helix follows. The purine and pyrimidine bases within this copolymer can also be distinguished based on current blockade traces (Akeson *et al*., 1999b; Deamer and Branton, 2002). Furthermore, poly U which lacks an ordered structure, translocates as a disordered but extended strand that can be distinguished by the difference in blockade time (Kasianowicz *et al*., 1996). Recent investigations also show that current blockade data contains information about RNA orientation pertaining to 5'-end or 3'-end entry into the pore (Butler *et al.*, 2006). For example, two RNA molecules, $A_{25}C_{50}$ and $C_{50}A_{25}$, with opposite orientations showed that 3'→5' translocation of the poly C segment causes a higher current obstruction than 5'→3' translocation (Butler *et al*., 2006). In another vein, the detection of RNA-protein interactions have also been analyzed with αHL channels (Astier *et al.*, 2007). In this experiment, the blockade duration for the translocation of oligonucleotide 5'-$C_{25}A_{25}$-3' was increased in the presence of a RNA binding ATPase protein P4. The long events disappeared with the addition of ATP due to the dissociation of the P4-RNA complex (Astier *et al.*, 2007). Furthermore, the measurement of the force applied on dsRNA molecules has been investigated using solid-state nanopores (van den Hout *et al*., 2010). The dsRNA is attached to an optically-trapped bead, which is manipulated by optical tweezers coupled with solid-state pores. The force needed to be applied on dsRNA was found to be slightly smaller than that of dsDNA (van den Hout *et al*., 2010).

1.2.1.3 DNA-Enzyme complex

The association and dissociation rates of DNA-enzyme interactions have been studied using nanopore force spectroscopy (Hornblower *et al*., 2007). Single-stranded DNA bound to Exonuclease I, does not translocate the pore due to the bulky enzyme, lodged at the top of the pore. However, the negative transmembrane potential pulls on the ssDNA which finally dissociates from the enzyme, releasing the ionic current blockade (Hornblower *et al*., 2007). Similarly, a 14 base pair DNA hairpin, with a 35 residue single-stranded overhang, was analyzed using αHL (Benner *et al*., 2007). The single-stranded end of the hairpin enters the pore, unfolds, and translocates with an average dwell time of 1 ms before dissociation. Yet when the DNA hairpin is bound to a Klenow fragment (KF) of *Escherichia coli DNA* polymerase I, the blockade current and number of events change. Furthermore, the DNA-KF (binary state) complex has little effect on the dwell time duration, but the presence of the correct substrate, for example dGTP, causes a dramatic increase in the dwell time, indicating a stable ternary complex of DNA-KF-dGTP (Benner *et al*., 2007; Hurt *et al*., 2009; Deamer, 2010).

1.2.2 Nanopore sensing of peptides and proteins

1.2.2.1 Analysis of peptides

The first report on nanopore analysis of peptides was reported by Lee and co-workers in 2004 (Sutherland *et al*., 2004b). This group analyzed peptides having repeats of $(Gly\text{-}Pro\text{-}Pro)_n$ where n = 1, P1; n = 2, P2 or n = 3, P3 that were terminated with ferrocene (Fc). These peptides exist as mixtures of single, double or collagen-like triple helices. Also, the single strand may exist in two different conformations, such as single linear strands or folded U-shaped strands. Nanopore analysis using an αHL pore clearly showed all of the different conformations that these peptides adopt, based on their blockade currents and durations (Sutherland *et al*., 2004b). Furthermore, all peptides could be distinguished from one another which also included their intermediate conformations (Sutherland *et al*., 2004b). In another approach, a series of negatively charged α-helical peptides containing a fluorenylmethoxycarbonyl (Fmoc) group at the N-terminus were analyzed using αHL and aerolysin pores (Stefureac *et al.*, 2006). This study helped identify two types of events. The first, stated as type-I or bumping events, comprise small current blockades and longer current

durations whereas the type-II or translocation events have larger current blockades and shorter durations. This study demonstrates that single-molecule nanopore analysis can provide important structural information with regard to peptide-pore interactions. Another important observation in this study was the influence of the dipole moment on peptide translocation. The dipole moment increases the probability for peptides to translocate (Stefureac *et al.*, 2006).

Following these preliminary studies with peptides, nanopore analysis of a set of β-hairpin peptides with various folding properties was reported by Movileanu and co-workers (Goodrich *et al*., 2007). The amino acid sequence of the β-hairpin peptide was from the C terminal residue of the B1 domain of protein G. The three negatively charged β-hairpins named as Ac-G40, G41 and K41 contained < 5%, ~ 30%, and ~ 50% fraction of the folded peptide, respectively (Goodrich *et al*., 2007). Nanopore analysis and Langevin molecular dynamics showed that the unfolded peptides have shorter translocation times compared to the folded peptides. An important observation was that at a similar force of 3.8 pN, the average dwell time of the long-lived events for the hairpin peptides, Ac-G40, G41, and K41 were 730 μs, 1150 μs and 1210 μs, respectively (Goodrich *et al*., 2007). These data suggest an increase in blockade duration with an increase in the folded fraction of the peptide. Also, an increase in transmembrane potential revealed an exponential decrease in the event duration for these long-lived events. These results demonstrate that the translocation time depends on the applied voltage (Goodrich *et al*., 2007).

Recently, Lee's laboratory analyzed a series of tethered peptides with αHL (Meng *et al*., 2010). Peptides comprising 12 amino acids were tethered via a terminal cysteine to mono-, di-, tri- and tetrabromomethyl-substituted benzene to construct bundles of one to four peptide strands. Nanopore analysis of these peptide bundles at different applied potentials of -50, -100 and -150 mV helped to identify a new set of events called "intercalation events", in addition to the bumping (Figure 1.10A) and translocating events (Figure 1.10C) mentioned in Stefureac *et al*., 2006 (Meng *et al*., 2010). An "intercalation event" is used to describe those molecules that transiently enter the pore but do not translocate. These events give large current blockades, and their blockade duration increases with increasing voltage (Figure 1.10B) (Meng *et al*., 2010). These molecules diffuse back using the same route they entered the pore. On the other hand for a translocation event, the molecule threads through the pore with large current blockades, where the blockade time decreases with increasing voltage (Figure 1.10C). This study is important

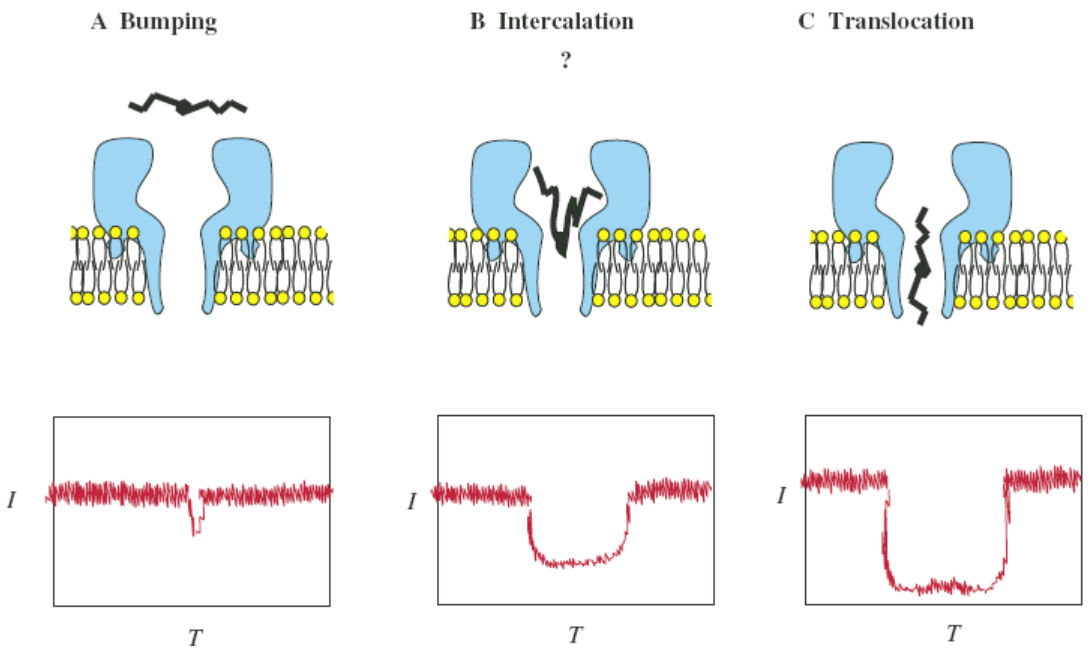

Figure 1.10 Types of events (top) with corresponding event profiles (bottom). (A) Shows a bumping event comprising a small blockade current and short duration. (B) Shows an intercalation event comprising a larger blockade current where the molecule enters the pore but does not translocate. (C) Shows a translocation event comprising a larger blockade current and blockade duration where the molecule threads through the pore. (Reprinted by permission from Meng *et al*., 2010. Copyright 2010 European Peptide Society and John Wiley & Sons, Ltd)

because events having large current blockades could be either an intercalation or a translocation event, and they can only be distinguished if voltage studies are carried out (Meng *et al*., 2010).

Engineered αHL pores have also proven to be useful for peptide analysis. Variant αHL pores with negatively charged binding sites within the lumen facilitated the translocation of cationic peptides in contrast to hydrophobic peptides (Wolfe *et al*., 2007). In addition, the interaction of a small positively charged ~ 25-residue polypeptide with αHL containing an acidic ring (aspartic acid) engineered to the *cis* and *trans* entrance of the pore increased the total event frequency (Mohammed and Movileanu, 2008; Movileanu, 2008). In another approach, the study of protease kinetics for enzyme-peptide interactions was analyzed using αHL pores (Zhao *et al*., 2009). New current blockades and blockade durations were recorded due to enzymatic cleavage of the peptide in contrast to the event profiles obtained for the substrate only (Zhao *et al*., 2009).

In a different vein, the interaction of peptides with divalent metal ions was investigated using a small 28-residue zinc finger peptide, Zif268 (Stefureac and Lee, 2008). Zif268 is comprised of a β-sheet, α-helix, and a turn motif. In the absence of Zn(II), only weak binding to its target DNA was seen due to the unfolded conformation of the peptide. Using nanopore analysis, in the absence of Zn(II), the peptide translocated with a large current blockade of -80 pA and a corresponding translocation-to-bumping events ratio of 2.49. But in the presence of equimolar Zn(II), translocation-to-bumping events ratio decreased to 0.69. The reduction in translocation events is due to folding of the peptide on binding with Zn(II) (Stefureac and Lee, 2008). Another report on peptide-metal analysis using nanopores was reported for the prion peptides within the octarepeat region (Stefureac *et al*., 2010). The N-terminus of the cellular prion protein, PrP^{C}, is involved in the binding of copper at the four octarepeat regions (PHGGGWGQ) located between residues 51 and 91 (Berlett and Stadtman, 1997; Miura *et al*., 1999). Nanopore analysis of prion peptides, Octa2 $(PHGGGWGQ)_2$, Octa4 $(PHGGGWGQ)_4$, and PrP(106-126) in the presence of divalent cations (Cu(II), Mg(II), Mn(II) and Zn(II)) were conducted using an αHL pore. All three peptides translocate freely through the αHL in the absence of divalent metal ions. However in the presence of Cu(II), translocation events decreased for PrP(106-126), Octa2 and Octa4 in the presence of equimolar, 16-fold, and 64-fold excess Cu(II) concentrations, respectively. The addition of Zn(II) caused some changes to the event parameters, but Mg(II) and Mn(II) had no effect on the translocation parameters. These

experiments demonstrate that conformational changes due to complex formation in the presence of divalent metal ions can be distinguished using nanopore technology (Stefureac *et al*., 2010).

1.2.2.2 Analysis of folded and unfolded proteins

The translocation of proteins in the presence of a chemical denaturant using αHL pores was first reported by Auvray and co-workers (Oukhaled *et al*., 2007). In the absence of guanidinium hydrochloride (Gdn-HCl), the 370-residue long maltose binding protein (MBP) displayed no current blockades. The translocation of the unfolded MBP was observed between concentrations of 0.8 M to 1.35 M of Gdn-HCl (Oukhaled *et al*., 2007). In contrast, current blockades, which were assumed to be translocations, were observed for a small 86-residue protein (Stefureac *et al*., 2008). The wild-type 86-residue long histidine-containing protein (HPr) remains uncharged at neutral pH. The structure of HPr contains two α-helices and four β-strands that fold into an open-faced β-sandwich (Jia *et al*., 1993; Napper *et al*., 1996). Single point mutations of HPr, comprising S34D and T34N were also analyzed using these nanopores. Surprisingly, a single conservative substitution of threonine to asparagine without changing the overall charge of the protein was sufficient to alter the event profile. The authors speculate that T34N may unfold differently or may interact differently with the pore compared to wild-type HPr. Yet the S34D variant of HPr which is negatively charged assists in the unfolding and translocates the pore (Stefureac *et al*., 2008). Lee and co-workers also investigated metal-protein interactions using an intrinsically disordered myelin basic protein (Baran *et al*., 2010). In the absence of divalent metal ions the myelin basic protein apparently translocates in an unfolded conformation. The addition of divalent metal ions, Cu(II) and Zn(II) reduced the translocation events to 28% and 52%, respectively, indicating a more compact conformation in the presence of metal ions (Baran *et al*., 2010).

In another approach, an engineered αHL pore containing a tethered polyethylene glycol (PEG) which also contained a covalently attached biotinyl group linked to the untethered end, was used to analyze the binding of streptavidin (Movileanu *et al*., 2000). The binding of a low-affinity streptavidin variant was detected at the *cis* side through transient current blockades but with rare captures on the *trans* side of the pore (Howorka *et al*., 2000; Movileanu *et al*., 2000). Similarly, electrostatic traps of aspartic acid rings engineered onto the limiting aperture and stem (*trans* side) of αHL, were used to study protein-protein interactions (Mohammad *et al*.,

2008). The protein analyte (pb_2-Ba) used for these experiments was made by fusing together the positively charged pre-sequences of the N-terminal region of pre-cytochrome b_2(pb_2) and the N-terminus of the small ribonuclease barnase (Ba). Pre-sequences of varying length were used to prepare the protein analyte. The interaction of pb_2-Ba with αHL was greatly enhanced by these electrostatic traps. This study also demonstrates some important factors that affect protein-protein interactions which include length of the pre-sequence, the location of the electrostatic trap, and the ionic strength of the electrolyte solution (Mohammad *et al*., 2008).

The use of solid-state pores as protein biosensors is popular due to the capacity to manufacture larger-sized pores (Siwy *et al*., 2005). A 5 nm diameter solid-state pore was used to detect bovine serum albumin (BSA) when added to the negatively biased compartment (Han *et al*., 2006). Similarly, a ~ 16 nm diameter Si_3N_4 pore was used for the analysis of BSA which was added to the *cis* compartment of the chamber with pH variations from pH < 5 to pH 7 (Fologea *et al*., 2007). At pH < 5, BSA is positively charged and only translocates the pore when the *trans* side is negatively biased. However, when the pH of the electrolyte solution was increased to pH 7, BSA would only translocate the pore when the *cis* side was negatively biased because at pH 7 the protein has an overall negative charge (Fologea *et al*., 2007). This group was also able to distinguish between fibrinogen and BSA using the event distribution plots for these proteins (Fologea *et al*., 2007). A new approach, where dsDNA filaments were coated with the protein RecA and then analyzed using solid-state pores, was first reported by Dekker and co-workers (Smeets *et al*., 2009; Kowalczyk *et al*., 2010). Si_3N_4 pores which had diameters ranging from 20-35 nm was used for the RecA coated dsDNA complex which exhibited large current durations as compared to the profiles obtained for dsDNA molecules. More recently, Si_3N_4 pores have also been used to detect the native, folded and unfolded conformational states of the protein, bovine β-lactoglobulin variant a (β-Lga) (Talaga and Li, 2009). These experiments were conducted in the presence of varying concentrations of the denaturant urea, and the results suggested that nanopores can distinguish between the folding states of the protein (Talaga and Li, 2009). The authors suggested that when a pro-sequence segment of a polypeptide chain in the protein enters the pore, the volume excluded helps distinguish between folded states. This analysis also suggested that most of the protein molecules translocate in a linear, looped or unfolded configuration (Talaga and Li, 2009). Furthermore, the analysis of the protein avidin across Si_3N_4 pores revealed electroosmotic (the motion of liquid induced by an

applied potential across porous material) transport may reverse electrophoretic transport (Firnkes *et al*., 2010).

1.2.2.3 Analysis of protein-antibody complexes using solid-state pores

The first publication on protein-antibody complexes analyzed with solid-state pores was reported from Charles Martin's group (Siwy *et al*., 2005). Gold-plated conical nanopores were used for the detection of biotin/streptavidin, protein G/immunoglobulin, and the protein, ricin/ricin-antibody complexes (Siwy *et al*., 2005). The biotin, protein-G, and ricin were attached to Au via a thiolated biotin, biotinylated protein G, and biotinylated ricin derivative, respectively (Siwy *et al*., 2005). When the protein binds to the corresponding analyte, a complete blockade of the ionic current was observed (Siwy *et al*., 2005). In another study, BSA and a BSA-Fab complex were investigated using a PEG-thiol group attached to a gold-plated conical nanotube (Sexton *et al*., 2007). The tip of these gold-plated solid-state pores had a diameter of ~ 17 nm. The current-pulse duration (τ) for BSA was 520 ms and changed to 2200 ms when complexes were formed with the anti-BSA-Fab fragments. The current pulse signatures obtained for BSA and the BSA/Fab complexe were also different (Sexton *et al*., 2007). Furthermore, latex colloids were analyzed using a polydimethylsiloxane (PDMS) pore which was 7 μm long and 1 μm wide (Saleh and Sohn, 2003). Latex colloids coated with streptavidin can be differentiated from a complex of latex colloids-streptavidin and colloids-streptavidin/ anti-streptavidin antibody (Saleh and Sohn, 2003). The main goal of this study was to detect an increase in the magnitude of the pulse caused by an increase in volume due to complex formation. Histograms showing the number of events *vs*. colloid diameter clearly depict the difference between latex colloids coated with streptavidin and the complex (Saleh and Sohn, 2003). In a similar strategy, a 28 nm diameter Si_3N_4 pore was used to distinguish between β-human chroionic gonadotropin (β-hCG) and β-hCG-antibody complex (Han *et al*., 2008). The experiments with antibody only showed large translocation blockade currents whereas the β-hCG-antibody complex reduced translocation events due to the change in electrophoretic mobility of the antibody when bound to β-hCG (Han *et al*., 2008).

1.2.3 Analyte detection using covalent and non-covalent adaptors

The αHL pore has been used to covalently link tethered ligands, antibodies, lectins, and

enzymes for the analysis of specific molecules (Movileanu *et al*., 2000; Howorka *et al*., 2000, 2004; Xie *et al*., 2005). A covalently attached protein kinase inhibitor peptide (PKIP) at the *trans* entrance of the pore interacts with the catalytic subunit C of cAMP-dependent protein kinase (PKA) (Xie *et al*., 2005). PKIP is tethered to a cysteine at position 129 through a disulfide link and a tetraethylene glycol (TEG) linker. The binding of PKA C subunit to PKIP is monitored by the change in ionic current through the pore (Xie *et al*., 2005). In a similar strategy, an engineered αHL pore containing a covalently attached polyethylene glycol (PEG) bound to biotin was used for the analysis of complex formation (Movileanu *et al*., 2000). Due to the capture of streptavidin and anti-biotin monoclonal antibody (IgG1) to biotin, it was observed that the tethered biotinyl group moved from one side of the pore (*cis*) to the other side (*trans*) (Movileanu *et al*., 2000). A set of large current blockades was also obtained when the engineered αHL pore containing the tethered arm of biotin was incorporated into a lipid bilayer. When wild-type streptavidin was added to the *cis* side of the bilayer, the large blockades disappeared (Movileanu *et al*., 2000). Addition of the wild-type streptavidin to the *trans* side caused a permanent current blockade. Similar results were also obtained when IgG1 was added to the *cis* and *trans* side of the lipid bilayer. In contrast, when a mutant form of streptavidin was added, transient current blockades were obtained as compared to the permanent blockades obtained with wild-type. This indicates low affinity capture between the mutant streptavidin and biotin. The distinct current blockade signatures obtained from nanopore analysis helps distinguish these interactions (Movileanu *et al*., 2000).

In another aspect, the reaction cycle of a covalently attached dithiobis-2-nitrobenzoic acid (DNTB) at cysteine 117 that forms a disulfide bond with αHL, was monitored by the change in blockade currents (Luchian *et al*., 2003). An increase in the open pore current of the engineered αHL pore was seen when DNTB formed the disulphide bond. However when the disulfide link was cleaved with DTT, the open pore current was reversed. Nanopore analysis was able to detect these short lived intermediate processes (Luchian *et al*., 2003). Similarly, an azobenzene derivative (photochemical dyes which can convert from the *trans* to *cis* isomer by using light at 380 nm wavelength) covalently attached to the αHL pore, can be photo-induced to change configurations (Loudwig and Bayley, 2006). The difference in open pore current between the *trans* and *cis* configurations of azobenzene help detect this izomerization event (Loudwig and Bayley. 2006). Finally, it has also been possible to detect protein-ligand

interactions using lectin which was previously explained in section 1.1.3.2 (Howorka *et al*., 2004).

A non-covalently bound molecular adapter, β-cyclodextrin (βCD), fitted into the lumen of an engineered αHL pore, was able to detect organic ligands and small drugs (Gu *et al*., 1999). Similarly, the interaction of 2-deoxyribonucleoside 5'monophosphate with the non-covalent adapter heptakis-(6 deoxy-6 amino)-β-cyclodextrin, positioned at M113R in αHL, gave distinct current blockades for each base (Astier *et al*., 2006). In a another study, Cucubit[6]uril (CB6) lodged into the lumen of αHL was shown to act as a carrier but not as an adapter (Braha *et al*., 2005). The interactions of tetrahydrofuran (THF) with CB6 in the presence of Na^+ ions could be distinguished by the different event profiles generated for the number of counts *vs*. blockade current (Braha *et al*., 2005).

1.3 Single-molecule sensing for bioanalytical applications

1.3.1 Nanopore sensors for genomic screening

Single-molecule nanopore sensors have been used recently to detect barcoded DNA. This label-free method could be useful in human genomics and diagnostic applications (Mirsaidov *et al*., 2010). Artificial nucleic acid analogs are mostly used in the study of hybridization and mismatch of specific DNA sequences. Peptide nucleic acids (PNA) are a class of artificial nucleic acid analogs that can be synthesized to bind one of the dsDNA strands. This PNA-tagged genomic fragment showed a characteristic secondary current blockade signature when compared to the untagged dsDNA (Singer *et al*., 2010). The concept of nanopore sequencing, discussed in detail earlier, has the advantage of being a label-free, amplification-free, and minimal sample preparation method. Additionally, it also has the potential for direct sequencing of genomic DNA (Bayley and Sanghera, 2008). For example, the use of molecular beacons (luminescent probes used for the identification of nucleic acids) coupled with solid-state nanopore arrays, was shown to allow for the sequencing 50-250 bases per second per nanopore (McNally *et al*., 2010; Krasnoperov *et al*., 2010). This method incorporates a two step reaction. First, each nucleotide on the target DNA sequence is converted to a pre-defined sequence of oligonucleotides followed by subsequent hybridization with molecular beacons that contain specific fluorophores. Second, this DNA-beacon complex

is electrophoretically driven through a 5 nm Si_3N_4 pore which reads each base through an optical detector (McNally *et al*., 2010).

1.3.2 Nanopores as diagnostic protein biosensors

Anthrax is an acute disease that affects mostly animals, but it can also be transmitted to humans (Friedlander *et al*., 1993). The three anthrax toxins known as the protective antigen (PA83), lethal factor (LF), and edema factor (EF) are secreted from *Bacillus anthracis* (Halverson *et al*., 2005). The anthrax protein PA63, synthesized from the cleavage of PA83, forms transmembrane ion channels that can act as pores in reconstituted lipid bilayers. When nanopore analysis using pores formed from protein PA63 was carried out in the presence of protein LF, it decreased the conductance of channel PA63. Further analysis showed that the complex between protein LF and PA63 also formed effective channels (Halverson *et al*., 2005). However, at positive applied potentials, protein EF blocks the channel formed by PA63. This method may be useful as a nanopore-based biosensor for the diagnostic testing of anthrax (Halverson *et al*., 2005; Kasianowickz *et al*., 2008). As mentioned earlier (section 1.2.2.3), another example of nanopores as protein biosensors is the detection of ricin-antibody complex (Siwy *et al*., 2005). Ricin, a protein toxin obtained from the castor bean plant, is poisonous if inhaled, injected or ingested (Audi *et al*., 2005). Thus, protein-protein or protein-antibody interactions which cause conformational changes in the complex can be identified with nanopores that show different event parameters.

1.3.3 Other single-molecule methods

Single-molecule fluorescence resonance energy transfer (FRET) is the most popular and general method for studying individual molecules (Ha *et al*., 1996). The general principal is that the dipole-dipole interactions between two fluorophores transfers energy depending on the distance of the donor and acceptor groups (van Holde and Zlatanova, 2006; Zlatanova and van Holde, 2006). This spectroscopic method can measure distance changes in the range of 20 Å – 80 Å (Ha, 2001). The applications of FRET require intramolecular and intermolecular labeling. Conformational changes in macromolecules, the folding/unfolding of macromolecules, and the structural changes of enzymes during catalysis can be analyzed, and may provide information pertaining to receptor-ligand and enzyme-substrate interactions (Weiss, 2000). For FRET

experiments, DNA can be immobilized onto quartz surfaces through a biotinylated BSA (Biotin-BSA) complex that sticks to the surface which is then attached to a separate biotin-DNA complex tagged with donor and acceptor fluorophores via multivalent neutravidin (Zhuang *et al*., 2000; Ha, 2001; Ha *et al*., 2002). For protein analysis, the quartz surfaces may be coated with PEG to reduce nonspecific binding (Sofia *et al*., 1998).

Another non-invasive single-molecule method is the use of optical tweezers or optical traps (Oddershede *et al*., 2003). An optical tweezer is created by focusing a laser beam onto a small region that has limited diffraction. The electromagnetic field created on this small region can capture a dielectric sphere when placed on this spot (Ashkin, 1997; van Holde and Zlatanova, 2006; Roy *et al*., 2008). The radiation pressure from the laser beam is able to trap small particles. Forces in the pico Newton (pN) range can be applied on the object of interest with nanometer range displacement. Optical tweezers have been used to study kinesins, myosins (motor proteins), and DNA processing enzymes (Selvin and Ha, 2008). Optical tweezers have also been incorporated with nanopore force spectroscopy to analyze the force exerted on DNA molecules (Keyser *et al*., 2006b; Dekker, 2007). Another similar single-molecule method uses magnetic traps. A magnetic trap or magnetic tweezer can be set up by placing two strong magnets above the sample holder of an inverted microscope (Strick *et al*., 2000). Super paramagnetic beads aligned in a strong magnetic field can also be used to tether molecules of interest on to the beads and the sample chamber (Neuman and Nagy, 2008). The applied force and displacement of these single molecules can then be measured. For example, magnetic tweezers have been used to study DNA gyrase (a nucleic acid enzyme that maintains negative supercoiling of DNA) and DNA topoisomerase IV (enzyme that maintains the regulatory DNA topology in the cell) (Charvin *et al*., 2000; Strick *et al*., 2000; Gore *et al*., 2006). These experiments showed that in the presence of ATP, DNA gyrase becomes significantly less processive as DNA tension increases, and in the absence of ATP, topoisomerase IV binds the supercoiled DNA in a cooperative manner (Charvin *et al*., 2000; Gore *et al*., 2006).

Atomic force microscopy (AFM) is another single-molecule method used to study the unfolding of proteins, nucleic acids, and the breaking of covalent bonds (Lee *et al*., 1994; Grandbois *et al*., 1999; Fernandez and Li, 2004). The atomic force microscope consists of a cantilever with a sharp tip, that is above a piezoelectric scanner (piezoelectric materials have a

permanent dipole moment across a unit cell) (Cumpson *et al*., 2004). A detection laser is reflected off the cantilever to a position-sensitive detector, measuring the displacement of the lever after it scans the sample surface (Neuman and Nagy, 2008). AFM has been used for single-molecule force-extension studies of DNA and proteins (Lee *et al*., 1994). The tip of the cantilever is tethered to the sample and the retraction of the tip helps determine the force on the sample (Lee *et al*., 1994; Fernandez and Li, 2004; Bustamante *et al*., 1994). These experiments investigated the interacting forces between two DNA strands and also the physical basis of protein folding reactions. (Lee *et al*., 1994; Fernandez and Li, 2004). For single-stranded DNA, the force needed to rupture the interchain and intrachain interactions between these strands can be measured and quantified in the nano Newton (nN) range (Lee *et al*., 1994). The folding trajectory of a single molecule of ubiquitin was observed where the protein was first unfolded and then extended at high force. This stretching force was then removed, causing the protein to refold in a natural process that was monitored using AFS (Fernandez and Li, 2004). In another study, the active transcription rate of RNA polymerase on DNA, which was loosely immobilized on a mica surface, was investigated using AFM (Adelman *et al*., 2002).

1.4 Prions

1.4.1 Structure and function

Prions are small proteinaceous infectious particles devoid of viruses, plasmids and viroids (Prusiner, 1982). Prion diseases are fatal neurodegenerative diseases thought to arise from the post-translational conversion of normal cellular prion protein (PrP^{C}) to an oligomeric β-sheet-rich form known as the scrapie isoform (PrP^{Sc}) (Borchelt *et al*., 1990; Caughey *et al* 1990, 2001; Caughey, 2001; Norstorm and Mastrianni, 2006). The fundamental event in the formation of PrP^{Sc} is the conversion of α-helices in PrP^{C} into β-sheets. PrP^{C} has a high α- helix content (42%) and a low β-sheet content (3%) whereas PrP^{Sc} has a high β-sheet composition (43%) and a reduced α-helical content of 30% (Pan *et al*., 1993). This β-sheet-rich isoform, PrP^{Sc}, often displays intermolecular associations that assemble to form characteristic amyloids in the propagation of prion infectivity (Stöhr *et al*., 2008). The prion protein [approximately 253 amino acid (a.a.) residues in mammals] is post-translationally modified to form the mature PrP^{C} (Aguzzi *et al*., 2008). After the translocation of the bovine prion protein into the endoplasmic reticulum (ER) lumen, the attachment of two N-linked carbohydrate moieties at

Asn^{181} and Asn^{197} are initiated with the cleavage of the N-terminal signal peptide (a.a.1-22) (Heller *et al*., 2003). Then, prior to the addition of a glycosylphosphatidylinositol (GPI) anchor at Ser^{231}, the C-terminal signal peptide (a.a.231-264) is cleaved. Subsequently, a disulphide bond is formed between Cys^{179} and Cys^{214} (Figure 1.11a) (Heller *et al*., 2003; Orsi and Sitia, 2007; Aguzzi *et al*., 2008). Mature PrP^{C} (a.a. 23-230) is a highly conserved ~ 35 kDa protein (Hegde *et al*., 1998).

The first nuclear magnetic resonance (NMR) structure for the globular region of mouse PrP^{C} (a.a.121-231), containing two anti-parallel β strands and three α-helices, was reported in 1996 (Riek *et al*., 1996). Since this first report, many PrP^{C} structures derived from different organisms have been studied and been shown to have similarly folded globular domains (Donne *et al*., 1997; Liu *et al*., 1999; Zahn *et al*., 2000). The prion protein is composed of two domains (Figure 1.11b): a C-terminal region that is structured and globular, and the N-terminus which is an unstructured region from (a.a. 23-121) (Viles *et al*., 1999; Aronoff-spencer *et al*., 2000; Zahn *et al*., 2000; Burns *et al*., 2002). The NMR structure of the globular domain in the bovine prion protein contains three α-helices comprising residues 144-154 (Helix 1), 173-194 (Helix 2), and 200-226 (Helix 3) and two short anti-parallel β-strands comprising residues 128-131 and 161-164. Helices 2 and 3 are connected by a disulphide bond (Garcia *et al*., 2000).

PrP^{Sc} is partially hydrolyzed by proteases to form a protease-resistant core designated as PrP 27-30 (apparent molecular weight of 27-30 kDa), while PrP^{C} is completely degraded under the same conditions (McKinley *et al*., 1983, 1991; Safar *et al*., 1993). Due to the insolubility of PrP^{Sc}, its structure has not been elucidated using conventional X-ray crystallography or NMR spectroscopy. Electron crystallography has been used to study the structure of PrP 27-30 (Wille *et al*., 2002). The two-dimensional crystals of PrP 27-30 were negatively stained with heavy metals and revealed three negatively charged densities near the center of a trimeric region in the unit cell with parallel β-helices (Wille *et al*., 2002, 2007, 2009).

Even though the function of PrP^{C} has not yet been fully established, many possibilities have been suggested (Linden *et al*., 2008). The cellular prion protein is concentrated in the nervous system but is also expressed in most tissues. The N-terminal region of PrP^{C} is involved in the binding of copper, preferentially Cu(II) at the four octarepeat regions (PHGGGWGQ) located between residues 51 and 91 (Viles *et al*., 1999). Free Cu(II) is highly cytotoxic due to the formation of reactive oxygen species (ROS) from redox reactions. Therefore, the binding of

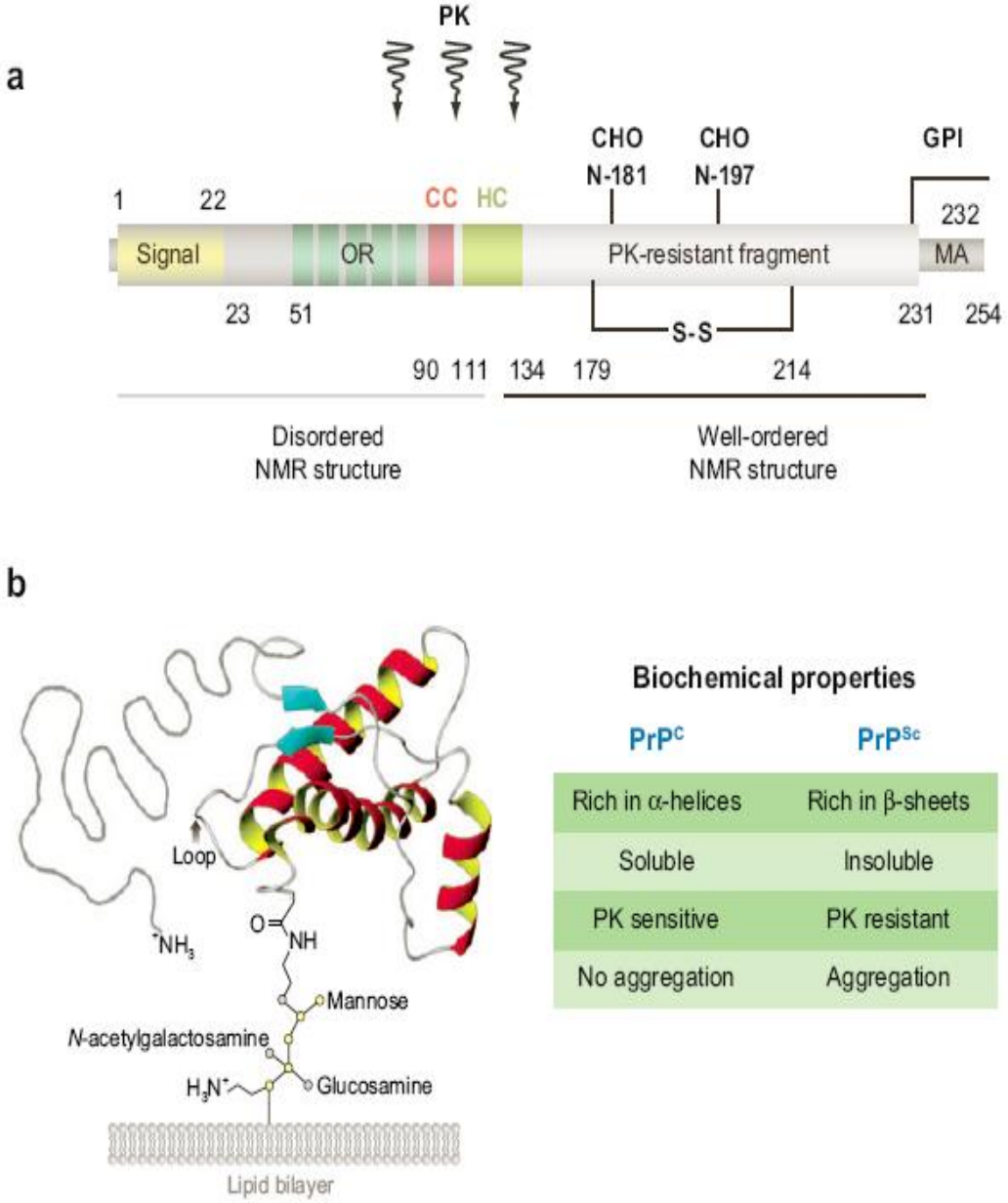

Figure 1.11 The structure and biochemical properties of PrP^{C}. (a) Shows the posttranslational modifications of PrP^{C}. N-terminal signal peptide in yellow; proteinase-K resistant core in grey; cleavage site for the formation of PrP^{Sc} is depicted in arrows; charged cluster (CC) in pink; hydrophobic core (HC) in green; S-S is the disulfide bond; membrane anchor (MA); glycosylphosphatidyl inositol (GPI); glycosylation sites (CHO); nuclear magnetic resonance (NMR). (b) Shows the tertiary structure of PrP^{C}. The biochemical properties of PrP^{C} and PrP^{Sc} are stated at the bottom right. (Reprinted by permission from Aguzzi *et al*., (2008). Copyright 2008 by Annual Reviews).

copper to PrP^C protects the cell from oxidative damage (Berlett and Stadtman, 1997; Miura *et al*., 1999; Viles *et al*., 1999; Burns *et al*., 2002; Aronoff-Spencer *et al*., 2000). Binding of Cu(II) to PrP^C also stimulates endocytosis of PrP^C which can generate an antioxidative defence (Vassallo and Herms, 2003).

The interaction of PrP^C as a specific receptor for laminin was investigated for its role in memory formation. The interaction of PrP^C in the hippocampal (major component of the brain) and laminin play a critical role in memory processing by the activation of protein kinase A (PKA) and extracellular regulated kinase (ERK1) or ERK2 signal pathways (Coitinho *et al*., 2006). Since PrP^C is a membrane protein, its interactions may be useful in signal transduction pathways. PrP (a.a.106-126) activates the tyrosine kinases, Lyn and Syk, which in turn releases intracellular calcium, and activates the protein kinase C and calcium-sensitive tyrosine kinase pathways which finally lead to the activation of mitogen activated protein (MAP) kinases ERK1 and ERK2 (Combs *et al*., 1999; Herms *et al*., 2001). Though PrP-null mice (Nagasaki mice, Rcm0 mice, and Zurich II mice) developed normally, they showed progressive ataxia, and Purkinje cell degeneration at later stages of their life span (Sakaguchi *et al*., 1996; Rossi *et al*., 2001). PrP^C deficient mice do not form PrP^{Sc} for at least 13 months after inoculation of the infective agent (Bueler *et al*., 1993). Due to PrP^C and PrP^{Sc} having the same identical sequence, no specific immune response is generated in prion diseases (Aucouturier *et al*., 2000). The effects of PrP^C on the immune system suggest that PrP^C is down-regulated in the presence of granulocyte maturation and is up-regulated during the maturation of antigen presenting cells (Isaacs *et al*., 2006).

1.4.2 Prion diseases

Prion diseases are infectious diseases of protein conformation that are known as transmissible spongiform encephalopathies (TSE's) (Prusiner, 1998). Prion diseases are mainly characterized by the loss of memory and motor control, dementia, paralysis, and wasting (Weissmann, 1996; Zahn *et al*., 2000). TSE's include Kuru, Creutzfeldt-Jakob disease (CJD), fatal familial insomnia (FFI), and Gerstmann-Sträussler-Scheinker syndrome (GSS) in humans; scrapie in sheep; bovine spongiform encephalopathy (BSE) in cows; chronic wasting disease (CWD) in captive mule deer and elk; transmissible mink encephalopathy (TME); and feline

pongiform encephalopathy (FSE) in domestic and captive cats (Klatzo *et al*., 1959; Hartsough and Burger, 1965; Roos *et al*., 1973; Williams and Young, 1980; Wells *et al*., 1987; Gambetti *et al*., 1995; Ghetti *et al*., 1995; Wood *et al*., 1997; Lezmi *et al*., 2003; Lysek *et al*., 2005).

In humans, Kuru emerged as a prion disease restricted to the Fore linguistic group due to the practice of ritualistic cannibalism in the Eastern Highland Province of Papuao New Guinea (Gajdusek *et al*., 1957). However, the disease has since disappeared due to termination of this ritualistic practice and also due to a novel protective prion protein variant, G127V, that was found to be exclusively present in the Kuru prevalent region (Mead *et al*., 2009). There are many forms of CJD. Sporadic CJD (sCJD) is caused in the absence of an infective agent, genetic linkage or somatic mutation (Masters *et al*., 1978). In a study done on sCJD in 1998, a dominant-negative protective polymorphism at E219K was discovered (Shibuya *et al*., 1998). Another form of CJD, known as familial CJD (fCJD) is due to extra inserts of the octarepeat region that can range from one to nine additional repeats compared to the four repeats usually present in humans (Owen *et al*., 1989). Furthermore, a point mutation, E200K, has also been genetically linked to fCJD in Libyan Jews (Goldfarb *et al*., 1990). In a more troubling perspective, a new form known as variant CJD (vCJD) has been linked to the consumption of BSE-infected meat in Britain, Ireland, Italy, and France (Bruce *et al*., 1997; Spencer *et al*., 2002). Finally, iatrogenic CJD is due to the transmission of the infective agent in contaminated neurosurgical instruments, human growth hormone, human dura mater grafts, corneal grafts, and depth electrodes (Nevin *et al*., 1960; Koch *et al*., 1985; Thadani *et al*., 1988; Uchiyama *et al*., 1994; Brown *et al*., 1992). Genetically-linked Gerstmann-Sträussler-Scheinker syndrome is due to P102L, A117V, F198S or Q217R mutations that occur in humans (Hsiao *et al*., 1989; Prusiner, 1989). FFI has been recorded in more than 30 families around the world and is genetically linked to a combination of D178N mutation occurring with M129 (Goldfarb *et al*., 1992; Gambetti *et al*., 1995).

In sheep, scrapie was the first spongiform encephalopathy reported in 1732 in England. Different breeds of sheep have different susceptibility to scrapie. For example, the Suffolk breeds in the USA are highly susceptible to scrapie (Hunter *et al*., 1993, 1997). Sheep having Q171R, a dominant-negative polymorphism, are protected from scrapie (Hunter *et al*., 1993; Westaway *et al*., 1994). In cattle, the BSE outbreak in Britain in the late 1980's not only caused the mandatory slaughter of thousands of animals but has also been linked to vCJD in the

younger population (Wells *et al*., 1987). Transmission of the infective agent was suspected to have come from the meat and bone meal (MBM) fed to cows contaminated with waste from sheep populations infected with scrapie (Wilesmith *et al*., 1991). Rapid post-mortem screening of animal brains for BSE has improved the safety of the meat industry and also lowered the chance of another epidemic. In cervids, CWD was first discovered in Colorado in the late 1960s. At present, the CWD outbreak has been a growing concern due to the rapid horizontal transmission of this contagious disease (Miller *et al*., 1998; Gross and Miller, 2001). An antimortem diagnostic tool for testing CWD is the biopsy of tonsils which might help control the spreading of the disease (Wild *et al*., 2002; Wolfe *et al*., 2002). In other animals, TME is a rare disease first discovered in ranched mink in Wisconsin. Only adult minks are affected by TME and have a minimum incubation period of seven months (Marsh, 1976). The first case of FSE which affected a captive cheetah born in France was reported in 2003 (Lezmi *et al*., 2003). Another report on the maternal transmission of FSE has also been published (Bencsik *et al*., 2009).

1.4.3 Prion strains

One of the most difficult concepts to understand in the prion field is the existence of different prion strains. The simplest approach to the concept of prion strains is that prion strains arise due to the different conformations of PrP^{Sc}. These can self-replicate using template-assisted conversion or a seeded nucleation pathway (Prusiner *et al*., 1990; Jarrett and Lansbury, 1993; Cohen and Prusiner, 1998; Bartz *et al*., 2000; Peretz *et al*., 2001a; Meier *et al*., 2003). The first documented evidence for the existence of prion strains was in goats and was published in 1961 (Pattison and Millson, 1961). The report accounts for two distinct clinical phenotypes called "scratching" and "nervous", which were observed in goats infected by the same scrapie agent. The different genetic background of the goats may have played a role in the development of these new strains (Morales *et al*., 2007a). Two strains of TME were serially passaged to hamsters. The HYPER (HY) strain of the TME agent produces hyperexcitability and cerebellar ataxia in hamsters, while the DROWSY (DY) strain shows progressive lethargy. The PrP^{Sc} isolated from hamsters from these two distinct biologic strains of the TME agent had different biochemical and physical properties (Bessen and Marsh, 1992). As stated by Aguzzi and Calella, "prion strains" can be interpreted as "infective agents having the ability to exhibit

distinct prion-disease phenotypes when transmitted to identical hosts" (Aguzzi and Calella, 2009).

Prion strains can be classified due to their distinct *in vivo* alterations and different biochemical characteristics. The main *in vivo* markers are incubation time, neuropathology of the brain and clinical symptoms (Figure 1.12) (Collinge and Clark, 2007). The incubation period is calculated as the time interval between inoculation of the infectious agent and the onset of clinical symptoms (Bruce *et al*., 2002). Intra-species transmission of the infective agent is remarkably repeatable. This was evident in a serial mouse passage study where the same mouse strain recorded an incubation time with a standard error of less than 2% of the mean incubation period (Bruce, 1993). Infection by interspecies transmission is slow and causes prolonged incubation periods which are different for each strain. The inability to transmit the infective agent between different mammalian species as compared to intra-species transmission is known as the "species barrier" (Peretz *et al*., 2001a; Moore *et al*., 2005). The incubation time for the first transmission of infectious prions from humans with CJD to mice was between 300 to 800 days. The second passage of these infective agents from mice to mice only takes ~120 days while the same incubation time was observed for the third passage from mice to mice (Tateishi *et al*., 1996). The species barrier is very effective for rabbits which have not yet been infected by various prions (Morales *et al*., 2007a). Transgenic mouse models were used to verify the species barrier which proves that differences in the primary structure of PrP between the donor-PrP^{Sc} and the recipient-PrP^{C} help stabilize the transmission barrier (Prusiner *et al*., 1990; Collinge *et al*., 1991; Palmer *et al*., 1991). For example, transgenic mice expressing Syrian hamster prions were highly susceptible to the disease when inoculated with the infective agent from hamsters (Bruce *et al*., 1994; Prusiner *et al*., 1990). However, the prion strain responsible for the efficient transmission of BSE to humans causing vCJD does not follow the species barrier rule (Bruce *et al*., 1994, 1997). Perhaps the type of prion strain also affects the ease of transmission from one species to another (Collinge and Clark, 2007). The biochemical characteristics of strains show different banding pattern in Western blots following proteolysis (Figure 1.12B) (Collinge and Clark, 2007; Telling *et al*., 1996; Collinge *et al*., 1996; Collinge and Rosser, 1996). Multiple strains generated from scrapie infected prions (Figure 1.12A) when serially passaged to mice showed that a single strain may retain its original biochemical and neuropathological characteristics, even after passaging through different

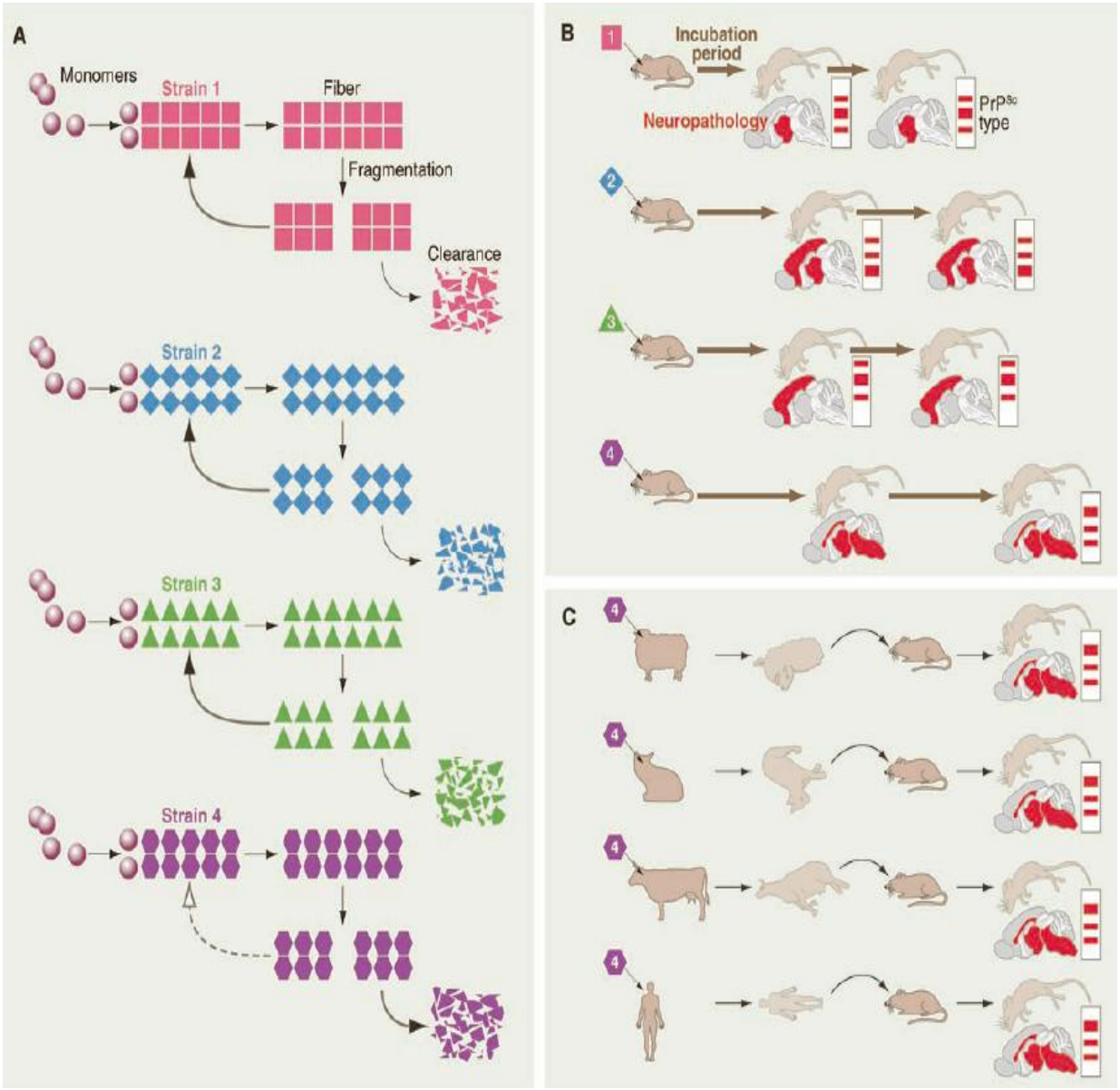

Figure 1.12 Diagram explaining prion strains. Image (A) shows the propagation of prion strains by the template assisted conversion which requires the recruitment of PrP^{C} monomers to the different PrP^{Sc} strains to generate more of the specific strain. Image (B) shows that strains can be characterized due to their different neuropathology, incubation period and Western blots. Image (C) shows a single strain may retain its characteristics, even after serial passage and re-isolation in the original host (Reprinted by permission from Collinge and Clark, 2007. Copyright 2007 AAAS).

species and finally re-isolating it from the original mice (Figure 1.12C) (Fraser *et al*., 1973; Bruce *et al*., 1994; Collinge and Clark, 2007).

1.4.4 Interaction of metal ions with prion protein

The unstructured N-terminal region of PrP^C contains four repeats of an eight-residue sequence PHGGGWGQ known as the octapeptide repeat region (Figure 1.13) which is highly conserved among species (Wopfner *et al*., 1999; Millhauser, 2007). Interestingly, Cu(II) binds to the octapeptide repeat region and this binding is one of the main functions of PrP^C in Cu(II) homoestasis. Though copper is an essential trace metal, it can also be toxic in excess quantity (Hornshaw *et al*., 1995a, b; Brown *et al*., 1997; Stöckel *et al*., 1998; Viles *et al*., 1999; Whittal *et al*., 2000; Millhauser, 2007). The binding of Cu(II) assists in the endocytosis of PrP^C (Pauly and Harris, 1998). Wild-type nerve cells in culture have shown resistance to oxidative stress and ROS generated by Cu(II) as compared to cells lacking PrP^C, indicating the requirement for the octarepeat region (Brown *et al*., 1998a). PrP knockout mice are susceptible to tissue damage through lipid oxidation as compared to wild-type mice (Klamt *et al*., 2001). It has been shown that the binding of Cu(II) to PrP^C causes structural changes and may cause different misfolding patterns (Viles *et al* ., 1999).

A crystal structure of Cu(II) bound to the HGGGW peptide revealed that Cu(II) co-ordinates with three nitrogen atoms (one from histidine) and one oxygen atom as an equatorial ligand in addition to an axial water molecule to form a square-pyramidal complex (Burns *et al*., 2002). At physiological pH, the affinity for binding Cu(II) (K_d) in the square-pyramidal complex is ~ 1-9 µM (Garnett and Viles, 2003; Walter *et al*., 2006; Wells *et al*., 2006). Cu(II) binds the octapeptide repeat region at Histidine (His) 60, His 68, His 76, and His 84 (Viles *et al*., 1999; Jones *et al*., 2005; Klewpatinond *et al*., 2008). Additional binding sites for copper outside the octarepeat region have been identified at His 95 and His 110 (Klewpatinond and Viles, 2007a, b). It has also been shown that the binding of Cu(II) to the full length recombinant prion protein first occurs between the octapeptide repeat region and at His 95 or 110 with subsequent loading to the octapeptide repeat region (Klewpatinond *et al*., 2008). Many articles have been published on the affinity of Cu(II) to PrP^C (Jackson *et al*., 2001; Kramer *et al*., 2001; Thompsett *et al*., 2005; Walter *et al*., 2006; Wells *et al*., 2006). The binding affinity of Cu(II) to the full length prion has an approximate K_d value of ~10 nM

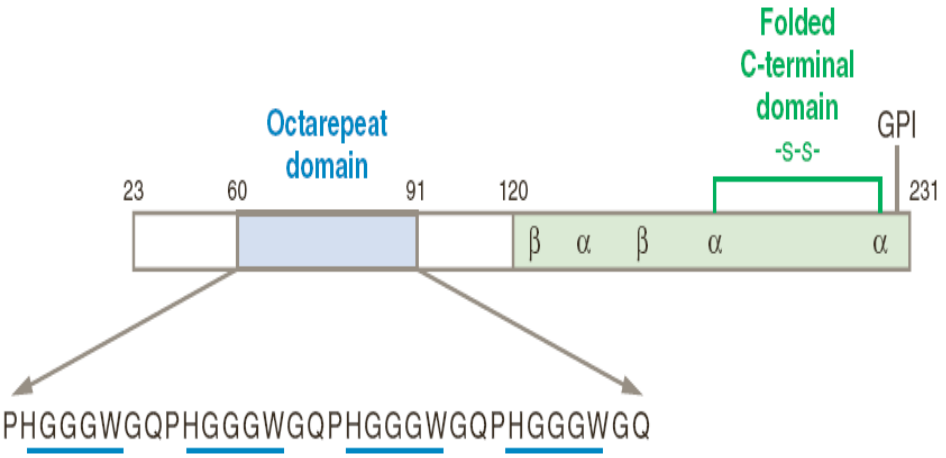

Figure 1.13 The octapeptide repeat region in PrP^{C}. The octapeptide repeat domain (blue) comprises four, eight-residue long PHGGGWGQ sequences. (Reprinted by permission from Millhauser, 2007. Copyright 2007 Annual Reviews).

(Viles *et al*., 2008). *In vitro* studies on the affinity of copper to denatured PrP^{Sc} showed an increase in protease resistivity and infectivity (Pauly and Harris, 1998; Quaglio *et al*., 2001; Sigurdsson *et al*., 2003; Kuczius *et al*., 2004; Singh *et al*., 2010). The recombinant full length cellular prion protein binds several metal ions other thancopper. The binding of Zn(II), Mn(II), Fe(II) and Ni(II) has been confirmed in many prion-metal interaction studies (Pan *et al*., 1992; Hornshaw *et al*., 1995a, b; Brown *et al*., 2000; Jackson *et al*., 2001; Jones *et al*., 2004, 2005; Basu *et al*., 2007). Zn(II) has also been associated with the induction of prion endocytosis and PrP^{C} binding (Pauly and Harris, 1998; Perera and Hooper, 2001; Qin *et al*., 2002). Zn(II) binds the octapeptide repeat region with a dissociation constant of approximately ~ 200 µM, which is much lower than that of copper binding (Walter *et al*., 2007). The interaction of Fe(II) with PrP^{C} depends mostly on the conformation of PrP^{C} and not a specific amino acid sequence (Singh *et al*., 2010). It has been suggested that PrP^{C} may act as an iron transporter from the endosomes to the cytosol (Miura *et al*., 2005). Furthermore, using a confocal single-molecule detection system, the binding of Mn(II) caused a pro-aggregatory effect at low micromolar concentrations (Giese *et al*., 2004). Another study which used vibrational raman spectroscopy and ultraviolet circular dichroism showed that Mn(II) reinforced the α-helix content to ~ 30% as compared to the opposing effect of Cu(II) (Zhu *et al*., 2008).

1.4.5 Therapeutics and treatment for prion diseases

Cell culture models have been used for the study of various therapeutic agents designed to reduce the propagation of PrP^{Sc}. Polyanionic glycans such as pentosan polysulphate (PPS) and dextran sulphate (DS) have been reported to decrease PrP^{Sc} levels in scrapie infected cells (Caughey and Raymond, 1993; Caughey *et al*., 1994; Barret *et al*., 2003). Heteropolyanionic-23 (HPA-23) is an antiviral compound that delays the onset of the formation of scrapie in mice and hamsters following inoculation of the infective agent. HPA-23 is strain dependent and has less effect if administered after post-infection (Kimberlin and Walker, 1983, 1986). Heparin sulfate also reduced the accumulation of PrP^{Sc} in scrapie infected cell cultures (Caughhey and Raymond., 1993; Gabizon *et al*., 1993). In an opposing effect, both heparin sulphate and PPS stimulate the cell-free conversion of PrP^{Sc} (Wong *et al*., 2001). Congo Red (CR) dye is mainly used in the staining of histopathological samples. The administration of CR to hamsters during intracerebral and intraperitoneal inoculation delayed the onset of scrapie, but did not have an

effect if administered after intracerebral inoculation (Ingrosso *et al*., 1995; Poli *et al*., 2004). Suramin (polysulphonated naphthyl urea) reduced the level of PrP^{Sc} in scrapie-infected neuroblasma (cancer) cells (ScN2a) and also prolonged the incubation time for the disease in hamsters when administered during intraperitoneal (injection of a substance into the body cavity) inoculation (Ladogana *et al*., 1992; Nunziante *et al*., 2005). Polycationic compounds such as dentritic polyamines (polypropyleneimine, polyethyleneimine and polyamidoamide), phosphorous-containing dentrimers, and lipopolyamines, all reduced pre-existing PrP^{Sc} in ScN2a cells (Supattapone *et al*., 1999, 2001; Winklhofer and Tatzelt, 2000; Solassol *et al*., 2004). Many other compounds such as amphotericin B, porphyrins, acridine and phenothiazine have also been tested for the reduction of PrP^{Sc} (Caughey *et al*., 1998; Mange *et al*., 2000; Korth *et al*., 2001). While amphotericin B delayed the onset of disease in hamsters, porphyrins, acridine, and phenothiazine reduced the level of PrP^{Sc} in ScN2a cell cultures (Pocchiari *et al*., 1987, 1989; Adjou *et al*., 1995, 1999, 2000).

In the development of therapeutic agents for prion disease, one of the main obstacles that has to be overcome is that the drugs have to cross the blood-brain barrier (BBB). The administration of quinacrine, an antimalarial drug, to CJD patients with an initial dose of 1000 mg, followed by a 300 mg daily dosage thereafter, showed hepatic toxicity (Prusiner *et al*., 2004). The development of anti-PrP antibodies for PrP^{C} has also been useful in reducing the propagation of PrP^{Sc} in cell cultures by a mechanism whereby PrP^{C} specific antibodies bind PrP^{C} and hence reduce the pool of available PrP^{C} needed for scrapie transformation (Enari *et al*., 2001; Peretz *et al*., 2001b; Gilch *et al*., 2003). Peripherally infected scrapie mice that were passively immunized with anti-PrP antibodies showed a significant reduction in PrP^{Sc} levels in spleen samples (Heppner *et al*., 2001; White *et al*., 2003). In summary, many other therapeutic agents have been discovered in cellular *in vitro* studies which are too extensive to mention at this point. For example, RNA aptamers (short strands of oligonucleotides), RNA interference strands, Statins (drugs used to reduce cholesterol levels), copper, dominant-negative inhibitors coupled with protein-X (a putative cofactor for prion conversion) mimetics, curcumin (major component in turmeric), dimethyl sulphoxide, and passive immunization with monoclonal antibodies have been investigated (Trevitt and Collinge, 2006).

1.5 Diagnostic methods for prion diseases

1.5.1 Bioassays using PrP conformation

The BSE crisis in Britain and its link to vCJD has raised the extremely important question; can we detect PrP^{Sc} in human blood samples? At present, there is no pre-mortem testing for human or animal prion diseases. The only positive diagnosis is post-mortem brain histology testing. Clinical symptoms are the main factors that assist in early diagnosis of human prion disease. Rodent models have been used to test the level PrP^{Sc} in blood. Blood samples collected from rodents infected with scrapie prions revealed a 1 pg/ml [~100 infectious units (IU) in 1 ml or ~ $3x10^{-14}$ M] detection limit in the blood buffy coat at the onset of symptomatic disease (Brown, 2001; Brown *et al*., 2001). During incubation, the detection limit is estimated at a 10 fold lower value of 10 IU or 0.1 pg/ml (~ 3×10^{-15} M). The number of molecules in plasma and red blood cells are estimated to be 5-10 folds lower than that present in the buffy coat (Brown *et al*., 1998b). Human and cattle blood samples would contain much lower numbers of PrP^{Sc} molecules. At present, there is no direct test for this level of sensitivity, but an amplification step, for example the protein misfolding cyclic amplification (PMCA) assay can be used to increase the detection limit in blood (Soto, 2004). PrP^{C} has been detected in blood plasma, milk, and urine (Narang *et al*., 2005; Franscini *et al*., 2006; Thackray *et al*., 2006). PrP^{Sc} has also been reported in the urine of hamsters, cattle and humans but the elevated levels of PrP^{C} (0.3 - 4.7 ng/ml) in naturally infected sheep urine samples cannot be explained (Shaked *et al*., 2001; Andrievskaiai *et al*., 2008). Further investigations to establish if the increase of urinary PrP^{C} is accompanied by scrapie infectivity in urine, needs to be explored (Andrievskaiai *et al*., 2008).

The PrP^{Sc} conformational-dependent immunoassay (Inpro, CDI by Beckman Coulter) is an excellent method used to differentiate PrP^{C} and denatured PrP^{Sc}. These antibodies do not bind to native PrP^{Sc} (Figure 1.14) (Safar *et al*., 1998, 2002). The antibody binds only a conformationally-dependent epitope that is always accessible in PrP^{C} but only becomes exposed in PrP^{Sc} after denaturation. For this purpose, all samples are divided into two aliquots (Bellon *et al*., 2003). One aliquot is denatured using 4 M (final concentration) Gdn-HCl and heating at 83ºC for 6 minutes, while the other aliquot is left untreated. The assay includes a sandwich immunoassay coupled with fluorescence labeled antibody fragments to detect prions (Bellon *et al*., 2003). For the sandwich enzyme-linked immunosorbent assay (ELISA), microtitre plates

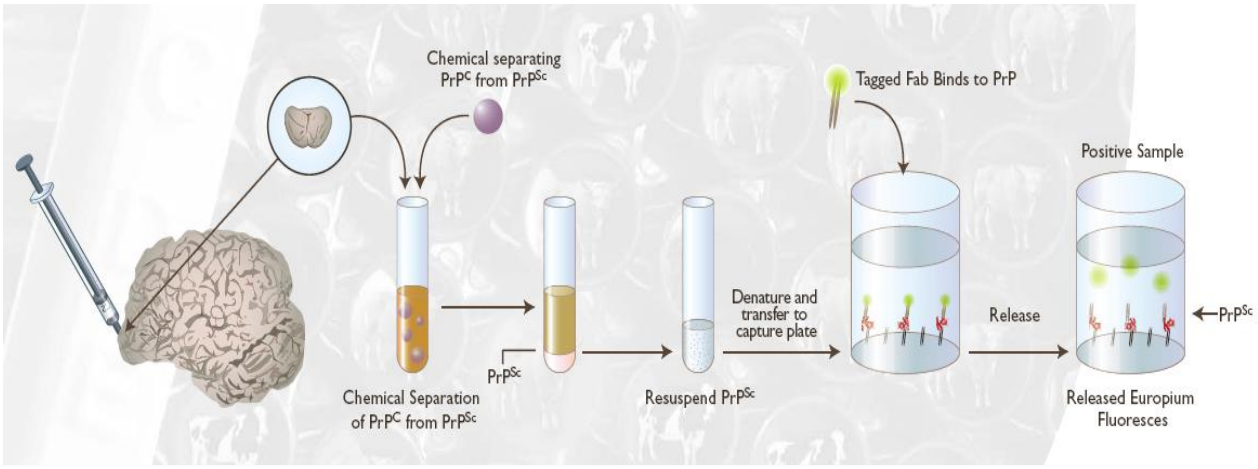

Figure 1.14 InPro conformational-dependent immunoassay (CDI). First the sample is processed to chemically separate PrP^{C} from PrP^{Sc}. Denatured PrP^{Sc} is then transferred to capture plates that utilize a fluorescent tagged Fab residue which is released for positive samples. (Reprinted with permission from InPro CDI Robust BSE testing Kit-BR-9918A; product licensed under patents from Inpro Biotechnology Inc, South San Francisco, California. Founded by Stanley B. Prusiner. Copyright 2005 Beckman Coulter, Inc).

are coated with 10 µg monoclonal antibodies (mAbs) followed by the loading of denatured and native samples. Following incubation, a labeled detection antibody fragment is added. The presence of the disulphide bond enhances the detection of mAb binding, in contrast to the reduced sample which is treated with 3.3 mM dithiothreitol (DTT) for 6 minutes (Bellon *et al*., 2003). These experiments suggest that mAb binding depends on the correctly formed disulphide bridge between Cys 179 and Cys 214. The detection limit for CDI is 0.5 - 5.0 pmol and is a highly sensitive test independent of the proteinase K digestion step.

With respect to protein conformation, the production of conformational antibodies that can specifically bind PrP^{Sc} but not PrP^{C} is a very key advance. In a study done by Korth and co-workers, an IgM monoclonal antibody named 15B3, that immunoprecipitated bovine, murine, and human PrP^{Sc} but not PrP^{C} was produced in 1997 (Korth *et al*., 1997). However further studies using this antibody have not been published as of yet. In another study, immunoprecipitation, plate-capture immunoassay, and flow cytometry assays showed that an antibody raised against the epitope, tyrosine-tyrosine-arginine, bound PrP^{Sc} and not PrP^{C} (Paramithiotis *et al*., 2003). Furthermore, these antibodies not only recognize protease resisitant PrP but also misfolded protease sensitive prion protein (Paramithiotis *et al*., 2003). The YYR motif is blocked in PrP^{C} but is available in PrP^{Sc}. Another PrP^{Sc} specific antibody called V5B2 bound PrP^{Sc} (and not PrP^{C}) to brain samples of CJD patients (Curin Serbec *et al*., 2004). RNA aptamers have also been used to specifically interact with the N-terminus of recombinant PrP^{C} and native PrP^{C} but not with native PrP 27-30. This study suggests that PrP^{SC} specific RNA aptamers may be able to screen infective samples in the future (Weiss *et al*., 1997).

1.5.2 Bioassays using PK-resistant PrP

Current diagnostics for prion diseases mainly use the proteinase K digestion method to validate the presence of PrP^{Sc} (McKinley *et al*., 1983; Meyer *et al*., 1986). This conventional method produces PrP 27-30, a ~142 amino acid residue fragment from PrP^{Sc}, in the presence of proteinase K, where ~ 67 amino acids from the N-terminus are completely digested (McKinley *et al*., 1991). Commercially available assay kits from *Prionics-Check Western test*, CEA/*BioRad test*, *Enfer test*, and *Prionics-Check LIA test* are being routinely used in government laboratories, university laboratories, and other research facilities for post-mortem

detection of PrP^{Sc} (Soto, 2004). The method used by *prionics-check western test* is as follows: A sample containing the obex region of the brain is first homogenized followed by the addition of proteinase K (Soto, 2004). The samples are then loaded on to a SDS-polyacrylamide gel for electrophoresis. Next, Western blot analysis is carried out using monoclonal antibody 6H4. The antibody binds epitope DYEDRYYRE which contains the Helix-1 region of the bovine prion protein. The detection limit of the test is in 5.0 - 20 pmol (Schaller *et al*., 1999; Oesch *et al*., 2000; Soto, 2004). The CEA/*BioRad test* consists of two distinct phases, a concentration phase followed by a sandwich immunoassay (Soto, 2004). In the first phase brain samples are homogenized and treated with proteinase K. The PrP^{Sc} is then concentrated using centrifugation, followed by the addition of a denaturant to dissolve the PrP^{Sc} pellet. In the, second phase the denatured sample is added to micro plates containing an immobilized monoclonal antibody (capture antibody) which binds PrP^{Sc}. The plates are then washed and a second monoclonal antibody coupled to an enzyme (antibody-peroxidase), which binds another site of PrP^{Sc}, is added. The binding of the second antibody is proportional to the immobilized sample which is detected by enzyme activity (Moynagh and Schimmel 1999; Grassi *et al*., 2001; Bennion and Daggett, 2002). The detection limit in this test is 0.5-2.0 pmol (Soto, 2004). The Prionics-*Check LIA test* developed by Biffiger and co-workers used two different monoclonal antibodies for the capture and detection of PrP 27-30 (Biffiger *et al*., 2002). In this method, brain samples are first homogenized followed by proteinase K digestion. These samples are then pre-treated with assay buffer and incubated for 60 minutes with detection antibodies that are conjugated with horseradish peroxidase. These pre-treated samples are then loaded onto micro plates precoated with a capture antibody (6H4) (Biffiger *et al*., 2002). A chemiluminescence substrate for peroxidase is then added and the emitted light is measured using a luminometer (Biffigner *et al*., 2002). The detection limit of this assay is between 1.0-5.0 pmol (Soto, 2004). The diagnostic *Enfer test* uses a rapid sample extraction procedure coupled to a chemiluminescence's ELISA method (Soto, 2004). The procedure includes homogenization, extraction, and proteinase K digestion of brain samples followed by simple ELISA detection. The detection limit for this test is 1.0-10 pmol (Moynagh and Schimmel, 1999; Bennion and Daggett, 2002; Soto, 2004). Methods such as cell blot and slot blot have also been developed for the detection of PrP^{Sc} (Bosque and Prusiner, 2000). In the cell blot method, cells infected with prions are plated on cover slips which are placed on a 24-well plate.

After 4 days of incubation in culture medium, the cover plates are removed (Bosque and Prusiner, 2000). The slot blot method utilizes BSE infected brain tissue or cell lysates that are filtered using a commercially available slot blot device that include a nitrocellulose or cellulose acetate membrane, followed by proteinase K detection (Winklhofer *et al*., 2001). Other methods that use the proteinase K digestion step include immunohistochemistry, cell culture assays, and protein misfolding cyclic amplification (PMCA) based methods (McBride *et al*., 1988; Klohn *et al*., 2003; Castilla *et al*., 2005).

PMCA is a technique for accelerated prion replication. It is based on the observations that the transmissible agent for prion diseases is PrP^{Sc} (Saborio *et al*., 2001). The PMCA method is a two step process (Figure 1.15) (Soto *et al*., 2002; Castilla *et al*., 2005; Morales *et al*., 2007b). First, samples containing extremely small amounts of PrP^{Sc} are incubated with excess amounts of PrP^{C} which then converts $PrP^{C} \rightarrow PrP^{Sc}$. In the second step, sonication is used to disrupt the aggregates that act as seeds for further conversion and amplification of PrP^{C} to the infective conformation (Figure 1.15A). This is achieved by repetitive cycles of serial dilution of the newly synthesized PrP^{Sc} with fresh brain homogenate samples (Figure 1.15B). The final product is subjected to proteinase K digestion followed by gel electrophoresis (Soto *et al*., 2002; Castilla *et al*., 2005; Morales *et al*., 2007b). PMCA is a very useful tool for prion diagnostic assays. A detection limit of 6-12 pg ($0.2 - 0.4 \times 10^{-15}$ mol) of PrP^{Sc} after a 10000 fold dilution and 10 cycles has been successfully described (Telling, 2001).

1.5.3 Bioassays using aggregation of PrP

A method to detect PrP^{Sc} aggregates in cerebrospinal fluid (CSF) was first reported by Kretzschmar and co-workers (Bieschke *et al*., 2000). Prion protein aggregates in CSF samples from patients with suspected CJD were labeled with specific antibody probes that were tagged with a fluorescent dye. The intensity of these signals was measured using a confocal-dual color fluorescence spectrometer that produced a detection limit of 2 pM concentrations for aggregated PrP^{Sc} (Bieschke *et al*., 2000). In another study, a novel enzyme-linked immunosorbent assay that reacts specifically with dimers or aggregates of PrP was reported by, Sy and coworkers (Pan *et al*., 2005). Most of the current *in vitro* diagnostic methods use proteinase K resistivity or treatment with Gdn-HCl that denatures the protein which in turn assists the binding of mAbs to hidden epitopes. On the other hand, the mAb, 11G5, reacted

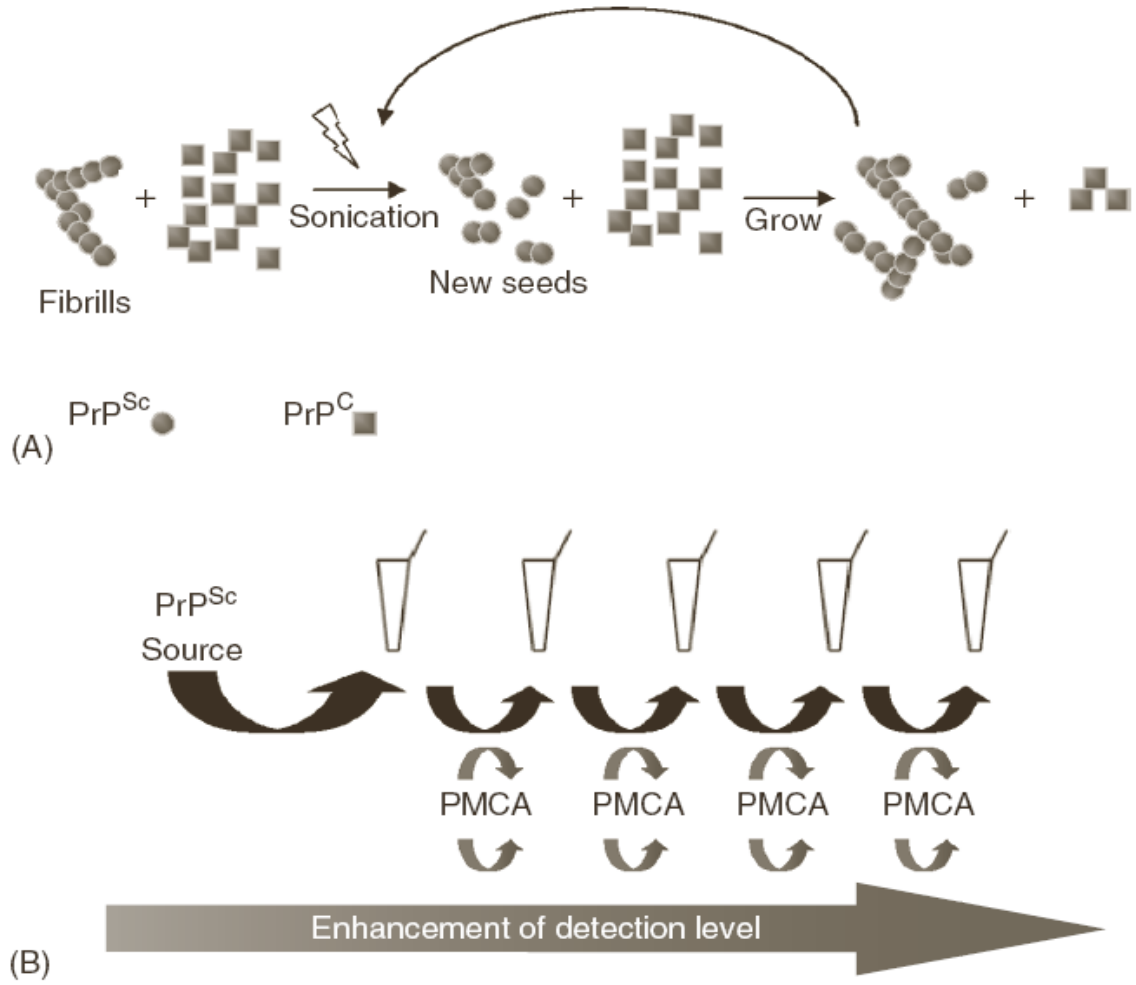

Figure 1.15 Protein misfolding cyclic amplification (PMCA). Image (A) shows incubation of large amounts of PrP^{C} with small amounts of PrP^{Sc} followed by sonication which forms new seeds that are then incubated at 37 ºC for the conversion of $PrP^{C} \rightarrow PrP^{Sc}$. Image (B) shows newly synthesized PrP^{Sc} is diluted in new aliquots of normal brain homogenates (Reprinted with permission from Morales *et al.*, 2007b (Microbial food contamination, second edition). Copyright 2010 Taylor and Francis Group, LLC).

with both dimers and PrP^{Sc} aggregates. The epitope region covered by 11G5 is a.a.114-130 which includes the β-strand (a.a.128-131). This aggregated ELISA method had a detection limit of 0.006 μg to 0.06 μg of PrP. Furthermore, these authors speculate that dimers andaggregates of PrP may share similarities in this conformational region that leads to the conversion of $PrP^{C} \rightarrow PrP^{Sc}$ (Pan *et al*., 2005).

At present there are many methods and protocols available for *in vitro* conversion of the recombinant prion protein to amyloid fibrils (Apetri *et al*., 2005; Breydo *et al*., 2005; Ryou and Mays, 2008). Most conversion methods require a source of PrP^{Sc}, which is incubated with PrP^{C} for the scrapie conversion (Raeber *et al*., 1992; Kocisko *et al.*, 1994; Lucassen *et al*., 2003; Deleault *et al.*, 2005; Atarashi *et al*., 2007, 2008). In contrast, a novel *in vitro* cell- free method that does not require a source of PrP^{Sc} for the formation of amyloid fibrils was developed by Baskakov and co-workers (Baskakov *et al*., 2002). The recombinant Syrian hamster prion protein (a.a. 90-231) was refolded into a β-oligomeric isoform at pH 3.7 in the absence of PrP^{Sc} with 5 M urea and was monitored by circular dichroism (Baskakov *et al*., 2002). These β-oligomers can then be converted into amyloid fibrils using constant shaking at 37 ºC under acidic conditions (Baskakov *et al*., 2002; Baskakov *et al*., 2004; Bocharova *et al*., 2005). Fibrils formation was monitored by staining the samples with congo red (CR) dye or the fluorescent dye thioflavin T (ThT) (Baskakov *et al*., 2002). ThT fluoresces only when bound to fibrils and does not interfere with fibril formation (Bourhim *et al*., 2007). Recently, Prusiner's laboratory developed an *in vitro* protease-sensitive synthetic prion that was formed using an unseeded polymerization method (Colby *et al*., 2010). For this purpose, the production of amyloid fibrils at 37ºC in 3 M urea and pH 5.0 using recombinant mouse PrP (a.a. 89-230) was monitored using a ThT binding assay (Baskakov *et al*., 2002; Legname *et al*., 2004; Colby *et al*., 2010). These recombinant PrP amyloids transmitted prion disease to transgenic mice that overexpressed the N-terminally truncated prion protein. These amyloid fibers proved to be highly infectious but remained protease sensitive (Colby *et al*., 2010). Furthermore, prions isolated from these sick animals transmitted the disease to healthy animals (Colby *et al*., 2010).

1.6 Thesis objectives

Single-molecule nanopore analysis is an attractive analytical method which can be developed to identify specific conformational changes that occur in proteins and peptides.

Prion diseases are thought to arise from the misfolding and aggregation of the normal cellular prion protein, PrP^{C} to an oligomeric β-sheet rich form known as the scrapie isoform, PrP^{Sc} (Prusiner, 1982). The research performed in this thesis presents the initial foundation and proof of principle for the development of an electrophoretic prion detector.

The preliminary work includes nanopore analysis of peptides protected with an acetyl or an Fmoc group and peptides having different secondary structures such as α-helical and β-sheet hairpin conformations. These experiments were designed to study the interactions between peptides and pores and to gain a more detailed view of the effects of peptide conformation on translocation or intercalation.

The next sets of experiments were designed in an effort to try and develop an electrophoretic prion detector using αHL pores. First, peptides with different secondary structures within the recombinant bovine prion protein were analyzed. The goal of this set of experiments was to investigate if small peptides from α-helical and β-sheet segments in the bPrP would give specific blockade current (I) and blockade time (T) signatures with nanopores. The next objective of this project was to determine if the full length recombinant bovine prion protein, bPrP (a.a. 25-242) interacts with the αHL pore. For this purpose, different voltages were also used with different orientations with respect to the location of the negative potential at the *cis* or *trans* side of the lipid bilayer.

Another objective of this project was to demonstrate that the conformation of the prion protein can be modulated by binding divalent metal ions. The N-terminal region of PrP^{C} is involved in the binding of copper, at the four octapeptide repeat regions (PHGGGWGQ) located between residues 51 and 91 (Viles *et al*., 1999). Furthermore, PrP^{C} also binds several other metal ions other than copper (Quaglio *et al*., 2001; Todorova-Balvay *et al*., 2001; Burns *et al*., 2003; Morante *et al*., 2004; Leach *et al*., 2006). Based on these findings, nanopore analysis of bPrP(25-242) in the presence of Cu(II), Zn(II), Ni(II), and Mn(II) was carried out.

The addition of anti-PrP antibodies to prion proteins and peptides while recording the difference in the number of events is a positive approach towards a diagnostic test for BSE. The next sets of experiments were designed to identify distinct conformational changes that occurred due to complex formation between antibodies and prion peptides and proteins.

Recently it has also been demonstrated that proteins can translocate the αHL pore, especially in the presence of denaturing agents which aid in protein unfolding (Oukhaled *et al*.,

2007; Stefureac *et al*., 2008). The next objective was to identify conformational changes that occurred in bPrP in the presence of Gdn-HCl. The conformational changes that occur due to complex formation was further investigated by the addition of antibodies to the unfolded bPrP(25-242). Based on these objectives, a non-prion peptide was also analyzed.

The N-terminus signal prion peptides have potent antiprion effects. Peptide PrP (a.a. 1-30) significantly reduced PrP^{Sc} levels in prion infected mouse neuronal hypothalamic cells but had no effect on PrP^{C} levels in noninfected cells (Löfgren *et al*., 2008). Based on these findings, the next objective of this project was to determine if the conformation of the prion protein can be modulated using signal prion peptides. For this purpose, we used the N- and C-terminal signal prion peptides.

The fundamental event in the formation of PrP^{Sc} is the conversion of α-helices in PrP^{C} into β-sheets (Pan *et al*., 1993). The final goal of this project was to demonstrate if fibril formation of the full length bPrP was possible at low concentrations of Gdn-HCl so as to monitor the folding intermediates using αHL nanopores.

2.0 MATERIALS AND METHODS

2.1 Chemical and biological reagents, supplies, and equipment

A list containing all the chemical and biological reagents, equipment, and supplies are presented in Table 2.1. The names and addresses of the pharmaceutical companies are listed in Table 2.2.

2.2 Nanopore detection of peptides

2.2.1 Acetylated and Fmoc protected peptides

Acetylated peptides, Ac-$D_2A_{14}K_2$ and Ac-$D_2A_7PA_6K_2$ and Fmoc-protected peptides, Fmoc-$D_2A_{14}K_2$ and Fmoc-$D_2A_7PA_6K_2$ were analyzed. The Fmoc-protected peptides were greater than 90% pure, while peptide Ac-$D_2A_7PA_6K_2$ was 96% pure. Stock solutions of 10 mg/mL for the acetylated peptides and 5 mg/mL for the Fmoc-protected peptides were prepared in 10 mM potassium phosphate (KH_2PO_4/K_2HPO_4) buffer with 1.0 M KCl at pH 7.8. The electrolyte solution for nanopore experiments was also 1.0 M KCl in 10 mM potassium phosphate buffer at pH 7.8. Once a stable α-hemolysin pore insertion was detected (fewer than 3 pores), 20-30 µL of the acetylated peptides or 10 µL of the Fmoc-protected peptides were added to the 1.5 mL *cis* chamber proximal to the aperture. The experiments were carried out using an Axopatch 200B amplifier connected to a CV203BU head-stage at 22 ± 1ºC with an applied potential of -100 mV at the *cis* side and at a bandwidth of 10 KHz. The blockade current populations were obtained by fitting the blockade current distribution with the Gaussian function. The lifetime data were obtained by fitting each blockade duration distribution with a single exponential function.

2.2.2 The capped and uncapped β-sheet hairpin peptides

The capped (Ac-SESYINPDGTWTVTE-NH_2) and uncapped (SESYINPDGTWTVTE) β-sheet hairpin peptides with purities of 72% and 79%, respectively, were analyzed. Mass spectrometry was performed on all peptides to confirm molecular weight. Stock solutions of 10 mg/mL were prepared in 10 mM potassium phosphate buffer with 1.0 M KCl at pH 7.8 for nanopore analysis. Nanopore experiments were carried out as stated in section 2.2.1 using 2 µL of stock peptide solutions.

Table 2.1 Chemical and biological reagents, equipment, and supplies

Item	Supplier
Chemical and biological reagents	
1,2-diphytanoyl-sn-glycero-3-phosphocholine in $CHCl_3$	Avanti Polar Lipids
Ac-$D_2A_{14}K_2$ peptide	Sigma-Genosys
Ac-$D_2A_7PA_6K_2$ pepide	Sigma-Genosys
Argon (gaseous)	Praxair
2-[*N*-cyclohexylamino]ethanesulfonic acid (CHES)	Sigma-Aldrich
$CuSO_4.5H_2O$	Sigma-Aldrich
Decane (anhydrous)	Sigma-Aldrich
Ethylenediaminetetraacetic acid (EDTA)	BDH
Fmoc-$D_2A_{14}K_2$ peptide	Chi Scientific
Fmoc-$D_2A_7PA_6K_2$ peptide	Chi Scientific
Fmoc-α helical hairpin peptide (FNMQCQRRFYEALHDPNLNEEQRNAKIKSIRDDC) with a disulfide link at Cys 5 & 34	Chi Scientific
Guanidine Hydrochloride (Gdn-HCl)	EM SCIENCE
Hydrochloric acid (HCl)	BDH
Manganese Chloride ($MnCl_2.4H_20$)	Fisher Scientific
Nickel Chloride ($NiCl_2.6H_20$)	Sigma-Aldrich
Nitrogen (gaseous)	Praxair
Peptide RG-23 RYSPTSPSYSPTSPSYSPTSPSG	Chi Scientific
Potassium Chloride (KCl)	Sigma-Aldrich
PrP(1-24): MVKSHIGSWILVLFVAMWSDVGLC	American Peptide
PrP(106-126): KTNMKHMAGAAAAGAVVGGLG	Anaspec
PrP(143-169): SAMSRPLIHFGNDYEDRYYRENMYRYP	Sigma-Genosys
Ac-PrP(145-162): Ace-DSRPLIHFGSDYEDRYYR	Sigma-Genosys
PrP (155-162): DYEDRYYR	Sigma-Genosys
PrP(243-264): VILFSSPPVILLISFLIFLIVG	American Peptide

Sodium phosphate, dibasic (Na_2HPO_4)	Sigma-Aldrich
Sodium phosphate, monobasic (NaH_2PO_4)	Sigma-Aldrich
Trifluoroacetic acid (TFA)	Sigma-Aldrich
Tris-[hydroxymethyl] aminomethane (Tris)	Sigma
Tris-2-carboxyetyhyl-phosphine hydrochloride (TCEP)	Fluka Biochemika
Zinc Chloride ($ZnCl_2$)	BDH
α-hemolysin (αHL)	Sigma-Aldrich
α-helical hairpin peptide(FNMQCQRRFYEALHDPNLNEEQRNAKIKSIRDDC) with a disulfide link at Cys 5 & 34	Sigma-Genosys
capped β-sheet hairpin peptide (Ac-SESYINPDGTWTVTE-NH_2)	Sigma-Genosys
uncapped β-sheet hairpin peptide (SESYINPDGTWTVTE)	Sigma-Genosys

Equipment and supplies

Active-air floating table	Kinetic Systems
Automatic Pipettes and tips	Eppendorf
Axopatch 200B amplifier	Axon Instruments
Barnstead Thermolyne Labquake	Barnstead Thermolyne
Basic pH meter	Fisher
Digitat 1322A digitizer	Axon Instruments
DynaPro-MS800 DLS instrument	Wyatt Technology
F-2500 fluorescence spectrophotometer	Hitachi
Falcon tubes	VWR
Faraday cage	Warner Instruments
Headstage model CV203BU	Axon Instruments
Microcentrifuge tubes	VWR
Microliter syringes	Hamilton
ONEAC PC750A power supply	ONEAC
pClamp 9.0 software	Axon Instruments

Perfusion bilayer chamber and cup	Warner Instruments
Size 000 paintbrushes	Island Blue
Syringes and needles	Becton Dickinson
Welch vacuum pump	Thomson Industries

Table 2.2 Pharmaceutical companies and addresses

Company	**Address**
American Peptide	American Peptide Company, Inc., Sunnyvale, CA, USA.
Anaspec	Anaspec, Fremont, CA, USA.
Avanti Polar Lipids	Avanti Polar Lipids, Alabaster, AL,USA
Axon Instruments	Axon Instruments, Foster City, CA, USA.
Barnstead Thermolyne	Barnstead Thermolyne, Dubuque, IA, USA.
BDH	British Drug House, Saskatoon, SK, Canada.
Beckton Dickinson	Beckton Dickinson and Co., Franklin Lakes, NJ, USA.
Chi Scientific	Chi Scientific, Maynard, MA, USA.
EM SCIENCE	EM Industries Inc., Gibbstown, NJ, USA.
Eppendorf	Eppendorf AG, Hamburg, Germany.
Fluka Biochemika	Fluka Biochemika, Buchs, Switzerland.
Hamilton	Hamilton, Reno, NV, USA.
Hitachi	Hitachi Ltd., Tokyo, Japan.
Island Blue	Island Blue Art Supplies, Victoria, BC, Canada.
ONEAC	ONEAC, Libertyville, IL,USA
Praxair	Praxair, Inc., Saskatoon, SK, Canada.
Sigma	Sigma Chemical Company, St.Louis, MO, USA.
Sigma-Aldrich	Sigma-Aldrich Canada Ltd., Oakville, ON, Canada.
Sigma-Genosys	Sigma-Genosys, The Woodlands, TX, USA.
Thomson Industries	Thomson Industries Inc., Louisville, KY, USA.
VWR	VWR, Mississauga, ON, Canada.
Warner Instruments	Warner Instruments, Hamden, CT, USA.
Wyatt Technology	Wyatt Technology Corporation, Santa Barbara, CA, USA.

2.2.3 The α-helical hairpin peptides

The α-helical hairpin peptide (FNMQCQRRFYEALHDPNLNEEQRNAKIKSIRDDC), containing a disulfide link at Cys 5 & 34, with and without Fmoc was analyzed (see Figure 3.6 on page 91) (Du and Gai, 2006). The Fmoc-α-helical hairpin peptide was 85% pure while the peptide without Fmoc had a purity of 79%. Mass spectrometry was performed on all peptides to confirm molecular weight. Stock solutions of 3.3 mg/mL (Fmoc-α-helical hairpin peptide) and 5 mg/mL (α-helical hairpin peptide, without Fmoc) were prepared in 10 mM potassium phosphate buffer with 1.0 M KCl at pH 7.8 for nanopore analysis. The experiments for the α-helical hairpin peptide that did not contain Fmoc were performed in three separate buffers, using 20-40 µL of peptide solution. The three buffers were: 1.0 M KC1 in 10 mM phosphate buffer at pH 7.0, 1.0 M KC1 in 10 mM Tris-HCl buffer at pH 8.5 and 1.0 M KCl in 10 mM CHES buffer at pH 9.0. The reason for the higher pH range was to confer negative charges on the unlinked sulfur atoms at Cys 5 and 34. Tris-2-carboxyethyl-phosphine hydrochloride (TCEP) was used as the reducing agent to produce the unlinked or reduced sample of the α-helical hairpin peptide. The concentration of TCEP was at least 10 or 20 times greater than that of the peptide.

For the Fmoc-α-helical hairpin peptide, the electrolyte solution was 1.0 KCl in 10 mM potassium phosphate at pH 7.0 and 10 µL peptide solutions were used for nanopore analysis. TCEP was also used to produce the reduced form of the peptide. Nanopore experiments were carried out as stated in section 2.2.1.

2.3 Nanopore detection of prion peptides and proteins

Prion peptides, PrP(155-165):DYEDRYYRENM, and PrP(168-178):YPNQVYYRPMD were generous gifts from Dr. Olga Andrievskaia, from the Canadian Food Inspection Agency, Nepean, Ontario, Canada (Andrievskaia *et al* ., 2006). Mass spectrometry was performed on all peptides to confirm molecular weight. Peptides, PrP (155-162): DYEDRYYR, Ac-PrP(145-162):Ac-DSRPLIHFGSDYEDRYYR and PrP(143-169):SAMSRPLIHFGNDYEDRYYRENM YRYP were also analyzed. These peptides contain a α-helical region (a.a. 155-162) and a β-strand sequence (a.a. 172-175). PrP(143-169) was 98% pure, while the mass of all the other peptides were confirmed with mass spectrometry. Peptide stock solutions of 5 mg/mL were prepared in 10 mM potassium phosphate buffer with 1.0 M KCl at pH 7.8 for nanopore

analysis. Nanopore experiments were carried out using 10 µL stock peptide solutions with a working buffer, 1.0 M KCl, 10 mM phosphate buffer at pH 7.8. The recombinant bovine prion protein (bPrP, net charge +8) containing residues 25-242 with a C-terminal His5 tag was also a generous gift from Dr. Olga Andrievskaia (Andrievskaia *et al*., 2006). A 1 mg/mL prion protein stock solution was prepared in 10 mM Tris-HCl buffer with 0.1 mM EDTA at pH 8.0 for all nanopore experiments. Nanopore analysis was carried out as stated in section 2.2.1, using 20 µL of bPrP in 1.0 M KCl and 10 mM phosphate buffer at pH 7.8. When the prion protein was used in the experimental method stated in section 2.2.1, it was known as "vestibule up-stream" (with *cis* side negative). The same analysis method was repeated for the prion protein but at applied potentials of -50 mV and -150 mV.

The prion protein was also analyzed by adding the protein to the *trans* side of the cup which contains the stem of αHL and also the positive electrode. This orientation is known as "stem down-stream" for the positively charged protein.

2.4 Prion protein and metal interactions

2.4.1 Nanopore detection of prion protein-metal interactions

Stock solutions of Cu(II), Zn(II), Ni(II), Mn(II), and EDTA were prepared. First, 20-70 µl of the 1 mg/ml stock protein was added to the 1.5 mL *cis* chamber, proximal to the aperture. Then the divalent metal ion solution was added to the *cis* side of the chamber and mixed very gently with a pipette tip. The concentration of the divalent metal ion was kept at least 10 times greater than that of the protein. For example, when the concentration of bPrP in the cup was 2.8 µmol/L, the Cu(II) concentration was kept at 28 µmol/L. This solution was then left to incubate for 15-30 minutes. Nanopore analysis was carried out as stated in section 2.2.1, using 1.0 M KCl in 10 mM Tris-HCl buffer at pH 7.8.

2.4.2 Dynamic light scattering

Dynamic light scattering (DLS) is a technique used to determine particle size (Fratantoni *et al*., 1984). The basic theory behind DLS is that when a laser light is focused on a solution with particles in Brownian motion, the scattered light intensity fluctuates (Maurer-Spurej *et al*., 2006). The interaction of light with a moving particle causes a Doppler shift. This in turn changes the wavelength of the incoming light which is related to the size of the

particle. There are two main assumptions for DLS ("Dynamic Light Scattering" by Sartor, M., University of California, San Diego). First, the particles are in Brownian motion and second that Stokes-Einstein relation can be easily applied for the diffusion coefficient, D:

$$D=K_BT/6\pi\eta R_H \qquad \text{Equation 2.1}$$

Where K_B, is the Boltzmann constant, T is the temperature in Kelvin degrees (the experiments in this thesis were conducted at room temperature), $\pi = 22/7$, η, is the viscosity of the solvent and R_H is the hydrodynamic radius of the particles been analyzed. Using this equation, the radius of molecules can be calculated (Maurer-Spurej *et al*., 2006; "Dynamic Light Scattering" by Sartor, M., University of California, San Diego).

DLS measurements were performed using a DynaPro-MS800 DLS instrument located at the Saskatchewan Structural Science Centre (SSSC), University of Saskatchewan. DLS was used to analyze the particle size of the full length bovine prion protein and complexes formed in the presence of Cu(II) and Mn(II). The protein (bPrP) having a concentration of 15-20 µg/mL was investigated in the presence of divalent metal ions, Cu(II) and Mn(II) where the concentration of the divalent metal ion was kept at least 10 times greater than that of the protein. The standard molecular weight (Mw) of the proteins was calculated from the hydrodynamic radius of the particles, using the standard curve model that is applied for the globular proteins:

$$Mw = [(R_{H\ factor}) \times R_H]^{\ power} \qquad \text{Equation 2.2}$$

Where the $R_{\ H\ factor}$ is 1.68 and the power is 2.3398. The factor and power are derived from the molecular dimensions of globular proteins and pullulans (homopolysaccaride consisting of maltotriose units) families (Bugs *et al*., 2004).

The result summary obtained from DLS experiments includes the following parameters: D ($x10^{-9}$ cm^2/s), R_H (nm), Intensity (%) and Mw (kDa). The data were then plotted in graphs having a y-axis of intensity (%) or mass (%) *vs* the logarithmic value of the hydrodynamic radius, log R_H (nm).

2.5 Nanopore detection of antibody-peptide interactions

Monoclonal antibody Jel352 which binds the epitope YSPTSPS was prepared and purified in Dr. Jeremy Lee's Laboratory (Moyle, *et al*., 1989). The concentration of the stock solution of Jel352 was 1.84 mg/mL. Stock solutions of 5 mg/mL RG23 were prepared in 1 M

KCl, 10 mM phosphate buffer at pH 7.8. Control experiments were carried out with peptide PrP(168-178). 2 µL peptide solutions were incubated with varying concentrations of antibody for 1 hour, at room temperature. These solutions were then added to the *cis* chamber proximal to the aperture. The electrolyte solution used for the nanopore experiments was 1.0 M KCl in 10 mM potassium phosphate buffer at pH 7.8. Nanopore analysis was carried out as stated in section 2.2.1.

2.6 Prions and antibody

2.6.1 Nanopore detection of prion peptide-antibody interactions

Monoclonal antibody, M2188, binds epitope, ^{146}SRPLIHFG^{153} in the bovine prion was a generous gift from Dr. Olga Andrievskaia. The expression and purification of this antibody is presented in Andrievskaia *et al*., 2006. The concentration of the M2188 stock solution was 2.44 mg/mL. Prion, antibody interactions with the peptides, Ac-PrP(145-162) and PrP(143-169) containing the epitope SRPLIHFG were analyzed with M2188 using an αHL pore. Control experiments were carried out with peptide, PrP(168-178). 5 µL from 5 mg/mL stock peptide solutions was incubated with varying concentrations of antibody for 1 hour at room temperature. These solutions were added to the *cis* chamber proximal to the aperture. The electrolyte solution for nanopore analysis was 1.0 M KCl in 10 mM potassium phosphate buffer at pH 7.8. Nanopore experiments were carried out as stated in section 2.2.1.

Peptide SN4:GSVYYRPPRYYVPRYYVSGSVYYRPPRYYVPRYYVGSS was a generous gift from Dr. Scott Napper (University of Saskatchewan, Department of Biochemistry, and VIDO, 120 Veterinary Road, Saskatoon, Saskatchewan). Polyclonal antibodies, SN4Ab and SN6Ab, which bind the epitope ^{172}VYYRP^{176}, were also kind gifts from Dr. Scott Napper (Paramithiotis *et al*., 2003 and Hedlin *et al*., 2010). Antibody SN4Ab had a concentration of 1.35 mg/mL while antibody SN6Ab had a concentration of 3.6 mg/mL. 5 mg/mL stock solutions of the peptide SN4 were prepared in 10 mM potassium phosphate buffer with 1.0 M KCl at pH 7.8. Prion peptide, antibody interactions for peptides, SN4 and PrP(168-178) containing the epitope VYYRP was analyzed as follows: 1 µL from 5 mg/mL stock peptide solutions were incubated with varying concentrations of antibody for 1 hour at room temperature. Nanopore analysis was carried out as stated in section 2.2.1.

2.6.2 Nanopore detection of prion protein-antibody interactions

Prion protein-antibody interactions were studied using bPrP and antibodies M2188 and SN4Ab. A 1 mg/mL bPrP stock solution was prepared in 10 mM Tris-HCl buffer with 0.1 mM EDTA at pH 8.0. 20 µL from the stock protein solution were incubated with varying concentrations of antibody for 1 hour at room temperature. Nanopore analysis was carried out as stated in section 2.2.1, using 1.0 M KCl in 10 mM potassium phosphate buffer at pH 7.8.

2.6.3 Nanopore detection of the unfolded prion protein-antibody interactions

20 µL from the prion protein stock solution (1 mg/mL) were denatured using 0.9 M Gdn-HCl. After incubating this premix for 5-10 minutes at room temperature, the interaction of antibodies, M2188 and SN6Ab were investigated in separate nanopore experiments. The addition of antibody at a protein: immunoglobulin ratio of 2:1 was then incubated for 15 minutes. This solution was then added to the *cis* chamber proximal to the aperture. Nanopore experiments were carried out as stated in section 2.2.1, using 1.0 M KCl in 10 mM potassium phosphate buffer at pH 7.8. The final concentration of Gdn-HCl in the *cis* chamber was 0.018 M.

2.7 Nanopore detection of signal prion peptides and protein interactions

Signal prion peptides, PrP(1-24): MVKSHIGSWILVLFVAMWSDVGLC and PrP(243-264):VILFSSPPVILLISFLIFLIVG were analyzed. Mass spectrometry was performed on these peptides to confirm their molecular weights. PrP(106-126):KTNMKHMAGAAAAG AVVGGLG was also analyzed, and had a purity of over 95%. Control experiments were conducted with peptide RG23(RYSPTSPSYSPTSPSYSPTSPSG). Stock peptide solutions of 1 mg/mL were prepared in 10 mM potassium phosphate buffer with 1.0 M KCl at pH 7.8 for all nanopore experiments. 1 mg/mL bPrP solutions were prepared in 10 mM Tris-HCl buffer with 0.1 mM EDTA at pH 8.0. 20 µL of protein solution was incubated with peptide PrP(1-24) at a peptide-to-protein molar ratio of 1:1 for 1 hour at room temperature. This solution was then added to the *cis* chamber proximal to the aperture. The same analysis was repeated with peptides, PrP(243-264), PrP(106-126), and RG23. Nanopore analysis was carried out as stated in section 2.2.1, using 1.0 M KCl in 10 mM potassium phosphate buffer at pH 7.8.

2.8 Aggregation of the full length prion protein

2.8.1 Method for prion protein aggregation and nanopore detection

Here we attempted to aggregate the full length bovine prion protein, bPrP(25-242), with a C-terminal His5 tag at pH 7.5 using the method described by Aperti *et al*, 2005. However, that group used an N-terminaly truncated human prion protein, PrP(90-231) with 1 M or 2 M Gdn-HCl (Aperti *et al*, 2005). 1 mg/mL prion protein stock solutions were prepared in 10 mM Tris-HCl buffer with 0.1 mM EDTA at pH 8.0. The master mix contained: 125 µL of 40 µM (1 mg/mL) of bPrP(25-242), 5 µL of 1 M Tris-HCl at pH 7.4, and 20.37 µL of 6.38 M Gdn-HCl. The final concentration of Gdn-HCl was 0.86 M in this mixture. This sample was incubated at 37ºC and continuously rotated at 8 rotations per minute (rpm) using a Barnstead Thermolyne Labquake rotator. 20µL samples were withdrawn at different time intervals of 0, 18, 25, 44, and 68 hours followed by nanopore analysis using αHL pores. The electrolyte solution for nanopore experiments was 1.0 M KCl in 10 mM potassium phosphate buffer at pH 7.8. Nanopore anlysis was carried out as stated in section 2.2.1.

2.8.2 Thioflavin T fluorometric assay

For the formation of fibrils, a fluorometric Thioflavin T (ThT) was measured using an F-2500 Fluorescence spectrophotometer. Samples were withdrawn at 0, 18, 25, 44, and 68 hours and transferred to a quartz cell containing 10 µM ThT in 50 mM phosphate at pH 6.4. After 30 seconds of incubation, the fluorescence of ThT was measured at 482 nm upon excitation at 450 nm. The final prion protein concentration in the ThT buffer was 0.415 µM. A stock solution of 1 mg/mL (3.14 mM) ThT was prepared by dissolving dry powder in deionized water in the dark. Using this stock solution, 10 µM ThT solutions in 50 mM phosphate buffer at pH 6.4 were prepared fresh daily for the fluorometric assay.

2.9 The patch-clamp experimental apparatus

2.9.1 The patch-clamp Instrument

Single-molecule nanopore analysis was conducted using a patch-clamp apparatus as shown in Figure 2.1. The patch-clamp apparatus is made up of a Faraday cage (Warner Instrument) containing the perfusion unit (Warner Instruments), headstage (model CV203BU,

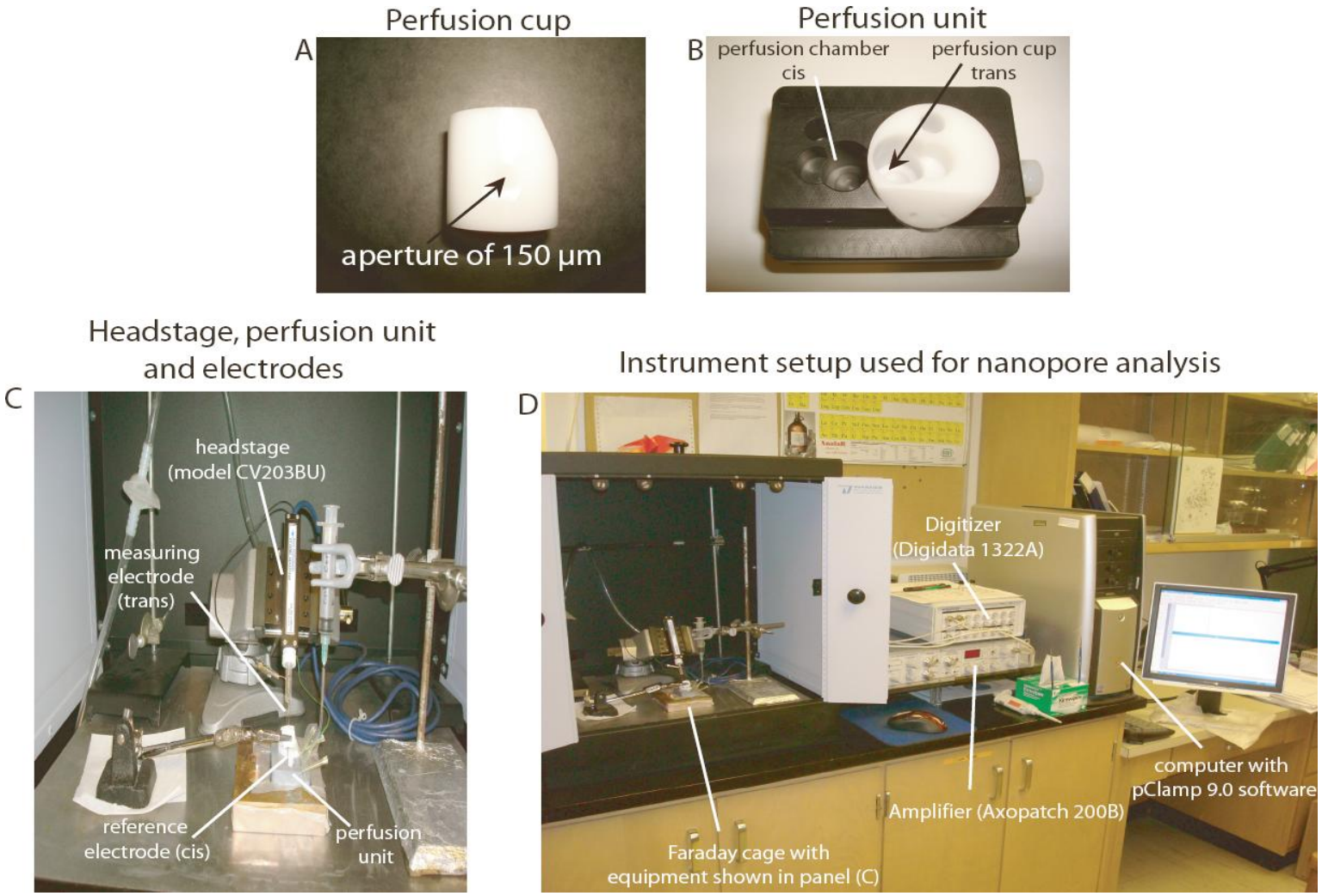

Figure 2.1 Images of the patch-clamp instrumental set up. Photograph (A) is the perfusion cup containing the 150 µm aperture. Photograph (B) is the perfusion unit comprising the perfusion chamber and cup. Photograph (C) shows the headstage, perfusion unit and electrodes in the Faraday cage. Photograph (D) shows the entire patch-clamp instrumental setup comprising the Faraday cage, digitizer, amplifier and computer with pClamp 9.0 software.

Axon Instruments), measuring and reference electrodes which are connected to the digitizer (Digidata 1322A, Axon Instruments) and amplifier (Axopatch 200B, Axon Instruments). This entire set of instruments as shown in Figure 2.1C, is connected to a computer (Figure 2.1D). pClamp 9.0 software, that records data which is also used for data analysis, is installed in this computer. The perfusion unit is made up of a black perfusion chamber and a white perfusion cup (Figure 2.1B). The white perfusion cup contains a 150 μm aperture (Figure 2.1A), on which the lipid bilayer is formed followed by the insertion of a biological nanopore of αHL or aerolysin. This perfusion unit separates the *cis* (outside) and *trans* (inside) compartments, which are filled with electrolyte solution and also contain the Ag/AgCl electrodes. The volume in each of these two compartments is approximately 1.5 mL. For all experiments stated in this thesis, a negative electric potential was applied to the *cis* compartment using the two Ag/AgCl electrodes. The measuring electrode located on the *trans* side of the cup was connected to a gold pin that was further connected to the headstage. The reference electrode on the *cis* side of the cup was also connected to the headstage. The perfusion unit is encased in a solid block of copper that was placed on an active-air floating table (Kinetic Systems) located inside the Faraday cage. The signals that are transmitted from the headstage are converted from voltage to current by the amplifier, and further converted from analog to digital by the digitizer. The patch-clamp instrumental setup was powered through an ONEAC power supply that helps protect the network and also reduce electronic noise.

2.9.2 The formation of a synthetic lipid bilayer and pore insertion

First, 75 μL aliquots of the lipid 1,2-diphytanoyl-sn-glycero-3-phosphocholine in $CHCl_3$ (Avanti Polar Lipids) were stored in Kimble vials at -20^0C. Before each experiment, one aliquot was dried under vacuum and then re-dissolved in decane to a final concentration of 30 mg/mL. The lipid suspension was then applied on both sides of the 150 μm aperture located on the white perfusion cup using a size 000 paintbrush (Island Blue paintbrush). The excess lipid was dried under a jet of nitrogen. As mentioned in section 2.9.1, the bilayer cup has two compartments of about 1.5 mL each, which are termed *cis* and *trans*. Once the lipid bilayer is dried, the *cis* and *trans* compartments are filled with approximately 1.5 mL of 1.0 M KCl, 10 mM potassium phosphate (KH_2PO_4/K_2HPO_4) buffer at pH 7.8. If different buffers were used they have been stated in each experimental method. A negative transmembrane potential of

100 mV was usually applied using the Ag/AgCl electrodes immersed in electrolyte solution, where anions are driven from *cis* to *trans*. To ensure the quality of the newly formed membrane, the capacitance was monitored using the pClamp 9.0 software and a value of 7-9 pF indicates a stable membrane into which a biological pore can insert with ease. Furthermore, a 0 pA ionic currentshould be recorded for a well-sealed membrane between the *cis* and *trans* compartments. Following the formation of a lipid bilayer, 5-10 μL of 2.0 μg/mL, α-hemolysin or aerolysin solutions were injected adjacent to the aperture on the *cis* side. At an applied voltage of -100 mV, a current jump of 100 pA or 50 pA was recorded for a single pore of αHL or aerolysin, respectively. If more than one pore of αHL or aerolysin was inserted, an open pore current that is multiplied by the number of pores was observed. Once stable pore insertion was detected, a solution of the molecules of interest was added to the *cis* side, proximal to the aperture (Figure 2.2). The experiments were carried out at 22 ± 1°C.

2.9.3 Data recording and collection

The Axopatch 200B patch-clamp amplifier was connected directly to the headstage which forms an interface between the sample being analyzed and the main instrument device. The amplifier receives data from the sample and also filters the data while holding a constant applied voltage (Molleman, 2008). The data were recorded as "fixed-length events". This means that the data are continuously digitized and displayed, but only saved for segments of specified duration (pClamp 9.0 User's Guide, 2005). The Axopatch 200B patch-clamp amplifier contains a low pass Bessel filter, which filters out all other frequencies except the signal of interest. The use of filters enhances the signal-to-noise ratio.

2.9.4 Raw data analysis and software

Raw Clampex data were analyzed using the Clampfit 9.2 software, part of the pClamp 9.0 package, from Axon Instruments. The Clampfit 9.2 software includes three main types of windows: analysis, results and layout. In addition, a system lab book and data file index window is also featured. Recorded Clampex data are first opened using the Clampfit-analysis window. This opened data that are viewed on the analysis window are then auto-scaled using the command "auto scale all y axes". Following this, the "view and data display" command is used to display the data as a series of concatenated episodes. All the data analysis performed in

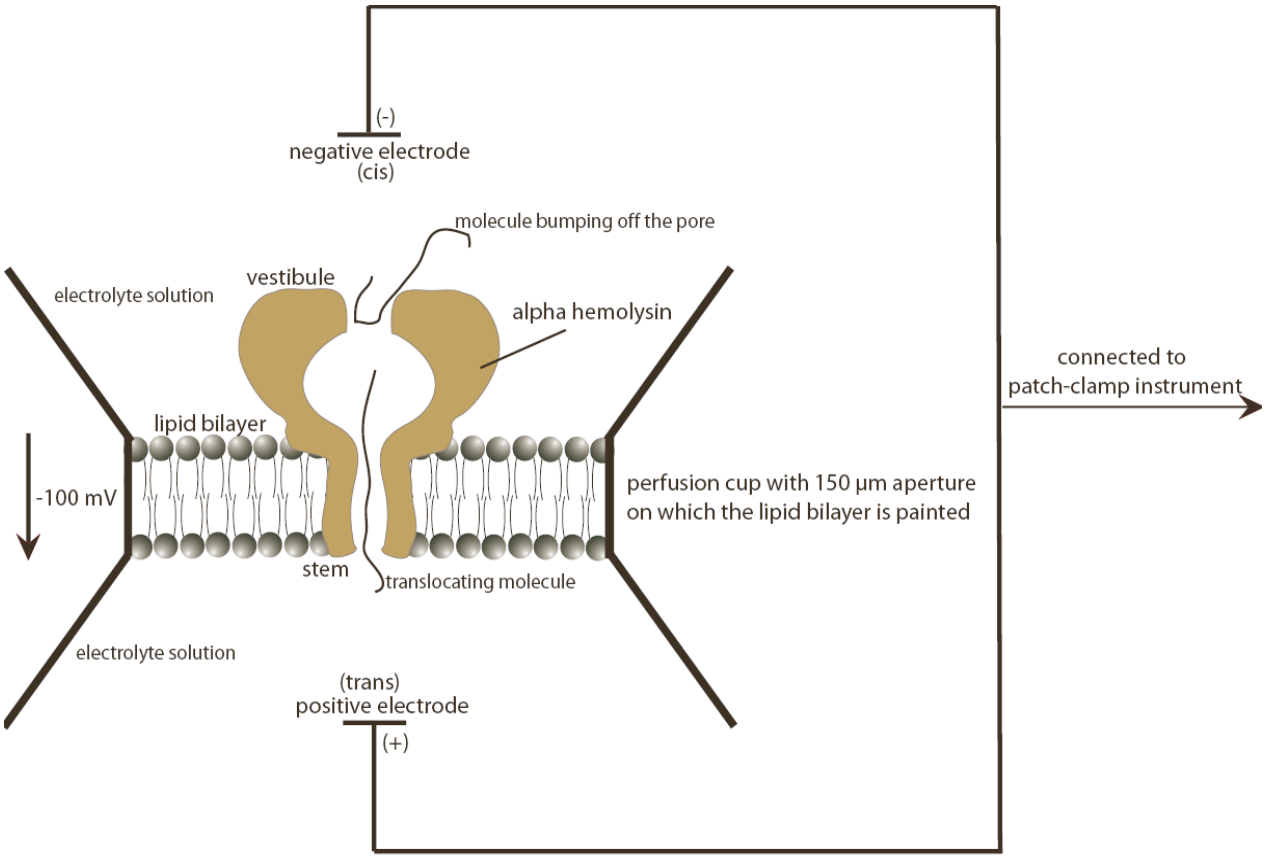

Figure 2.2 Schematic of an α-hemolysin pore embedded into a lipid bilayer. The lipid bilayer is painted across the 150 µm aperture located on the perfusion cup. The perfusion unit separates the *cis* and *trans* sides. A negative potential of -100 mV is applied through the Ag/AgCl electrodes. The bumping and translocation events of a molecule are shown. Intercalation events are not shown.

this thesis used the "single-channel analysis" command which is displayed in the "event detection" tab. The recorded data are now displayed on the screen with the y-axis presenting the amplitude of current blockade as "I Patch (pA)" and the x-axis as "Time (ms)" which represents the blockade time shown. The amplitude of current blockade is due to the molecule interacting with the pore and displacing a volume of electrolyte solution, while the blockade time can be stated as the transport time or the time taken for a molecule to interact with the pore (Henriquez *et al*., 2004).

The interaction of a molecule with the pore can be stated as an "event" which is characterized by two parameters, the current blockade (**I**), and blockade time (**T**) (Figure 2.3). In general, events are of three types and are designated as bumping, intercalation and translocation events (Stefureac *et al*., 2006; Meng *et al*., 2010). The bumping events also called type-I events have a small current blockade and are due to molecules that bump into the pore and then slowly diffuse away (Sutherland *et al*., 2004b; Stefureac *et al*., 2006). The type-II events which could be intercalation or translocation have larger current blockades (Stefureac *et al*., 2006; Meng *et al*., 2010). An intercalation event has been described in which molecules transiently enter the pore but do not translocate. These events comprise large current blockades in which the blockade duration increases with increasing voltage (Meng *et al*., 2010). As these molecules do not translocate, they diffuse back into the electrolyte solution using the same route they entered the pore. The translocation events are assigned to molecules that are transported through the pore where the blockade time decreases with increasing voltage (Akeson *et al*., 1999b; Sutherland *et al*., 2004b; Stefureac *et al*., 2006). As both of these type-II events comprise large current blockades, they can only be distinguished from one another if voltage studies are carried out.

Once a set of recorded data has been identified, a continuous segment is selected for Clampfit 9.2 analysis. First, a baseline is set at the open pore current level which is marked as a horizontal line depicting level zero. Then a level two detection threshold was performed for all data. The first base line was placed for the detection of type-I events and is marked as horizontal level one. The same was done to detect the type-II events by placing a baseline marked as horizontal level two. All the data analyzed in this thesis used this level two detection threshold which can easily identify type-I and type-II event populations (Figure 2.3). The

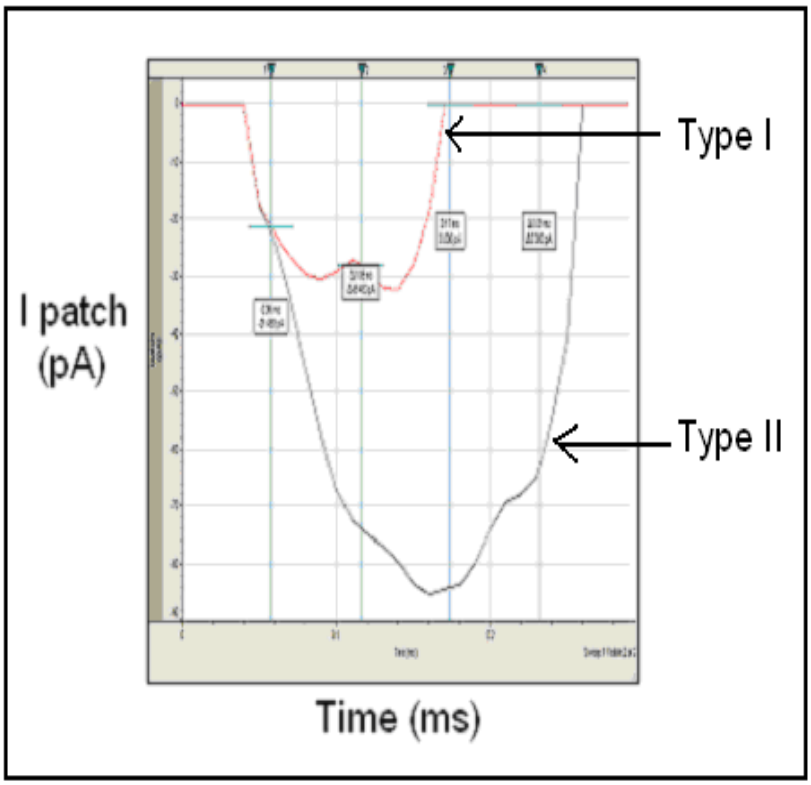

Figure 2.3 The types of events recorded with an α-hemolysin pore. The plot consist of blockade current (I) vs. blockade time (T). The type-I events having smaller blockade currents are designated as bumping events and the type-II events comprising larger blockade currents could be either intercalation or translocation events.

ignore duration for events was set at 0.1 ms and the search region was set at cursor 1 and 2 which depicts the vertical lines shown as number 1 and number 2. Vertical cursor lines 3 and 4 are ignored for this analysis. Once the "event viewer" window pops up, a nonstop analysis is conducted. After the analysis of a segment of recorded data is complete, the "event viewer" window is closed and the analyzed data are listed in the results window in a separate spreadsheet, named as "events". The data are then transferred to a separate spreadsheet and then the cycle begins with the selection at another segment for analysis.

The rise time of the instrument (Tr), is the time taken for a signal to change from a lower to higher value. This instrument uses a clampfit digital filter known as a lowpass Bessel filter. Tr can be calculated as $0.33/f_{c,}$ where fc is the frequency of the filter. The experiments conducted in this thesis used a rise time of 50 μs or more, where below this level events are considered too fast to be measured. Once the raw data analysis was complete, it was transferred to Origin 7.0 (OriginLab Corporation, Northampton, MA). The blockade current populations were obtained by fitting the blockade current distribution with the Gaussian function. The lifetime data were obtained by fitting each blockade duration distribution with a single exponential function. The bin increments for the blockade current and blockade time were set at 1 pA and 0.05 ms, respectively.

3.0 RESULTS

3.1 Analysis of acetylated and Fmoc protected peptides

3.1.1 Introduction

Nanopore analysis of peptides using αHL pores has been previously reported by Lee and co-workers (Sutherland *et al*., 2004a, b; Stefureac *et al*., 2006; Stefureac and Lee, 2006; Meng *et al*., 2010). Fluorenylmethyloxycarbonyl (Fmoc) is a protecting group for amines which is added to the amino terminus of an amino acid (Carpino and Han, 1972). Previous studies using Fmoc protected peptides revealed that these peptides translocate through the αHL and aerolysin pores more easily compared to the unprotected peptides (Stefureac *et al*., 2006). This group used a set of negatively charged α-helical peptides for their analysis. All peptides having a general formula of Fmoc-$D_xA_yK_z$ where x and z were 1, 2 or 3 and y was 10, 14, 18 or 22 translocated through the αHL pore with blockade currents ranging between -62 pA and -78 pA (Stefureac *et al*., 2006). Recently, peptides comprising 12 amino acids that were tethered via a terminal cysteine to mono-, di-, tri-, and tetrabromomethyl-substituted benzene to construct bundles were analyzed at different applied potentials of -50, -100 and -150 mV. This analysis helped to identify a new set of events called "intercalation events" in addition to the bumping and translocation events mentioned in Stefureac *et al*., 2006 (Meng *et al*., 2010). The rationale for the experiments presented below was first to study the interactions between peptides and pores and to try and gain a more detailed view of the effects of acetylation and Fmoc. Second, I wanted to verify whether the introduction of one proline residue at the center of these peptides, which can cause a turn, bend or kink in the peptide conformation, was adequate to block the pore.

3.1.2 Nanopore detection of Ac-$D_2A_{14}K_2$, Ac-$D_2A_7PA_6K_2$, and Fmoc-$D_2A_7PA_6K_2$

Three peptides, Ac-$D_2A_{14}K_2$, Ac-$D_2A_7PA_6K_2$, and Fmoc-$D_2A_7PA_6K_2$ were analyzed using αHL pores. All peptides had a net negative charge of -1 (at pH 7.8) and were 18 amino acids in length. The nanopore experiments and data analysis were performed as described in the Materials and Methods section. The interaction of the peptide with the pore can be stated as an event, which is characterized by two parameters, the current blockade i_{block}, and blockade time t_{block} (Figure 3.1). In general, events are three types, and have been previously described in section 2.9.4. The analyzed data were arranged in histograms by plotting the intensities of current blockade *vs*. the number of events. The data analysis, in which the number of events is

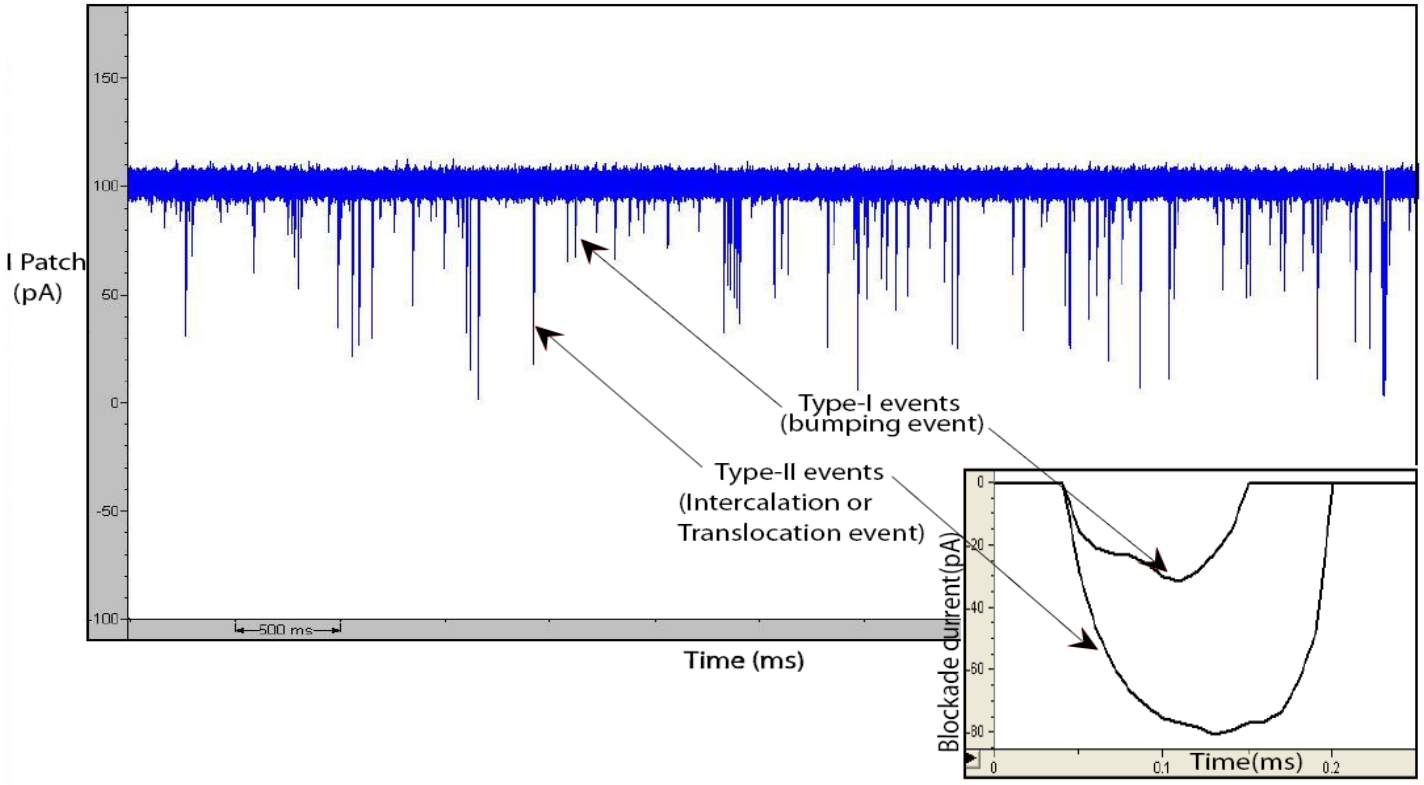

Figure 3.1 A plot of blockade current, I (pA) *vs*. blockade time, T (ms) for a string of ionic current pulses for the capped-β hairpin peptide. The inset shows an expanded view of typical type-I events having smaller blockade currents, designated as bumping events and the type-II events comprising larger blockade currents which could be either intercalation or translocation events.

counted for each 1 pA increment in the i_{block}, was used to plot the graphs. Each blockade current distribution was fitted with a first order decay function to obtain the blockade time histograms. The bin increment for the blockade duration was set at 0.05 ms.

For peptide Ac-$D_2A_{14}K_2$, the blockade current and blockade time histograms are shown in Figure 3.2 and the parameters are listed in Table 3.1. The Ac-$D_2A_{14}K_2$ peptide has a net negative charge and thus will be driven through the αHL pore due to the negative potential applied on the *cis* side of the bilayer cup. Upon addition of Ac-$D_2A_{14}K_2$ to the *cis* side of the chamber, the rate of data acquisition was slow and the peptide displayed two event populations with approximately equal number of events under each population peak which were fitted with a Gaussian distribution. Due to the single Gaussian distribution for both type-I and type-II events, we can conclude that only monomers are present in the peptide solution, whereas if complexes are formed they would give rise to multiple peaks (Sutherland *et al*., 2004b). Alternatively, if complexes are forming, they must be very weak and do not affect the type-II events (Stefureac *et al*., 2006). The average blockade current values for peptide Ac-$D_2A_{14}K_2$, for type-I ($\mathbf{I_1}$) and type-II ($\mathbf{I_2}$) events were -26 pA and -64 pA, respectively, with corresponding blockade time values ($\mathbf{T_1}$) and ($\mathbf{T_2}$) of 0.08 ms and 0.09 ms. The ratio for the type-I ($\mathbf{A_1}$) to type-II ($\mathbf{A_2}$) events for peptide Ac-$D_2A_{14}K_2$ was 0.95:1. The same peptide protected with Fmoc, analyzed by Stefureac *et al*., 2006 was used to compare the difference with the acetylated version. For comparison, the current blockade and blockade time histograms for Fmoc-$D_2A_{14}K_2$ were also included in Figure 3.2 and the parameters were listed in Table 3.1. However, peptide Fmoc-$D_2A_{14}K_2$ displayed only a single Gaussian distribution of type-II events. The average current blockade for Fmoc-$D_2A_{14}K_2$, for the type-II ($\mathbf{I_2}$) events was -65 pA with a corresponding blockade time value ($\mathbf{T_2}$) of 0.34 ms. Thus, acetylating a peptide reduces the number of type-II events as compared to Fmoc which increases it. The data also reveal that the blockade current for the type-II events is essentially the same for both peptides, but the blockade duration is much smaller for peptide Ac-$D_2A_{14}K_2$.

The Ac-$D_2A_7PA_6K_2$ peptide contains a proline which causes a turn or kink in the α-helix (Cheng and Chang, 1999). For peptides Ac-$D_2A_7PA_6K_2$ and Fmoc-$D_2A_7PA_6K_2$, the blockade current and time histograms are shown in Figure 3.3 and the parameters are listed in Table 3.2. When peptide Ac-$D_2A_7PA_6K_2$ was added to the *cis* side of the bilayer cup, the rate of data acquisition was as slow as for peptide Ac-$D_2A_{14}K_2$. However the histogram of the blockade

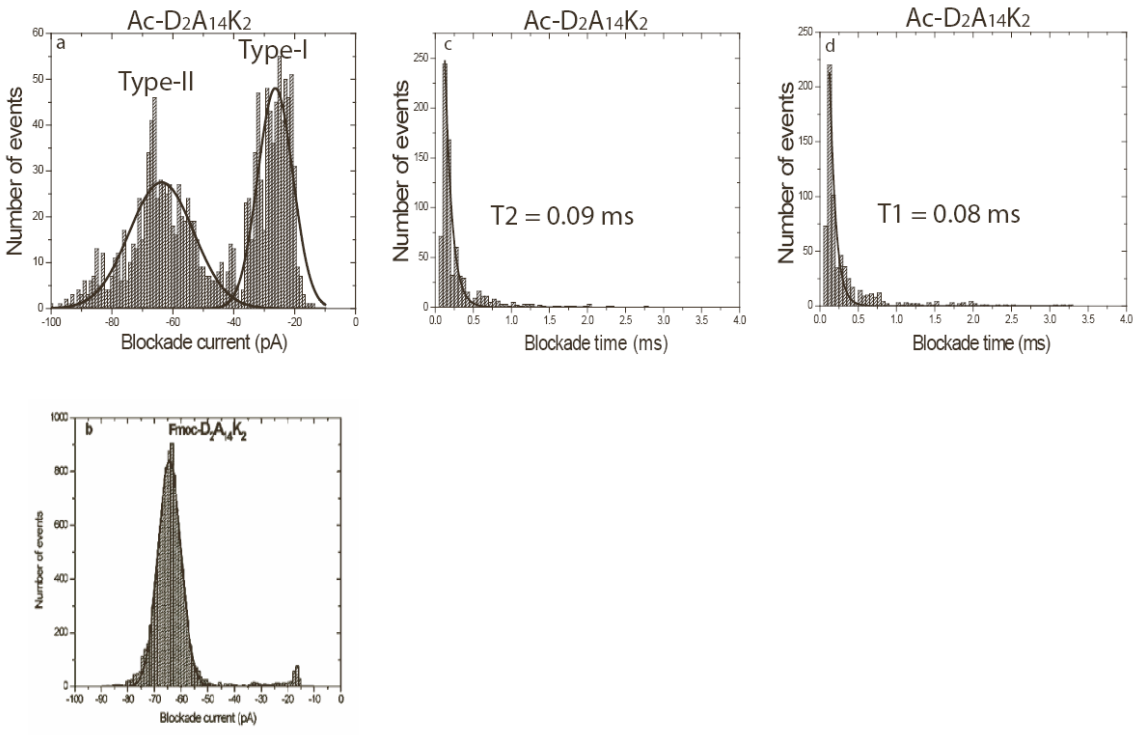

Figure 3.2 Current blockade histograms for (a) Ac-$D_2A_{14}K_2$ and (b) Fmoc-$D_2A_{14}K_2$ tested on αHL pores at pH 7.8. The histogram for Fmoc-$D_2A_{14}K_2$ was obtained from Stefureac *et al*., 2006. Single Gaussian functions have been fitted for each population of events and each of the two blockade current distributions was fitted with a first order decay function to obtain the blockade time shown in panels (c) and (d). Parameters are presented in Table 3.1. (Figure 3.2b was reprinted by permission from Stefureac *et al*., 2006. Copyright 2006 American Chemical Society.)

Table 3.1. Interaction parameters of the acetylated and Fmoc protected peptides with αHL pores[a].

Peptide	**I_1 (pA)**	**I_2 (pA)**	**T_1 (ms)**	**T_2 (ms)**	**A_1**	**A_2**	**A_1/A_2**	**W_1**	**W_2**
Ac-$D_2A_{14}K_2$	-26	-64	0.08	0.09	693	728	0.95	11.4	21.1
Fmoc-$D_2A_{14}K_2$	-	-65	-	0.34	-	9505	-	-	8.3

[a] **I** is the current blockade and **T** is the time of blockade. The subscripts 1 and 2 refer to Type-I and Type-II event populations presented in Figure 3.2. $\mathbf{A_1}$ and $\mathbf{A_2}$ are the number of events of each population. $\mathbf{W_1}$ and $\mathbf{W_2}$ are the peak widths at half-height. Fmoc-$D_2A_{14}K_2$ data was obtained from Stefureac *et al*., 2006. (The error is estimated to be ±1 pA for **I** and ±10% for **T**)

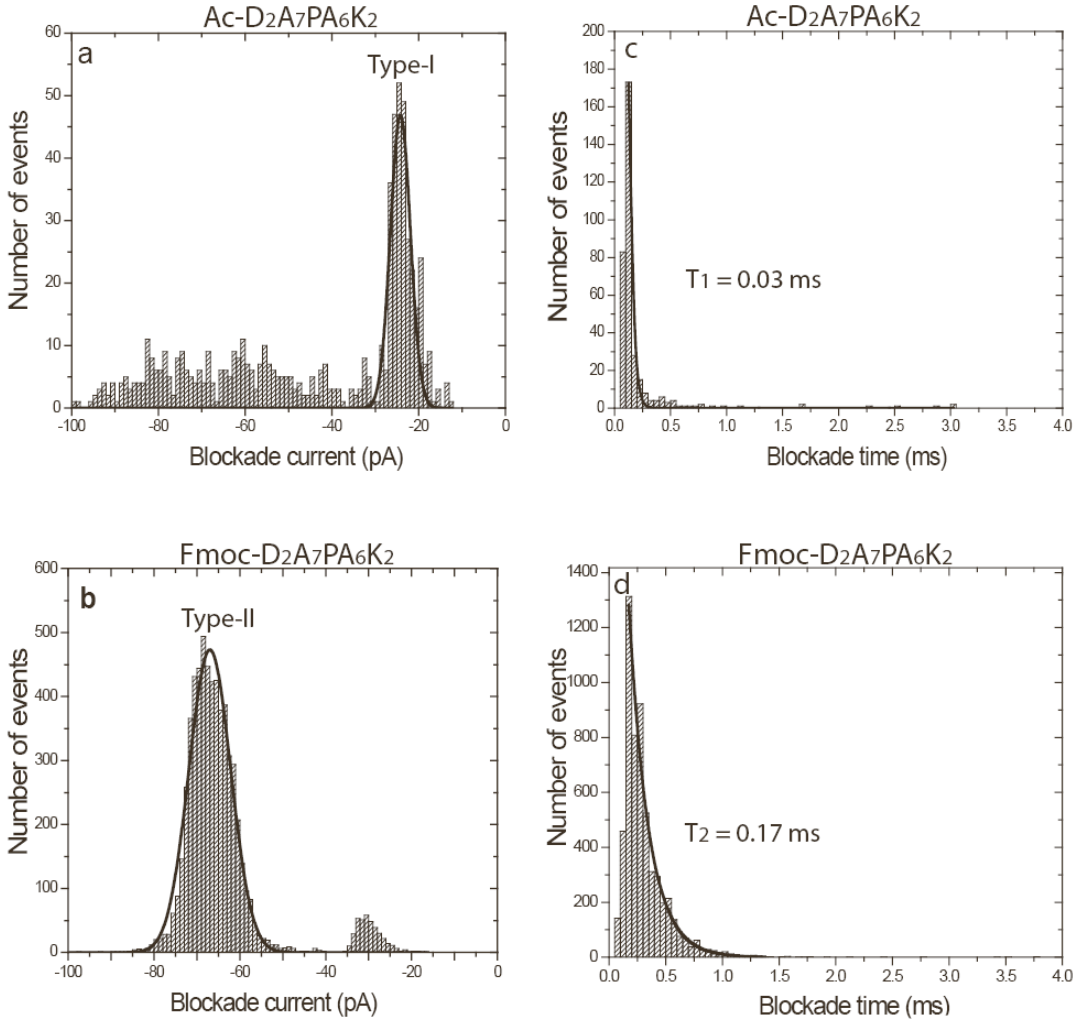

Figure 3.3 Current blockade histograms for (a) Ac-$D_2A_7PA_6K_2$ and (b) Fmoc-$D_2A_7PA_6K_2$ tested on αHL pores at pH 7.8. Single Gaussian functions have been fitted for each population of events and each blockade current distribution was fitted with a first order decay function to obtain the blockade time shown in panels (c) and (d). Parameters are presented in Table 3.2.

Table 3.2 Interaction parameters of the acetylated and Fmoc protected peptides which include a proline at position 10[a].

Peptide	**I_1 (pA)**	**I_2 (pA)**	**T_1 (ms)**	**T_2 (ms)**	**A_1**	**A_2**	**A_1/A_2**	**W_1**	**W_2**
Ac-$D_2A_7PA_6K_2$	-24	-	0.03	-	292	-	-	4.7	-
Fmoc-$D_2A_7PA_6K_2$	-	-67	-	0.17	-	5750	-	-	9.5

[a] **I** is the current blockade and **T** is the time of blockade. The subscripts 1 and 2 refer to Type-I and Type-II event populations presented in Figure 3.3. $\mathbf{A_1}$ and $\mathbf{A_2}$ are the number of events of each population. $\mathbf{W_1}$ and $\mathbf{W_2}$ are the peak widths at half-height. (The error is estimated to be ±1 pA for **I** and ±10% for **T**)

current for peptide Ac-$D_2A_7PA_6K_2$ (Figure 3.3a) appears different from peptide Ac-$D_2A_{14}K_2$, with only a single Gaussian distribution for the type-I events and no clear peak for the type-II events can be discerned. The type-II event populations are dispersed with varying blockade current values ranging from -40 pA to -100 pA. Therefore it would appear that many conformations of the Ac-$D_2A_7PA_6K_2$ peptide are present in the peptide solution which may form multiple complexes that do not readily intercalate or translocate the pore. The average blockade current values for the type-I ($\mathbf{I_1}$) events were -24 pA with a corresponding blockade time value ($\mathbf{T_1}$) of 0.04 ms. These results show that the addition of a proline in the middle of an acetylated peptide further reduces the number of type-II events. In contrast, the histogram of the blockade current for peptide Fmoc-$D_2A_7PA_6K_2$ (Figure 3.2b) gave a single population of type-II events having an average blockade current ($\mathbf{I_2}$) of -67 pA with a corresponding blockade time ($\mathbf{T_2}$) of 0.17 ms. Thus, acetylation of the N-terminus of peptide $D_2A_7PA_6K_2$ decreased the number of type-II events as compared to the Fmoc- $D_2A_7PA_6K_2$.

3.2 Analysis of hairpin peptides

3.2.1 Introduction

3.2.1.1 The structure of α-helical and β-sheet hairpin peptides

In light of the results above, we were encouraged to go a step further and study the interactions of peptides that had different secondary structures. Do different types of secondary structures such as α-helical and β-sheet regions in small peptides give specific signatures with nanopore analysis? These data may help to interpret the conformational changes and folding patterns that take place during peptide-pore interactions. For this purpose, a 15-residue β-hairpin and a 34 residue α-helical hairpin which also contained a disulfide link were analyzed.

β-hairpins are the simplest models for the study of protein folding. They consist of two antiparallel β-strands linked by a turn or a short loop (Wu and Brooks, 2004). Conformational studies of β-hairpins provide insight into the early events of protein folding (Blanco *et al.*, 1994). The folding energetics of β-hairpins have been developed using computational models, but only a few experimental studies have been reported. Among them, infra red (IR) and temperature-jump (T-jump) studies demonstrate that the folding of a β-hairpin is consistent with the hydrophobic collapse model (Pande and Rokhsar, 1999). The hydrophobic collapse model

is mainly applied to the folding pathway of proteins which first fold into native secondary structures and then collapse due to the hydrophobic effect that go to form the globular structure (Sadqi *et al*., 2003). Using a fluorescence T-jump technique, the folding of a 16 residue β-hairpin fragment from the C-terminal amino acid sequence 41-56, of protein GB1 (immunoglobulin G binding protein located on the cell wall of group G *Streptococci* containing the immunoglobulin G binding domain B1) at room temperature was 6 μs, which is 30 times slower than that of α-helix formation (Kobayashi *et al*., 1995; Xu *et al*., 2003). The folding of a β-hairpin follows the basic laws of protein folding, which include hydrogen bonding, hydrophobic interactions and a two state behavior (Munoz *et al*., 1997). Furthermore, the formation of a β-hairpin in the GB1 peptide was studied using multi-probed thermodynamic characterization, which is a study of the folding/unfolding equilibrium by measuring temperature-dependence on the structural features such as absorption, fluorescence, CD and NMR. It was found that the β-hairpin formation is a first-order phase transition between two states without any distinguishable intermediates (Honda *et al*., 2000).

The α-helical hairpin is a helix-turn-helix motif, which consists of two antiparallel helices connected by a reverse turn. The most important aspect in the structure of the α-helical hairpin is that it resembles a protein folding intermediate (Fezoui *et al*., 1994). IR and T-jump studies suggest that the folding of α-helical hairpins is ultra fast with a rate of (~ 4.0×10^5 s^{-1}) and the hydrophobic cluster stabilizes the native structure (Du and Gai, 2006). The helix-turn-helix is also an important structure for DNA-binding proteins (Huffman and Brennan, 2002).

3.2.2. Nanopore detection of α-helical and β-sheet hairpin peptides

Three peptides were analyzed; a capped (Ac-SESYINPDGTWTVTE-NH_2) and an uncapped (SESYINPDGTWTVTE) 15-residue β-hairpin and a 34 residue α-helical hairpin (FNMQCQRRFYEALHDPNLNEEQRNAKIKSIRDDC), with a disulfide link between Cys 5 & 34. The structure and dimensions of the capped and uncapped β-hairpins are shown in Figure 3.4 and both peptides have a net negative charge of -3 and are 15 amino acids in length. For the capped and uncapped β-hairpins, the blockade current and blockade time histograms are shown in Figure 3.5 and the parameters are listed in Table 3.3. For both the capped and uncapped β-hairpins there was a single Gaussian distribution for each population of events. Due to the single Gaussian distribution for both type-I and type-II events, we can conclude that

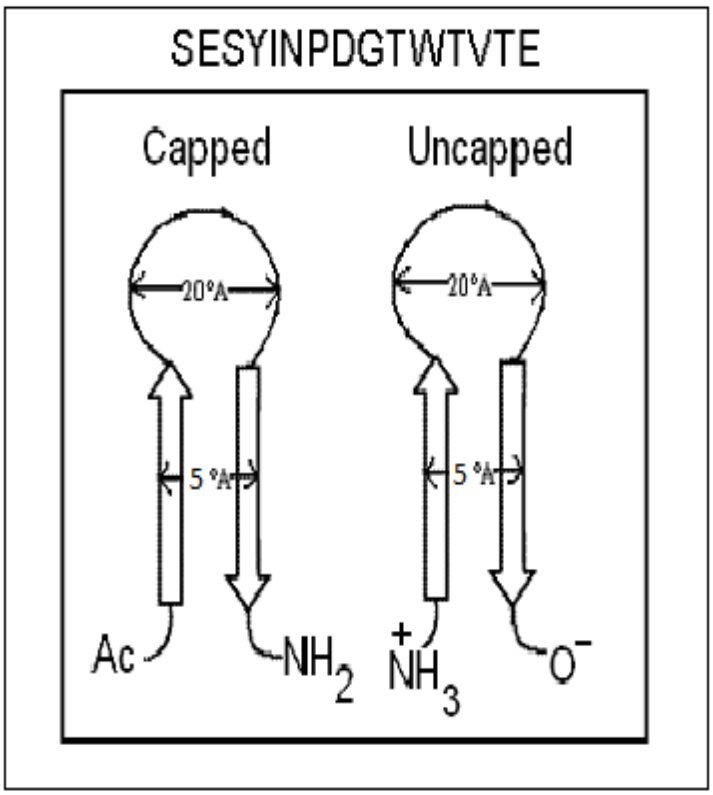

Figure 3.4 Diameter of the loop and the distance between the β-strands of the capped and uncapped β-hairpin peptides calculated using Spartan software program (SpartanModel). The dimensions are given in Ångstroms (Å).

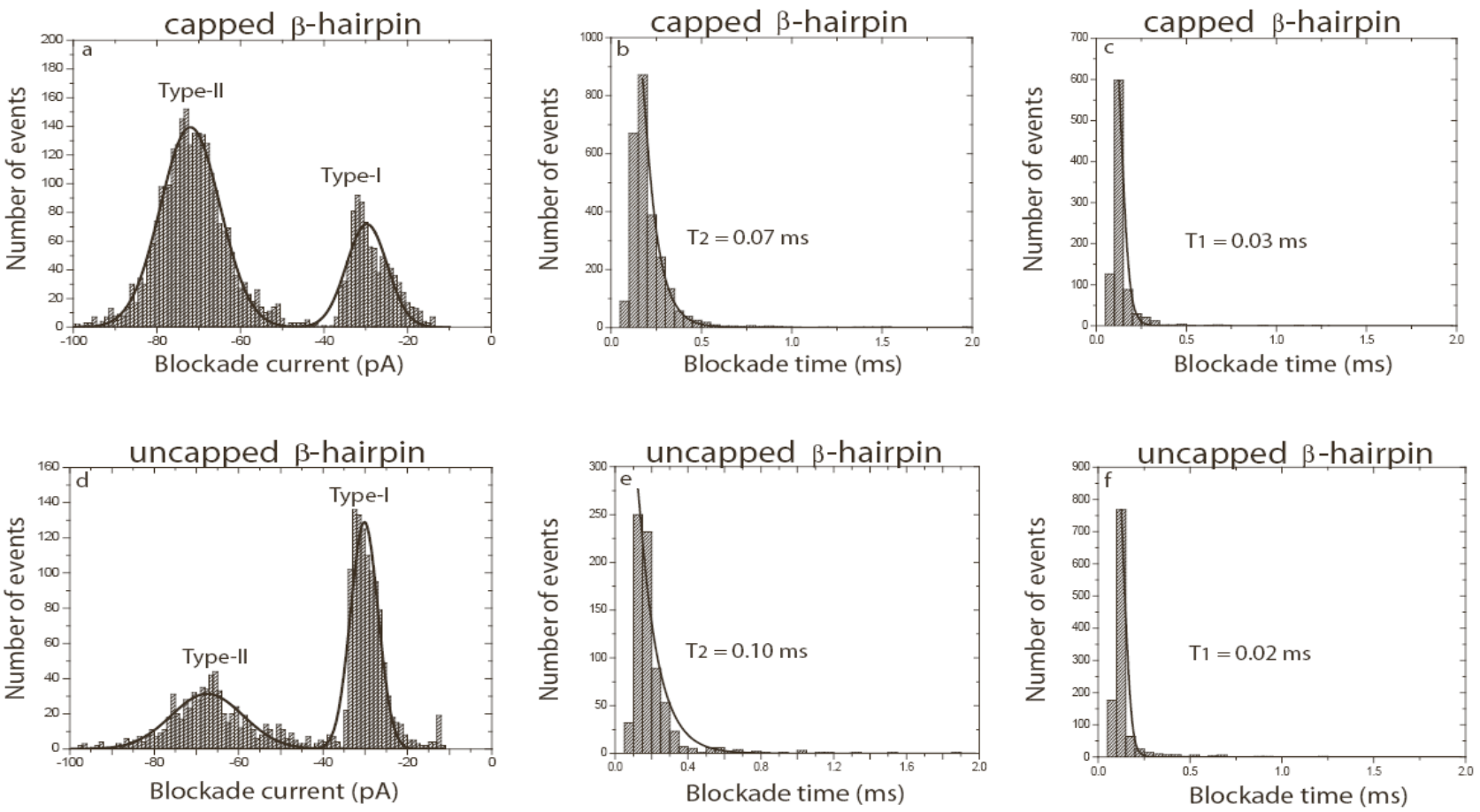

Figure 3.5 Current blockade histograms for (a) capped β-hairpin and (d) uncapped β-hairpin at pH 7.8. Single Gaussian functions have been fitted for each population of events and each blockade current distribution was fitted with a first order decay function to obtain the blockade time shown in panels (b-c) and (e-f). Parameters are presented in Table 3.3.

Table 3.3 Interaction parameters of the capped and uncapped β-hairpin peptides [a].

Peptide	I_1 (pA)	I_2 (pA)	T_1 (ms)	T_2 (ms)	A_1	A_2	A_1/A_2	W_1	W_2
β-hairpins									
capped	-30	-72	0.03	0.07	892	2567	0.347	9.6	14.1
uncapped	-30	-67	0.02	0.10	1107	703	1.575	6.3	17.0

[a] **I** is the current blockade and **T** is the time of blockade. The subscripts 1 and 2 refer to Type-I and Type-II event populations presented in Figure 3.5. $\mathbf{A_1}$ and $\mathbf{A_2}$ are the number of events of each population. $\mathbf{W_1}$ and $\mathbf{W_2}$ are the peak widths at half-height. (The error is estimated to be ±1 pA for **I** and ±10% for **T**).

only monomers are present in the peptide solution. The ratio of type-II ($\mathbf{A_2}$) to type-I ($\mathbf{A_1}$) events for the capped β-hairpin peptide was 2.87:1 which decreased to 0.63:1 for the uncapped β-hairpin peptide. Thus, the uncapped β-hairpin may fold more, causing a reduction in the type-II events as compared to the capped β-hairpin.

First, the analysis of the α-helical hairpin peptide that did not contain an Fmoc at the N-terminus was performed at different pH values of 7.0, 8.5, and 9.0 using three separate buffers. TCEP was used as the reducing agent to produce the unlinked form of the α-helical hairpin peptide. The concentration of TCEP was kept at least 10 times greater than that of the peptide. The reason for an increase in pH was to confer a negative charge on the two Cys derivatives at position 5 and 34 in the unlinked peptide (Figure 3.6a). For the crosslinked α-helical hairpin peptide that did not contain Fmoc, there was a single Gaussian distribution for each population of events. However, the number of type-I events for the crosslinked α-helical hairpin peptide (without Fmoc) at all the above mentioned pH values was much higher compared to the type-II events. When TCEP was used to form the unlinked peptide, the overall distribution for each population did not change significantly. These results suggest that in the absence of Fmoc, crosslinked and unlinked α-helical hairpins give very few type-II events.

Due to the results obtained for peptide Fmoc-$D_2A_7PA_6K_2$ which was stated in section 3.1, where the number of type-II events increased when the acetyl group was substituted by Fmoc, it was decided to add an Fmoc to the N-terminus of the 34 residue α-helical hairpin (Figure 3.6b). The results for the Fmoc-crosslinked and Fmoc-unlinked α-helical hairpin peptides are shown in Figure 3.7 and the parameters are listed in Table 3.4. These results are different from the α-helical hairpin without Fmoc. The results for Fmoc-crosslinked α-helical hairpin are unusual in that there are three peaks, with two peaks being roughly Gaussian and depicting type-I and type-II events at -31 pA and -74 pA respectively (Figure 3.7a). The peak centered between -40 and -50 pA may represent either N- or C-terminal entry into the pore or a different conformation. However, the number of events between -40 to -50 pA decreased for the Fmoc-unlinked form (Figure 3.7b). For the Fmoc-crosslinked α-helical hairpin, the ratio of type-II/type-I events was approximately 1:1. Upon the addition of TCEP this ratio increased to approximately 3:1. These results suggest that Fmoc-crosslinked and Fmoc-unlinked α-helical hairpins do interact with αHL pores and cause current blockade events of type-I and type-II.

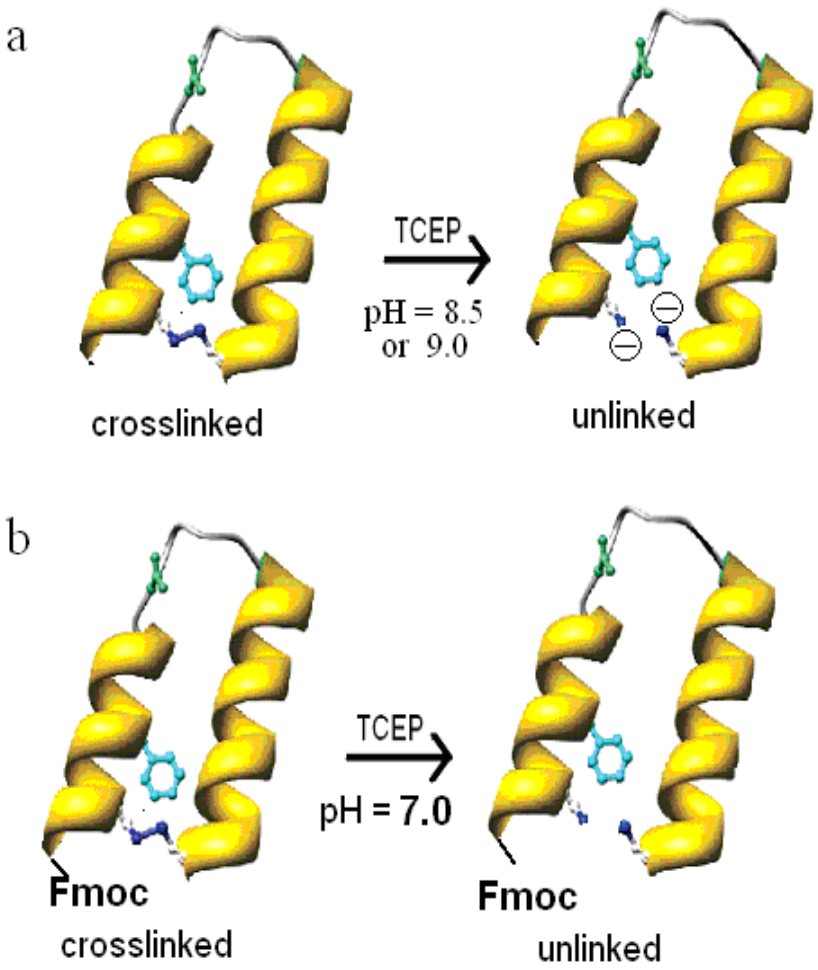

Figure 3.6 α-helical hairpins containing the disulfide link at Cys 5 & 34 shown in dark blue. (a) The reaction with TCEP at pH 8.5 and 9.0 gives a negative charge at Cys 5 and 34 in the unlinked hairpin. (b) The N-terminal of the α-helical hairpin is protected with Fmoc and when TCEP is added at pH 7.0, no charge is present in the unlinked peptide. Modified from Du and Gai, 2006. (Reprinted by permission from Du and Gai, 2006. Copyright 2006 American Chemical Society.)

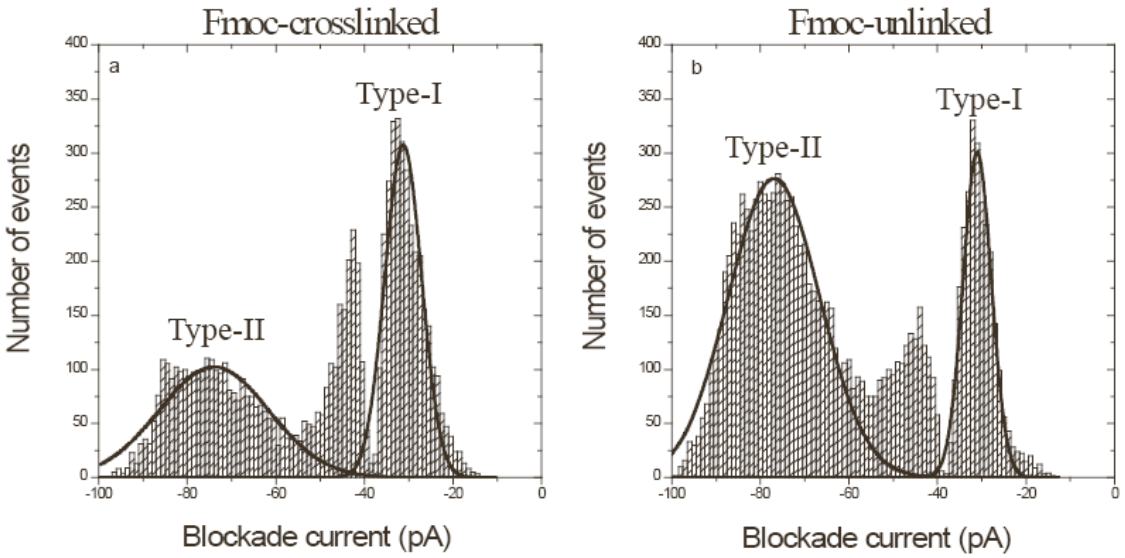

Figure 3.7 Current blockade histograms for the (a) Fmoc-crosslinked and (b) Fmoc-unlinked α-helical hairpin tested on αHL pores at pH 7.0. Parameters are presented in Table 3.4.

Table 3.4. Interaction parameters of the Fmoc-crosslinked and Fmoc-unlinked α-helical hairpin peptides at pH 7.0 [a].

Peptide	I_1 (pA)	I_2 (pA)	T_1 (ms)	T_2 (ms)	A_1	A_2	A_1/A_2	W_1	W_2
Fmoc-α-helical hairpin									
Fmoc-crosslinked	-31	-74	0.07	0.28	3173	3174	0.99	7.0	24.7
Fmoc-unlinked	-31	-77	0.07	0.24	2435	7130	0.34	6.2	20.5

[a] **I** is the current blockade and **T** is the time of blockade. The subscripts 1 and 2 refer to Type-I and Type-II event populations presented in Figure 3.7. $\mathbf{A_1}$ and $\mathbf{A_2}$ are the number of events of each population. $\mathbf{W_1}$ and $\mathbf{W_2}$ are the peak widths at half-height. (The error is estimated to be ±1 pA for **I** and ±10% for **T**).

3.3 Nanopore analysis of prion peptides and proteins

3.3.1 Introduction

The long term goal of this work was to develop an electrophoretic prion detector using αHL pores. The prion protein has been implicated in a number of neurodegenerative diseases, called transmissible spongiform encephalopathies (TSEs) (Prusiner, 2001; Cobb *et al*., 2009). In normal tissue, the prion protein is soluble and protease sensitive and the secondary structure is mostly α-helical (PrP^{C}). In the disease state, the protein aggregates and is insoluble, becomes protease resistant, and adopts a mostly β-sheet structure (PrP^{Sc}) (Morillas *et al*., 2001; Bennion *et al*., 2004;). The aggregated PrP^{Sc} eventually leads to neuronal apoptosis similar to other protein misfolding diseases such as Alzheimer's and Parkinson's disease (Chiti *et al*., 2006; Gaggelli *et al*., 2006; Lansbury *et al*., 2006;Uversky *et al*., 2008). In contrast to the latter, prion diseases are transmissible because PrP^{Sc} can cause the conversion of PrP^{C} to more PrP^{Sc} in an autocatalytic reaction (Saborio *et al*., 2001; Collinge *et al*., 2007; Castilla *et al*., 2008; Cobb *et al*., 2009). Although the incidence of the disease in humans is low, there is evidence that it can be transmitted by consuming infected meat from livestock (Prusiner, 2001). As well, there is no reliable pre-mortem test, and so the discovery of a single sick animal has led to the mandatory slaughter of the whole herd. Thus, the development of a simple diagnostic test for TSE before the occurrence of neurological symptoms is imperative.

First, we wanted to investigate if small peptides having α-helical and β-sheet sequences in prions would give specific signatures with nanopore analysis. Second, we wanted to investigate if the full length recombinant bovine prion protein (bPrP) gives type-I or type-II events. For this purpose, bPrP was analyzed at different voltages. In addition, bPrP was also analyzed in the presence of TCEP which reduced the disulfide bond in the protein, as well as EDTA a metal chelating agent which sequesters divalent metal ions. Experiments were also conducted using different orientations with respect to the location of the negative potential in the *cis* or *trans* side of the lipid bi-layer.

3.3.2 α-helical and β-sheet prion peptide analysis with α-hemolysin and aerolysin

Three peptides derived from bPrP: PrP(155-162):DYEDRYYR, PrP(145-162):Ac-DSRPLIHFGSDYEDRYYR that substituted M with D at position 145, and PrP(168-178):YPNQVYYRPMD that substituted V with M at position 177, were analyzed (bPrP

sequence from NCBI: P10279, gi130910). Peptides PrP(155-162) and PrP(145-162) contained the α-helical region 155-162, while peptide PrP(168-178) contained the β-strand segment 172-175. In addition, PrP(168-178) was also analyzed using an aerolysin pore.

Peptide PrP(155-162) has a net negative charge of -1 and the histogram of blockade current and time are shown in Figure 3.8 (a-d) and the parameters are listed in Table 3.5. PrP(155-162) is unusual in that it gives three peaks, with each peak being roughly Gaussian. The peak 1 in Figure 3.8a centered at -30 pA is due to type-I events, whereas peaks 2 and 3 which are centered at -50 pA and -60 pA are type-II events. The simplest explanation is that the peaks represent either N- or C-terminal entry to the pore or that the peptide can adopt two different conformations. The blockade current values for PrP(155-162) are not unreasonable as the peptide is only 8 amino acids in length and may not be able to form a stable α-helical structure as compared to the results obtained for the negatively charged Fmoc-α-helical peptides.

The acetylated PrP(145-162) is neutral and displayed two event populations that were fitted with Gaussian distributions [Figure 3.8 (e-g)]. Surprisingly, even though PrP(145-162) is only 18 amino acids in length, it showed a higher blockade current of -87 pA for type-II events. Also, for PrP(145-162) the blockade time for the type-II events was 0.23 ms compared to 0.01 ms recorded for the 18 amino acid long Ac-$D_2A_{14}K_2$.

The blockade current and time histograms for PrP(168-178) are shown in Figure 3.8 (h-k) and parameters in Table 3.5. At an applied voltage of 100 mV, the open current for αHL is 100 pA, whereas for aerolysin it is 50 pA. Analysis of PrP(168-178) with αHL displayed a single population of type-II events which was fitted with a Gaussian distribution. Again, surprisingly PrP(168-178) which contains only 11 amino acids showed a higher blockade current of -74 pA for the type-II events. However, when PrP(168-178) was analyzed with the aerolysin pore (Figure 3.8j), in addition to the type-II event population that was roughly Gaussian, a small increase in the number of bumping events were also seen.

3.3.3 Prion protein analysis with α-hemolysin

3.3.3.1 Nanopore analysis of bPrP at -50 mV, -100 mV and -150 mV

The full length bPrP, having a net charge of +8 at pH 7.8 and containing residues 25-242 with a C- terminal His5 tag, was analyzed. The protein was added to the *cis* side of the

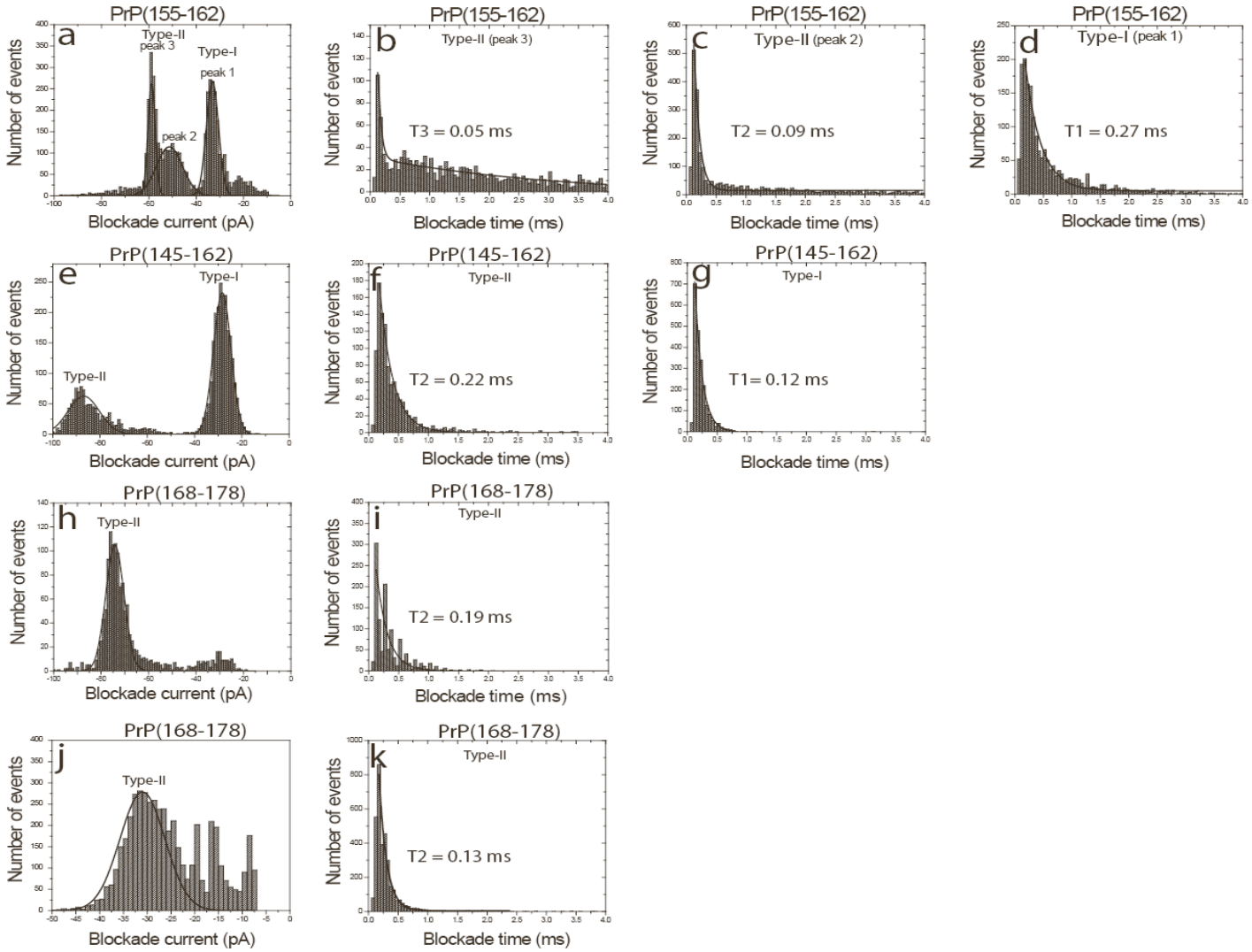

Figure 3.8 Current blockade histograms for prion peptides. (a) PrP(155-162), (e) PrP(145-162) contains the α-helical region and PrP(168-178) in (h) and (j) contains the β-sheet region in bovine prion protein. Peptides shown in histograms (a), (e) and (h) were tested on αHL pores while histogram (j) was tested on aerolysin. Histograms of blockade time are shown in (b-d), (f-g), (i) and (j). Parameters are presented in Table 3.5.

Table 3.5. Interaction parameters of the recombinant bovine prion peptides [a].

Peptide	I_1 (pA)	I_2 (pA)	I_3 (pA)	T_1 (ms)	T_2 (ms)	T_3 (ms)	A_1	A_2	A_3	A_1/A_2	W_1	W_2	W_3
(i) Tested with αHL													
PrP(155-162)	-33	-51	-59	0.27	0.09	0.05	1709	1571	1571	-	4.9	10.9	2.8
PrP(145-162)	-28	-	-87	0.12	-	0.22	2154	-	1040	2.07	7.2	-	13.1
PrP(168-178)	-	-	-74	-	-	0.19	-	-	1013	-	-	-	7.64
(ii) Tested with aerolysin													
PrP(168-178)	-	-	-31	-	-	0.13	-	-	3292	-	-	-	9.39

[a] **I** is the current blockade and **T** is the time of blockade. The subscripts 1 and 2, 3 refer to Type-I and Type-II events, respectively. The current blockade histograms are shown in Figure 3.8. A_1, A_2 and A_3 are the number of events of each population. W_1, W_2 and W_3 are the peak widths at half-height. (The error is estimated to be ±1 pA for **I** and ±10% for **T**).

chamber, which also contained the vestibule of αHL and the negative electrode. This type of analysis is defined as "vestibule up-stream" for positively charged molecules because any interactions with the pore will be diffusion-controlled (Figure 3.9). After the addition of the protein, a complete profile could be accumulated in approximately 3-4 hours (Figure 3.10). With a single pore insertion, the rate of data acquisition was slow. The histograms for the blockade current and time are shown in Figure 3.11 and the parameters are listed in Table 3.6. For αHL, the open pore current is directly proportional to the applied voltage. At -50 mV, very few translocations were observed (Figure 3.11a); presumably because the potential was not sufficiently large to unfold the protein even if it enters the vestibule of the pore. However at -100 mV (Figure 3.11b), bPrP displayed two events populations corresponding to type-I ($\mathbf{I_1}$= -27 pA) and type-II ($\mathbf{I_2}$= -65 pA) events which were fitted with a Gaussian distribution. The ratio of type-I ($\mathbf{A_1}$) to type-II ($\mathbf{A_2}$) events was 1.37:1 with approximately 42% being type-II events. This ratio decreased to 1.20:1 when EDTA was added (Figure 3.11d). At -150 mV (Figure 3.11c), bPrP still displayed two event populations, corresponding to type-I ($\mathbf{I_1}$=-39 pA) and type-II ($\mathbf{I_2}$= -102 pA) events which were fitted with a Gaussian distribution. The percentage of translocation events did not change significantly and only increased to 45%. Finally, no significant change was observed for bPrP in the presence of TCEP. Although translocation of such a large molecule may appear unlikely, further justification and a model for the type-II events are presented in section 4.3.1 and Figure 4.1c.

3.3.3.2 Analysis of bPrP, stem down-stream

After formation of stable pores in the lipid membrane, the protein was added to the *trans* side of the chamber, which contained the stem of αHL and also the positive electrode. bPrP has a net positive charge and thus will be driven through the pore when added to the *trans* side. This type of analysis is defined as "stem down-stream". The histograms of blockade current and time are shown in Figure 3.12 and the parameters are listed in Table 3.7. Again, bPrP displayed two events populations corresponding to type-I ($\mathbf{I_1}$= -27 pA) and type-II ($\mathbf{I_2}$= -71 pA) events which were fitted with a Gaussian distribution. The ratio of type-I ($\mathbf{A_1}$) to type-II ($\mathbf{A_2}$) events reduced to 0.85 as compared to 1.37 when analyzed vestibule up-stream. Also, the blockade time for bPrP when added stem down-stream was approximately twice as large compared to vestibule up-stream.

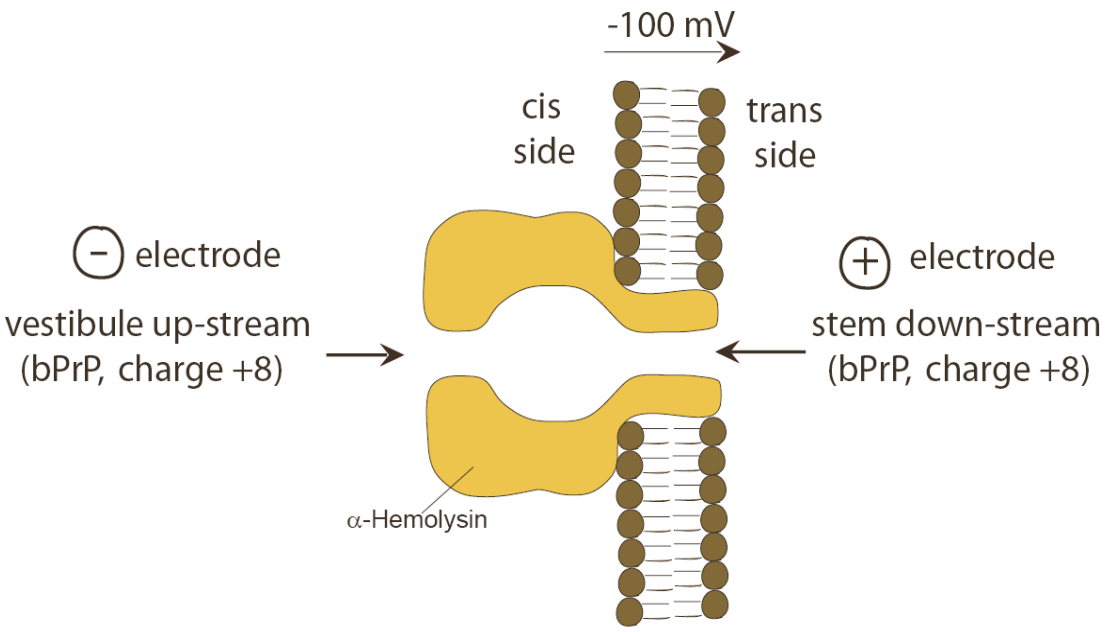

Figure 3.9 The α-hemolysin pore depicting vestibule up-stream and stem down-stream orientations for bPrP.

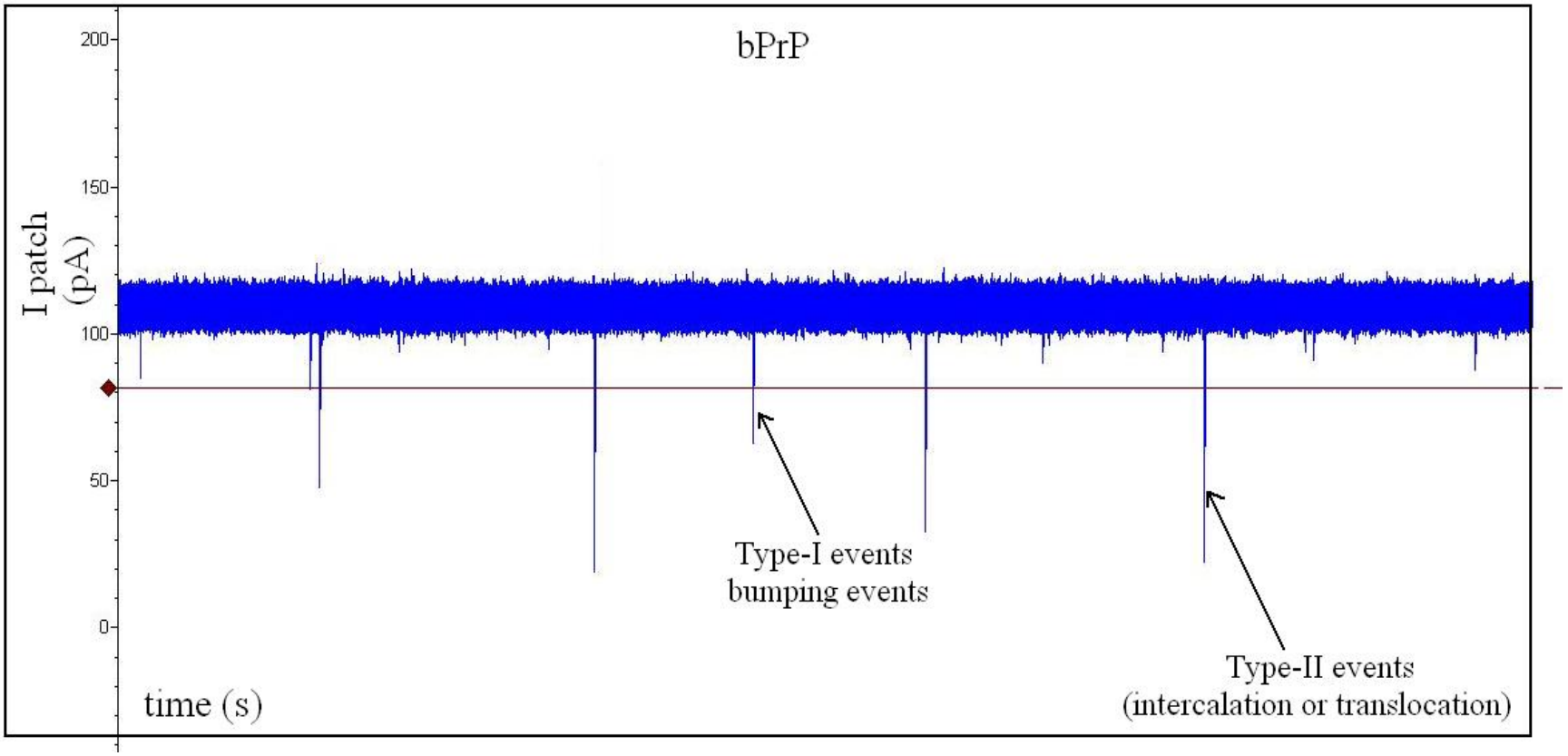

Figure 3.10 Current traces for bPrP with a single pore of αHL. Events are recorded for vestibule up-stream experiments. Typical type-I and type-II events are shown.

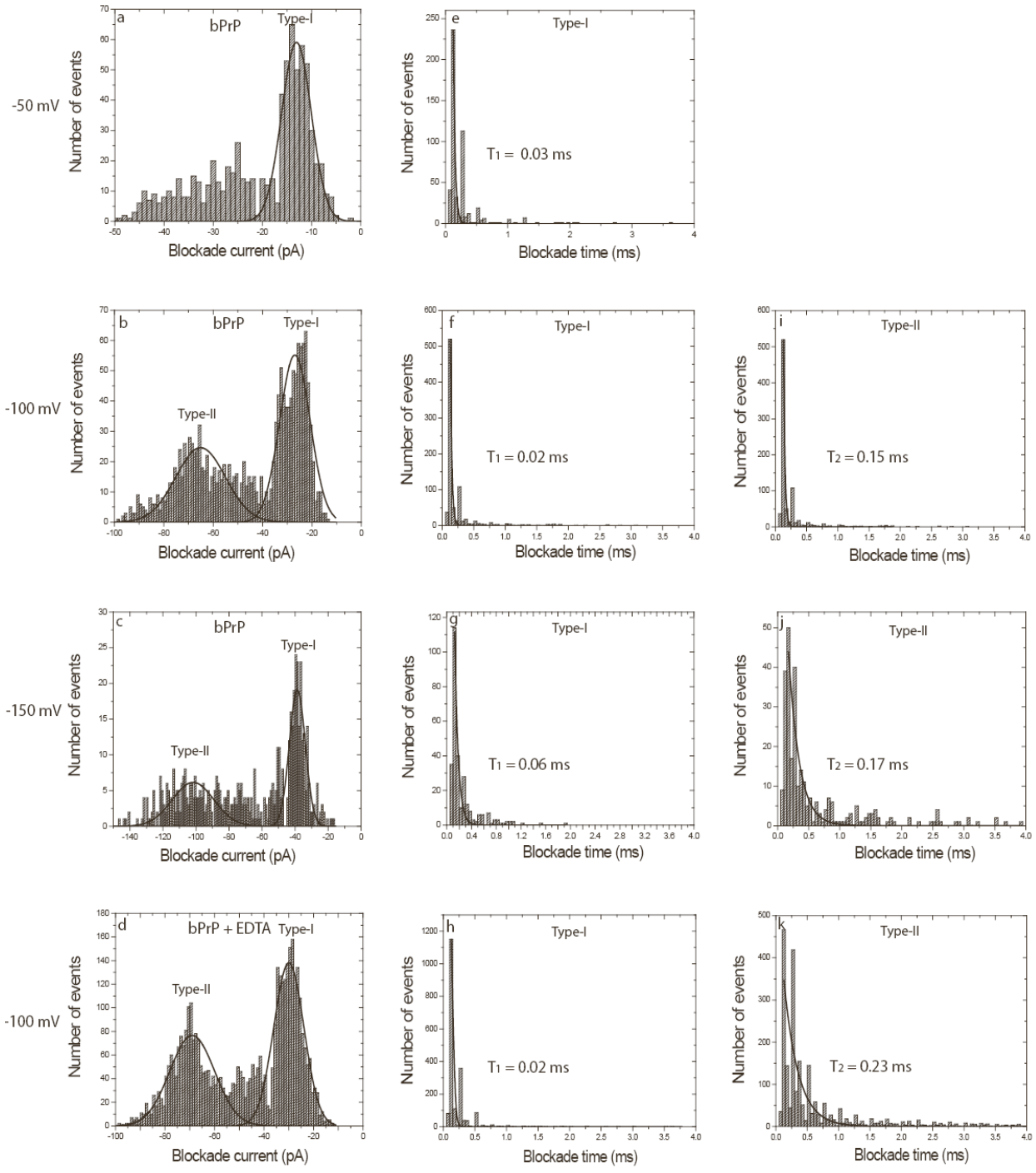

Figure 3.11 Current blockade histograms for bPrP added vestibule up-stream. (a) -50 mV, (b) -100mV, (c) -150mV, and (d) bPrP with EDTA at -100mV tested on αHL pores at pH 7.8. Histograms of blockade time are shown in (e), (f-i), (g-j), (i) and (h-kj). Parameters are presented in Table 3.6.

Table 3.6. Interaction parameters of the recombinant bovine prion protein [a].

Voltage (mV)	I_1 (pA)	I_2 (pA)	T_1 (ms)	T_2 (ms)	A_1	A_2	A_1/A_2	W_1	W_2
(i) bPrP (vestibule up-stream with *cis* side negative)									
-50	-13	-	0.03	-	446	-	-	5.9	-
-100	-27	-65	0.02	0.13	853	619	1.37	12.2	20.0
-150	-39	-102	0.06	0.17	230	193	1.19	9.2	25.0
(ii) bPrP + EDTA (vestibule up-stream with *cis* side negative)									
-100	-30	-69	0.02	0.23	2098	1735	1.20	12	18.0

[a] **I** is the current blockade and **T** is the time of blockade. The subscripts 1 and 2 refer to Type-I and Type-II event populations presented in Figure 3.11. $\mathbf{A_1}$ and $\mathbf{A_2}$ are the number of events of each population. $\mathbf{W_1}$ and $\mathbf{W_2}$ are the peak widths at half-height. (The error is estimated to be ±1 pA for **I** and ±10% for **T**).

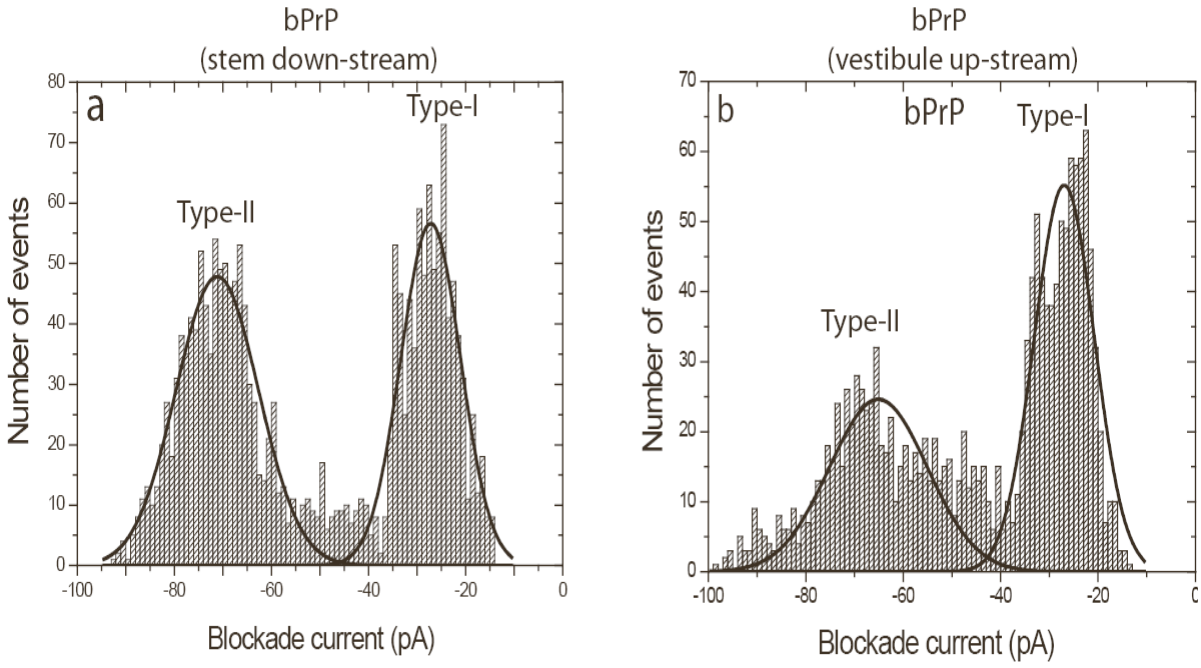

Figure 3.12 Current blockade histograms for bPrP at -100 mV at pH 7.8. (a) bPrP added stem down-stream. (b) bPrP added vestibule up-stream. Parameters are presented in Table 3.7.

Table 3.7 Interaction parameters of the recombinant bovine prion protein added stem down-stream and vestibule up-stream.

Voltage (mV)	I_1 (pA)	I_2 (pA)	T_1 (ms)	T_2 (ms)	A_1	A_2	A_1/A_2	W_1	W_2
Stem down-stream									
-100	-27	-71	0.06	0.29	873	1018	0.85	12.1	17.0
Vestibule up-stream									
-100	-27	-65	0.02	0.13	853	619	1.37	12.2	20.0

[a] **I** is the current blockade and **T** is the time of blockade. The subscripts 1 and 2 refer to Type-I and Type-II event populations presented in Figure 3.12. $\mathbf{A_1}$ and $\mathbf{A_2}$ are the number of events of each population. $\mathbf{W_1}$ and $\mathbf{W_2}$ are the peak widths at half-height. (The error is estimated to be ±1 pA for **I** and ±10% for **T**).

3.4 Analysis of the interaction of metal ions with prion protein

3.4.1 Introduction

The binding of metal ions to PrP^C has received considerable attention because there is evidence from multiple lines of research that it can cause changes in conformation (Todorova – Balvay *et al*., 2001;Quaglio *et al*., 2001; Burns *et al*., 2003; Morante *et al*., 2004; Leach *et al*., 2006). It has been shown that Cu(II) binding causes structural changes in PrP^C, suggesting that the misfolding and fibrillization of PrP^C may be profoundly influenced by the presence of Cu(II). The octapeptide repeat (residues 60-91 in human) is highly conserved and contains four tandem sequences of PHGGGWGQ. As many as six Cu(II) molecules can bind to human PrP^C, whereas two bind initially to His_{95} and His_{110}; these histidine residues are between the octapeptide repeats and the structured domain (Figure 3.13). The other four bind to His_{60}, His_{68}, His_{76}, and His_{84} at the four octapeptide repeat sequences (Viles *et al*., 2008). Elimination of this region does not prevent formation of PrP^{Sc}, but addition of further repeats increases the likelihood of the development of spontaneous TSE, confirming the region's importance in disease pathogenesis (Goldfarb *et al*., 1991; Croes *et al*., 2004).

The affinity for other divalent metal ions is reasonably lower (Stockel *et al*., 1998; Millhauser, 2004). Cu(II) binding to the octapeptide repeat may influence the folding of the C-terminal domain and cause self-association of the protein (Wells *et al*., 2006; Thompsett and Brown, 2007). The rationale for the experiments presented below was to demonstrate that the conformation of the prion protein can be modulated by binding divalent metal ions. Therefore, nanopore analysis of bPrP in the presence of Cu(II), Zn(II), Ni(II), and Mn(II))was carried out.

3.4.2 Nanopore detection of bPrP(25-242) with metal ions

An investigation of the effect of metal ions on bPrP is shown in Figure 3.14 and the results are summarized in Table 3.8. As described earlier, in the absence of metal ions, bPrP showed two distinct populations corresponding to type-I and type-II events (Figure 3.14a). Upon addition of Cu(II) (bPrP at 2.8 $\mu mol.L^{-1}$ and Cu(II) at 28 $\mu mol.L^{-1}$) the type-II events disappeared and the value of the blockade current for the type-I ($\mathbf{I_1}$) events decreases by about 7 pA. The bumping peak becomes much sharper as was observed previously for Zn(II) binding to a Zn-finger protein (Stefureac and Lee, 2008). However, the conformational change induced by Cu(II) was readily reversed by the addition of an excess of EDTA (Figure 3.14f). The addition of

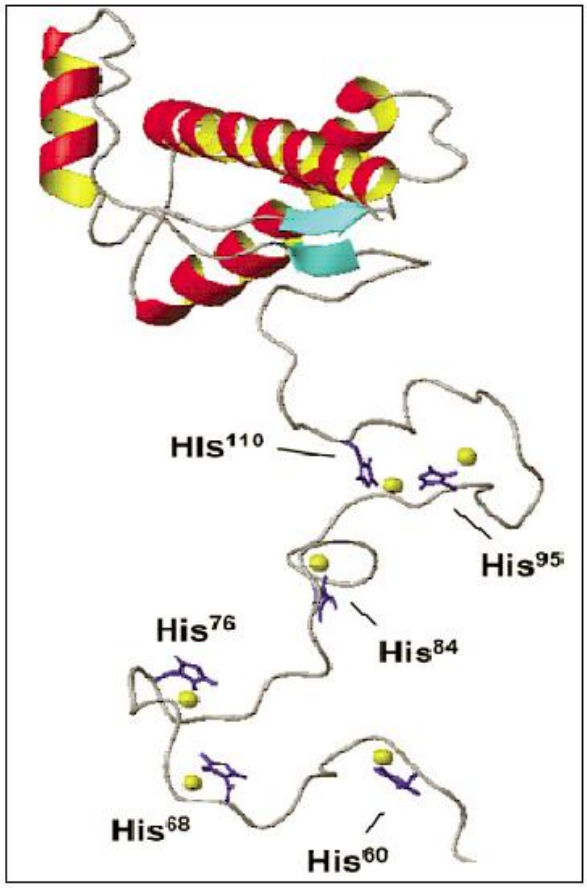

Figure 3.13 Human PrP^{C} structure with six Cu(II) binding sites. Residues 60-90 constitute the octarepeat regions and the structured helical region is from 126-231. (Reprinted by permission from Viles *et al*., 2008. Copyright 2008 The Biochemical Society)

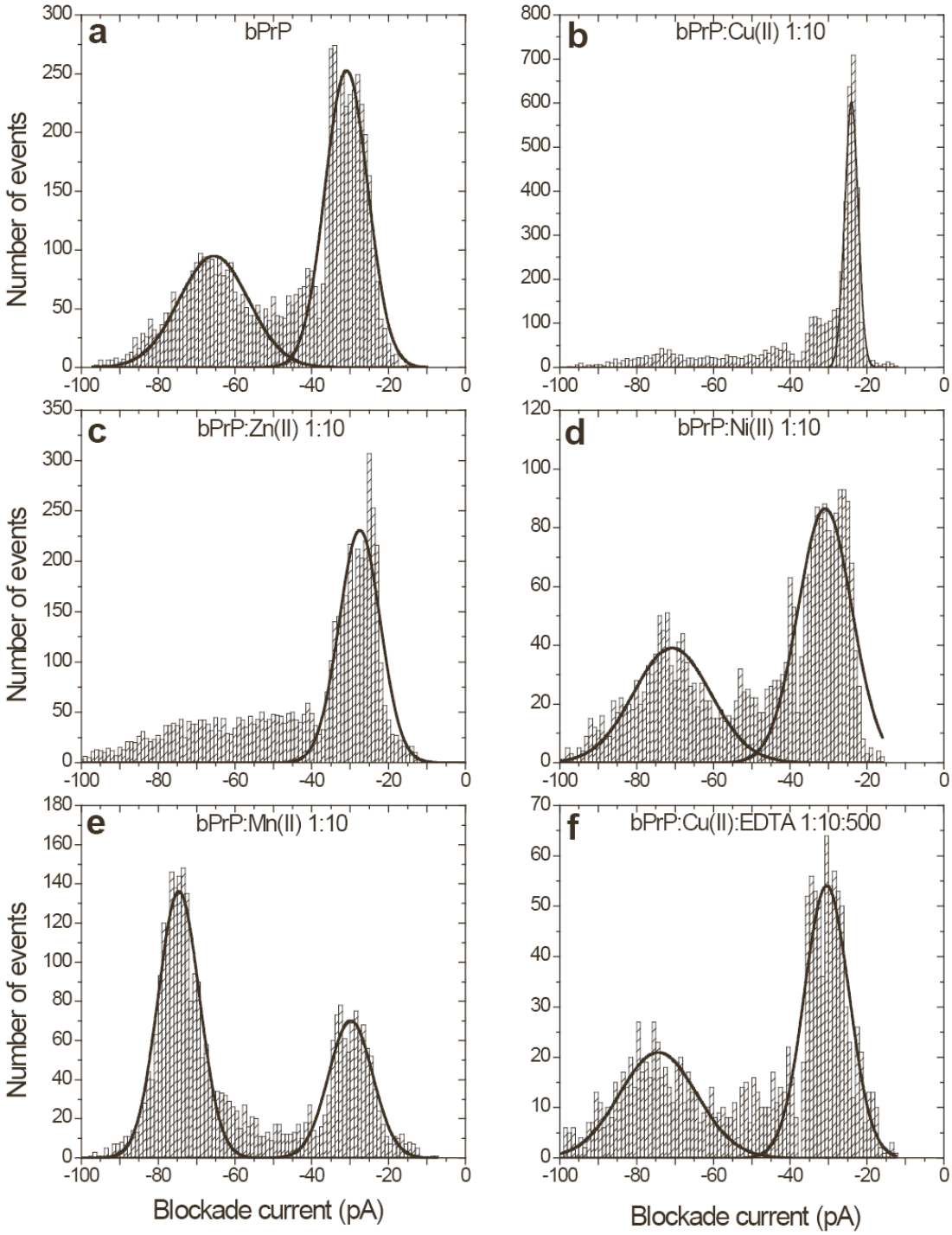

Figure 3.14 Current blockade histograms for metal prion interactions. (a) bPrP, (b) with Cu(II) 10 X, (c) with Zn(II) 10 X, (d) with Ni(II) 10 X, (e) with Mn(II) 10 X, and (f) after the addition of Cu(II), then EDTA. Parameters are stated in Table 3.8.

Table 3.8 Event parameters for bPrP and metal interactions[a].

Compound	I_1 (pA)	I_2 (pA)	T_1 (ms)	T_2 (ms)	A_1	A_2	A_2/A_1	W_1	W_2
bPrP	-31	-66	0.03	0.30	3524	2148	0.6	11.0	18.0
bPrP : Cu(II) 1:10	-24	-	0.20	-	2608	-	-	3.0	-
bPrP : Zn(II) 1:10	-28	-	0.12	-	3108	-	-	10.5	-
bPrP : Ni(II) 1:10	-31	-71	0.12	0.30	1519	983	0.6	13.9	20.0
bPrP : Mn(II) 1:10	-30	-75	0.03	0.29	1006	1839	1.8	11.3	10.6
bPrP:Cu(II):EDTA 1:10:500	-31	-74	0.02	0.20	788	527	0.7	11.5	20.0

[a] **I** is the current blockade and **T** is the time of blockade. The subscripts 1 and 2 refer to Type-I and Type-II event populations presented in Figure 3.1 4. **A_1 and A_2** are the number of events per pore per minute for each population. **W_1** and **W_2** are the peak widths at half-height. (The error is estimated to be ±1 pA for **I** and ±10% for **T**).

Zn(II) (Figure 3.14c) clearly decreases the proportion of type-II events, but the changes in the bumping peak are less pronounced than with Cu(II). The effect of Ni(II) (Figure 3.14d) was tested as a control because of the presence of the His-tag on the bPrP, but there was little change compared to Cu(II) or Zn(II). Surprisingly, the addition of Mn(II) (Figure 3.14e) caused a significant increase in the proportion of type-II events with the type-I ($\mathbf{A_1}$) to type-II ($\mathbf{A_2}$) ratio increasing from 0.6 to 1.8. Thus, Mn(II) appears to promotes translocation.

3.4.3 Dynamic light scattering of bPrP(25-242) with metal ions

Dynamic light scattering (DLS) experiments of bPrP in the presence of Cu(II) and Mn(II) was performed as stated in the Material and Methods section. The data were plotted on graphs having a y-axis of intensity (%) or mass (%) *vs* the logarithmic value of the hydrodynamic radius; log R_H (nm) as shown in Figure 3.15. The hydrodynamic radius, R_H, of bPrP particles at a concentration of 100 μg/mL was determined to be 2.55 nm with a molecular weight (Mw) of 29.09 kDa. In the presence of Cu(II), aggregation was observed with a R_H value of approximately 230.8 nm and a Mw ~ 2.30 X 10^7. Yet when Mn(II) was added, the value of R_H was 3.51 nm while the molecular weight was approximately 75.94 kDa, which was about twice the molecular weight of bPrP. The concentration of the divalent metal ions in these experiments was kept at least 10 times greater than that of the protein. The measurements observed for DLS indicate that the binding of Cu(II) to bPrP caused the hydrodynamic radii of bPrP to increase almost 75 fold while the presence of Mn(II) only changed the bPrP radii by 1 nm. These data support the results obtained with nanopore analysis.

3.5 Nanopore detection of antibody peptide interactions

3.5.1 Introduction

The next experiments were designed to identify distinct conformational changes that occurred due to complex formation between antibodies and peptides. For this purpose, the evolutionarily conserved C-terminal heptapeptide repeat domain sequence Tyr-Ser-Pro-Thr-Ser-Pro-Ser, of the largest subunit polypeptide (RPO21) of eukaryotic RNA polymerase II that binds to specific monoclonal antibodies developed in Lee's laboratory was used (Moyle *et al*., 1989). These monoclonal antibodies known as Jel351, Jel352, Jel354 and Jel355 inhibited the initiation of transcription from mammalian promoters *in vitro*.

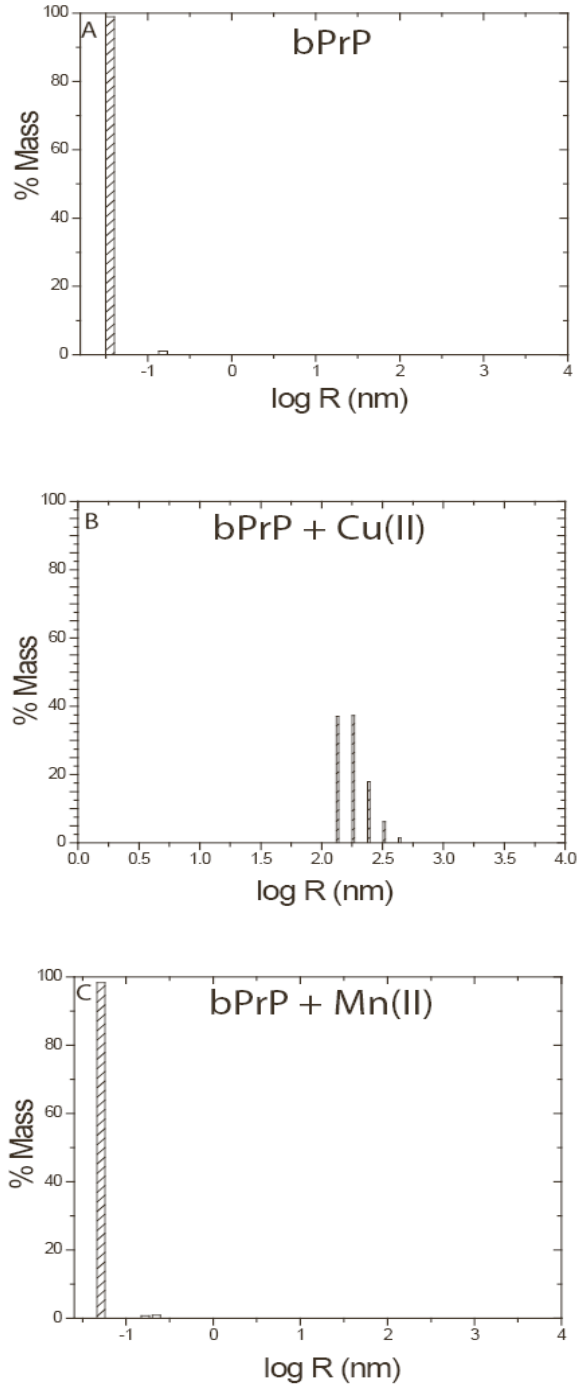

Figure 3.15 Dynamic light scattering measurements of bPrP. The x-axis and y-axis show the logarithmic value of the hydrodynamic radius, R_H *vs*. the percentage of mass. Graph (A), shows bPrP in the absence of metal ions. Graph (B) shows bPrP in the presence of Cu(II). Graph (C) shows bPrP in the presence of Mn(II).

3.5.2 Nanopore analysis of Jel352 and peptide RG23

Nanopore analysis is used as a novel method to investigate these interactions. The experiments presented below used a 23 residue peptide, RG23, which has a net charge of +1 at pH 7.8. Peptide RG23:RYSPTSPSYSPTSPSYSPTSPSG contains the sequence YSPTSPS which is the epitope for Jel352. The blockade current histograms for RG23 and a control peptide, PrP(168-178), are shown in Figure 3.16 and the parameters are listed in Table 3.9. Peptide RG23, showed a single Gaussian distribution of type-II events with a peak centered at -75 pA. On the addition of Jel352 at a peptide-to-antibody ratio of 2:1, the number of type-II events were reduced to approximately half with the new presence of an additional peak of type-I events (Figure 3.16b). The ratio for the type- I($\mathbf{A_1}$) to type-II ($\mathbf{A_2}$) was 0.85. The antibody by itself (Figure 3.16c) also gave rise to a number of events that were subtracted from the event profile of the complex (Figure 3.16d). Alternatively, the apparent events may be due to impurities within the antibody preparation. Intermediate ratios of antibody/peptide were also studied.

As a control, the same analysis was repeated with PrP(168-178), which does not contain the epitope for Jel352 (Figure 3.16f). It is clear from the event profile that no significant interaction can be detected, although there seemed to be a small increase in the number of type-II events, with almost double the peak width at half height (Table 3.9). In Figure 3.16g, the appearance of a negative bumping peak in addition to about a 30% decrease in the type-II events, suggested that the complex gave rise to fewer events.

3.6 Analysis of antibody prion interactions

3.6.1 Introduction

Although the concentration of PrP^{Sc} is highest in the brain, it is also found in lymphoid tissue, blood, urine, saliva, and milk (Soto, 2004; Grinkevich *et al*., 2005; Seeger *et al*., 2005; Sage, 2006). Thus, a non-invasive diagnostic test is possible but it would have to be extremely sensitive since the detection limit would have to be of the order of 100 molecules per ml of blood during the presymptomatic phase (Hill *et al*., 1997). The test would also have to be extremely specific since PrP^{C} is present on the surface of many cell types (Caughey and Baron, 2006). For this reason, several groups have explored the use of antibodies which can distinguish between PrP^{C} and PrP^{Sc} based upon the exposure of different epitopes in the two forms (Demart *et al*.,

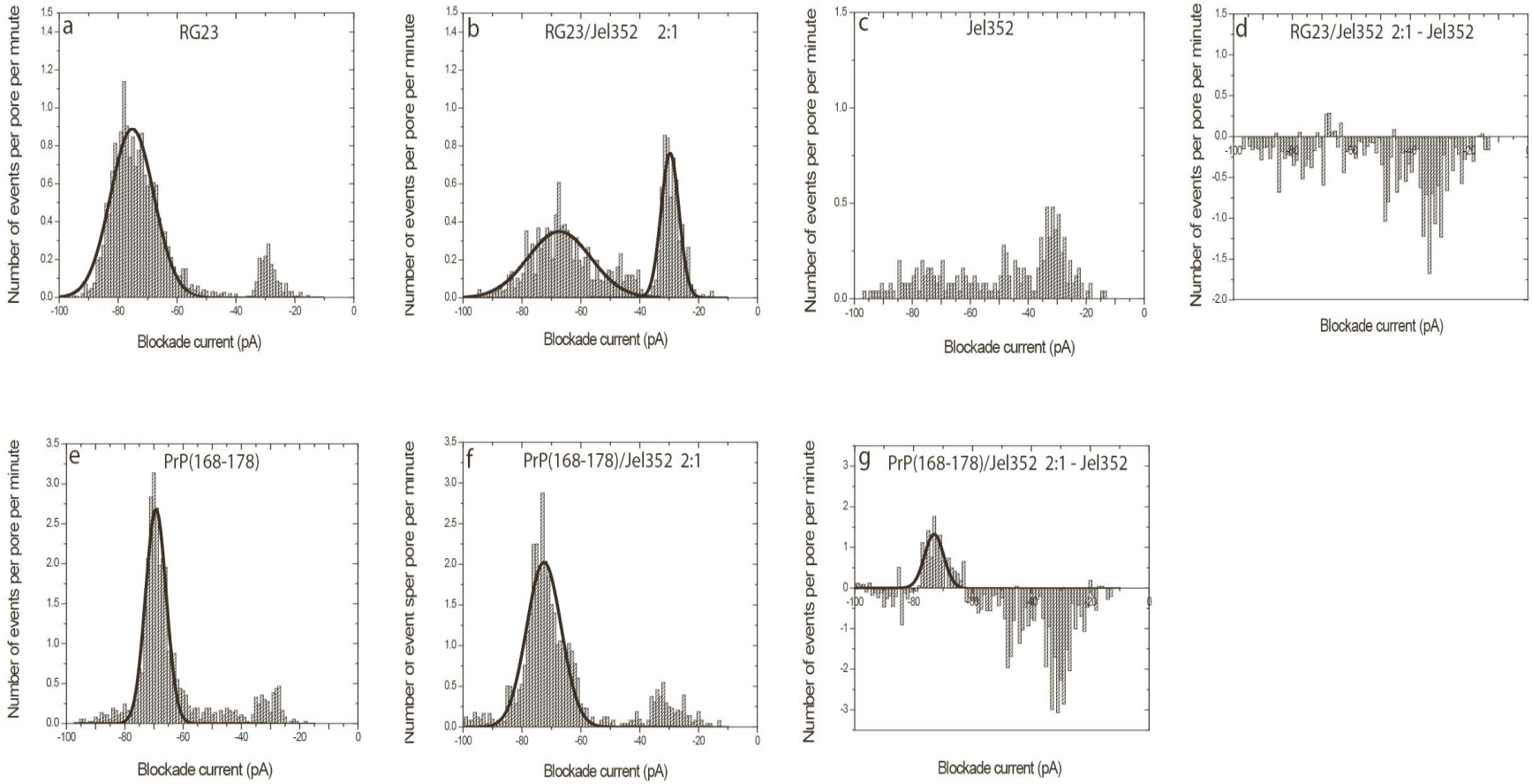

Figure 3.16 Current blockade histograms for peptide and Jel352 interactions. (a)RG23; (b) RG23 with Jel352, 2:1 ratio; (c) Jel352 alone; (d) subtraction of Jel352 from panel (b); (e) PrP(168-178); (f) PrP(168-178) with Jel352, 2:1 ratio; (g) subtraction of Jel352 from panel(f). Parameters are presented in Table 3.9.

Table 3.9 Event parameters for RG23, RG23/Jel352 complex, PrP(168-178), and PrP(168-178)/Jel352 complex[a]

Compound	I_1 (pA)	I_2 (pA)	T_1 (ms)	T_2 (ms)	A_1	A_2	A_1/A_2	W_1	W_2
RG23	-	-75	-	0.16	1.6	16.4	0.09	-	14.6
RG23/Jel352 2:1	-30	-67	0.06	0.12	7.2	8.4	0.85	5.9	21.3
PrP(168-178)	-	-70	-	0.26	-	27.6	-	-	6.7
PrP(168-178)/Jel352 2:1	-	-72	-	0.22	-	32.1	-	-	11.6

[a] **I** is the current blockade and **T** is the time of blockade. The subscripts 1 and 2 refer to Type-I and Type-II event populations presented in Figure 3.16. **A_1 and A_2** are the number of events per pore per minute for each population. **W_1** and **W_2** are the peak widths at half-height. (The error is estimated to be ±1 pA for **I** and ±10% for **T**).

1999; Paramithiotis *et al*., 2003; Andrievskaia *et al*., 2006; Polymenidou *et al*., 2008). One promising epitope is VYYRP, residues 171-175 in the bovine sequence, which is buried in PrP^{C} but is available as part of an exposed β-sheet in PrP^{SC} (Paramithiotis *et al*., 2003). There is also evidence that antibodies can be used therapeutically by blocking conversion or helping to clear PrP^{SC} from infected cells (Heppner *et al*., 2001; Antonyuk *et al*., 2009).

The next set of experiments was designed to identify distinct conformational changes that occurred due to complex formation between antibodies and prion peptides and proteins. Previous work with peptides showed that the parameters **I** and **T** are dependent on many factors such as length, charge, hydrophobicity, and even the dipole moment of the peptide (Sutherland *et al.*, 2004b; Stefureac *et al*., 2006; Wolfe *et al* ., 2007; Movileanu, 2008;). In addition, conformational changes can be detected (Goodrich *et al*., 2007; Stefureac and Lee, 2008). For example, in the absence of metal ions, Zn-finger peptides can readily translocate, but upon binding Zn(II) the peptide folds into a rigid conformation which is now too large to pass through the pore (Stefureac and Lee, 2008). Similarly, larger molecular complexes have been studied using solid state pores. For example, when an antibody Fab fragment binds to its target, the current blockade increases so that the free and bound forms can be distinguished (Siwy *et al*., 2005; Dekker, 2007; Hurt *et al*., 2009). Here we provide evidence that PrP^{C} can also give type-II events, even though it contains a disulphide bond (see Section 3.3.3). However, as shown in Figure 3.17, the type-II events for the prion peptide or protein are eliminated upon binding antibody so that antibody specificity can still be investigated. It has been shown previously that both β-hairpins and disulphide-linked Fmoc-α-helical hairpins can give type-II events, suggesting that a single disulphide bond is not sufficient to prevent type-II events (Goodrich *et al*., 2007 and results in section 3.2).

3.6.2 Nanopore detection of PrP(145-162) with antibody M2188

A novel detection method for antibody prion interactions that use αHL pores was investigated. Peptide PrP(145-162) containing epitope SRPLIHFG for antibody M2188 (IgG) was analyzed. Nanopore detection of antibody prion interactions were analyzed as described in the Materials and Methods section. At these concentrations, a complete profile could be accumulated in approximately 2-3 hours. The histograms of blockade current for PrP(145-162)

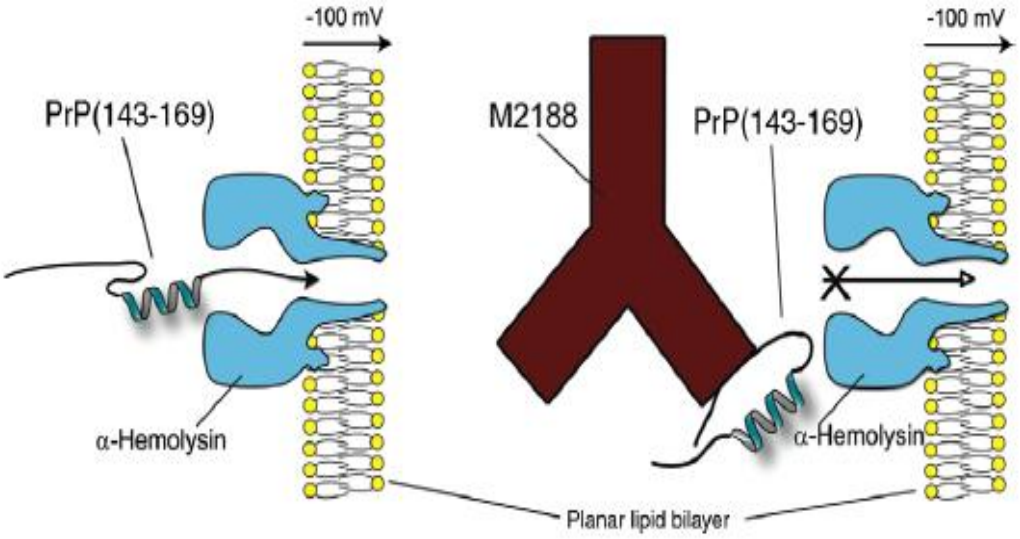

Figure 3.17 Antibody binding to a peptide will prevent translocation. The antibody is not drawn to scale.

with and without M2188 are shown in Figure 3.18 and parameters are listed in Table 3.10. In an attempt to conserve antibody, lower concentration of peptide was used. The results for PrP(145-162) was previously explained in detail in section 3.3.2 (Figure 3.18a). On the addition of antibody M2188 (Figures 3.18b-e) at a peptide-to-immunoglobulin G (IgG) ratio of 256:1, 128:1, 64:1 and 32:1, only type-I events were observed. For PrP(145-162), the total number of events per pore per minute was 163. In the presence of M2188, at a peptide-to-IgG ratio of 256:1, 128:1, 64:1, and 32:1 this number changed to 119, 110, 85, and 52, respectively. The results obtained for PrP(145-162) are unusual, due to the high drop in the number of events at low concentrations of M2188. For example, only a 6% reduction in the total number of events is expected at a peptide-to-IgG ratio of 32:1, assuming the antibody has two binding sites. However, at this ratio a ~ 68% reduction in the total number of events was observed. To address this problem a different peptide was analyzed.

3.6.3 Nanopore detection of PrP(143-169) and PrP(168-178) with antibody M2188

PrP(143-169):SAMSRPLIHFGNDYEDRYYRENMYRYP (the epitope for antibody M2188 is underlined) with a net charge of +1 was analyzed. As a control, the same analysis was repeated with PrP(168-178):YPNQVYYRPMD having a net charge of zero, which does not contain the epitope for antibody M2188. For PrP(143-169), a complete profile could be accumulated in about one hour. Typical traces for PrP(143-169) with and without antibody are shown in Figure 3.19. The histogram of blockade current for PrP(143-169) is shown in Figure 3.20A and the event parameters are listed in Table 3.11. Also, the histograms of blockade duration are presented in Figure 3.21. PrP(143-169) is unusual in that it gives three peaks, with each peak being roughly Gaussian. As shown previously, the peak centered at – 30 pA is due to bumping events whereas those at -50 pA and -80 pA are type-II events. The simplest explanation is that the peaks represent either N- or C-terminal entry to the pore or two different conformations. Currently, these possibilities cannot be distinguished. On the addition of antibody M2188 (Figure 3.20B) at a ratio of 2:1 (peptide: M2188), the number of events is reduced and no clear peak for the type-II events can be discerned. The antibody by itself (see Figure 3.23C in section 3.6.4) also gave rise to a significant number of events that were subtracted from the event profile of the complex (Figure 3.20C). In this case, the average number of type-II events was reduced even further, although the event profile in the bumping

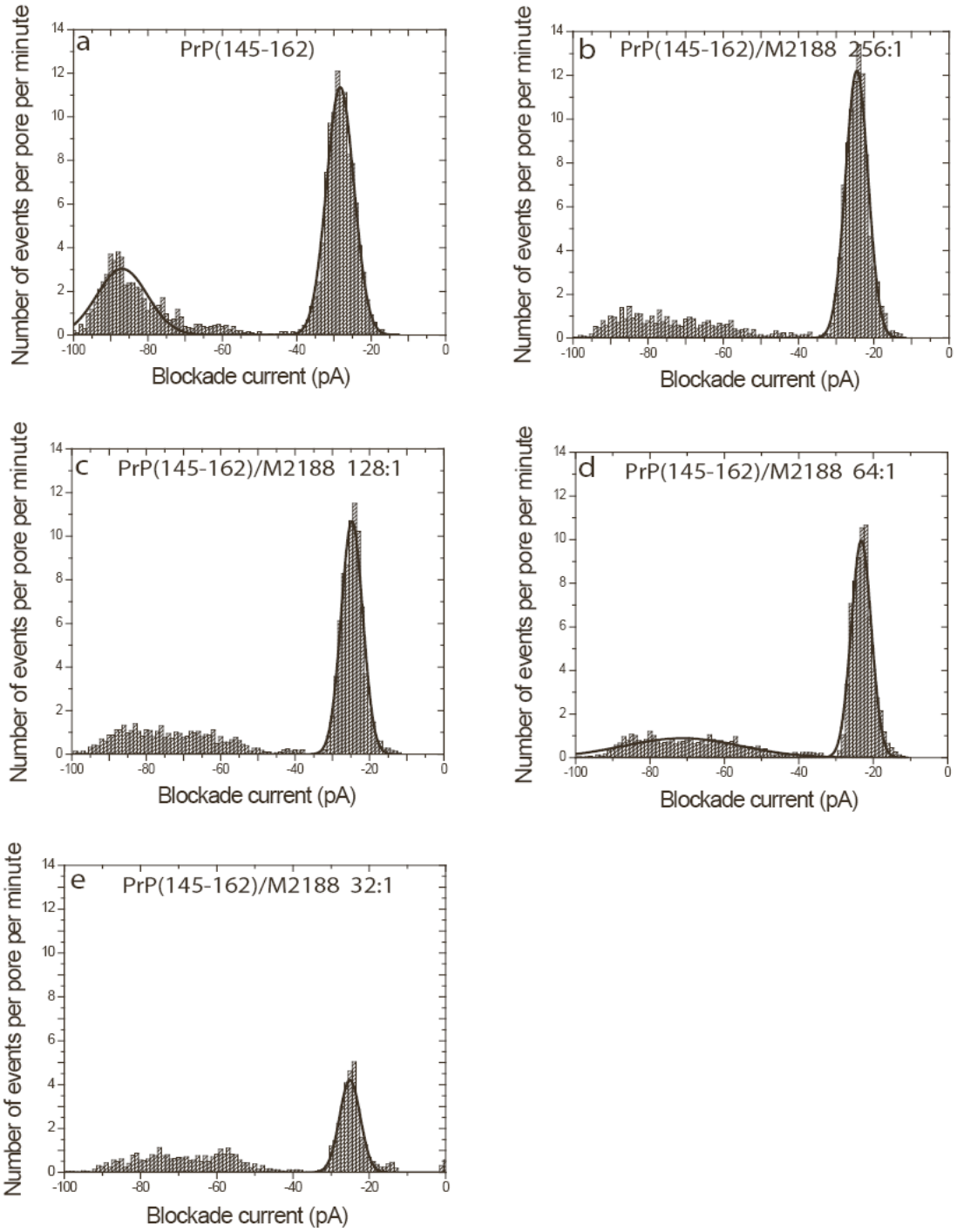

Figure 3.18 Current blockade histograms for PrP(145-162) and M2188 interactions. (a) PrP(145-162); (b) PrP(145-162) with M2188, 256:1 ratio: (c) PrP(145-162) with M2188, 128:1 ratio; (d) PrP(145-162) with M2188, 64:1 ratio; (e) PrP(145-162) with M2188, 32:1 ratio tested on αHL pores at pH 7.8. Parameters are presented in Table 3.10.

Table 3.10 Event parameters for PrP(145-162) and PrP(145-162)/M2188 complex[a].

Compound	I_1 (pA)	I_2 (pA)	T_1 (ms)	T_2 (ms)	A_1	A_2	W_1	W_2
PrP(145-162)	-28	-87	0.12	0.22	106	57	7.2	13.1
PrP(145-162)/M2188 256:1	-25	-	0.11	-	89	-	5.5	-
PrP(145-162)/M2188 128:1	-25	-	0.12	-	75	-	5.6	-
PrP(145-162)/M2188 64:1	-24	-	0.11	-	65	-	5.1	-
PrP(145-162)/M2188 32:1	-25	-	0.11	-	28	-	4.9	-

[a] **I** is the current blockade and **T** is the time of blockade. The subscripts 1 and 2 refer to Type-I and Type-II event populations presented in Figure 3.18. $\mathbf{A_1}$ and $\mathbf{A_2}$ are the number of events per pore per minute for each population. $\mathbf{W_1}$, and $\mathbf{W_2}$ are the peak widths at half-height. (The error is estimated to be ±1 pA for **I** and ±10% for **T**).

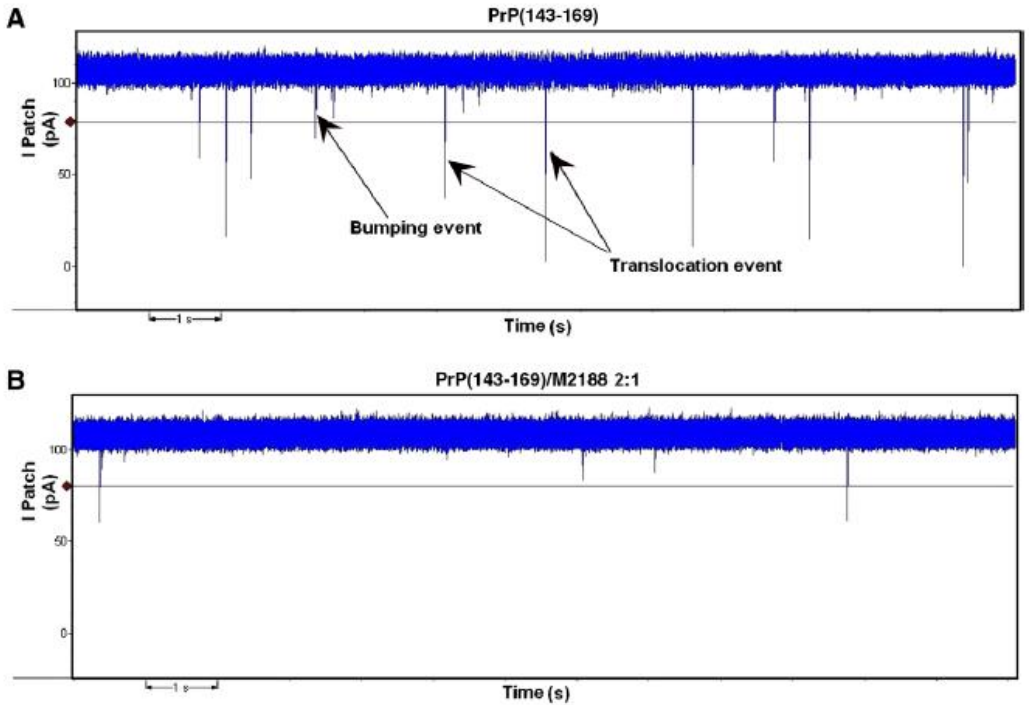

Figure 3.19 Current traces for PrP(143-169) without antibody (A) and with antibody (B). Typical bumping and translocation events are indicated. In the presence of antibody, the event frequency is decreased and those events that do occur are mostly bumping.

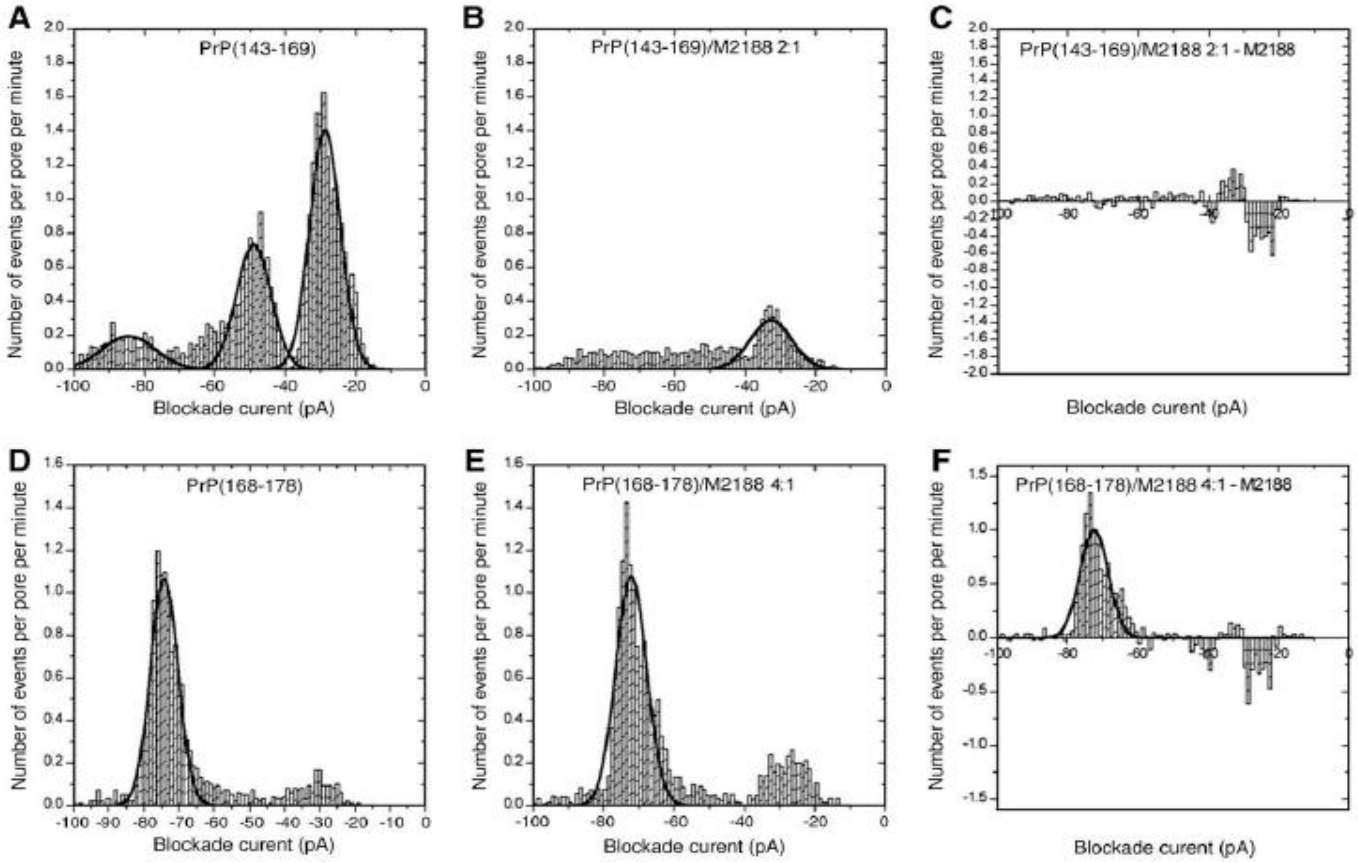

Figure 3.20 Current blockade histograms for prion peptide and M2188 interactions. (A) PrP(143-169); (B) PrP(143-169) with M2188, 2:1 ratio; (C) subtraction of M2188 from panel B; (D) PrP(168-178); (E) PrP(168-178) with M2188,4:1 ratio; (F) subtraction of M2188 from panel E. Parameters are presented in Table 3.11.

Table 3.11 Event parameters for PrP(143-169), PrP(143-169)/M2188 complex, PrP(168-178), and PrP(168-178)/M2188 complex[a]

Compound	I_1 (pA)	I_2 (pA)	I_3 (pA)	T_1 (ms)	T_2 (ms)	T_3 (ms)	A_1	A_2	A_3	W_1	W_2	W_3
PrP(143-169)	-29	-49	-84	0.16	0.25	0.41	15.6	9.6	4.3	8.5	9.6	15.0
PrP(143-169)/M2188 2:1	-32	-	-	0.02	-	-	3.7	-	-	11.7	-	-
PrP(168-178)	-	-	-74	-	-	0.19	-	-	12.0	-	-	7.6
PrP(168-178)/M2188 4:1	-	-	-72	-	-	0.27	-	-	13.5	-	-	8.5

[a] **I** is the current blockade and **T** is the time of blockade. The subscript 1 and 2, 3 refer to type-I and Type-II events, respectively. Event populations are presented in Figure 3.20. $\mathbf{A_1}$, $\mathbf{A_2}$ and $\mathbf{A_3}$ are the number of events per pore per minute for each population. $\mathbf{W_1}$, $\mathbf{W_2}$ and $\mathbf{W_3}$ are the peak widths at half -height. (The error is estimated to be ±1 pA for **I** and ±10% for **T**).

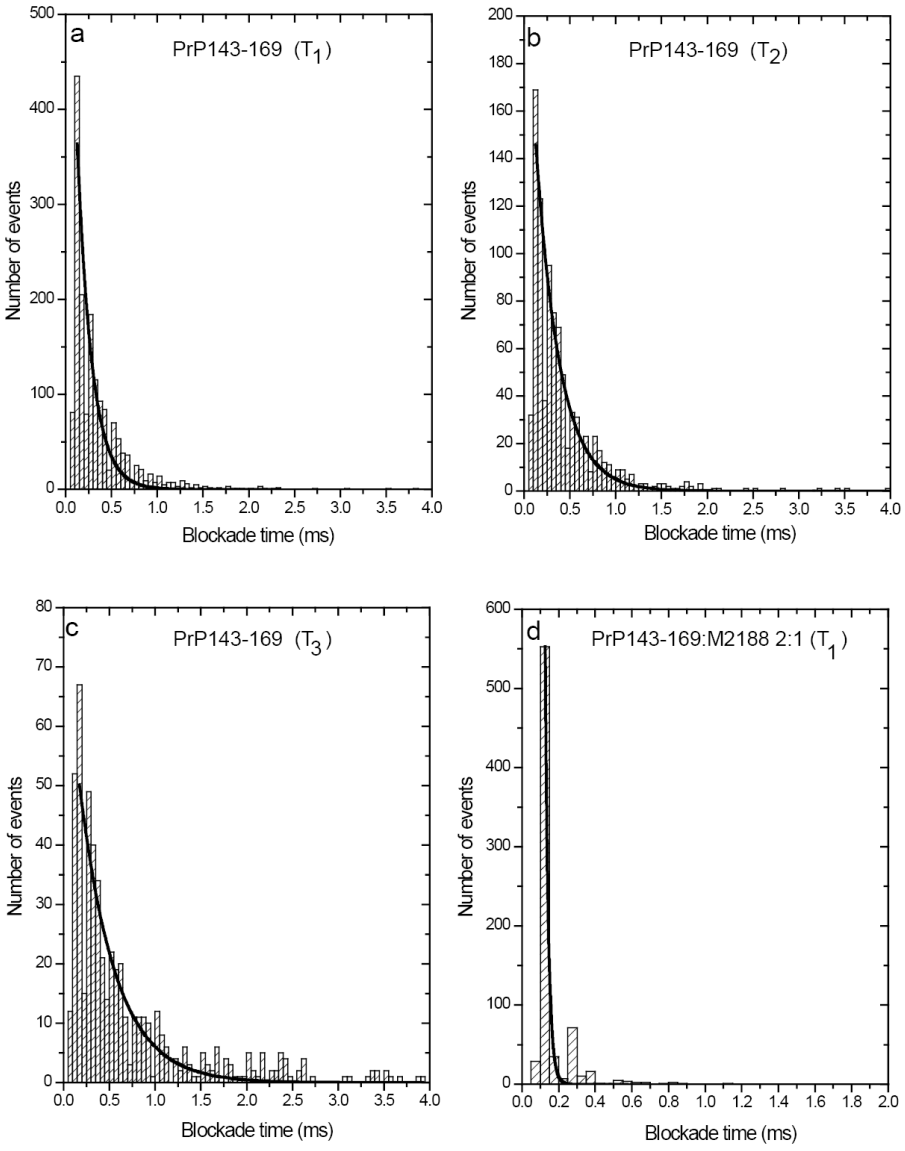

Figure 3.21 Histograms of blockade times for PrP(143-169). (a) PrP(143-169) peak 1, (b) PrP(143-169) peak 2, (c)PrP(143-169) peak 3, and (d) peak 1 with antibody. The best fit single exponential is shown. The values are listed in Table 3.10.

region appears to be more complex.

PrP(168-178), which does not contain the epitope for antibody M2188, was analyzed (Figures 3.20D-F). It is clear from the event profiles that no significant interaction was detected, although there appeared to be a small increase in the blockade time for the type-II events (Table 3.11). Intermediate ratios of antibody/peptide were also studied and the results are summarized in Figure 3.22. No significant change in the number of events was detected with PrP(168-178), whereas the total number of events was reduced to approximately 12% at the highest ratio of antibody with PrP(143-169).

3.6.4 Nanopore detection of bPrP(25-242) with antibody M2188

Experiments with the full-length bPrP are shown in Figure 3.23A and the event parameters are listed in Table 3.12. The peak centered at −65 pA, which is due to type-II events, is much broader than that for the peptide; this may be caused by different orientations of the protein as it enters the pore or different modes of unfolding as it passes through the pore. The ratio of the type-II ($\mathbf{A_2}$) to type-I ($\mathbf{A_1}$) events is approximately 1:2. On the addition of antibody, no clear peak for the type-II events can be seen and the ratio of type-II ($\mathbf{A_2}$) to type-I ($\mathbf{A_1}$) events decreases to approximately 1:10. Compared with the PrP peptides, the total number of events per pore per minute is much lower and so subtraction of the control with antibody alone (Figure 3.23C) is more important. The antibody alone shows a sharp bumping peak at approximately −24 pA and a few events with blockade currents above −40 pA. It seems very unlikely that the latter represent type-II events of the antibody because it is an order of magnitude larger than the pore and contains multiple, very stable β-sheet domains with several disulfide bonds. Alternatively, the apparent type-II events may be due to impurities within the antibody preparation. After subtraction (Figure 3.23D), the average number of events with a blockade current above −30 pA is insignificant, but there is now a large negative bumping peak between -20 pA and -30 pA.

3.6.5 Nanopore detection of peptides SN4 and PrP(168-178) with antibody SN4Ab

The interaction of peptide SN4 and PrP(168-178) with antibody SN4Ab were analyzed. Peptide SN4 contained six copies of epitope ^{172}VYYRP^{176} compared to a single copy in PrP(168-178). SN4Ab binds residue ^{172}VYYRP^{176} which is blocked in PrP^{C} but available in

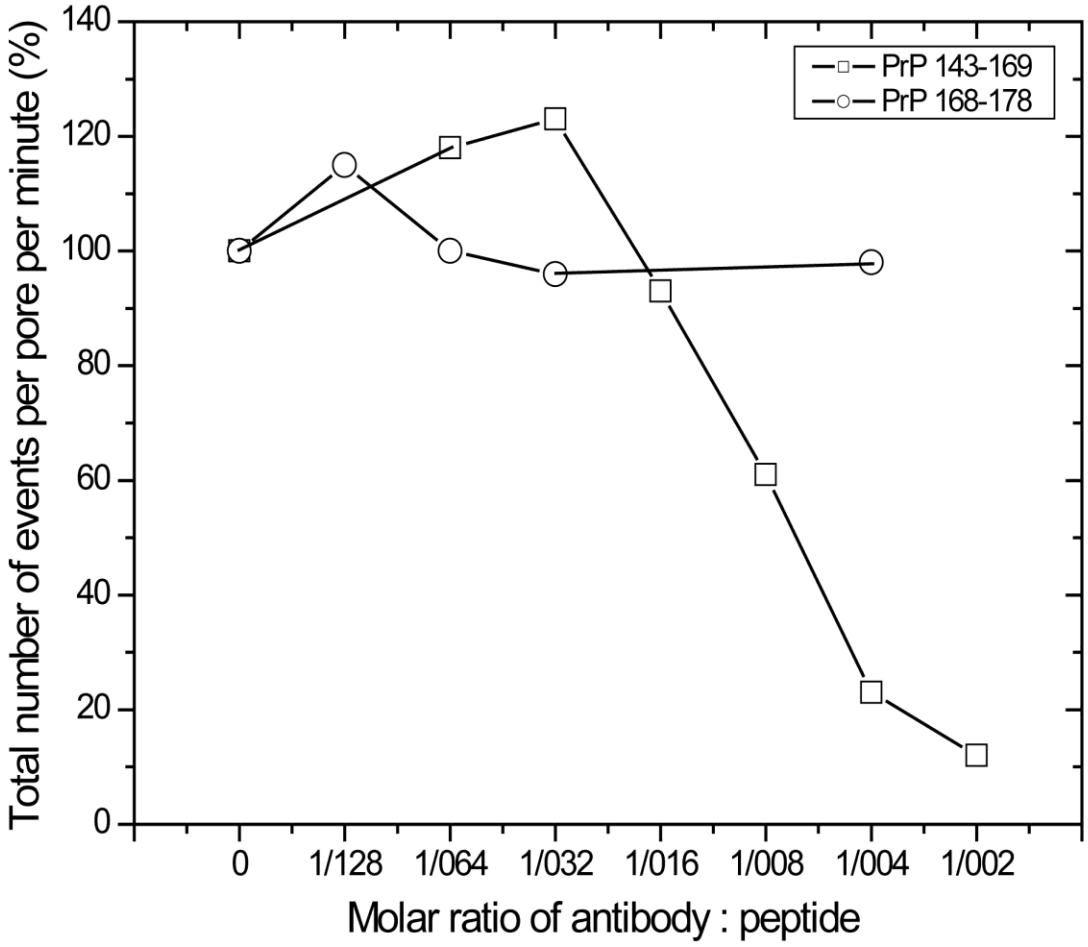

Figure 3.22 Numbers of translocation events as a function of antibody (M2188): peptide ratio for the two peptides. To conserve antibody, only single experiments were performed for each ratio. In the absence of antibody, the reproducibility was estimated to be ± 20%.

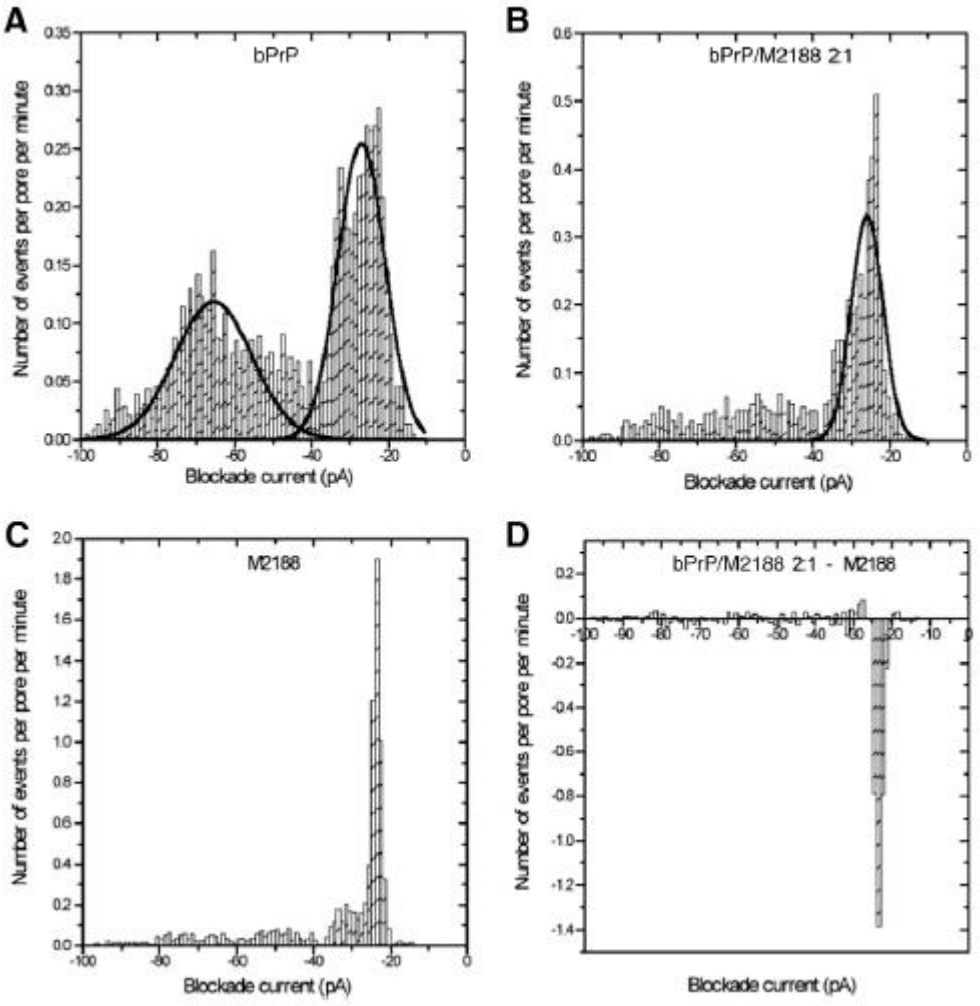

Figure 3.23 Current blockade histograms for prion protein and M2188 interactions. (A) bPrP, (B) bPrP with M2188 at a 2:1 ratio, (C) M2188 alone, and (D) subtraction of panel C from panel B. The values are listed in Table 3.12.

Table 3.12 Event parameters for bPrP,bPrP/M2188 complex, and M2188[a]

Compound	I_1 (pA)	I_2 (pA)	T_1 (ms)	T_2 (ms)	A_1	A_2	W_1	W_2
bPrP	-27	-65	0.02	0.15	3.7	3.4	12.2	20.0
bPrP/M2188 2:1	-26	-	0.19	-	3.5	-	8.0	-
M2188	-23	-	0.12	-	6.6	-	2.1	-

[a] **I** is the current blockade and **T** is the time of blockade. The subscripts 1 and 2 refer to Type-I and Type-II event populations presented in Figure 3.23. $\mathbf{A_1}$ and $\mathbf{A_2}$ are the number of events per pore per minute for each population. $\mathbf{W_1}$ and $\mathbf{W_2}$ are the peak widths at half-height. (The error is estimated to be ±1 pA for **I** and ±10% for **T**).

PrP^{Sc}. The results for peptides SN4 and PrP(168-178) are shown in Figure 3.24 and the parameters are present in Table 3.13. In the absence of antibody, PrP(168-178) displayed a single population of type-II events with a peak centered at -74 pA. On the addition of antibody SN4Ab (Figure 3.24b) at a peptide-to-antibody ratio of 2:1, the number of type-II events were reduced by ~ 55%, after the background for antibody was subtracted (Figure 3.24c). The antibody alone shows bumping events, at approximately −30 pA and a few events with blockade currents above −40 pA (Figure 3.24c). Alternatively, the apparent events may be due to impurities within the antibody preparation as proposed earlier in section 3.5.2. Peptide SN4 has a net charge of +6 and is 38 amino acids in length. Peptide SN4 displayed two event populations of type-I and type-II events with peaks centered at -28 pA and -71 pA, respectively. On the addition of antibody SN4Ab, (Figure 3.24e) at a peptide-to-antibody ratio of 2:1, the number of events was reduced and no clear peak for the type-II events was discerned. Also, the number of type-I events was increased by 36%. The bumping peak became much sharper as was observed previously for the prion and Cu(II) interactions.

3.6.6 Nanopore detection of bPrP(25-242) with antibody SN4Ab

Experiments with the full-length bPrP are shown in Figure 3.25 and the parameters are listed in Table 3.14. The results for bPrP as seen previously, displayed two event populations of type-I and type-II events with peaks centered at -31 pA and -68 pA, respectively (Figure 3.25a). On the addition of antibody SN4Ab (Figure 3.25b) at a protein-to-antibody ratio of 2:1, the blockade current for the type-II events increased to -79 pA while the ratio for the type-II ($\mathbf{A_2}$) to type-I ($\mathbf{A_1}$) events did not change. The number of type-II and type-I events was reduced by 23% and 70%, respectively, after subtraction of the control with antibody alone (Figure 3.25c).

3.7 Analysis of antibody interactions with the unfolded prion protein

3.7.1 Introduction

Recently it has been demonstrated that proteins can translocate the αHL pore, especially in the presence of denaturing agents which aid in protein unfolding (Oukhaled *et al*., 2007; Stefureac *et al*., 2008). The rationale for the experiments presented below was to study conformational changes that occurred in bPrP(25-242) in the presence of Gdn-HCl. Furthermore,

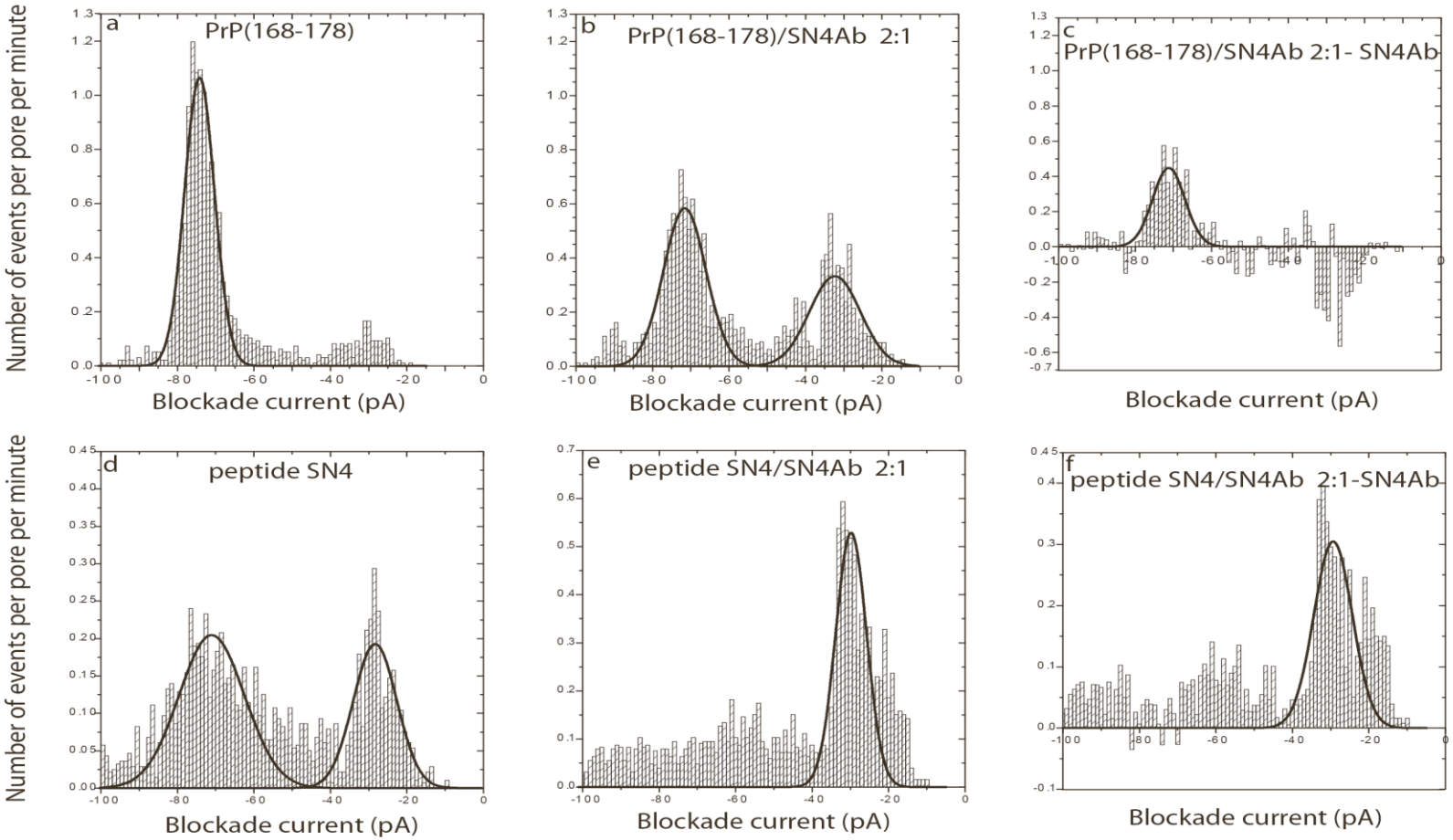

Figure 3.24 Current blockade histograms for peptide and SN4Ab interactions (a) PrP(168-178); (b) PrP(168-178) with SN4Ab, 2:1 ratio; (c) subtraction of SN4Ab from panel (b); (d) peptide SN4 ;(e) peptide SN4 with SN4Ab, 2:1 ratio; (f) subtraction of SN4Ab from panel (e). Parameters are presented in Table 3.13.

Table 3.13 Event parameters for PrP(168-178), PrP(168-178)/SN4Ab complex, peptide SN4, and peptide SN4/SN4Ab complex[a]

Compound	I_1 (pA)	I_2 (pA)	T_1 (ms)	T_2 (ms)	A_1	A_2	A_1/A_2	W_1	W_2
PrP(168-178)	-	-74	-	0.19	-	12.0	-	-	7.6
PrP(168-178)/SN4Ab 2:1	-32	-71	0.09	0.27	5.5	8.1	0.67	13.2	11.0
Peptide SN4	-28	-71	0.03	0.20	2.7	4.4	0.62	11.2	17.0
Peptide SN4/SN4Ab 2:1	-30	-	0.02	-	5.3	-	-	8.0	-

[a] **I** is the current blockade and **T** is the time of blockade. The subscripts 1 and 2 refer to Type-I and Type-II event populations presented in Figure 3.24. $\mathbf{A_1}$ and $\mathbf{A_2}$ are the number of events per pore per minute for each population. $\mathbf{W_1}$ and $\mathbf{W_2}$ are the peak widths at half-height. (The error is estimated to be ±1 pA for **I** and ±10% for **T**)

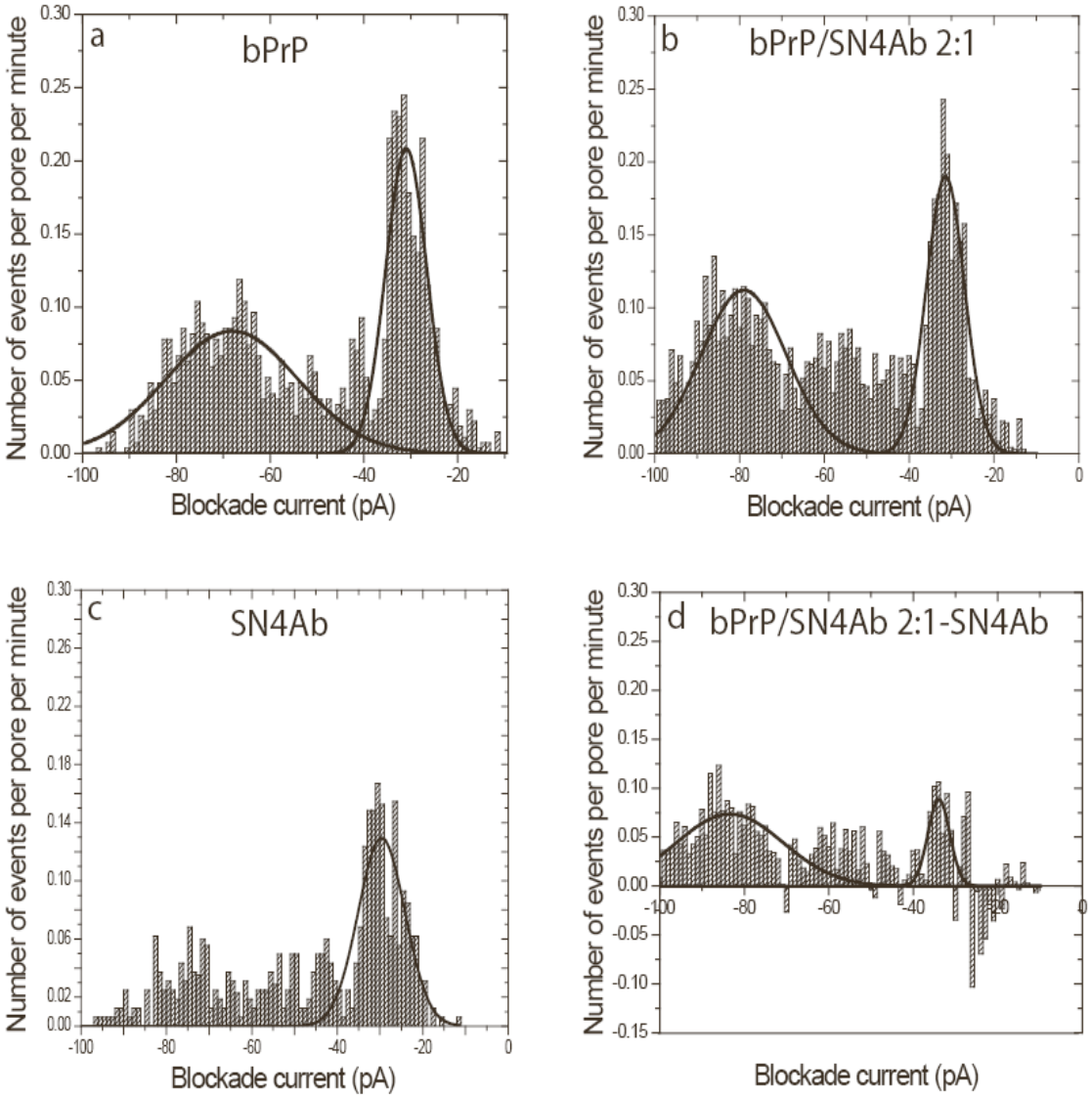

Figure 3.25 Current blockade histograms for prion protein and SN4Ab interactions. (a) bPrP, (b) bPrP with SN4Ab at a 2:1 ratio, (c) SN4Ab alone, and (d) subtraction of panel (c) from panel (b). The values are listed in Table 3.14.

Table 3.14 Event parameters for bPrP, bPrP/SN4Ab complex, and SN4Ab[a]

Compound	I_1 (pA)	I_2 (pA)	T_1 (ms)	T_2 (ms)	A_1	A_2	A_1/A_2	W_1	W_2
bPrP	-31	-68	0.01	0.17	2.3	3.0	0.76	8.7	28.2
bPrP/SN4Ab 2:1	-31	-79	0.02	0.12	2.1	2.8	0.75	8.9	28
SN4Ab	-30	-	0.03	-	1.8	-	-	10.9	-

[a] **I** is the current blockade and **T** is the time of blockade. The subscripts 1 and 2 refer to Type-I and Type-II event populations presented in Figure 3.25. $\mathbf{A_1}$ and $\mathbf{A_2}$ are the number of events per pore per minute for each population. $\mathbf{W_1}$ and $\mathbf{W_2}$ are the peak widths at half-height. (The error is estimated to be ±1 pA for **I** and ±10% for **T**).

the conformational changes that occur due to complex formation were further investigated by the binding of antibodies M2188 and SN6Ab. As mentioned earlier, M2188 binds the epitope ^{146}SRPLIHFG^{153} available in PrP^{C} whereas SN6Ab binds residues ^{172}VYYRP^{176} which are blocked in PrP^{C} but available in PrP^{Sc}.

3.7.2 Nanopore detection of the unfolded bPrP(25-242) with antibodies, M2188 and SN6Ab

First, bPrP was pre-treated with 0.9 M Gdn-HCl. Experiments with the full-length bPrP are shown in Figure 3.26 and the event parameters are listed in Table 3.15. Analysis of bPrP in the presence of Gdn-HCl displayed a single population of type-II events with a peak centered at -73 pA (Figure 3.26b). A three fold increase in the number of type-II events and also an increase in the blockade current ($\mathbf{I_2}$) by about 5 pA was observed. The final concentration of Gdn-HCl in the cup was 18 mM. Thus, this treatment suggests full or partial unfolding of bPrP resulting in an increase of type-II events.

Then, antibodies M2188 and SN6Ab were analyzed. The results for the interactions of the unfolded bPrP in the presence of M2188 or SN6Ab are shown in Figure 3.27(a-d) and Figure 3.27(e-h), respectively. The parameters are listed in Table 3.16. On the addition of M2188 (Figure 3.27b), at a protein-to-antibody ratio of 2:1, the number of events are reduced and no clear peak for the type-II events can be discerned. As previously mentioned, the antibody by itself (Figure 3.27c) also gives rise to a significant number of events that were subtracted from the event profile for the complex (Figure 3.27d). In this case, the average number of type-II events is reduced even further, although the event profile in the bumping region appears to be more complex.

However on the addition of SN6Ab (Figure 3.27b), at a protein-to-antibody ratio of 2:1, a two fold increase of the type-II events was observed. In addition, an increase in the blockade current ($\mathbf{I_2}$) of about 10 pA was apparent. In the presence of SN6Ab, the blockade duration for the type-II events increased from 0.11 to 0.23 ms. The VYYRP epitope is blocked in bPrP but may be accessible in the unfolded bPrP.

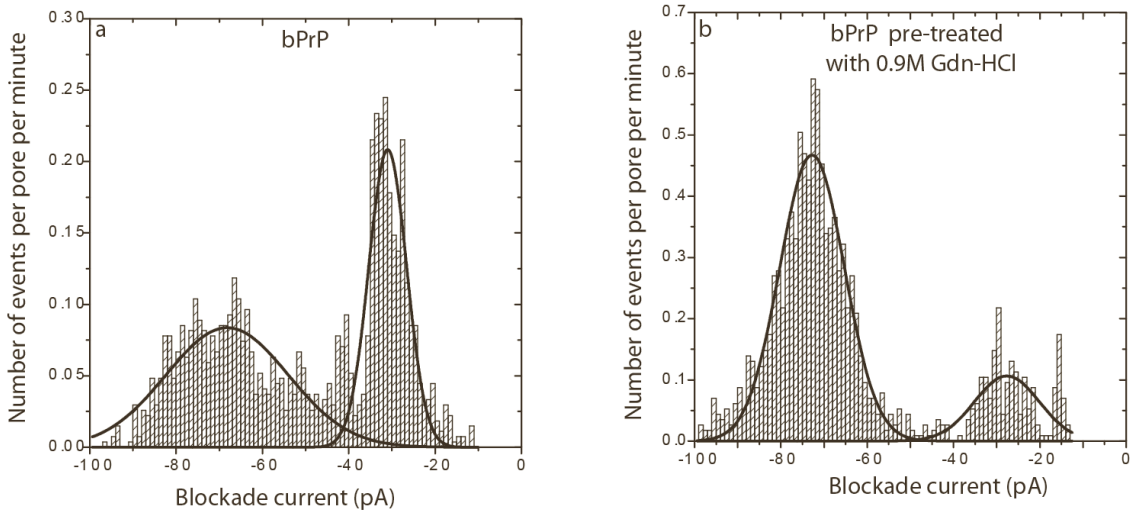

Figure 3.26 Current blockade histograms for bPrP in the presence of Gdn-HCl. (a) bPrP and (b) bPrP pre-treated with 0.9 M Gdn-HCl. The values are listed in Table 3.15.

Table 3.15 Event parameters for bPrP and bPrP pre-treated with 0.9M Gdn-HCl[a]

Compound	I_1 (pA)	I_2 (pA)	T_1 (ms)	T_2 (ms)	A_1	A_2	A_1/A_2	W_1	W_2
bPrP	-31	-68	0.01	0.17	2.3	3.0	0.76	8.7	28.2
bPrP pre-treated with 0.9M Gdn-HCl	-28	-73	0.02	0.11	2.0	8.8	0.22	14.9	14.9

[a] **I** is the current blockade and **T** is the time of blockade. The subscripts 1 and 2 refer to Type-I and Type-II event populations presented in Figure 3.26. $\mathbf{A_1}$ and $\mathbf{A_2}$ are the number of events per pore per minute for each population. $\mathbf{W_1}$ and $\mathbf{W_2}$ are the peak widths at half-height. (The error is estimated to be ±1 pA for **I** and ±10% for **T**).

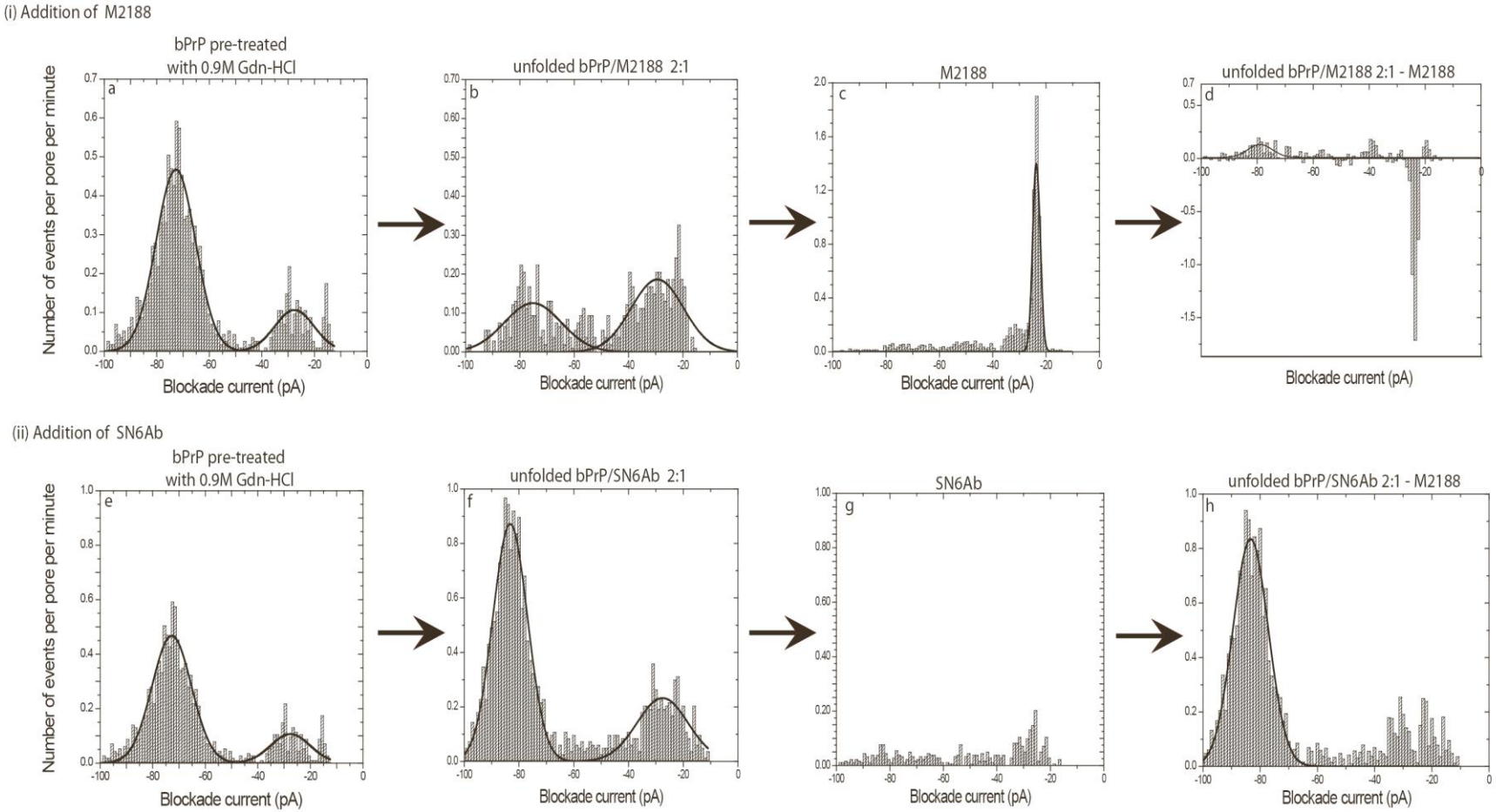

Figure 3.27 Current blockade histograms for the unfolded bPrP and antibody interactions. (a,e) bPrP pre-treated with 0.9M Gdn-HCl, (b) unfolded bPrP with M2188, 2:1 ratio, (c) M2188 alone, (d) subtraction of panel (c) from panel (b), (f) unfolded bPrP with SN6Ab, 2:1 ratio, (g) SN6Ab alone and (h) subtraction of panel (g) from panel (f). The y-axis of histogram (a) and (e) are different. The values are listed in Table 3.16.

Table 3.16 Event parameters for bPrP pre-treated with 0.9M Gdn-HCl, unfolded bPrP/M2188 complex, unfolded bPrP/SN6Ab complex, M2188 and SN6Ab[a]

Compound	I_1 (pA)	I_2 (pA)	T_1 (ms)	T_2 (ms)	A_1	A_2	A_1/A_2	W_1	W_2
bPrP pre-treated with 0.9M GdnHCl	-28	-73	0.02	0.11	2.0	8.8	0.22	14.9	14.9
Unfolded bPrP/ M2188 2:1	-29	-75	0.02	0.23	4.4	3.2	1.15	19.2	20.8
Unfolded bPrPl/ SN6Ab 2:1	-27	-83	0.01	0.23	5.4	13.8	0.39	18.65	12.61
M2188	-23	-	0.12	-	6.6	-	-	2.1	-
SN6Ab	-	-	-	-	1.3	-	-	-	-

[a] **I** is the current blockade and **T** is the time of blockade. The subscripts 1 and 2 refer to bumping (Type-I) and translocation (Type-II) event populations presented in Figure 3.27. $\mathbf{A_1}$ and $\mathbf{A_2}$ are the number of events per pore per minute for each population. $\mathbf{W_1}$ and $\mathbf{W_2}$ are the peak widths at half-height. (The error is estimated to be ±1 pA for **I** and ±10% for **T**).

3.8 Analysis of prion protein and signal prion peptide interactions

3.8.1 Introduction

After the translocation of PrP into the endoplasmic reticulum (ER) lumen, the attachment of the two N-linked carbohydrate moieties at Asn^{181} and Asn^{197} is initiated along with the cleavage of the N-terminal signal peptide (a.a.1-22). Then, prior to the addition of a glycosylphosphatidylinositol (GPI) anchor at Ser^{231}, the C-terminal signal peptide (a.a. 231-264) is cleaved. Subsequently a disulphide bond is formed between Cys^{179} and Cys^{214} (see Introduction, Figure 1.11a). The N-terminus signal prion peptides have potent antiprion effects. bPrP(1-30) significantly reduced PrP^{Sc} levels in prion infected mouse neuronal hypothalamic cells but had no effect on PrP^{C} levels in noninfected cells (Löfgren *et al*., 2008). PrP(106-126) binds the plasma membrane and initiates aggregation of PrP^{C}, which then is weakly proteinase K resistant (Gu *et al*., 2002). Studies on the C-terminal signal peptide including any amino acid sequence within the PrP(231-264) region have not been published as yet. The N- and C-terminal cleavages may be important in the generation of soluble and membrane-bound forms of the protein that are biologically active (Harris *et al*., 1993). Here we investigated the interactions between PrP(1-24) or PrP(243-264) with bPrP. We also investigated the interaction of PrP(106-126), which is known to cause aggregation to the prion protein.

3.8.2 Nanopore detection of bPrP(25-242) with signal prion peptides

Interaction of bPrP with PrP(1-24)**:**MVKSHIGSWILVLFVAMWSDVGLC or PrP(243-264):VILFSSPPVILLISFLIFLIVG was analyzed. Control experiments were also conducted with peptide RG23 in presence of bPrP. The analysis of peptides PrP(1-24), PrP(243-264) or RG23 with bPrP was done as stated in the Material and Methods section. PrP(1-24) has an overall net charge of +1 and is highly hydrophobic with limited solubility in phosphate buffer. As a result, PrP(1-24) does not give consistent nanopore results. The results for PrP(1-24) and bPrP are shown in Figure 3.28(a-d) and the parameters are listed in Table 3.17. PrP(1-24) displayed two peaks with each peak being roughly Gaussian (Figure 3.28b). The peaks centered at -29 pA and -69 pA was due to type-I and type-II events, respectively. The ratio for the type-I ($\mathbf{A_1}$) to type-II ($\mathbf{A_2}$) was 0.26 to 1. On the addition of PrP(1-24) to bPrP (Figure 3.28c) at a peptide-to-protein molar ratio of 1:1, the number of events is reduced, when compared to the theoretical sum of the histograms for PrP(1-24) and bPrP (Figure 3.28d).

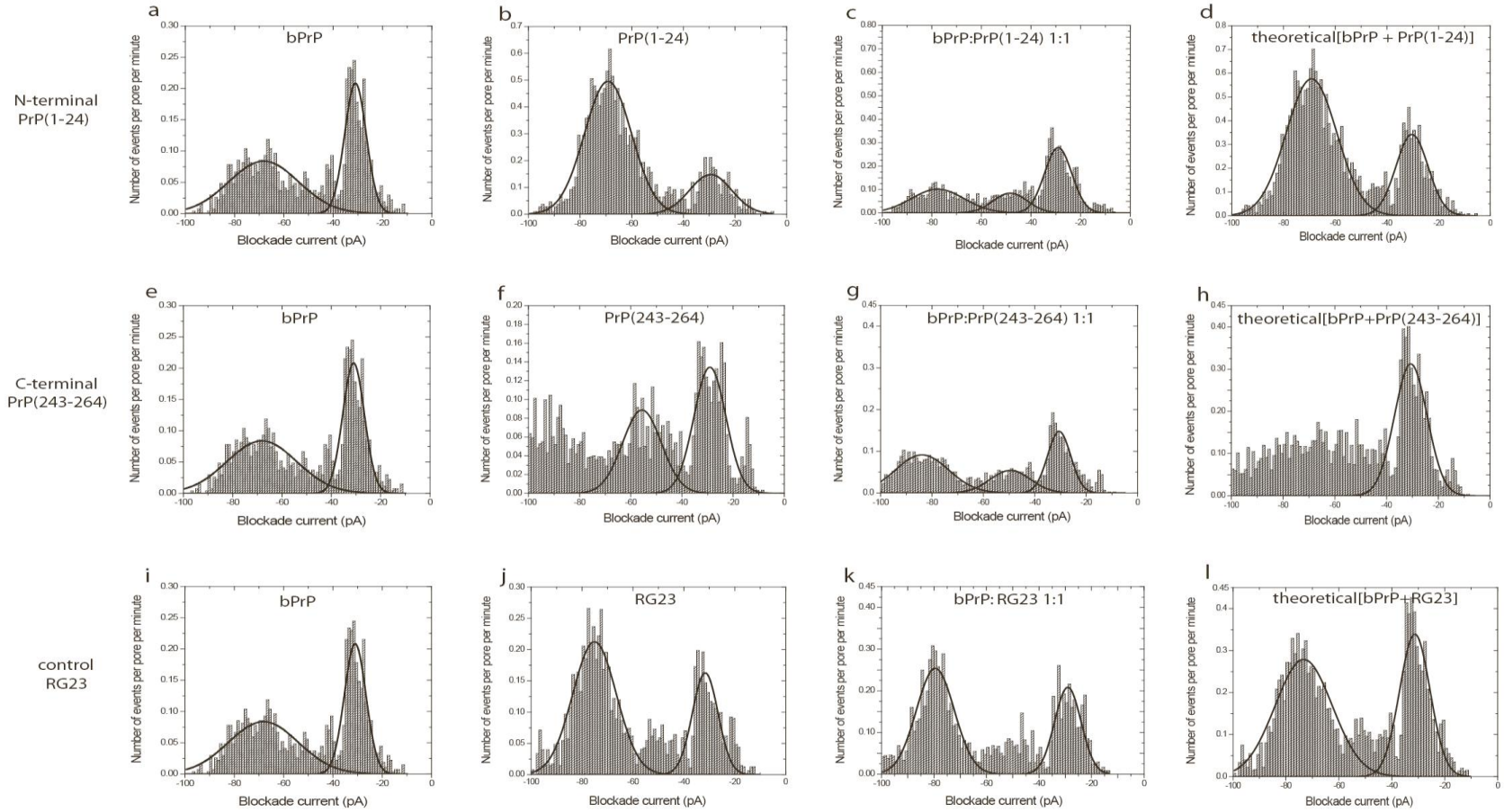

Figure 3.28 Current blockade histograms for signal prion peptides and bPrP interactions. (a,e,i) bPrP; (b) PrP(1-24); (c) PrP(1-24) with bPrP,1:1 ratio; (d) sum of panel(a) and panel(b); (f) PrP(243-264); (g) PrP(243-264) with bPrP,1:1 ratio; (h) sum of panel(e) and panel (f); (j) control peptide RG23; (k) RG23 with bPrP,1:1 ratio; (l) sum of panel(i) and panel(j). Parameters are presented in Table 3.17.

Table 3.17 Event parameters for bPrP, PrP(1-24), PrP(1-24)/bPrP complex, PrP(243-264), PrP(243-264)/bPrP complex, RG23, and RG23/bPrP complex[a]

compound	I_1 (pA)	I_2 (pA)	T_1 (ms)	T_2 (ms)	A_1	A_2	A_1/A_2	W_1	W_2
bPrP	-31	-68	0.01	0.17	2.3	3.0	0.76	8.7	28.2
PrP(1-24)	-29	-69	0.04	0.18	3.0	11.3	0.26	16.2	18.2
bPrP:PrP(1-24) 1:1	-29	-78	0.02	0.13	3.8	2.7	1.40	10.8	21.1
Theoretical sum of bPrP & PrP(1-24) histograms	-30	-69	-	-	5.3	14.1	0.37	12.3	19.5
PrP(243-264)	-29	-	0.02	-	2.1	-	-	12.3	-
bPrP:PrP(243-264) 1:1	-30	-84	0.02	0.03	1.6	2.3	0.69	8.7	20.5
Theoretical sum of bPrP & PrP(243-264) histograms	-31	-	-	-	4.9	-	-	12.5	-
RG23	-32	-75	0.02	0.11	2.0	4.5	0.44	10.0	17.9
bPrP:RG23 1:1	-29	-79.	0.03	0.16	2.6	4.5	0.57	10.0	14.3
Theoretical sum of bPrP & RG23 histograms	-31	-73	-	-	4.8	7.5	0.64	11.4	21.5

[a] **I** is the current blockade and **T** is the time of blockade. The subscripts 1 and 2 refer to bumping (Type-I) and translocation (Type-II) event populations presented in Figure 3.28. $\mathbf{A_1}$ and $\mathbf{A_2}$ are the number of events per pore per minute for each population. $\mathbf{W_1}$ and $\mathbf{W_2}$ are the peak widths at half-height. (The error is estimated to be ±1 pA for **I** and ±10% for **T**).

Other groups have also shown using Western blots, that bovine PrP(1-30) significantly reduced PrP^{Sc} levels in chronically infected prion cell lines (Löfgren *et al*., 2008).

The analysis of PrP(243-264) and bPrP is also shown in Figure 3.28(e-h) and the parameters are listed in Table 3.17. PrP(243-264) with a net charge of zero and displayed two peaks with each peak being roughly Gaussian. The peaks centered at -29 pA and -60 pA were due to type-I and type-II events, respectively. In addition, events between -80 pA and -100 pA were also observed. These events do not follow a Gaussian distribution. Therefore, PrP(243-264) may have more than one conformation. Alternatinely, the peaks may represent N- or C-terminal entry into the pore. Upon the addition of PrP(243-264) to bPrP (Figure 3.28g) at a peptide-to-protein ratio of 1:1, there was an increase in the blockade current for the type-II events and a subsequent reduction in the number of type-I events when compared to the theoretical sum of PrP(243-264) and bPrP (Figure 3.28h). These novel results suggest that the N-terminal and C-terminal prion peptides interact with the prion protein and cause conformational changes in $bPrP^{C}$.

A similar analysis was performed with a control peptide RG23, shown in Figure 3.28 (i-l) and the parameters listed in Table 3.17. RG23 has an overall net charge of +1 and displayed two peaks with each peak being roughly Gaussian. The peaks centered at -32 pA and -75 pA were due to type-I and type-II events, respectively (Figure 3.26j). On the addition of RG23 to bPrP (Figure 3.28k), at a peptide-to-protein ratio of 1:1, the number of type-II events remained the same. When this event profile was compared to the theoretical sum of RG23 and bPrP (Figure 3.28l), only a -6 pA reduction in the type-II events was seen for the sum of graphs. The ratio for the type-I ($\mathbf{A_1}$) to type-II ($\mathbf{A_2}$) for the premix of RG23 and bPrP was 0.57 to 1. However, for the theoretical sum of RG23 and bPrP this ratio only changed to 0.64:1.

3.8.3 Nanopore detection of bPrP(25-242) with PrP(106-126)

A similar analysis was performed using PrP(106-126):KTNMKHMAGAAAAGAVVGGLG which has an overall net charge of +3 at pH 7.8. The results are shown in Figure 3.29 and the parameters are listed in Table 3.18. PrP(106-126) displayed two event populations with each peak being roughly Gaussian (Figure 3.29b and e). The peaks centered at -29 pA and -72 pA were due to type-I and type-II events, respectively. Upon the addition of PrP(106-126) to bPrP (Figure 3.29c), at a peptide-to-protein

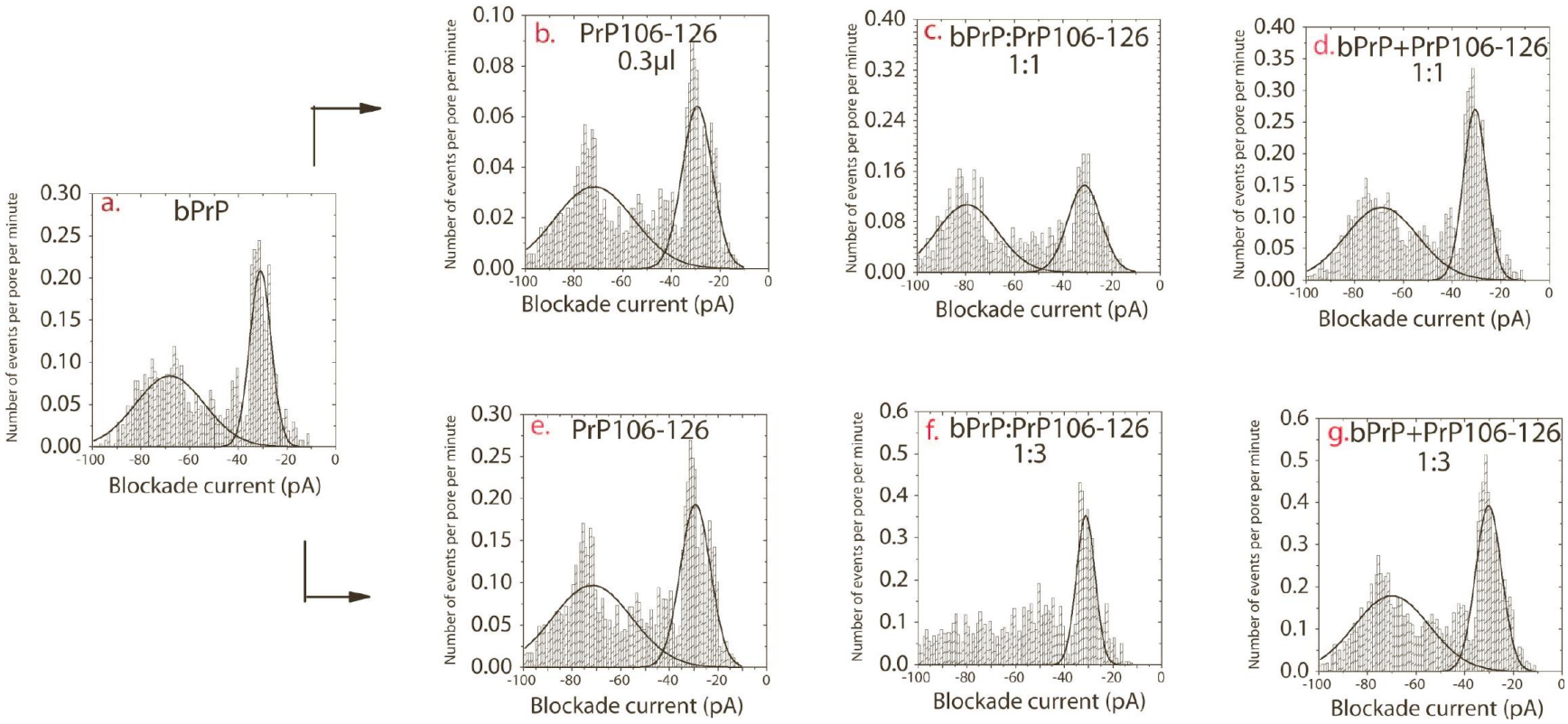

Figure 3.29 Current blockade histograms for PrP(106-126) and bPrP interactions. (a) bPrP; (b,e) PrP(106-126); (c) bPrP with PrP(106-126), 1:1 ratio; (d) sum of panel (a) and panel (b); (f) bPrP with PrP(106-126), 1:3 ratio; (g) sum of panel (a) and panel (e). Parameters are presented in Table 3.18.

Table 3.18 Event parameters for bPrP, PrP(106-126), bPrP/PrP(106-126) complex and the sum of bPrP with PrP(106-126)[a].

compound	I_1 (pA)	I_2 (pA)	T_1 (ms)	T_2 (ms)	A_1	A_2	A_1/A_2	W_1	W_2
bPrP	-31	-68	0.01	0.17	2.3	3.0	0.76	8.7	28.2
PrP(106-126) - 0.0016 mg/mL in the cup	-29	-72	0.02	0.19	0.9	1.3	0.91	12.3	32.3
bPrP:PrP(106-126) 1:1	-31	-79	0.02	0.19	2.3	3.3	0.69	13.6	25.0
Sum of bPrP & PrP(106-126) histograms for 1:1 molar ratio	-31	-69	-	-	3.2	4.2	0.76	9.5	29.7
PrP(106-126) – 0.005 mg/mL in the cup	-29	-72	0.02	0.19	2.9	3.9	0.74	12.3	32.3
bPrP:PrP(106-126) 1:3	-31	-	0.02	-	3.3	-	-	7.4	-
Sum of bPrP & PrP(106-126) histograms for 1:3 molar ratio	-30	-70	-	-	5.2	6.8	0.76	10.6	30.7

[a] **I** is the current blockade and **T** is the time of blockade. The subscripts 1 and 2 refer to Type-I and Type-II event populations presented in Figure 3.29. $\mathbf{A_1}$ and $\mathbf{A_2}$ are the number of events per pore per minute for each population. $\mathbf{W_1}$ and $\mathbf{W_2}$ are the peak widths at half-height. (The error is estimated to be ±1 pA for **I** and ±10% for **T**).

molar ratio of 1:1,an increase in the number of events was observed. However, when PrP(106-126) and bPrP were added at a peptide-to-protein molar ratio of 3:1, the number of events was reduced and no clear peak for the type-II events could be discerned (Figure 3.29f).

3.9 Analysis of prion protein aggregation

3.9.1 Introduction

Prion diseases are thought to arise from the misfolding and aggregation of the normal cellular prion protein, PrP^{C} into an oligomeric β-sheet-rich form known as the scrapie isoform, PrP^{SC} (Prusiner, 1982). A study on the rates of hydrogen/deuterium exchange demonstrated that the most likely route for the conversion of PrP^{C} to PrP^{Sc} is through a highly unfolded state rather than through a highly organized folding intermediate (Hosszu *et al*., 1999). *In vitro* conversion of full length recombinant prion protein is possible under neutral or slightly acidic pH (between 5.0 to 7.5) with Gdn-HCl (up to 2 M) or Urea (up to 4 M) (Breydo *et al*., 2008). Also, the N-terminal truncated recombinant human PrP(90-231) can be converted to a variety of oligomeric β-sheet rich structures (Apetri *et al*., 2005). The formation of amyloid fibrils can be monitored using a thioflavin T (ThT) fluorescence assay. ThT is known to bind to proteins containing β-sheets and to fluoresce only in the bound configuration (Bourhim *et al*., 2007). ThT fluorescence of fibrils can vary due to different PrP variants, and the exact values depend on several factors, including purity of the protein and conditions of fibril formation (Breydo *et al*., 2008). The rationale for the experiments presented below was to demonstrate if fibril formation of the full length bPrP was possible at low concentrations of Gdn-HCl so as to monitor the folding intermediates (Apetri *et al*., 2005).

3.9.2 Nanopore detection of bPrP(25-242) aggregation

For this purpose we used the protocol stated in Apetri *et al*., 2005 but pre-mixed bPrP(25-242) with 0.86 M Gdn-HCl at pH 7.5. Following continuous rotation at 8 rpm and at 37ºC, samples were withdrawn at different time intervals of 0, 18, 25, 44, and 68 hours. These samples were analyzed using nanopores at pH 7.8, followed by a fluorometric ThT assay. Results for the nanopore analysis are shown in Figure 3.30 and the parameters are listed in Table 3.19. On the addition of 0.86 M Gdn-HCl, at 0 hours (Figure 3.30b) bPrP displayed a single population of type-II events with a peak centered at -73 pA (Figure 3.30b). A three fold

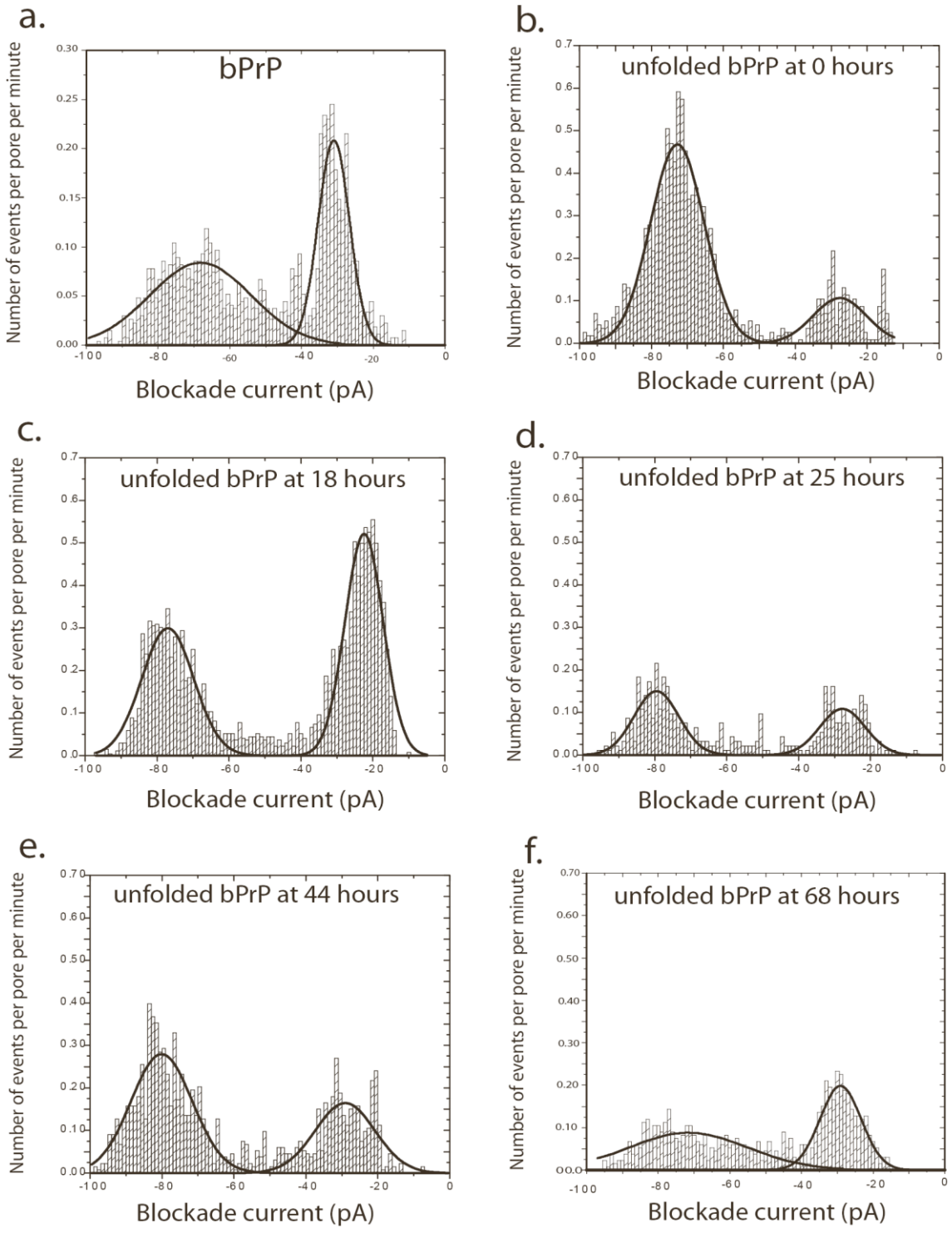

Figure 3.30 Current blockade histograms for the unfolded bPrP. (a) bPrP, (b) unfolded bPrP with Gdn-HCl at 0 hours, (c) unfolded bPrP with Gdn-HCl at 18 hours, (d) unfolded bPrP with Gdn-HCl at 25 hours, (e) unfolded bPrP with Gdn-HCl at 44 hours, and (f) unfolded bPrP with Gdn-HCl at 68 hours. Parameters are presented in Table 3.19.

Table 3.19 Event parameters for bPrP and the unfolded bPrP with Gdn-HCl: samples analyzed at 0, 18, 25, 44, and 68 hours[a]

compound	I_1 (pA)	I_2 (pA)	T_1 (ms)	T_2 (ms)	A_1	A_2	A_1/A_2	W_1	W_2
bPrP	-31	-68	0.01	0.17	2.3	3.0	0.76	8.7	28.2
unfolded bPrP with Gdn-HCl at 0 hours	-28	-73	0.02	0.11	2.0	8.8	0.22	14.9	14.9
unfolded bPrP with Gdn-HCl at 18 hours	-22	-77	0.03	0.23	6.9	5.4	1.27	10.5	14.3
unfolded bPrP with Gdn-HCl at 25 hours	-28	-79	0.03	0.24	1.7	2.3	0.73	12.4	12.2
unfolded bPrP with Gdn-HCl at 44 hours	-29	-80	0.02	0.25	3.4	5.9	0.57	16.5	16.8
Unfolded bPrP with Gdn-HCl at 68 hours	-29	-71	0.02	0.07	2.8	3.6	0.77	11.4	33.01

[a] **I** is the current blockade and **T** is the time of blockade. The subscripts 1 and 2 refer to Type-I and Type-II event populations presented in Figure 3.30. $\mathbf{A_1}$ and $\mathbf{A_2}$ are the number of events per pore per minute for each population. $\mathbf{W_1}$ and $\mathbf{W_2}$ are the peak widths at half-height. (The error is estimated to be ±1 pA for **I** and ±10% for **T**).

increase in the number of type-II events and also an increase in the blockade current ($\mathbf{I_2}$) by about 5 pA was observed. The following nanopore results were observed after 18, 25, 44, and 68 hours. When compared to the 0 hour experiment, at 18 hours (Figure 3.30c), a decrease in type-II and an increase in type-I events was observed. The ratio for the type-I ($\mathbf{A_1}$) to type-II ($\mathbf{A_2}$) at 18 hours was 1.27:1. When compared to the 18 hour experiment, at 25 hours (Figure 3.30d), a further decrease in both type-I and type-II events was observed. The ratio for the type-I ($\mathbf{A_1}$) to type-II ($\mathbf{A_2}$) events reduced to 0.73:1. When compared to the 25 hour experiment, at 44 hours (Figure 3.30e), a two fold increase in both the type-II and type-I events was observed. The ratio for the type-I ($\mathbf{A_1}$) to type-II ($\mathbf{A_2}$) events further reduced to 0.57:1. When compared to the 44 hour experiment, at 68 hours (Figure 3.30f) a decrease in both type-I and type-II events was observed. However the ratio for the type-I ($\mathbf{A_1}$) to type-II ($\mathbf{A_2}$) events increased to 0.77:1. So these results do not show any trend except that a decrease in the number of type-II events is observed in Figures 3.30(c-f), when compared with the unfolded protein at zero hours.

The ThT assay (Figure 3.31) only showed a threefold increase in fluorescence after 68 hours, whereas other groups have observed a 20-30 fold increase in ThT fluorescence. However these groups used the N-terminal truncated human PrP(90-231) with 1 M or 2 M Gdn-HCl (Apetri *et al*., 2005).

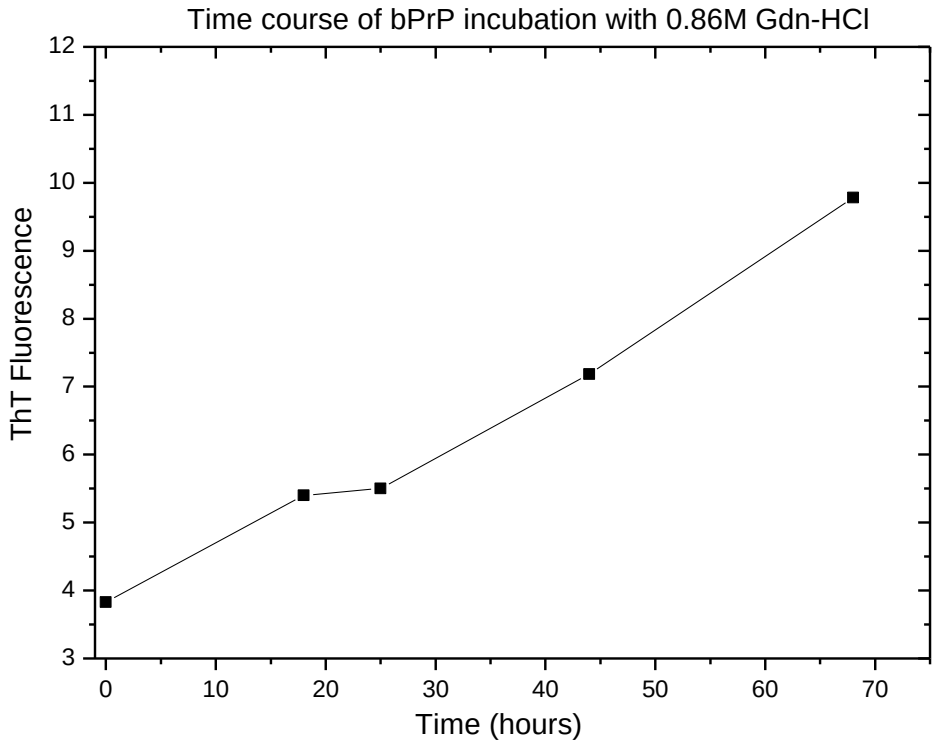

Figure 3.31 Effect of thioflavin T fluorescence on bPrP(25-242) with 0.86 M Gdn-HCl

4.0 DISCUSSION

4.1 Acetylated *vs.* Fmoc protected peptides

The experiments were designed to gain insight into the effect of Fmoc, acetylation or proline substitution on negatively charged α-helical peptides. For simple α-helical peptides that are negatively charged, it seems reasonable to assume that the type-II events are translocations. In support of this, the blockade current and time increased with the length of the helix (Stefureac *et al*., 2006).

As shown in the results (Figures 3.2 and 3.3), Fmoc peptides gave more translocations than acetylated peptides. For example, Ac-$D_2A_{14}K_2$ and Fmoc-$D_2A_{14}K_2$ are identical except for the protecting group; yet Ac-$D_2A_{14}K_2$ displayed approximately equal numbers of bumping and translocation events, whereas Fmoc-$D_2A_{14}K_2$ showed only translocations. The addition of Fmoc increased the overall hydrophobicity of the peptide which may decrease the interaction with the outside of the pore and favors translocation. Furthermore, as the aromatic ring of Fmoc is highly polarizable, this may help to steer the peptide into the pore, again increasing the number of translocations. A similar effect has also been observed for a group of negatively charged α-helical peptides. These peptides did not translocate in the absence of Fmoc (Stefureac *et al*., 2006). In another study, the addition of a toluene molecule to a peptide made a large difference in the number of type-II events. For example, a 12 amino acid long peptide, tethered via a terminal cysteine to monobromomethyl-substituted benzene, gave more type-II events than the untethered peptide (Meng *et al*., 2010).

Another important observation was the effect of proline on α-helical peptides. For example, Ac-$D_2A_{14}K_2$ and Ac-$D_2A_7PA_6K_2$ are identical except for a proline residue at the tenth position. The proline may cause a bend or kink in the peptide conformation. Peptide Ac-$D_2A_{14}K_2$ displayed two event populations with approximately equal number of events for each population whereas Ac-$D_2A_7PA_6K_2$ had only bumping events. Thus, the addition of a proline in the middle of an acetylated peptide appears to further reduce the number of translocation events.

One the other hand, peptides Fmoc-$D_2A_{14}K_2$ and Fmoc-$D_2A_7PA_6K_2$ showed similar histograms of blockade current with single peaks, comprising translocation events. For Fmoc-$D_2A_7PA_6K_2$, a decrease in the blockade time was the only change in the event parameters. This observation suggests that when a proline is added to the middle of an Fmoc peptide, it will

unfold easier into a linear conformation and thus can enter the pore and thread faster than an α-helix. These experiments show that nanopore analysis can be a useful tool to identify small changes in event parameters.

4.2 β-sheet and α-helical hairpin peptides

These experiments were initiated to study the effects of β-sheet and α-helical hairpin conformations on translocation or intercalation. As shown in section 3.2, the capped and uncapped β-sheet hairpins have different event parameters. The uncapped β-hairpin forms a more stable "U" shaped conformation due to the electrostatic interactions between the positively charged N-terminus and the negatively charged C-terminus, thus reducing the number of translocations (see Figures 3.4 and 3.5). This result also suggests that the uncapped β-hairpin has a higher proportion of the folded "U" shaped hairpin population in solution. This observation also agrees with the unpublished data stated in Xu *et al*., 2003. However, these interactions are diminished in the capped peptide. Presumably, the capped β-hairpin may unfold more easily to form a linear conformation that helps to orient molecules to enter the pore, causing a greater number of type-II events.

The next question that arises is; are these type-II events in the capped β-hairpin intercalations or translocations? The answer to this question can only be confirmed with voltage studies (Meng *et al*., 2010), but there are several factors that indicate these type-II events are translocations. First, folded molecules give larger blockade durations as compared to linear conformations (Goodrich *et al*., 2007). The blockade time for the type-II events in the capped peptide is smaller when compared with the uncapped. Second, the diameter of the α-hemolysin pore is 15 Å, whereas the diameter of the folded loop of the "U" shaped β-hairpin is about 20 Å (see Figure 3.4). Thus, for the unfolded peptide, the diameter can be estimated to be less than the diameter of α-hemolysin. This estimate is not unreasonable, as the average diameter calculated for the Fmoc protected α-helical peptides was about 8.8 Å, suggesting that these peptides may interact with the interior walls of the pore (Stefureac, R.I. thesis, page 117, Copyright 2006 Radu Ioan Stefureac). Third, because the peptide has an overall net charge of -3, molecules will be driven through the pore electrophoretically. However, the lower proportion of type-II events for the uncapped β-hairpin could be translocations or intercalations and cannot be differentiated without voltage studies (Meng *et al*., 2010).

As described earlier, the addition of Fmoc increases the number of type-II events. Similarly, the Fmoc-α-helical hairpin displayed equal numbers of both type-I and type-II events, whereas in the absence of Fmoc, the peptide gives very few type-II events (see Figures 3.6 and 3.7). When TCEP was added, the disulfide bond was reduced, creating an unlinked peptide. The crosslinked and unlinked α-helical hairpin without Fmoc showed no change in the histogram for blockade current in the presence of TCEP. However, for the Fmoc-unlinked-α-helical hairpin a significant increase in the proportion of type-II events was observed. Thus, the type-II events observed in the crosslinked and unlinked Fmoc-α-helical hairpin could be translocations, presuming that the two parallel helixes collapse on each other. On the other hand, the disulphide bond by itself is not expected to prevent translocation, since it is known that folded peptides can translocate (Goodrich *et al*., 2007). In addition, the increase in the proportion of type-II events in the unlinked hairpin is not unreasonable because the collapse of the two parallel helixes is less restricted in this conformation. From the event parameters, this collapsed model is favored as compared to the unfolded peptide adopting a linear conformation, because only a small change in blockade current was observed.

4.3 Prion peptide and protein analysis

The next group of experiments was initiated in an attempt to develop an electrophoretic prion detector. However, first small peptides from α-helical and β-sheet regions in prions were investigated. For example, PrP(155-162) and Ac-PrP(145-162) both contain an α-helical region 155-162; yet, PrP(155-162) has three peaks in the histogram of blockade current, whereas Ac-PrP(145-162) has only two with a larger number of bumping events. For PrP(155-162), the blockade current values for the type-II events were represented by peaks 2 and 3 (see Figure 3.8a), which are slightly lower compared to the negatively charged Fmoc-α-helical peptides (Stefuraec *et al*., 2006). Yet these values are not unreasonable as the peptide is only 8 amino acids in length and may not be able to form a stable α-helical structure. Presumably, these peaks represent either N- or C-terminal entry to the pore or two different conformations. On the other hand, the blockade current and time for the type-II events for Ac-PrP(145-162) are significantly greater as compared to PrP(155-162). However Ac-PrP(145-162) contains both an α-helical (a.a. 155-162) and a non-structured region (a.a. 145-154). Presumably, if the non-

structured region folds parallel to the α-helical segment, large blockade currents for these type-II events would be possible.

It remains unclear as to whether the type-II events observed for PrP(155-162) and Ac-PrP(145-162) represent translocations or intercalations. Again, the answer to this question can only be confirmed with voltage studies (Meng *et al*., 2010). However, for PrP(155-162) there are two factors that indicate peak 3 to be translocations. First, peak 3 has the highest blockade current of -59 pA that can represent translocations for a peptide with a linear conformation. This is reasonable when compared to a peptide with 14 amino acids that displayed a blockade current of -62 pA (Stefureac *et al*., 2006). Second, as the molecule has an overall negative charge this would help steer linear conformations into the pore. Similarly, the type-II events for Ac-PrP(145-162) could be translocations due to the large blockade current of -87 pA.

PrP(168-178) containing a β-sheet segment (a.a.172-175) was analyzed using α-hemolysin and aerolysin. With aerolysin, PrP(168-178) has two peaks in the histogram of blockade current whereas with α-hemolysin, only a single peak of type-II events can be discerned. Thus, the interactions between peptide and pore are dependent on the type and the structure of the pore. For example, even though both pores have similar diameters (Stefureac *et al*., 2006), the percentage block for the type-II events with aerolysin is 62% compared to 74% with α-hemolysin. Another observation was the increase in bumping events with aerolysin. Presumably, the lack of a vestibule in aerolysin may increase peptide collisions with the pore. Why do the type-II events with α-hemolysin have a large blockade current of -74 pA for a 11 amino acid peptide? One suggestion is that if two peptides enter the pore as a double stranded β-sheet, this would displace a greater volume of electrolyte solution, causing a higher blockade current (Henriquez *et al*., 2004).

4.3.1 Intercalation *vs*. translocation for the prion protein

The interaction of bPrP with αHL showed both type-I and type-II events with about 37% being type-II. There are several lines of evidence that indicate events with blockade currents (I_2) approximately equal to –65 pA for bPrP represent translocations. First, the proportion of translocations is dependent on the applied potential. At 50 mV, very few translocations are observed, presumably because the potential is not sufficiently large to unfold the protein even if it enters the vestibule of the pore. Second, theoretical studies have estimated that once a strand

has entered the pore, the free energy for translocation of the remainder of the protein can be small (Makarov, 2009). For example, the helix α1 region (DYEDRYYR) of bPrP contains three negative charges (underlined) which can enter the vestibule and eventually drag the rest of the protein through the pore. Another set of three negative charges located on the loop between helix α2 and α3 can facilitate translocation if this region is correctly oriented towards the vestibule. Finally, others have shown that the maltose binding protein of 370 residues can translocate especially in the presence of denaturing agents such as guanidinium hydrochloride (Oukhaled *et al*., 2007). Others in our laboratory have performed similar experiments with RNase A (124 residues) for which a majority of events appear to be translocations and the proportion increases upon addition of either guanidinium hydrochloride or reducing agents that break the disulphide bonds (B. Krasniqi, unpublished results). A model for the interaction of bPrP with the αHL pore is shown in Figure 4.1. The folded protein can approach the pore (Figure 4.1a) or enter the vestibule (Figure 4.1b) in orientations that do not allow it to translocate. These would be recorded as bumping events. Alternatively, a loop of protein may diffuse into the vestibule (Figure 4.1c). As mentioned earlier, once the negatively-charged residues at D(155), E(157), and D(158) at the N-terminus of helix α1 enter the vestibule, they will be pulled into the pore, due to the applied negative potential, eventually dragging the rest of the protein through as well. The disulphide bond by itself is not expected to prevent translocation, since it is known that folded peptides can translocate (Goodrich *et al*., 2007). When the voltage was increased to -150 mV the value of the blockade times for both types of events increased slightly.

On the other hand, when bPrP was added stem down-stream at +100 mV, an increase in the number of translocations was detected, as expected. This is because positively charged molecules will be driven through the pore. An increase in both the translocation blockade current and time suggests that the protein takes time to unfold and enter the pore due to the lack of a vestibule that may assist in capturing molecules.

4.4 Interaction of metal ions with prion proteins

The objective of these experiments was to demonstrate that the conformation of the prion protein can be modulated by binding divalent metal ions. As described in section 3.4, analysis of bPrP showed that about 37% were translocation events, but upon addition of Cu(II)

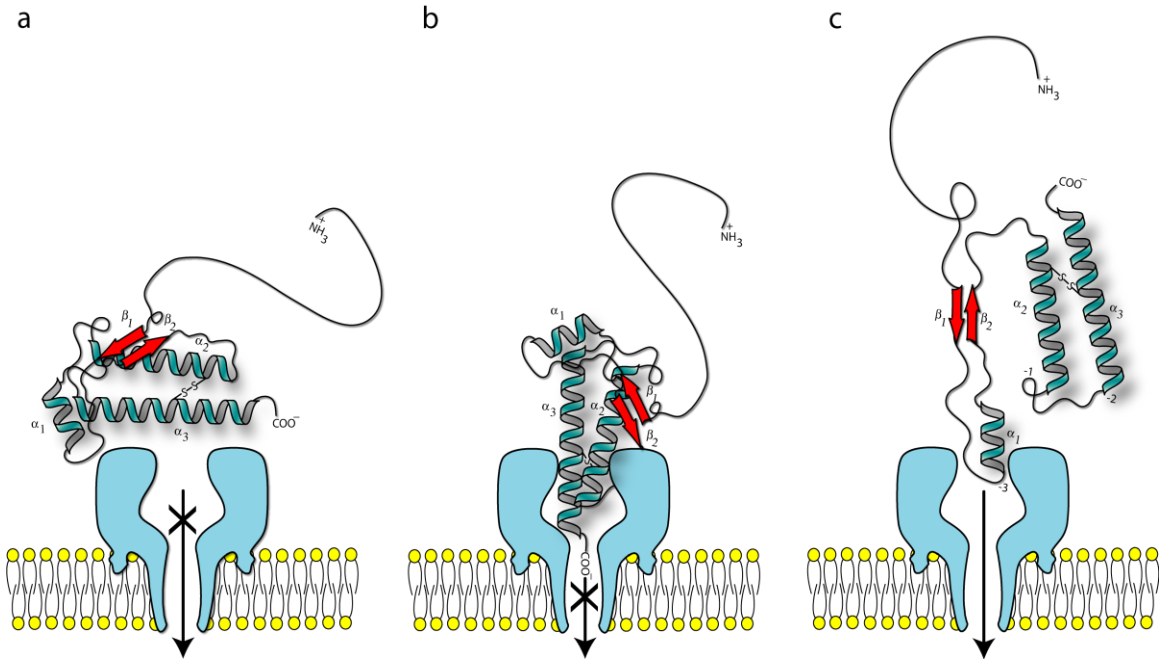

Figure 4.1 Model for the interaction of bPrP with the α-hemolysin pore. (a) and (b) represent bumping events whereas in (c) the initial orientation will allow the whole protein to translocate. (Reprinted by permission from Stefureac *et al*, 2010. Copyright 2010 NRC Research Press Journals.)

or Zn(II) these disappeared and only bumping events were recorded.

Although it may prove very difficult to provide direct evidence for translocation, it is clear that bPrP forms complexes with Zn(II), and especially with Cu(II), which cannot translocate. The bPrP–Cu(II) complex gives a very sharp bumping peak indicative of a single, well-ordered conformation. However, complex formation is readily reversed by the addition of EDTA, so there is no evidence that the Cu(II) complex can be identified with PrP^{Sc}, a result consistent with the work of others (Quaglio *et al*., 2001; Burns *et al*., 2003; Morante *et al*., 2004; Thompsett and Brown 2007). If the model mentioned earlier in Figure 4.1c is correct, it is not clear how complex formation could prevent translocation. One possibility is that the N-terminal loop now folds back onto helix α1, blocking entry to the vestibule. In support of this model, a recent Raman and circular dichroism study suggests that the addition of Cu(II) causes the loss of helix (α1) (Zhu *et al*., 2008). The effect of Mn(II) on bPrP (i.e., increasing the proportion of translocations) was most surprising, since there was no evidence that it bound to any of the prion peptides in the octarepeat region (Stefureac *et al*., 2010). It has been reported that Mn(II) can bind to another site centered at residue His95 (Brazier *et al*., 2008). Mn(II) can also cause structural changes, such as increasing the α-helical content from 25% to 30%, which may represent reinforcement or extension of the α1 helix (Zhu *et al*., 2008). In turn, an extended α- helix at this site may promote translocation. Ni(II) did not cause any significant changes. The effects of Cu(II) and Mn(II) on bPrP were also confirmed using DLS experiments.

In conclusion, we have demonstrated that nanopore analysis can be useful for interpreting conformational changes caused by the binding of metal ions. Since these experiments can be performed at very low protein concentrations, aggregation or precipitation of the protein is much less likely to occur and does not interfere.

4.5 Analysis of Jel352 and peptide interactions

These experiments were used to demonstrate complex formation that occurred due to antibody peptide interactions. Peptide RG23 can readily translocate through the pore, but on the addition of antibody Jel352, which binds the peptide, the number of translocations is decreased to about 50% before the subtraction of the control antibody. Presumably, this would be the case, if a single peptide molecule bound two antibody molecules (Figure 4.2a) using

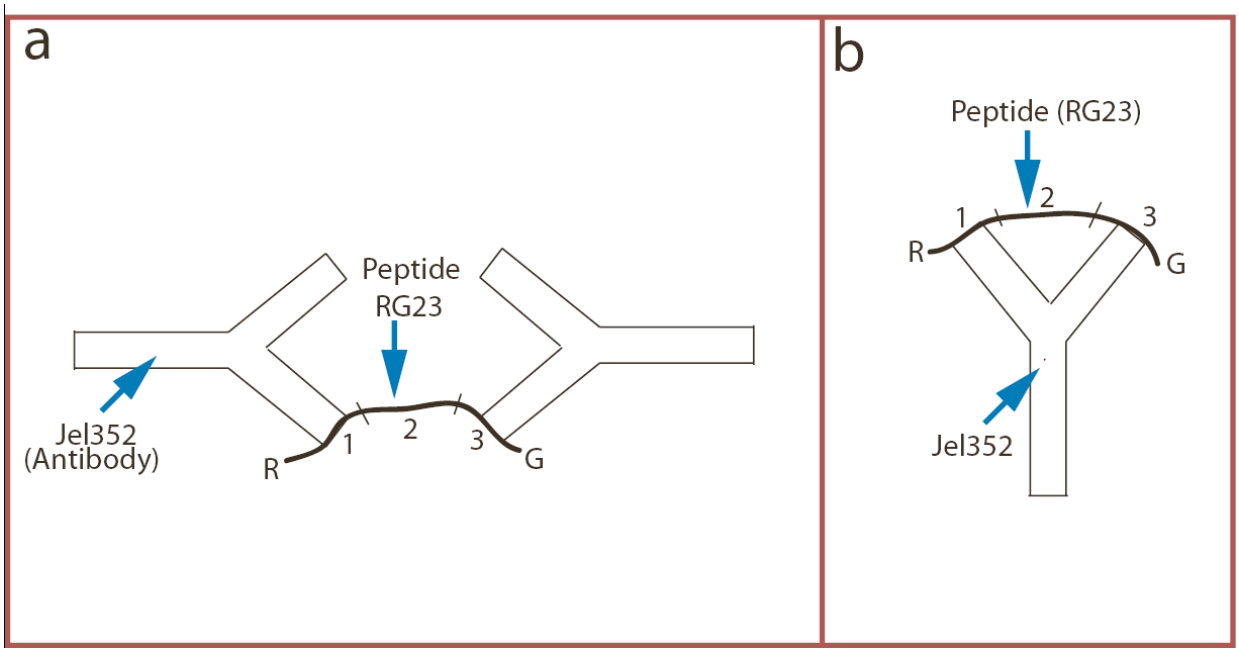

Figure 4.2 Schematic of Jel352 binding a single peptide RG23 at epitopes 1 and 3. RG23 contains a triple tandem heptarepeat unit of YSPTSPS numbered as 1, 2 and 3. YSPTSPS is the epitope for Jel352. (a) Schematic diagram of two Jel352 molecules binding a single peptide RG23. (b) Schematic of a single molecule of Jel352 binding a single peptide of RG23.

different epitopes or a single antibody binds to two epitopes on a single peptide (Figure 4.2b). The event profile of a control peptide, PrP(168-178), which does not bind the antibody showed no decrease in the number of events. But after the subtraction of antibody the total number of events is reduced to approximately 95% and 30% for RG23 and PrP(168-178), respectively. In conclusion, we have demonstrated that because the antibody-peptide complex is too large to translocate it diffuses much more slowly to the pore.

4.6 Analysis of antibody prion interactions

These studies were intended to demonstrate that complex formation can be monitored with nanopores. A prion peptide, PrP(143–169), can readily translocate through the pore, but on the addition of monoclonal antibody M2188, which binds the peptide, the number of translocations is reduced because the complex is too large to translocate. At a peptide-to-immunoglobulin G (IgG) ratio of 2:1, only bumping events were observed. The appearance of a negative peak (see Figure 3.20C) after the subtraction of the antibody suggests that the complex gives rise to fewer bumping events than does the sum of the peptide and antibody alone. This is not unreasonable given that complex formation reduces the number of molecular species. In addition, the complex may diffuse to the pore more slowly than the antibody alone, again giving rise to fewer bumping events. Alternatively, the individual molecules may interfere with each others access to the pore even in the absence of significant binding. The event profile of a control peptide PrP(168-178) that does not bind the antibody remained unchanged (see Figure 3.20E).

Similarly, the presence of M2188 prevents translocation of the full-length prion protein, bPrP (see Figure 3.23). The translocation peak centered at -65 pA is much broader than that for the peptide; this may be caused by different orientations of the protein as it enters the pore or different modes of unfolding as it passes through the pore. It is perhaps surprising that the translocation time (T_2) for bPrP is less than that for PrP(143-169). However, T_2 for maltose binding protein of 370 residues is also in the range of 0.2 ms, so the larger value for the peptide may be due to a strong interaction with the pore (Oukhaled *et al*., 2007). In addition, there are other values of blockade time that are difficult to understand, e.g. for example, the bumping events of PrP(143-169) and bPrP with and without antibody (see Tables 3.11 and 3.12). However, all four events are due to different structures or complexes, and currently the

relationship between blockade time and structure is not well understood; thus, predicting T values is not possible.

Though the work in this thesis represents experiments on complex formation between antibodies and peptides and proteins using a biological nanopore, α-hemolysin, there have been many previous publications with solid-state pores (Siwy *et al*., 2005; Sexton *et al*., 2007; Han *et al*., 2008). The protein-antibody complexes for protein G/immunoglobulin and ricin/ricin antibody were analyzed using gold-plated conical solid-state pores (Siwy *et al*., 2005). Protein-G and ricin were attached to Au using the biotinylated protein. When the protein bound the corresponding analyte, a complete blockade of the ionic current was observed (Siwy *et al*., 2005). Another report on the analysis of BSA and BSA/Fab complex were investigated using a PEG-thiol attached to a gold-plated conical nanotube, which displayed different current pulse signatures for BSA and the BSA/Fab complex (Sexton *et al*., 2007). A 28 nm diameter Si_3N_4 pore was used to distinguish between β-human chroionic gonadotropin (β-hCG) and β-hCG-antibody complex. The experiments with the antibody gave large blockade currents for translocation events, whereas on complex formation with β-hCG the translocations reduced. The authors speculated that the reduction in translocation events could be due to the change in the electrophoretic mobility of the antibody when bound to β-hCG (Han *et al*., 2008).

Similarly, the antibody SN4Ab, which binds PrP(168-178) and peptide SN4, reduced the number of translocation events (see Figure 3.24). PrP(168-178) has one epitope of VYYRP and the antibody, SN4Ab reduced the number of translocations by 55%. Alternatively, as explained earlier, PrP(168-178) may be translocating as a double stranded β-sheet which might block the access to the epitope. On the other hand, peptide SN4 has six epitopes and showed no clear translocation peak in the presence of antibody.

The event profile of bPrP that does not bind antibody SN4Ab showed an increase in the translocation blockade current (see Figure 3.25). However, after the subtraction of the antibody, a reduction in the number of bumping events suggests that a weak complex gives rise to fewer bumping events than does the sum of the peptide and antibody alone. Furthermore, these weak interactions are not sufficient to prevent translocations.

A three fold increase in the number of translocations with a decrease in bumping events was observed when bPrP was pre-treated with 0.9 M Gdn-HCl (see Figure 3.26). However, even though bPrP may be fully unfolded at first, the addition of 1 M KCl may cause it to

partially refold, as only a -5 pA increase in blockade current was observed. One possibility is that although the single disulfide link is still intact, the unfolding of helix α1 at the N-terminus, which is comprised of negatively charged amino acids, D(155), E(157), and D(158) may enhance entry into the vestibule and thread through the pore. Even though the unfolded bPrP can readily translocate the pore, the addition of antibody M2188 which binds the protein reduced the number of events with no clear translocations peak (see Figure 3.27d). In this case, as the location of the epitope for M2188 is at the unstructured N-terminus, it is not affected by unfolding and would still be accessible for binding.

On the other hand, the addition of antibody SN6Ab, which does not bind bPrP, increased the translocation events by 46% (see Figure 3.27h). This effect of SN6Ab could be due to weak interactions between antibody and the epitope sequence VYYRP, which is buried in bPrP (without Gdn-HCl) but may be available due to partial unfolding. The unfolded protein may then interact with the antibody which serves as a chaperone that brings molecules to the pore, and then break away (Figure 4.3). We have seen elsewhere that the binding of Fab to poly(dT)$_{45}$ increased the frequency of translocation events which suggests that the rigid form of the complex enhances translocation (Ying *et al*., 2010).

In conclusion, we have demonstrated that complex formation between antibodies and prion peptides and proteins can be detected by nanopore analysis. In principle, a nanopore can detect a single molecule; thus, this work represents the first step towards the development of a prion detector. The nanopore will provide the sensitivity and antibodies will provide the specificity to distinguish between PrP^{C} and PrP^{Sc}.

4.7 Analysis of signal prion peptide and protein interactions

These experiments were designed to study signal prion peptides binding to bPrP that may cause conformational changes, leading to changes in events parameters. The addition of signal prion peptides, PrP(1-24) and PrP(243-264) to bPrP changed the event parameters of the complex as compared to the sum of the peptide and protein alone. PrP(1-24) reduced the number of type-II events, suggesting that complex formation reduces the number of molecular species. The N-terminus signal prion peptides have potent antiprion effects. bPrP(1-30) significantly reduced PrP^{Sc} levels in prion infected mouse neuronal hypothalamic cells but had

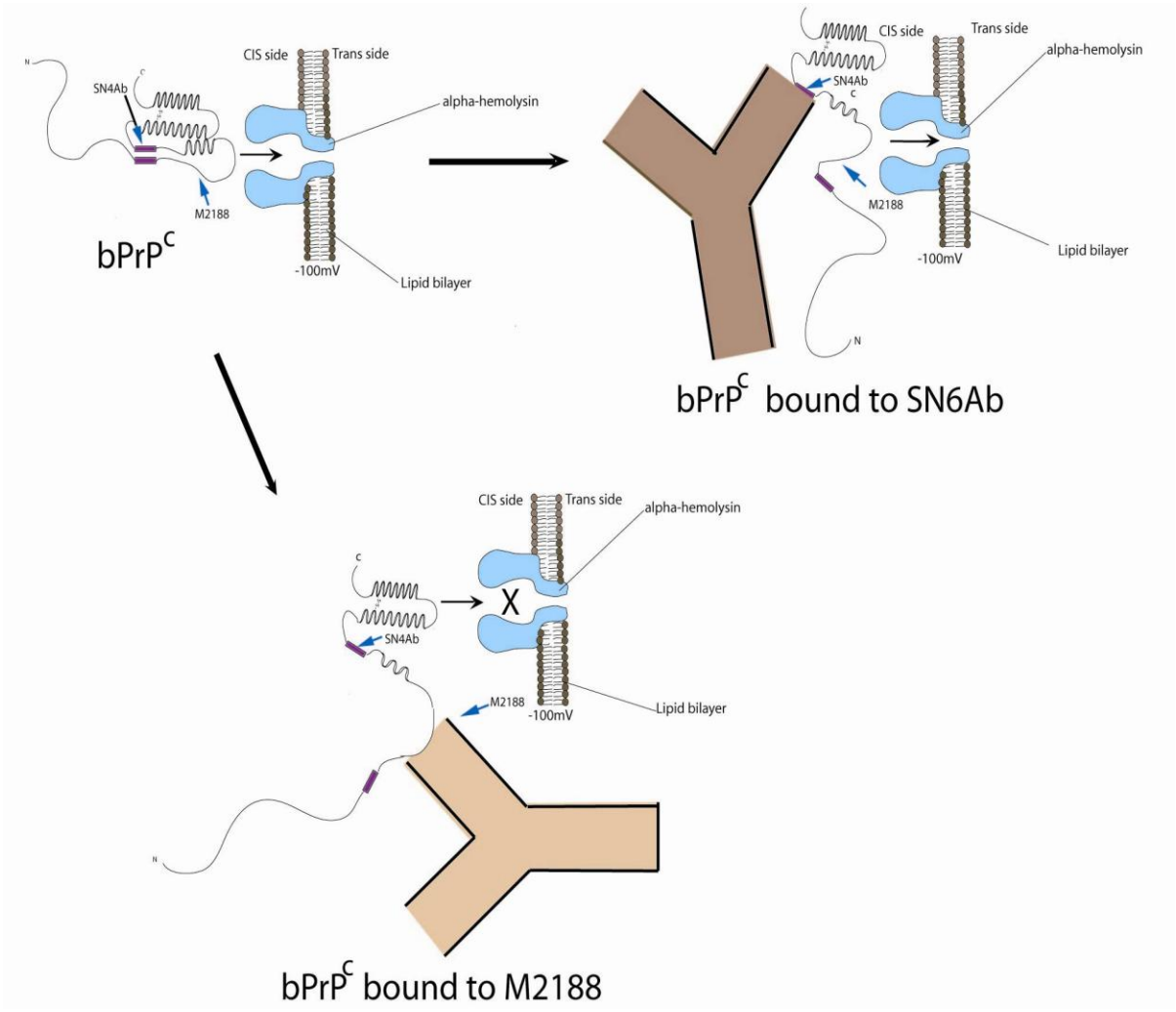

Figure 4.3 Schematic of the partially unfolded bPrP in the presence of antibodies, M2188 and SN6Ab tested on α-hemolysin.

no effect on PrP^C levels in noninfected cells (Lofgren *et al*., 2008). Surprisingly, this may be a new mechanism by which the hydrophobic sequence in PrP(1-24) interacts with PrP^C. Similarly, the addition of PrP(243-264) changed the translocation blockade current and reduced the number of bumping events, as compared to the sum of the peptide and protein alone. This is a new finding as no group has reported work on the C-terminal signal peptide. These signal peptides may be very important for the correct folding of native PrP^C. Furthermore, the two proteolytic cleavages may be important in the generation of soluble and membrane bound proteins (Harris *et al*., 1993; Heller *et al*., 2003; Orsi and Sitia, 2007). The interaction of PrP(106-126), which is known to cause *in vitro* fibrillogenicity and toxicity to neurons, reduced the number of translocation events (Jeong *et al*., 2010). PrP(106-126) binds the plasma membrane and initiates aggregation of PrP^C (Gu *et al*., 2002). The event profile of a control peptide changed very little when compared to the above mentioned peptide profiles.

These results suggest that the N-and C-terminal signal prion peptides interact with prion proteins and change the conformation of the complex which is readily detected by the change in event parameters. Therefore these findings relate to a new mechanism by which these signal peptides interact with prion protein (Figure 4.4). These observations also suggest that the N- and C-terminal signal peptides may be useful as therapeutic tools to reduce the pool of available PrP^C which serves as a template for the conversion of $PrP^C \rightarrow PrP^{Sc}$ (Aguzzi and Calella, 2009).

4.8 Analysis of prion protein aggregation

The final set of experiments was designed to study the possibility of fibril formation of the full length bovine prion protein at low concentrations of Gdn-HCl, so as to monitor the folding intermediates. When bPrP(25-242) was pre-treated with 0.86 M Gdn-HCl at pH 7.5, after 68 hours, aggregation was not possible. This may be due to the low concentration of Gdn-HCl. *In vitro* conversion of the full length recombinant prion protein is possible under neutral or slightly acidic pH (between 5.0 to 7.5) with Gdn-HCl (up to 2 M) or urea (up to 4 M) (Breydo *et al*., 2008). However, it has been reported that *in vitro* conversion of the N-terminal truncated human PrP(90-231) was possible using 1 M or 2 M Gdn-HCl (Aperti *et al*., 2005). Recently, 3 M urea was used in an unseeded method to convert mouse PrP(89-230) into a protease-sensitive synthetic prion (Colby *et al*., 2010).

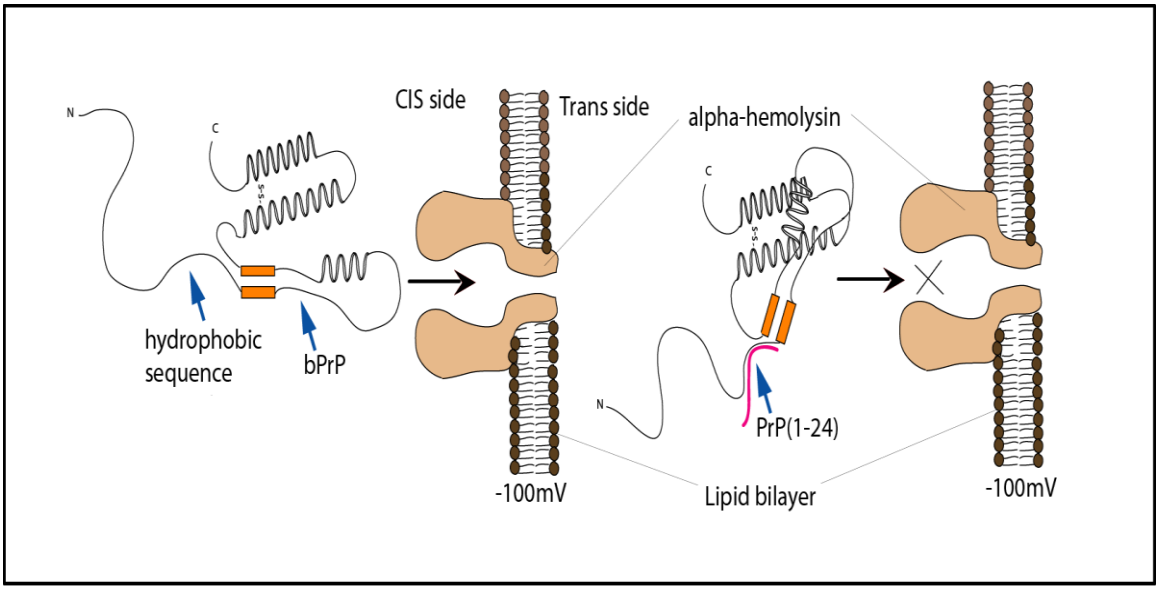

Figure 4.4 Schematic of the interactions between PrP(1-24) and bPrP tested on α-hemolysin. When PrP(1-24) interacts with bPrP a change in conformation occurs, which reduces the number of events.

These results suggests that the protein unfolds between the first 0-3 hours of the cycle and then starts to convert into a different conformation which gives similar event parameters as that of bPrP (Figure 4.5). The conformational conversion of $PrP^{C} \rightarrow PrP^{Sc}$ is an important biochemical pathway that is not well understood as yet. A study on the rates of hydrogen/deuterium exchange demonstrates that the most likely route for the conversion of $PrP^{C} \rightarrow PrP^{Sc}$ is through a highly unfolded state rather than through a highly organized folding intermediate (Hosszu *et al*., 1999). These findings suggest that nanopores can be used to monitor conformational changes that occur in proteins in the presence of a denaturant. These results further suggest that higher concentrations of Gdn-HCl should be used for the aggregation of the full length protein. However, these concentrations may affect the stability of the α-hemolysin pore. Finally, if aggregation is successful, a nanopore should detect no events because the aggregated complex will be too large to cause type-I or type-II events.

4.9 Future directions

Using nanopore analysis, the experiments presented in this thesis show that Cu(II) induces a conformational change in full-length bPrP(25-242) (see Figure3.14b). Briefly, native PrP^{C} can unfold and translocate through an α-hemolysin nanopore (see Figure 3.14a) but in the presence of Cu(II) a conformational change occurs which prevents translocation. Similarly, the addition of the N-terminal signal prion peptide PrP(1-24) also prevents translocation presumably because the complex cannot unfold (see Figure 3.28c). The ability of this technique to detect minor conformational differences within the protein and to assign distinctive signature spectra may offer a more sensitive and high-throughput methodology for describing conformational isomers of PrP.

The experiments presented in this thesis extended this technique with the use of prion-specific antibodies; the PrP/antibody complex is too large to translocate whereas unbound molecules are uneffected (Madampage *et al*., 2010). Additionally, the development of antibodies to different epitopes of PrP that enable conformational discrimination of PrP^{Sc} and PrP^{C} would be useful. These experiments provide proof of principle that conformational changes and PrP^{C}/antibody interactions are easily detected by nanopore analysis. The technique has the following advantages: speed - the results are available in 2-3 hours or less: specificity - provided by PrP^{C} or PrP^{Sc} specific antibodies; and sensitivity - the pore can theoretically detect

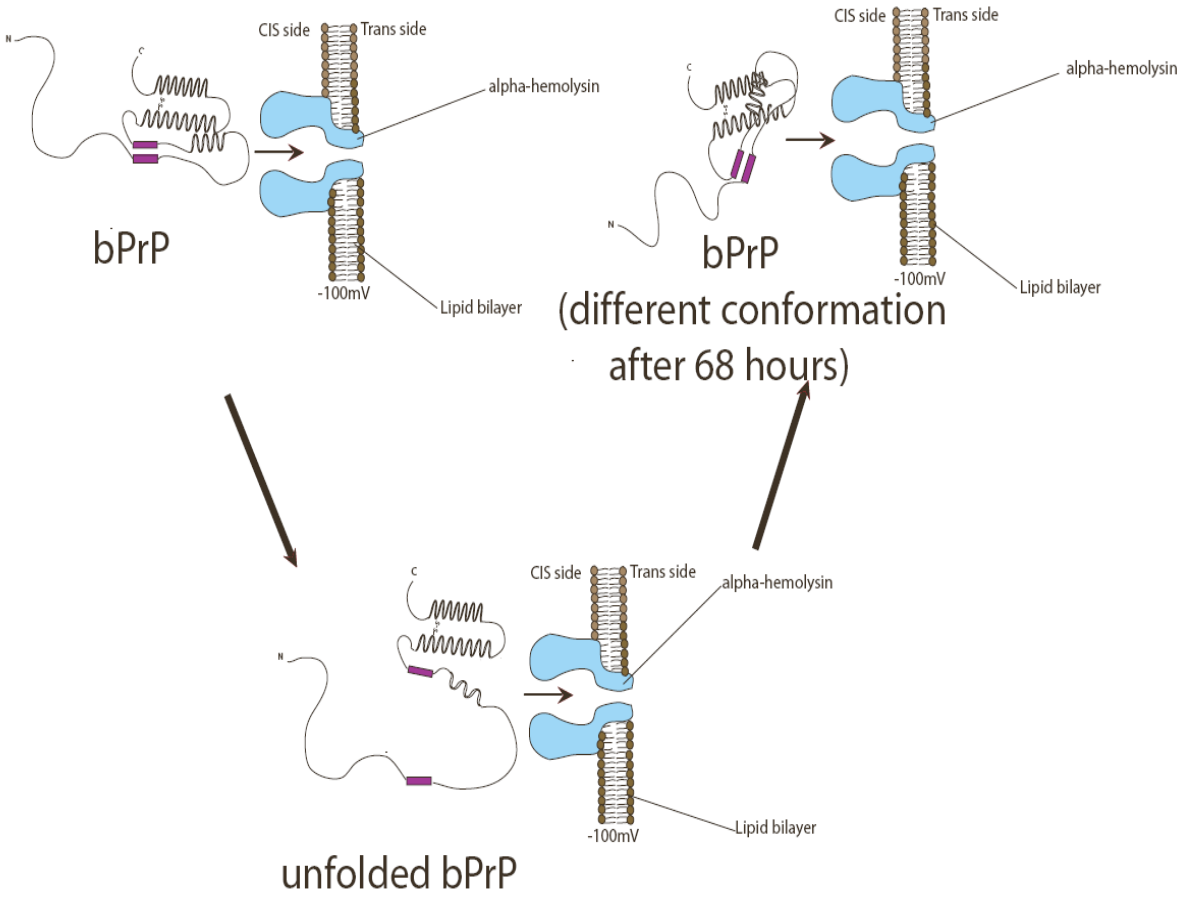

Figure 4.5 Schematic of the unfolding of bPrP pre-treated with 0.86 M Gdn-HCl.

a single molecule or complex. This type of test would be extremely beneficial for the meat industry as well as in the diagnosis of human prion diseases. Although the incidence of prion disease in humans is low, early detection would help patients seek medical advice. At present, PMCA, a technique for accelerated prion replication, is a useful tool for prion diagnostic assays (Saborio *et al*., 2001). A detection limit of 6-12 pg ($0.2\text{-}0.4\text{x}10^{-15}$ mol) of PrP^{Sc} after a 10000 fold dilution and 10 cycles has been successfully described (Telling, 2001).

Future work will include the development of a panel of prion proteins from different species which will "naturally" (have a preference to) misfold into different conformations based on the concept of the species barrier. Different conformations will expose different epitopes which can then be detected by specific antibodies (e.g VYYR is buried in PrP^{Sc}). Furthermore, PrP^{C} can be induced to convert to PrP^{Sc} and because of low concentrations; the altered conformation can be detected by nanopore analysis before PrP^{Sc} aggregates.

As mentioned earlier, an important finding of this work was the interactions between signal prion peptides and proteins. Further studies on the N- and C-terminal signal peptides may be useful as a therapeutic tool to reduce the pool of available PrP^{C} which serves as a template for the conversion of $PrP^{C} \rightarrow PrP^{Sc}$ (Aguzzi and Calella, 2009). Furthermore, nanopore analysis of drugs or peptides that bind to PrP which may cause conformational changes, leading to the prevention of conversion to PrP^{Sc} is very important.

Finally, the analytical method used for nanopore analysis in this thesis can be applied to the detection of other protein misfolding diseases such as Alzheimer's and Parkinsons. Similarly, if the protein is bound to an antibody, then translocation will be inhibited so that antibody discrimination of the native and misfolded conformations can be analyzed. In the long term, it is envisaged that these experiments will lead to the construction of a rapid and sensitive prion detector to detect PrP^{Sc} while also providing information on specific strains. The major additional requirement will be the production of solid-state nanopores with specific antibodies lining the pore.

5.0 REFERENCES

Abrami, L., Fivaz, M., and van der Goot, F.G. (2000). Adventures of a pore-forming toxin at the target cell surface. Trends Microbiol *8*, 168-172.

Adelman, K., La Porta, A., Santangelo, T.J., Lis, J.T., Roberts, J.W., and Wang, M.D. (2002). Single molecule analysis of RNA polymerase elongation reveals uniform kinetic behavior. P Natl Acad Sci USA *99*, 13538-13543.

Adjou, K.T., Demaimay, R., Deslys, J.P., Lasmezas, C.I., Beringue, V., Demart, S., Lamoury, F., Seman, M., and Dormont, D. (1999). MS-8209, a water-soluble amphotericin B derivative, affects both scrapie agent replication and PrPres accumulation in Syrian hamster scrapie. J Gen Virol *80 (Pt 4)*, 1079-1085.

Adjou, K.T., Demaimay, R., Lasmezas, C., Deslys, J.P., Seman, M., and Dormont, D. (1995). MS-8209, a new amphotericin B derivative, provides enhanced efficacy in delaying hamster scrapie. Antimicrob Agents Chemother *39*, 2810-2812.

Adjou, K.T., Privat, N., Demart, S., Deslys, J.P., Seman, M., Hauw, J.J., and Dormont, D. (2000). MS-8209, an amphotericin B analogue, delays the appearance of spongiosis, astrogliosis and PrPres accumulation in the brain of scrapie-infected hamsters. J Comp Pathol *122*, 3-8.

Aguzzi, A., and Calella, A.M. (2009). Prions: protein aggregation and infectious diseases. Physiol Rev *89*, 1105-1152.

Aguzzi, A., Sigurdson, C., and Heikenwaelder, M. (2008). Molecular mechanisms of prion pathogenesis. Annu Rev Pathol *3*, 11-40.

Akeson, M., Branton, D., Brandin, E., Kasianowicz, J., and Deamer, D. (1999a). Purine and pyrimidine nucleic acids produce distinctive current blockades in the alpha hemolysin pore. Biophys J *76*, A152-A152.

Akeson, M., Branton, D., Kasianowicz, J.J., Brandin, E., and Deamer, D.W. (1999b). Microsecond time-scale discrimination among polycytidylic acid, polyadenylic acid, and polyuridylic acid as homopolymers or as segments within single RNA molecules. Biophys J *77*, 3227-3233.

Aksimentiev, A., and Schulten, K. (2005). Imaging alpha-hemolysin with molecular dynamics: ionic conductance, osmotic permeability, and the electrostatic potential map. Biophys J *88*, 3745-3761.

Andrievskaiai, O., Algire, J., Balachandran, A., and Nielsen, K. (2008). Prion protein in sheep urine. J Vet Diagn Invest *20*, 141-146.

Andrievskaia, O., McRae, H., Elmgren, C., Huang, H., Balachandran, A., and Nielsen, K. (2006). Generation of antibodies against bovine recombinant prion protein in various strains of mice. Clin Vaccine Immunol *13*, 98-105.

Antonyuk, S.V., Trevitt, C.R., Strange, R.W., Jackson, G.S., Sangar, D., Batchelor, M., Cooper, S., Fraser, C., Jones, S., Georgiou, T., *et al.* (2009). Crystal structure of human prion protein bound to a therapeutic antibody. Proc Natl Acad Sci USA *106*, 2554-2558.

Apetri, A.C., Vanik, D.L., and Surewicz, W.K. (2005). Polymorphism at residue 129 modulates the conformational conversion of the D178N variant of human prion protein 90-231. Biochemistry *44*, 15880-15888.

Aronoff-Spencer, E., Burns, C.S., Avdievich, N.I., Gerfen, G.J., Peisach, J., Antholine, W.E., Ball, H.L., Cohen, F.E., Prusiner, S.B., and Millhauser, G.L. (2000). Identification of the Cu2+ binding sites in the N-terminal domain of the prion protein by EPR and CD spectroscopy. Biochemistry *39*, 13760-13771.

Ashkin, A. (1997). Optical trapping and manipulation of neutral particles using lasers. Proc Natl Acad Sci USA *94*, 4853-4860.

Astier, Y., Braha, O., and Bayley, H. (2006). Toward single molecule DNA sequencing: direct identification of ribonucleoside and deoxyribonucleoside 5'-monophosphates by using an engineered protein nanopore equipped with a molecular adapter. J Am Chem Soc *128*, 1705-1710.

Astier, Y., Kainov, D.E., Bayley, H., Tuma, R., and Howorka, S. (2007). Stochastic detection of motor protein-RNA complexes by single-channel current recording. Chemphyschem *8*, 2189-2194.

Atanasov, V., Atanasova, P.P., Vockenroth, I.K., Knorr, N., and Koper, I. (2006). A molecular toolkit for highly insulating tethered bilayer lipid membranes on various substrates. Bioconjug Chem *17*, 631-637.

Atanasov, V., Knorr, N., Duran, R.S., Ingebrandt, S., Offenhausser, A., Knoll, W., and Koper, I. (2005). Membrane on a chip: a functional tethered lipid bilayer membrane on silicon oxide surfaces. Biophys J *89*, 1780-1788.

Atarashi, R., Moore, R.A., Sim, V.L., Hughson, A.G., Dorward, D.W., Onwubiko, H.A., Priola, S.A., and Caughey, B. (2007). Ultrasensitive detection of scrapie prion protein using seeded conversion of recombinant prion protein. Nat Methods *4*, 645-650.

Atarashi, R., Wilham, J.M., Christensen, L., Hughson, A.G., Moore, R.A., Johnson, L.M., Onwubiko, H.A., Priola, S.A., and Caughey, B. (2008). Simplified ultrasensitive prion detection by recombinant PrP conversion with shaking. Nat Methods *5*, 211-212.

Aucouturier, P., Carp, R.I., Carnaud, C., and Wisniewski, T. (2000). Prion diseases and the immune system. Clin Immunol *96*, 79-85.

Audi, J., Belson, M., Patel, M., Schier, J., and Osterloh, J. (2005). Ricin poisoning: a comprehensive review. JAMA *294*, 2342-2351.

Bachman, M. (1999). Anisotropic silicon etching using KOH. Integrated nanosystems research facility. University of Califonia, Irvine, USA.

Banerjee, A., Mikhailova, E., Cheley, S., Gu, L.Q., Montoya, M., Nagaoka, Y., Gouaux, E., and Bayley, H. (2010). Molecular bases of cyclodextrin adapter interactions with engineered protein nanopores. Proc Natl Acad Sci USA *107*, 8165-8170.

Baran, C., Smith, G.S., Bamm, V.V., Harauz, G., and Lee, J.S. (2010). Divalent cations induce a compaction of intrinsically disordered myelin basic protein. Biochem Biophys Res Commun *391*, 224-229.

Barret, A., Tagliavini, F., Forloni, G., Bate, C., Salmona, M., Colombo, L., De Luigi, A., Limido, L., Suardi, S., Rossi, G., *et al.* (2003). Evaluation of quinacrine treatment for prion diseases. J Virol *77*, 8462-8469.

Bartz, J.C., Bessen, R.A., McKenzie, D., Marsh, R.F., and Aiken, J.M. (2000). Adaptation and selection of prion protein strain conformations following interspecies transmission of transmissible mink encephalopathy. J Virol *74*, 5542-5547.

Bashford, C.L., Alder, G.M., Fulford, L.G., Korchev, Y.E., Kovacs, E., MacKinnon, A., Pederzolli, C., and Pasternak, C.A. (1996). Pore formation by S. aureus alpha-toxin in liposomes and planar lipid bilayers: effects of nonelectrolytes. J Membr Biol *150*, 37-45.

Baskakov, I.V. (2004). Autocatalytic conversion of recombinant prion proteins displays a species barrier. J Biol Chem *279*, 7671-7677.

Baskakov, I.V., Legname, G., Baldwin, M.A., Prusiner, S.B., and Cohen, F.E. (2002). Pathway complexity of prion protein assembly into amyloid. J Biol Chem *277*, 21140-21148.

Basu, S., Mohan, M.L., Luo, X., Kundu, B., Kong, Q., and Singh, N. (2007). Modulation of proteinase K-resistant prion protein in cells and infectious brain homogenate by redox iron: implications for prion replication and disease pathogenesis. Mol Biol Cell *18*, 3302-3312.

Bayley, H. (1999). Designed membrane channels and pores. Curr Opin Biotechnol *10*, 94-103.

Bayley, H., and Martin, C.R. (2000). Resistive-pulse sensing – From microbes to molecules. Chem Rev *100*, 2575-2594.

Bayley, H., and Sanghera, G. (2008). Standard and pores. Nature *456*, 23-25.

Bellon, A., Seyfert-Brandt, W., Lang, W., Baron, H., Groner, A., and Vey, M. (2003). Improved conformation-dependent immunoassay: suitability for human prion detection with enhanced sensitivity. J Gen Virol *84*, 1921-1925.

Belmonte, G., Cescatti, L., Ferrari, B., Nicolussi, T., Ropele, M., and Menestrina, G. (1987). Pore formation by Staphylococcus aureus alpha-toxin in lipid bilayers. Dependence upon temperature and toxin concentration. Eur Biophys J *14*, 349-358.

Bencsik, A., Debeer, S., Petit, T., and Baron, T. (2009). Possible case of maternal transmission of feline spongiform encephalopathy in a captive cheetah. PLoS One *4*, e6929.

Benner, S., Chen, R.J., Wilson, N.A., Abu-Shumays, R., Hurt, N., Lieberman, K.R., Deamer, D.W., Dunbar, W.B., and Akeson, M. (2007). Sequence-specific detection of individual DNA polymerase complexes in real time using a nanopore. Nat Nanotechnol *2*, 718-724.

Bennion, B.J., and Daggett, V. (2002). Protein conformation and diagnostic tests: the prion protein. Clin Chem *48*, 2105-2114.

Bennion, B.J., DeMarco, M.L., and Daggett, V. (2004). Preventing misfolding of the prion protein by trimethylamine N-oxide. Biochemistry *43*, 12955-12963.

Berlett, B.S., and Stadtman, E.R. (1997). Protein oxidation in aging, disease, and oxidative stress. J Biol Chem *272*, 20313-20316.

Bernheimer, A.W., and Avigad, L.S. (1974). Partial characterization of aerolysin, a lytic exotoxin from Aeromonas hydrophila. Infect Immun *9*, 1016-1021.

Bessen, R.A., and Marsh, R.F. (1992). Biochemical and physical properties of the prion protein from two strains of the transmissible mink encephalopathy agent. J Virol *66*, 2096-2101.

Bezrukov, S.M., and Kasianowicz, J.J. (1997). The charge state of an ion channel controls neutral polymer entry into its pore. Eur Biophys J *26*, 471-476.

Bhakdi, S., Fussle, R., and Tranum-Jensen, J. (1981). Staphylococcal alpha-toxin: oligomerization of hydrophilic monomers to form amphiphilic hexamers induced through contact with deoxycholate detergent micelles. Proc Natl Acad Sci USA *78*, 5475-5479.

Bhat, U.G., and Gartel, A.L.(2008). Differencial sensitivity of human colon cancer cell lines to the nucleoside analogs ARC and DRB. Int J Cancer *122*, 1426-1429.

Bieschke, J., Giese, A., Schulz-Schaeffer, W., Zerr, I., Poser, S., Eigen, M., and Kretzschmar, H. (2000). Ultrasensitive detection of pathological prion protein aggregates by dual-color scanning for intensely fluorescent targets. Proc Natl Acad Sci USA *97*, 5468-5473.

Biffiger, K., Zwald, D., Kaufmann, L., Briner, A., Nayki, I., Purro, M., Bottcher, S., Struckmeyer, T., Schaller, O., Meyer, R., *et al.* (2002). Validation of a luminescence immunoassay for the detection of PrP(Sc) in brain homogenate. J Virol Methods *101*, 79-84.

Blanco, B.J., Rivas, G. and Serrano, L.: A short linear peptide that folds into a native stable β-hairpin in aqueous solution. Structural Biology 1994, *1*: 584-590

Bocharova, O.V., Breydo, L., Parfenov, A.S., Salnikov, V.V., and Baskakov, I.V. (2005). In vitro conversion of full-length mammalian prion protein produces amyloid form with physical properties of PrP(Sc). J Mol Biol *346*, 645-659.

Borchelt, D.R., Scott, M., Taraboulos, A., Stahl, N., and Prusiner, S.B. (1990). Scrapie and cellular prion proteins differ in their kinetics of synthesis and topology in cultured cells. J Cell Biol *110*, 743-752.

Bosque, P.J., and Prusiner, S.B. (2000). Cultured cell sublines highly susceptible to prion infection. J Virol *74*, 4377-4386.

Bourhim, M., Kruzel, M., Srikrishnan, T., and Nicotera, T. (2007). Linear quantitation of Abeta aggregation using Thioflavin T: reduction in fibril formation by colostrinin. J Neurosci Methods *160*, 264-268.

Braha, O., Walker, B., Cheley, S., Kasianowicz, J.J., Song, L., Gouaux, J.E., and Bayley, H. (1997). Designed protein pores as components for biosensors. Chem Biol *4*, 497-505.

Braha, O., Gu, L., Zhou, L., Lu, X., Cheley, S., and Bayley, H. (2000). Simultaneous stochastic sensing of divalent metal ions. Nature Biotechnology *18*, 1005-1007.

Braha, O., Webb, J., Gu, L.Q., Kim, K., and Bayley, H. (2005). Carriers versus adapters in stochastic sensing. Chemphyschem *6*, 889-892.

Branton, D., Deamer, D.W., Marziali, A., Bayley, H., Benner, S.A., Butler, T., Di Ventra, M., Garaj, S., Hibbs, A., Huang, X., *et al.* (2008). The potential and challenges of nanopore sequencing. Nat Biotechnol *26*, 1146-1153.

Brazier, M.W., Davies, P., Player, E., Marken, F., Viles, J.H., and Brown, D.R. (2008). Manganese binding to the prion protein. J Biol Chem *283*, 12831-12839.

Breydo, L., Bocharova, O.V., Makarava, N., Salnikov, V.V., Anderson, M., and Baskakov, I.V. (2005). Methionine oxidation interferes with conversion of the prion protein into the fibrillar proteinase K-resistant conformation. Biochemistry *44*, 15534-15543.

Breydo, L., Makarava, N. , Baskakov, V. (2008). Methods for conversion of prion protein into amyloid fibrils. Prion protein protocols, methods in molecular biology, *459*,105-115.

Brown, D.R., Hafiz, F., Glasssmith, L.L., Wong, B.S., Jones, I.M., Clive, C., and Haswell, S.J. (2000). Consequences of manganese replacement of copper for prion protein function and proteinase resistance. EMBO J *19*, 1180-1186.

Brown, D.R., Qin, K., Herms, J.W., Madlung, A., Manson, J., Strome, R., Fraser, P.E., Kruck, T., von Bohlen, A., Schulz-Schaeffer, W., *et al.* (1997). The cellular prion protein binds copper in vivo. Nature *390*, 684-687.

Brown, D.R., Schmidt, B., and Kretzschmar, H.A. (1998a). Effects of copper on survival of prion protein knockout neurons and glia. J Neurochem *70*, 1686-1693.

Brown, P. (2001). Creutzfeldt-Jakob disease: blood infectivity and screening tests. Semin Hematol *38*, 2-6.

Brown, P., Cervenakova, L., and Diringer, H. (2001). Blood infectivity and the prospects for a diagnostic screening test in Creutzfeldt-Jakob disease. J Lab Clin Med *137*, 5-13.

Brown, P., Preece, M.A., and Will, R.G. (1992). "Friendly fire" in medicine: hormones, homografts, and Creutzfeldt-Jakob disease. Lancet *340*, 24-27.

Brown, P., Rohwer, R.G., Dunstan, B.C., MacAuley, C., Gajdusek, D.C., and Drohan, W.N. (1998b). The distribution of infectivity in blood components and plasma derivatives in experimental models of transmissible spongiform encephalopathy. Transfusion *38*, 810-816.

Bruce, M.E. (1993). Scrapie strain variation and mutation. Br Med Bull *49*, 822-838.

Bruce, M.E., Boyle, A., Cousens, S., McConnell, I., Foster, J., Goldmann, W., and Fraser, H. (2002). Strain characterization of natural sheep scrapie and comparison with BSE. J Gen Virol *83*, 695-704.

Bruce, M.E., McBride, P.A., Jeffrey, M., and Scott, J.R. (1994). PrP in pathology and pathogenesis in scrapie-infected mice. Mol Neurobiol *8*, 105-112.

Bruce, M.E., Will, R.G., Ironside, J.W., McConnell, I., Drummond, D., Suttie, A., McCardle, L., Chree, A., Hope, J., Birkett, C., *et al.* (1997). Transmissions to mice indicate that 'new variant' CJD is caused by the BSE agent. Nature *389*, 498-501.

Buckley, J.T., Halasa, L.N., Lund, K.D., and MacIntyre, S. (1981). Purification and some properties of the hemolytic toxin aerolysin. Can J Biochem *59*, 430-435.

Buckley, J.T., Wilmsen, H.U., Lesieur, C., Schulze, A., Pattus, F., Parker, M.W., and van der Goot, F.G. (1995). Protonation of histidine-132 promotes oligomerization of the channel-forming toxin aerolysin. Biochemistry *34*, 16450-16455.

Bueler, H., Aguzzi, A., Sailer, A., Greiner, R.A., Autenried, P., Aguet, M., and Weissmann, C. (1993). Mice devoid of PrP are resistant to scrapie. Cell *73*, 1339-1347.

Bugs, M.R., Forato, L.A., Bortoleto-Bugs, R.K., Fischer, H., Mascarenhas, Y.P., Ward, R.J., and Colnago, L.A. (2004). Spectroscopic characterization and structural modeling of prolamin from maize and pearl millet. Eur Biophys J *33*, 335-343.

Burns, C.S., Aronoff-Spencer, E., Dunham, C.M., Lario, P., Avdievich, N.I., Antholine, W.E., Olmstead, M.M., Vrielink, A., Gerfen, G.J., Peisach, J., *et al.* (2002). Molecular features of the copper binding sites in the octarepeat domain of the prion protein. Biochemistry *41*, 3991-4001.

Burns, C.S., Aronoff-Spencer, E., Legname, G., Prusiner, S.B., Antholine, W.E., Gerfen, G.J., Peisach, J., and Millhauser, G.L. (2003). Copper coordination in the full-length, recombinant prion protein. Biochemistry *42*, 6794-6803.

Bustamante, C., Erie, D.A., and Keller, D. (1994). Biochemical and Structural Applications of Scanning Force Microscopy. Curr Opin Struc Biol *4*, 750-760.

Butler, T.Z., Gundlach, J.H., and Troll, M.A. (2006). Determination of RNA orientation during translocation through a biological nanopore. Biophys J *90*, 190-199.

Butler, T.Z., Pavlenok, M., Derrington, I.M., Niederweis, M., and Gundlach, J.H. (2008). Single-molecule DNA detection with an engineered MspA protein nanopore. Proc Natl Acad Sci USA *105*, 20647-20652.

Carpino, L.A., and Han, G.Y. (1972). 9-Fluorenylmethoxycarbonyl Amino-Protecting Group. Journal of Organic Chemistry *37*, 3404-3409.

Castilla, J., Saa, P., and Soto, C. (2005). Detection of prions in blood. Nat Med *11*, 982-985.

Castilla, J., Gonzalez-Romero, D., Saa, P., Morales, R., De Castro, J., and Soto, C. (2008). Crossing the species barrier by PrP(Sc) replication in vitro generates unique infectious prions. Cell *134*, 757-768.

Caughey, B. (2001). Interactions between prion protein isoforms: the kiss of death? Trends Biochem Sci *26*, 235-242.

Caughey, B., and Baron, G.S. (2006). Prions and their partners in crime. Nature *443*, 803-810.

Caughey, B., Brown, K., Raymond, G.J., Katzenstein, G.E., and Thresher, W. (1994). Binding of the protease-sensitive form of PrP (prion protein) to sulfated glycosaminoglycan and congo red [corrected]. J Virol *68*, 2135-2141.

Caughey, B., Neary, K., Buller, R., Ernst, D., Perry, L.L., Chesebro, B., and Race, R.E. (1990). Normal and scrapie-associated forms of prion protein differ in their sensitivities to phospholipase and proteases in intact neuroblastoma cells. J Virol *64*, 1093-1101.

Caughey, B., and Raymond, G.J. (1993). Sulfated polyanion inhibition of scrapie-associated PrP accumulation in cultured cells. J Virol *67*, 643-650.

Caughey, B., Raymond, G.J., Callahan, M.A., Wong, C., Baron, G.S., and Xiong, L.W. (2001). Interactions and conversions of prion protein isoforms. Adv Protein Chem *57*, 139-169.

Caughey, W.S., Raymond, L.D., Horiuchi, M., and Caughey, B. (1998). Inhibition of protease-resistant prion protein formation by porphyrins and phthalocyanines. Proc Natl Acad Sci USA *95*, 12117-12122.

Chakraborty, T., Huhle, B., Bergbauer, H., and Goebel, W. (1986). Cloning, expression, and mapping of the Aeromonas hydrophila aerolysin gene determinant in Escherichia coli K-12. J Bacteriol *167*, 368-374.

Chakraborty, T., Huhle, B., Hof, H., Bergbauer, H., and Goebel, W. (1987). Marker exchange mutagenesis of the aerolysin determinant in Aeromonas hydrophila demonstrates the role of aerolysin in A. hydrophila-associated systemic infections. Infect Immun *55*, 2274-2280.

Chang, H., Kosari, F., Andreadakis, G., Alam, M.A., Vasmatzis, G., and Bashir, R. (2004). DNA-mediated fluctuations in ionic current through silicon oxide nanopore channels. Nano Lett *4*, 1551-1556.

Charvin, G., Strick, T.R., Bensimon, D., and Croquette, V. (2005). Topoisomerase IV bends and overtwists DNA upon binding. Biophys J *89*, 384-392.

Cheley, S., Gu, L.Q., and Bayley, H. (2002). Stochastic sensing of nanomolar inositol 1,4,5-trisphosphate with an engineered pore. Chem Biol *9*, 829-838.

Chen, M., Khalid, S., Sansom, M.S., and Bayley, H. (2008a). Outer membrane protein G: Engineering a quiet pore for biosensing. Proc Natl Acad Sci USA *105*, 6272-6277.

Chen, M., Li, Q.H., and Bayley, H. (2008b). Orientation of the monomeric porin OmpG in planar lipid bilayers. Chembiochem *9*, 3029-3036.

Cheng, S.F., and Chang, D.K. (1999). Proline-induced kink in a helix arises primarily from dihedral angle energy: a molecular dynamics simulation on alamethicin. Chem Phys Lett *301*, 453-457.

Chiti, F., and Dobson, C.M. (2006). Protein misfolding, functional amyloid, and human disease. Annu Rev Biochem *75*, 333-366.

Clarke, J., Wu, H.C., Jayasinghe, L., Patel, A., Reid, S., and Bayley, H. (2009). Continuous base identification for single-molecule nanopore DNA sequencing. Nat Nanotechnol *4*, 265-270.

Cobb, N.J., and Surewicz, W.K. (2009). Prion diseases and their biochemical mechanisms. Biochemistry *48*, 2574-2585.

Cohen, F.E., and Prusiner, S.B. (1998). Pathologic conformations of prion proteins. Annu Rev Biochem *67*, 793-819.

Coitinho, A.S., Freitas, A.R., Lopes, M.H., Hajj, G.N., Roesler, R., Walz, R., Rossato, J.I., Cammarota, M., Izquierdo, I., Martins, V.R., and Brentani, R.R. (2006). The interaction between prion protein and laminin modulates memory consolidation. Eur J Neurosci *24*, 3255-3264.

Colby, D.W., Wain, R., Baskakov, I.V., Legname, G., Palmer, C.G., Nguyen, H.O., Lemus, A., Cohen, F.E., DeArmond, S.J., and Prusiner, S.B. (2010). Protease-sensitive synthetic prions. PLoS Pathog *6*, e1000736.

Cole, K.S. (1965). Electrodiffusion Models for Membrane of Squid Giant Axon. Physiol Rev *45*, 340-379.

Collinge, J., and Clarke, A.R. (2007). A general model of prion strains and their pathogenicity. Science *318*, 930-936.

Collinge, J., Palmer, M.S., and Dryden, A.J. (1991). Genetic predisposition to iatrogenic Creutzfeldt-Jakob disease. Lancet *337*, 1441-1442.

Collinge, J., and Rossor, M. (1996). A new variant of prion disease. Lancet *347*, 916-917.

Collinge, J., Sidle, K.C., Meads, J., Ironside, J., and Hill, A.F. (1996). Molecular analysis of prion strain variation and the aetiology of 'new variant' CJD. Nature *383*, 685-690.

Combs, C.K., Johnson, D.E., Cannady, S.B., Lehman, T.M., and Landreth, G.E. (1999). Identification of microglial signal transduction pathways mediating a neurotoxic response to amyloidogenic fragments of beta-amyloid and prion proteins. J Neurosci *19*, 928-939.

Conlan, S., and Bayley, H. (2003). Folding of a monomeric porin, OmpG, in detergent solution. Biochemistry *42*, 9453-9465.

Conlan, S., Zhang, Y., Cheley, S., and Bayley, H. (2000). Biochemical and biophysical characterization of OmpG: A monomeric porin. Biochemistry *39*, 11845-11854.

Cornell, B.A., Braach-Maksvytis, V.L., King, L.G., Osman, P.D., Raguse, B., Wieczorek, L., and Pace, R.J. (1997). A biosensor that uses ion-channel switches. Nature *387*, 580-583.

Coulter, W.H. (1953). US Pat., 2656508.

Croes, E.A., Theuns, J., Houwing-Duistermaat, J.J., Dermaut, B., Sleegers, K., Roks, G., Van den Broeck, M., van Harten, B., van Swieten, J.C., Cruts, M., *et al.* (2004). Octapeptide repeat insertions in the prion protein gene and early onset dementia. J Neurol Neurosurg Psychiatry *75*, 1166-1170.

Cumpson, P.J., Clifford, C.A., and Hedley, J. (2004). Quantitative analytical atomic force microscopy: a cantilever reference device for easy and accurate AFM spring-constant calibration. Meas Sci Technol *15*, 1337-1346.

Curin Serbec, V., Bresjanac, M., Popovic, M., Pretnar Hartman, K., Galvani, V., Rupreht, R., Cernilec, M., Vranac, T., Hafner, I., and Jerala, R. (2004). Monoclonal antibody against a peptide of human prion protein discriminates between Creutzfeldt-Jacob's disease-affected and normal brain tissue. J Biol Chem *279*, 3694-3698.

Deamer, D. (2010). Nanopore analysis of nucleic acids bound to exonucleases and polymerases. Annu Rev Biophys *39*, 79-90.

Deamer, D.W., and Akeson, M. (2000). Nanopores and nucleic acids: prospects for ultrarapid sequencing. Trends Biotechnol *18*, 147-151.

Deamer, D.W., and Branton, D. (2002). Characterization of nucleic acids by nanopore analysis. Acc Chem Res *35*, 817-825.

DeBlois, R.W., and Bean, C.P. (1970). Counting and Sizing of Submicron Particles by Resistive Pulse Technique. Review of Scientific Instruments *41*, 909-916.

DeGuzman, V.S., Lee, C.C., Deamer, D.W., and Vercoutere, W.A. (2006). Sequence-dependent gating of an ion channel by DNA hairpin molecules. Nucleic Acids Res *34*, 6425-6437.

Dekker, C. (2007). Solid-state nanopores. Nat Nanotechnol *2*, 209-215.

Deleault, N.R., Geoghegan, J.C., Nishina, K., Kascsak, R., Williamson, R.A., and Supattapone, S. (2005). Protease-resistant prion protein amplification reconstituted with partially purified substrates and synthetic polyanions. J Biol Chem *280*, 26873-26879.

Demart, S., Fournier, J.G., Creminon, C., Frobert, Y., Lamoury, F., Marce, D., Lasmezas, C., Dormont, D., Grassi, J., and Deslys, J.P. (1999). New insight into abnormal prion protein using monoclonal antibodies. Biochem Biophys Res Commun *265*, 652-657.

Derrington, I.M., Butler, T.Z., Collins, M.D., Manrao, E., Pavlenok, M., Niederweis, M., and Gundlach, J.H. (2010). Nanopore DNA sequencing with MspA. Proc Natl Acad Sci USA *107*, 16060-16065.

Donne, D.G., Viles, J.H., Groth, D., Mehlhorn, I., James, T.L., Cohen, F.E., Prusiner, S.B., Wright, P.E., and Dyson, H.J. (1997). Structure of the recombinant full-length hamster prion protein PrP(29-231): The N terminus is highly flexible. Proc Natl Acad Sci USA *94*, 13452-13457.

Du, D., and Gai, F. (2006). Understanding the folding mechanism of an alpha-helical hairpin. Biochemistry *45*, 13131-13139.

Enari, M., Flechsig, E., and Weissmann, C. (2001). Scrapie prion protein accumulation by scrapie-infected neuroblastoma cells abrogated by exposure to a prion protein antibody. Proc Natl Acad Sci U S A *98*, 9295-9299.

Fajardo, D.A., Cheung, J., Ito, C., Sugawara, E., Nikaido, H., and Misra, R. (1998). Biochemistry and regulation of a novel Escherichia coli K-12 porin protein, OmpG, which produces unusually large channels. J Bacteriol *180*, 4452-4459.

Faller, M., Niederweis, M., and Schulz, G.E. (2004). The structure of a mycobacterial outer-membrane channel. Science *303*, 1189-1192.

Fernandez, J.M., and Li, H. (2004). Force-clamp spectroscopy monitors the folding trajectory of a single protein. Science *303*, 1674-1678.

Fezoui, Y., Weaver, D.L., and Osterhout, J.J. (1994). De novo design and structural characterization of an alpha-helical hairpin peptide: a model system for the study of protein folding intermediates. Proc Natl Acad Sci U S A *91*, 3675-3679.

Firnkes, M., Pedone, D., Knezevic, J., Doblinger, M., and Rant, U. (2010). Electrically Facilitated Translocations of Proteins through Silicon Nitride Nanopores: Conjoint and Competitive Action of Diffusion, Electrophoresis, and Electroosmosis. Nano Lett *10*, 2162-2167.

Fivaz, M., Velluz, M.C., and van der Goot, F.G. (1999). Dimer dissociation of the pore-forming toxin aerolysin precedes receptor binding. J Biol Chem *274*, 37705-37708.

Fologea, D., Gershow, M., Ledden, B., McNabb, D.S., Golovchenko, J.A., and Li, J. (2005). Detecting single stranded DNA with a solid state nanopore. Nano Lett *5*, 1905-1909.

Fologea, D., Ledden, B., McNabb, D.S., and Li, J. (2007). Electrical characterization of protein molecules by a solid-state nanopore. Applied Physics Letters *91*, 053901-053903.

Franco-Obregon, A., and Lansman, J.B. (2002). Changes in mechanosensitive channel gating following mechanical stimulation in skeletal muscle myotubes from the mdx mouse. J Physiol-London *539*, 391-407.

Franscini, N., El Gedaily, A., Matthey, U., Franitza, S., Sy, M.S., Burkle, A., Groschup, M., Braun, U., and Zahn, R. (2006). Prion protein in milk. PLoS One *1*, e71.

Fraser, H., and Dickinson, A.G. (1973). Scrapie in mice. Agent-strain differences in the distribution and intensity of grey matter vacuolation. J Comp Pathol *83*, 29-40.

Friedlander, A.M., Welkos, S.L., Pitt, M.L., Ezzell, J.W., Worsham, P.L., Rose, K.J., Ivins, B.E., Lowe, J.R., Howe, G.B., Mikesell, P., and et al. (1993). Postexposure prophylaxis against experimental inhalation anthrax. J Infect Dis *167*, 1239-1243.

Fussle, R., Bhakdi, S., Sziegoleit, A., Tranum-Jensen, J., Kranz, T., and Wellensiek, H.J. (1981). On the mechanism of membrane damage by Staphylococcus aureus alpha-toxin. J Cell Biol *91*, 83-94.

Gabizon, R., Meiner, Z., Halimi, M., and Ben-Sasson, S.A. (1993). Heparin-like molecules bind differentially to prion-proteins and change their intracellular metabolic fate. J Cell Physiol *157*, 319-325.

Gaggelli, E., Kozlowski, H., Valensin, D., and Valensin, G. (2006). Copper homeostasis and neurodegenerative disorders (Alzheimer's, prion, and Parkinson's diseases and amyotrophic lateral sclerosis). Chem Rev *106*, 1995-2044.

Gambetti, P., Parchi, P., Petersen, R.B., Chen, S.G., and Lugaresi, E. (1995). Fatal familial insomnia and familial Creutzfeldt-Jakob disease: clinical, pathological and molecular features. Brain Pathol *5*, 43-51.

Gajdusek, D.C., and Zigas, V. (1957). Degenerative disease of the central nervous system in New Guinea; the endemic occurrence of kuru in the native population. N Engl J Med *257*, 974-978.

Garcia, F.L., Szyperski, T., Dyer, J.H., Choinowski, T., Seedorf, U., Hauser, H., and Wuthrich, K. (2000). NMR structure of the sterol carrier protein-2: implications for the biological role. J Mol Biol *295*, 595-603.

Garland, W.J., and Buckley, J.T. (1988). The cytolytic toxin aerolysin must aggregate to disrupt erythrocytes, and aggregation is stimulated by human glycophorin. Infect Immun *56*, 1249-1253.

Garnett, A.P., and Viles, J.H. (2003). Copper binding to the octarepeats of the prion protein. Affinity, specificity, folding, and cooperativity: insights from circular dichroism. J Biol Chem *278*, 6795-6802.

Ghetti, B., Dlouhy, S.R., Giaccone, G., Bugiani, O., Frangione, B., Farlow, M.R., and Tagliavini, F. (1995). Gerstmann-Straussler-Scheinker disease and the Indiana kindred. Brain Pathol *5*, 61-75.

Giese, A., Levin, J., Bertsch, U., and Kretzschmar, H. (2004). Effect of metal ions on de novo aggregation of full-length prion protein. Biochem Biophys Res Commun *320*, 1240-1246.

Gilch, S., Wopfner, F., Renner-Muller, I., Kremmer, E., Bauer, C., Wolf, E., Brem, G., Groschup, M.H., and Schatzl, H.M. (2003). Polyclonal anti-PrP auto-antibodies induced with dimeric PrP interfere efficiently with PrP^{Sc} propagation in prion-infected cells. J Biol Chem *278*, 18524-18531.

Goldfarb, L.G., Brown, P., McCombie, W.R., Goldgaber, D., Swergold, G.D., Wills, P.R., Cervenakova, L., Baron, H., Gibbs, C.J., Jr., and Gajdusek, D.C. (1991). Transmissible familial Creutzfeldt-Jakob disease associated with five, seven, and eight extra octapeptide coding repeats in the PRNP gene. Proc Natl Acad Sci U S A *88*, 10926-10930.

Goldfarb,L.G., Mitrova, E., Brown, P., Toh, B.H., and Gajdusek,D.C.(1990). Mutation in codon 200 of scrapie amyloid protein gene in two clusters of Creutzfeldt-Jakob disease in Slovakia. Lancet *336*, 514-515.

Goldfarb, L.G., Petersen, R.B., Tabaton, M., Brown, P., LeBlanc, A.C., Montagna, P., Cortelli, P., Julien, J., Vital, C., Pendelbury, W.W., and et al. (1992). Fatal familial insomnia and familial Creutzfeldt-Jakob disease: disease phenotype determined by a DNA polymorphism. Science *258*, 806-808.

Goodrich, C.P., Kirmizialtin, S., Huyghues-Despointes, B.M., Zhu, A., Scholtz, J.M., Makarov, D.E., and Movileanu, L. (2007). Single-molecule electrophoresis of beta-hairpin peptides by electrical recordings and Langevin dynamics simulations. J Phys Chem B *111*, 3332-3335.

Gore, J., Bryant, Z., Stone, M.D., Nollmann, M., Cozzarelli, N.R., and Bustamante, C. (2006). Mechanochemical analysis of DNA gyrase using rotor bead tracking. Nature *439*, 100-104.

Gouaux, E. (1997). Channel-forming toxins: Tales of transformation. Curr Opin Struc Biol *7*, 566-573.

Graham, M. (2003). The Coulter principle: Foundation of an industry. JALA *8*, 72-81.

Grandbois, M., Beyer, M., Rief, M., Clausen-Schaumann, H., and Gaub, H.E. (1999). How strong is a covalent bond? Science *283*, 1727-1730.

Grassi, J., Comoy, E., Simon, S., Creminon, C., Frobert, Y., Trapmann, S., Schimmel, H., Hawkins, S.A., Moynagh, J., Deslys, J.P., and Wells, G.A. (2001). Rapid test for the preclinical postmortem diagnosis of BSE in central nervous system tissue. Vet Rec *149*, 577-582.

Grinkevich,V., Issaeva, N., Hossain, S., Pramanik,A., and Selvannova, G. (2005). PrP^{Sc} in mammary glands of sheep affected by scrapie and mastitis. Nat. Med *11*, 1137-1138.

Grosman, C. (2003). Free-energy landscapes of ion-channel gating are malleable: changes in the number of bound ligands are accompanied by changes in the location of the transition state in acetylcholine-receptor channels. Biochemistry *42*, 14977-14987.

Gross, J.E., and Miller, M.W. (2001). Chronic wasting disease in mule deer: disease dynamics and control. J Wildlife Manage *65*, 205-215.

Gu, L.Q., Braha, O., Conlan, S., Cheley, S., and Bayley, H. (1999). Stochastic sensing of organic analytes by a pore-forming protein containing a molecular adapter. Nature *398*, 686-690.

Gu, Y., Fujioka, H., Mishra, R.S., Li, R., and Singh, N. (2002). Prion peptide 106-126 modulates the aggregation of cellular prion protein and induces the synthesis of potentially neurotoxic transmembrane PrP. J Biol Chem *277*, 2275-2286.

Guan, X., Gu, L.Q., Cheley, S., Braha, O., and Bayley, H. (2005). Stochastic sensing of TNT with a genetically engineered pore. Chembiochem *6*, 1875-1881.

Ha, T. (2001). Single-molecule fluorescence resonance energy transfer. Methods *25*, 78-86.

Ha, T., Enderle, T., Ogletree, D.F., Chemla, D.S., Selvin, P.R., and Weiss, S. (1996). Probing the interaction between two single molecules: fluorescence resonance energy transfer between a single donor and a single acceptor. Proc Natl Acad Sci U S A *93*, 6264-6268.

Ha, T., Rasnik, I., Cheng, W., Babcock, H.P., Gauss, G.H., Lohman, T.M., and Chu, S. (2002). Initiation and re-initiation of DNA unwinding by the Escherichia coli Rep helicase. Nature *419*, 638-641.

Halverson, K.M., Panchal, R.G., Nguyen, T.L., Gussio, R., Little, S.F., Misakian, M., Bavari, S., and Kasianowicz, J.J. (2005). Anthrax biosensor, protective antigen ion channel asymmetric blockade. J Biol Chem *280*, 34056-34062.

Hamill, O.P., Marty, A., Neher, E., Sakmann, B., and Sigworth, F.J. (1981). Improved Patch-Clamp Techniques for High-Resolution Current Recording from Cells and Cell-Free Membrane Patches. Pflug Arch Eur J Phy *391*, 85-100.

Han, A., Creus, M., Schurmann, G., Linder, V., Ward, T.R., de Rooij, N.F., and Staufer, U. (2008). Label-free detection of single protein molecules and protein-protein interactions using synthetic nanopores. Anal Chem *80*, 4651-4658.

Han, A., Schurmann,G., Mondin,G., Bitterli,R.A., Hegelbach,N.G., de Rooij, N.F., and Staufer,U.(2006). Sensing protein molecules using nanofabricated pores. Applied Physics Letters *88*, 093901-093903.

Harrell, C.C., Siwy, Z.S., and Martin, C.R. (2006). Conical nanopore membranes: controlling the nanopore shape. Small *2*, 194-198.

Harris, D.A., Huber, M.T., van Dijken, P., Shyng, S.L., Chait, B.T., and Wang, R. (1993). Processing of a cellular prion protein: identification of N- and C-terminal cleavage sites. Biochemistry *32*, 1009-1016.

Hartsoug.Gr, and Burger, D. (1965). Encephalopathy of Mink .I. Epizootiologic and Clinical Observations. Journal of Infectious Diseases *115*, 387-392.

Hedlin, P.D., Cashman, N.R., Li. Li., Jyotsana, G., Babiuk, L.A., Potter, A.A., Griebel,P., and Napper, S. (2010). Design and delivery of a cryptic PrP^{C} epitope for induction of PrP^{SC}-specific antibody responses. Vaccine *28*, 981-988.

Hegde, R.S., Mastrianni, J.A., Scott, M.R., DeFea, K.A., Tremblay, P., Torchia, M., DeArmond, S.J., Prusiner, S.B., and Lingappa, V.R. (1998). A transmembrane form of the prion protein in neurodegenerative disease. Science *279*, 827-834.

Heller, U., Winklhofer, K.F., Heske, J., Reintjes, A., and Tatzelt, J. (2003). Post-translational import of the prion protein into the endoplasmic reticulum interferes with cell viability: a critical role for the putative transmembrane domain. J Biol Chem *278*, 36139-36147.

Heng, J.B., Ho, C., Kim, T., Timp, R., Aksimentiev, A., Grinkova, Y.V., Sligar, S., Schulten, K., and Timp, G. (2004). Sizing DNA using a nanometer-diameter pore. Biophys J *87*, 2905-2911.

Henrickson, S.E., Misakian, M., Robertson, B., and Kasianowicz, J.J. (2000). Driven DNA transport into an asymmetric nanometer-scale pore. Phys Rev Lett *85*, 3057-3060.

Henriquez, R.R., Ito, T., Sun, L., and Crooks, R.M. (2004). The resurgence of Coulter counting for analyzing nanoscale objects. Analyst *129*, 478-482.

Heppner, F.L., Musahl, C., Arrighi, I., Klein, M.A., Rulicke, T., Oesch, B., Zinkernagel, R.M., Kalinke, U., and Aguzzi, A. (2001). Prevention of scrapie pathogenesis by transgenic expression of anti-prion protein antibodies. Science *294*, 178-182.

Herms, J.W., Tings, T., Dunker, S., and Kretzschmar, H.A. (2001). Prion protein affects Ca^{2+}-activated K^{+} currents in cerebellar purkinje cells. Neurobiol Dis *8*, 324-330.

Hill, A.F., Zeidler, M., Ironside, J., and Collinge, J. (1997). Diagnosis of new variant Creutzfeldt-Jakob disease by tonsil biopsy. Lancet *349*, 99-100.

Hille, B. (1992). Ionic channels of excitable membranes, second edition.(Sinauer Associates, Sunderland, MA).

Hladky, S.B., and Haydon, D.A. (1970). Discreteness of Conductance Change in Bimolecular Lipid Membranes in Presence of Certain Antibiotics. Nature *225*, 451-453.

Holden, M.A., and Bayley, H. (2005). Direct introduction of single protein channels and pores into lipid bilayers. Journal of the American Chemical Society *127*, 6502-6503.

Holden, M.A., Jayasinghe, L., Daltrop, O., Mason, A., and Bayley, H. (2006). Direct transfer of membrane proteins from bacteria to planar bilayers for rapid screening by single-channel recording. Nat Chem Biol *2*, 314-318.

Holly, R., and Hingerl, K. (2006). Fabrication of silicon vertical taper structures using KOH anisotropic etching. Microelectron Eng *83*, 1430-1433.

Honda, S., Kobayashi, N., and Munekata, E. (2000). Thermodynamics of a beta-hairpin structure: evidence for cooperative formation of folding nucleus. J Mol Biol *295*, 269-278.

Hornblower, B., Coombs, A., Whitaker, R.D., Kolomeisky, A., Picone, S.J., Meller, A., and Akeson, M. (2007). Single-molecule analysis of DNA-protein complexes using nanopores. Nat Methods *4*, 315-317.

Hornshaw, M.P., McDermott, J.R., and Candy, J.M. (1995a). Copper binding to the N-terminal tandem repeat regions of mammalian and avian prion protein. Biochem Biophys Res Commun *207*, 621-629.

Hornshaw, M.P., McDermott, J.R., Candy, J.M., and Lakey, J.H. (1995b). Copper binding to the N-terminal tandem repeat region of mammalian and avian prion protein: structural studies using synthetic peptides. Biochem Biophys Res Commun *214*, 993-999.

Hosszu, L.L., Baxter, N.J., Jackson, G.S., Power, A., Clarke, A.R., Waltho, J.P., Craven, C.J., and Collinge, J. (1999). Structural mobility of the human prion protein probed by backbone hydrogen exchange. Nat Struct Biol *6*, 740-743.

Howard, S.P., and Buckley, J.T. (1982). Membrane glycoprotein receptor and hole-forming properties of a cytolytic protein toxin. Biochemistry *21*, 1662-1667.

Howard, S.P., and Buckley, J.T. (1985). Activation of the hole-forming toxin aerolysin by extracellular processing. J Bacteriol *163*, 336-340.

Howard, S.P., and Buckley, J.T. (1986). Molecular cloning and expression in Escherichia coli of the structural gene for the hemolytic toxin aerolysin from Aeromonas hydrophila. Mol Gen Genet *204*, 289-295.

Howard, S.P., Garland, W.J., Green, M.J., and Buckley, J.T. (1987). Nucleotide sequence of the gene for the hole-forming toxin aerolysin of Aeromonas hydrophila. J Bacteriol *169*, 2869-2871.

Howorka, S., Cheley, S., and Bayley, H. (2001a). Sequence-specific detection of individual DNA strands using engineered nanopores. Nat Biotechnol *19*, 636-639.

Howorka, S., Movileanu, L., Braha, O., and Bayley, H. (2001b). Kinetics of duplex formation for individual DNA strands within a single protein nanopore. Proc Natl Acad Sci U S A *98*, 12996-13001.

Howorka, S., Movileanu, L., Lu, X.F., Magnon, M., Cheley, S., Braha, O., and Bayley, H. (2000). A protein pore with a single polymer chain tethered within the lumen. Journal of the American Chemical Society *122*, 2411-2416.

Howorka, S., Nam, J., Bayley, H., and Kahne, D. (2004). Stochastic detection of monovalent and bivalent protein-ligand interactions. Angew Chem Int Ed Engl *43*, 842-846.

Howorka, S., and Siwy, Z. (2009a). Nanopore analytics: sensing of single molecules. Chem Soc Rev *38*, 2360-2384.

Howorka, S., and Siwy, Z. (2009b). Nanopores: generation, engineering and single-molecule applications. Handbook of single molecule biophysics, Hinterdorfer, P., and Van Oijen, A. editors. (New York: Springer Science). pp.293-329.

Hsiao, K., Baker, H.F., Crow, T.J., Poulter, M., Owen, F., Terwilliger, J.D., Westaway, D., Ott, J., and Prusiner, S.B. (1989). Linkage of a prion protein missense variant to Gerstmann-Straussler syndrome. Nature *338*, 342-345.

Huffman, J.L., and Brennan, R.G. (2002). Prokaryotic transcription regulators: more than just the helix-turn-helix motif. Curr Opin Struct Biol *12*, 98-106.

Hunter, N., Goldmann, W., Benson, G., Foster, J.D., and Hope, J. (1993). Swaledale sheep affected by natural scrapie differ significantly in PrP genotype frequencies from healthy sheep and those selected for reduced incidence of scrapie. Journal of General Virology *74*, 1025-1031.

Hunter, N., Moore, L., Hosie, B.D., Dingwall, W.S., and Greig, A. (1997). Association between natural scrapie and PrP genotype in a flock of Suffolk sheep in Scotland. Veterinary Record *140*, 59-63.

Hurt, N., Wang, H., Akeson, M., and Lieberman, K.R. (2009). Specific nucleotide binding and rebinding to individual DNA polymerase complexes captured on a nanopore. J Am Chem Soc *131*, 3772-3778.

Hwa, I.A., Reimann, K., Lim, P.K., and Lai, L.C. (1999). Effects of insulin-like growth factors I and II on oestrone sulphatase activity in human breast cancer cell lines. Int J Mol Med *4*, 175-178.

Iacovache, I., Paumard, P., Scheib, H., Lesieur, C., Sakai, N., Matile, S., Parker, M.W., and van der Goot, F.G. (2006). A rivet model for channel formation by aerolysin-like pore-forming toxins. EMBO J *25*, 457-466.

Ingrosso, L., Ladogana, A., and Pocchiari, M. (1995). Congo red prolongs the incubation period in scrapie-infected hamsters. J Virol *69*, 506-508.

Isaacs, J.D., Jackson, G.S., and Altmann, D.M. (2006). The role of the cellular prion protein in the immune system. Clin Exp Immunol *146*, 1-8.

Jackson, G.S., Murray, I., Hosszu, L.L., Gibbs, N., Waltho, J.P., Clarke, A.R., and Collinge, J. (2001). Location and properties of metal-binding sites on the human prion protein. Proc Natl Acad Sci U S A *98*, 8531-8535.

Jarrett, J.T., and Lansbury, P.T., Jr. (1993). Seeding "one-dimensional crystallization" of amyloid: a pathogenic mechanism in Alzheimer's disease and scrapie? Cell *73*, 1055-1058.

Jeong, K., Suh, J., Chung, W.Y., Kye, Y.S., Kim, D., and Lee, T.Y. (2010). New Methodology for Estimation of the Prion Protein 106-126 Amyloid Aggregation. B Korean Chem Soc *31*, 1029-1030.

Jia, Z.C, Quail, J.W. Waygood, E.B., and Delbaere, L.T.J. (1993). The 2.0-angstrom resolution structure of *Escherichia coli* histidine-containing phosphocarrier protein HPr: A redetermination. J.Biol.Chem. *268*, 22490-22501.

Jirage, K.B., Hulteen, J.C., and Martin, C.R. (1997). Nanotubule-based molecular-filtration membranes. Science *278*, 655-658.

Jones, C.E., Abdelraheim, S.R., Brown, D.R., and Viles, J.H. (2004). Preferential Cu2+ coordination by His96 and His111 induces beta-sheet formation in the unstructured amyloidogenic region of the prion protein. J Biol Chem *279*, 32018-32027.

Jones, C.E., Klewpatinond, M., Abdelraheim, S.R., Brown, D.R., and Viles, J.H. (2005). Probing Cu^{2+} binding to the prion protein using diamagnetic Ni^{2+} and 1H NMR: the unstructured N terminus facilitates the coordination of six Cu^{2+} ions at physiological concentrations. J Mol Biol *346*, 1393-1407.

Kalman, E.B., Sudre, O., Vlassiouk, I., and Siwy, Z.S. (2009). Control of ionic transport through gated single conical nanopores. Anal Bioanal Chem *394*, 413-419.

Kang, X.F., Cheley, S., Guan, X.Y., and Bayley, H. (2006). Stochastic detection of enantiomers. Journal of the American Chemical Society *128*, 10684-10685.

Kasianowicz, J.J., and Bezrukov, S.M. (1995). Protonation dynamics of the alpha-toxin ion channel from spectral analysis of pH-dependent current fluctuations. Biophys J *69*, 94-105.

Kasianowicz, J.J., Brandin, E., Branton, D., and Deamer, D.W. (1996). Characterization of individual polynucleotide molecules using a membrane channel. Proc Natl Acad Sci USA *93*, 13770-13773.

Kasianowicz, J.J., Burden, D.L., Han, L.C., Cheley, S., and Bayley, H. (1999). Genetically engineered metal ion binding sites on the outside of a Channel's transmembrane beta-barrel. Biophys J *76*, 837-845.

Kasianowicz, J.J., Robertson, J.W., Chan, E.R., Reiner, J.E., and Stanford, V.M. (2008). Nanoscopic porous sensors. Annu Rev Anal Chem (Palo Alto Calif) *1*, 737-766.

Katz, B., and Miledi, R. (1972). Statistical Nature of Acetycholine Potential and Its Molecular Components. J Physiol-London *224*, 665-699.

Keyser, U.F., Koeleman, B.N., Van Dorp, S., Krapf, D., Smeets, R.M.M., Lemay, S.G., Dekker, N.H., and Dekker, C. (2006a). Direct force measurements on DNA in a solid-state nanopore. Nat Phys *2*, 473-477.

Keyser, U.F., van der Does, J., Dekker, C., and Dekker, N.H. (2006b). Optical tweezers for force measurements on DNA in nanopores. Review of Scientific Instruments *77*, 105105-1 to105105-9.

Kimberlin, R.H., and Walker, C.A. (1983). The antiviral compound HPA-23 can prevent scrapie when administered at the time of infection. Arch Virol *78*, 9-18.

Kimberlin, R.H., and Walker, C.A. (1986). Suppression of scrapie infection in mice by heteropolyanion 23, dextran sulfate, and some other polyanions. Antimicrob Agents Chemother *30*, 409-413.

Klamt, F., Dal-Pizzol, F., Conte da Frota, M.L., Jr., Walz, R., Andrades, M.E., da Silva, E.G., Brentani, R.R., Izquierdo, I., and Fonseca Moreira, J.C. (2001). Imbalance of antioxidant defense in mice lacking cellular prion protein. Free Radic Biol Med *30*, 1137-1144.

Klatzo, I., Gajdusek, D.C., and Zigas, V. (1959). Pathology of Kuru. Lab Invest *8*, 799-847.

Klewpatinond, M., Davies, P., Bowen, S., Brown, D.R., and Viles, J.H. (2008). Deconvoluting the Cu2+ binding modes of full-length prion protein. J Biol Chem *283*, 1870-1881.

Klewpatinond, M., and Viles, J.H. (2007a). Empirical rules for rationalising visible circular dichroism of Cu2+ and Ni2+ histidine complexes: applications to the prion protein. FEBS Lett *581*, 1430-1434.

Klewpatinond, M., and Viles, J.H. (2007b). Fragment length influences affinity for Cu2+ and Ni2+ binding to His96 or His111 of the prion protein and spectroscopic evidence for a multiple histidine binding only at low pH. Biochem J *404*, 393-402.

Klohn, P.C., Stoltze, L., Flechsig, E., Enari, M., and Weissmann, C. (2003). A quantitative, highly sensitive cell-based infectivity assay for mouse scrapie prions. Proc Natl Acad Sci U S A *100*, 11666-11671.

Koch, T.K., Berg, B.O., De Armond, S.J., and Gravina, R.F. (1985). Creutzfeldt-Jakob disease in a young adult with idiopathic hypopituitarism. Possible relation to the administration of cadaveric human growth hormone. N Engl J Med *313*, 731-733.

Kocisko, D.A., Come, J.H., Priola, S.A., Chesebro, B., Raymond, G.J., Lansbury, P.T., and Caughey, B. (1994). Cell-free formation of protease-resistant prion protein. Nature *370*, 471-474.

Korchev, Y.E., Alder, G.M., Bakhramov, A., Bashford, C.L., Joomun, B.S., Sviderskaya, E.V., Usherwood, P.N., and Pasternak, C.A. (1995a). Staphylococcus aureus alpha-toxin-induced pores: channel-like behavior in lipid bilayers and patch clamped cells. J Membr Biol *143*, 143-151.

Korchev, Y.E., Bashford, C.L., Alder, G.M., Kasianowicz, J.J., and Pasternak, C.A. (1995b). Low conductance states of a single ion channel are not 'closed'. J Membr Biol *147*, 233-239.

Korth, C., May, B.C., Cohen, F.E., and Prusiner, S.B. (2001). Acridine and phenothiazine derivatives as pharmacotherapeutics for prion disease. Proc Natl Acad Sci USA *98*, 9836-9841.

Korth, C., Stierli, B., Streit, P., Moser, M., Schaller, O., Fischer, R., Schulz-Schaeffer, W., Kretzschmar, H., Raeber, A., Braun, U., *et al.* (1997). Prion (PrPSc)-specific epitope defined by a monoclonal antibody. Nature *390*, 74-77.

Kowalczyk, S.W., Hall, A.R., and Dekker, C. (2010). Detection of local protein structures along DNA using solid-state nanopores. Nano Lett *10*, 324-328.

Kramer, M.L., Kratzin, H.D., Schmidt, B., Romer, A., Windl, O., Liemann, S., Hornemann, S., and Kretzschmar, H. (2001). Prion protein binds copper within the physiological concentration range. J Biol Chem *276*, 16711-16719.

Krasnoperov, L.N., Marras, S.A., Kozlov, M., Wirpsza, L., and Mustaev, A. (2010). Luminescent probes for ultrasensitive detection of nucleic acids. Bioconjug Chem *21*, 319-327.

Kuczius, T., Buschmann, A., Zhang, W., Karch, H., Becker, K., Peters, G., and Groschup, M.H. (2004). Cellular prion protein acquires resistance to proteolytic degradation following copper ion binding. Biol Chem *385*, 739-747.

Kullman, L., Winterhalter, M., and Bezrukov, S.M. (2002). Transport of maltodextrins through maltoporin: A single-channel study. Biophysical Journal *82*, 803-812.

Iacovache, I., Paumard, P., Scheib, H., Lesieur, C., Sakai, N., Matile, S., Parker, M.W., and van der Goot, F.G. (2006). A rivet model for channel formation by aerolysin-like pore-forming toxins. EMBO J *25*, 457-466.

Ladogana, A., Casaccia, P., Ingrosso, L., Cibati, M., Salvatore, M., Xi, Y.G., Masullo, C., and Pocchiari, M. (1992). Sulphate polyanions prolong the incubation period of scrapie-infected hamsters. J Gen Virol *73 (Pt 3)*, 661-665.

Lansbury, P.T., and Lashuel, H.A. (2006). A century-old debate on protein aggregation and neurodegeneration enters the clinic. Nature *443*, 774-779.

Leach, S.P., Salman, M.D., and Hamar, D. (2006). Trace elements and prion diseases: a review of the interactions of copper, manganese and zinc with the prion protein. Anim Health Res Rev *7*, 97-105.

Legname, G., Baskakov, I.V., Nguyen, H.O., Riesner, D., Cohen, F.E., DeArmond, S.J., and Prusiner, S.B. (2004). Synthetic mammalian prions. Science *305*, 673-676.

Lee, G.U., Chrisey, L.A., and Colton, R.J. (1994). Direct measurement of the forces between complementary strands of DNA. Science *266*, 771-773.

Lee, S.B., and Martin, C.R. (2002). Electromodulated molecular transport in gold-nanotube membranes. Journal of the American Chemical Society *124*, 11850-11851.

Lezmi, S., Bencsik, A., Monks, E., Petit, T., and Baron, T. (2003). First case of feline spongiform encephalopathy in a captive cheetah born in France: PrPsc analysis in various tissues revealed unexpected targeting of kidney and adrenal gland. Histochem Cell Biol *119*, 415-422.

Li, J., Gershow, M., Stein, D., Brandin, E., and Golovchenko, J.A. (2003). DNA molecules and configurations in a solid-state nanopore microscope. Nat Mater *2*, 611-615.

Li, J., Stein, D., McMullan, C., Branton, D., Aziz, M.J., and Golovchenko, J.A. (2001). Ion-beam sculpting at nanometre length scales. Nature *412*, 166-169.

Lin, J., Kolomeisky, A., and Meller, A. (2010). Helix-coil kinetics of individual polyadenylic acid molecules in a protein channel. Phys Rev Lett *104*, 158101.

Liu, A., Zhao, Q., and Guan, X. (2010). Stochastic nanopore sensors for the detection of terrorist agents: current status and challenges. Anal Chim Acta *675*, 106-115.

Liu, H., Farr-Jones, S., Ulyanov, N.B., Llinas, M., Marqusee, S., Groth, D., Cohen, F.E., Prusiner, S.B., and James, T.L. (1999). Solution structure of Syrian hamster prion protein rPrP(90-231). Biochemistry *38*, 5362-5377.

Lofgren, K., Wahlstrom, A., Lundberg, P., Langel, U., Graslund, A., and Bedecs, K. (2008). Antiprion properties of prion protein-derived cell-penetrating peptides. FASEB J *22*, 2177-2184.

Loudwig, S., and Bayley, H. (2006). Photoisomerization of an individual azobenzene molecule in water: an on-off switch triggered by light at a fixed wavelength. J Am Chem Soc *128*, 12404-12405.

Lucassen, R., Nishina, K., and Supattapone, S. (2003). In vitro amplification of protease-resistant prion protein requires free sulfhydryl groups. Biochemistry *42*, 4127-4135.

Luchian, T., Shin, S.H., and Bayley, H. (2003). Single-molecule covalent chemistry with spatially separated reactants. Angew Chem Int Ed Engl *42*, 3766-3771.

Lysek, D.A., Schorn, C., Nivon, L.G., Esteve-Moya, V., Christen, B., Calzolai, L., von Schroetter, C., Fiorito, F., Herrmann, T., Guntert, P., and Wuthrich, K. (2005). Prion protein NMR structures of cats, dogs, pigs, and sheep. Proc Natl Acad Sci USA *102*, 640-645.

Madampage, C.A., Andrievskaia, O., and Lee, J.S. (2010). Nanopore detection of antibody prion interactions. Anal Biochem *396*, 36-41.

Maglia, G., Henricus, M., Wyss, R., Li, Q., Cheley, S., and Bayley, H. (2009). DNA strands from denatured duplexes are translocated through engineered protein nanopores at alkaline pH. Nano Lett *9*, 3831-3836.

Maglia, G., Restrepo, M.R., Mikhailova, E., and Bayley, H. (2008). Enhanced translocation of single DNA molecules through alpha-hemolysin nanopores by manipulation of internal charge. Proc Natl Acad Sci USA *105*, 19720-19725.

Majd, S., Yusko, E.C., Billeh, Y.N., Macrae, M.X., Yang, J., and Mayer, M. (2010). Applications of biological pores in nanomedicine, sensing, and nanoelectronics. Curr Opin Biotechnol *21*, 439-476.

Makarov, D.E. (2009). Computer simulations and theory of protein translocation. Acc Chem Res *42*, 281-289.

Mange, A., Nishida, N., Milhavet, O., McMahon, H.E., Casanova, D., and Lehmann, S. (2000). Amphotericin B inhibits the generation of the scrapie isoform of the prion protein in infected cultures. J Virol *74*, 3135-3140.

Marsh, R.F. (1976). The subacute spongiform encephalopathies. Front Biol *44*, 359-380.

Martyn, J.A.J., Fagerlund, M.J., and Eriksson, L.I. (2009). Basic principles of neuromuscular transmission. Anaesthesia *64*, 1-9.

Marziali, A., and Akeson, M. (2001). New DNA sequencing methods. Annu Rev Biomed Eng *3*, 195-223.

Masters, C.L., Harris, J.O., Gajdusek, D.C., Gibbs, C.J. Jr., Bernouilli,C., and Asher, D.M.(1987). Creutzfeldt-Jakob disease: Patterns of worldwide occurrence and the significance of familial and sporadic clustering. Ann Neurol *5*, 177-188.

Mathe, J., Aksimentiev, A., Nelson, D.R., Schulten, K., and Meller, A. (2005). Orientation discrimination of single-stranded DNA inside the alpha-hemolysin membrane channel. Proc Natl Acad Sci USA *102*, 12377-12382.

Maurer-Spurej, E., Brown, K., Labrie, A., Marziali, A., and Glatter, O. (2006). Portable dynamic light scattering instrument and method for the measurement of blood platelet suspensions. Phys Med Biol *51*, 3747-3758.

May, A.K., Sawyer, R.G., Gleason, T., Whitworth, A., and Pruett, T.L. (1996). In vivo cytokine response to Escherichia coli alpha-hemolysin determined with genetically engineered hemolytic and nonhemolytic E. coli variants. Infect Immun *64*, 2167-2171.

McBride, P.A., Bruce, M.E., and Fraser, H. (1988). Immunostaining of scrapie cerebral amyloid plaques with antisera raised to scrapie-associated fibrils (SAF). Neuropathol Appl Neurobiol *14*, 325-336.

McCave, J.N., and Syvitski, J.P. (2007). Principles and methods of geological particle size analysis. Principles, methods and application of particle size analysis, Syvitski, J.P.M. editor. (Cambridge, UK: Cambridge university press). pp. 3-21.

McKinley, M.P., Bolton, D.C., and Prusiner, S.B. (1983). A protease-resistant protein is a structural component of the scrapie prion. Cell *35*, 57-62.

McKinley, M.P., Meyer, R.K., Kenaga, L., Rahbar, F., Cotter, R., Serban, A., and Prusiner, S.B. (1991). Scrapie prion rod formation in vitro requires both detergent extraction and limited proteolysis. J Virol *65*, 1340-1351.

McNally, B., Singer, A., Yu, Z., Sun, Y., Weng, Z., and Meller, A. (2010). Optical recognition of converted DNA nucleotides for single-molecule DNA sequencing using nanopore arrays. Nano Lett *10*, 2237-2244.

Mead, S., Whitfield, J., Poulter, M., Shah, P., Uphill, J., Campbell, T., Al-Dujaily, H., Hummerich, H., Beck, J., Mein, C.A., *et al.* (2009). A Novel Protective Prion Protein Variant that Colocalizes with Kuru Exposure. New Engl J Med *361*, 2056-2065.

Mehta, S., Hunter, D.J., Mugusi, F.M., Spiegelman, D., Manji, K.P., Giovannucci, E.L., Hertzmark, E., Msamanga, G.I., and Fawzi, W.W. (2009). Perinatal outcomes, including mother-to-child transmission of HIV, and child mortality and their association with maternal vitamin D status in Tanzania. J Infect Dis *200*, 1022-1030.

Meier, P., Genoud, N., Prinz, M., Maissen, M., Rulicke, T., Zurbriggen, A., Raeber, A.J., and Aguzzi, A. (2003). Soluble dimeric prion protein binds PrP(Sc) in vivo and antagonizes prion disease. Cell *113*, 49-60.

Meller, A., and Branton, D. (2002). Single molecule measurements of DNA transport through a nanopore. Electrophoresis *23*, 2583-2591.

Meller, A., Nivon, L., Brandin, E., Golovchenko, J., and Branton, D. (2000). Rapid nanopore discrimination between single polynucleotide molecules. Proc Natl Acad Sci USA *97*, 1079-1084.

Meller, A., Nivon, L., and Branton, D. (2001). Voltage-driven DNA translocations through a nanopore. Phys Rev Lett *86*, 3435-3438.

Menestrina, G. (1986). Ionic channels formed by Staphylococcus aureus alpha-toxin: voltage-dependent inhibition by divalent and trivalent cations. J Membr Biol *90*, 177-190.

Menestrina, G., Serra, M.D., and Prevost, G. (2001). Mode of action of beta-barrel pore-forming toxins of the staphylococcal alpha-hemolysin family. Toxicon *39*, 1661-1672.

Meng, H., Detillieux, D., Baran, C., Krasniqi, B., Christensen, C., Madampage, C., Stefureac, R.I., and Lee, J.S. (2010). Nanopore analysis of tethered peptides. J Pept Sci *16*, 701-708.

Meyer, R.K., McKinley, M.P., Bowman, K.A., Braunfeld, M.B., Barry, R.A., and Prusiner, S.B. (1986). Separation and properties of cellular and scrapie prion proteins. Proc Natl Acad Sci USA *83*, 2310-2314.

Miller, M.W., Wild, M.A., and Williams, E.S. (1998). Epidemiology of chronic wasting disease in captive Rocky Mountain elk. J Wildlife Dis *34*, 532-538.

Millhauser, G.L. (2004). Copper binding in the prion protein. Acc Chem Res *37*, 79-85.

Millhauser, G.L. (2007). Copper and the prion protein: methods, structures, function, and disease. Annu Rev Phys Chem *58*, 299-320.

Mirsaidov, U.M., Wang, D.Q., Timp, W., and Timp, G. (2010). Molecular diagnostics for personal medicine using a nanopore. Wires Nanomed Nanobi *2*, 367-381.

Miura, T., Hori-i, A., Mototani, H., and Takeuchi, H. (1999). Raman spectroscopic study on the copper(II) binding mode of prion octapeptide and its pH dependence. Biochemistry *38*, 11560-11569.

Miura, T., Sasaki, S., Toyama, A., and Takeuchi, H. (2005). Copper reduction by the octapeptide repeat region of prion protein: pH dependence and implications in cellular copper uptake. Biochemistry *44*, 8712-8720.

Mohammad, M.M., and Movileanu, L. (2008). Excursion of a single polypeptide into a protein pore: simple physics, but complicated biology. Eur Biophys J *37*, 913-925.

Mohammad, M.M., Prakash, S., Matouschek, A., and Movileanu, L. (2008). Controlling a single protein in a nanopore through electrostatic traps. Journal of the American Chemical Society *130*, 4081-4088.

Molleman, A. (2008). Patch clamping: An introductory guide to patch clamp electrophysiology. (John Wiley and Sons Ltd). pp 5-41.

Montal, M., and Mueller, P. (1972). Formation of bimolecular membranes from lipid monolayers and a study of their electrical properties. Proc Natl Acad Sci USA *69*, 3561-3566.

Moore, R.A., Vorberg, I., and Priola, S.A. (2005). Species barriers in prion diseases-brief review. Arch Virol Suppl, 187-202.

Morales, R., Abid, K., and Soto, C. (2007a). The prion strain phenomenon: molecular basis and unprecedented features. Biochim Biophys Acta *1772*, 681-691.

Morales, R., Gonzales, D., Soto, C., and Castilla, j. (2007b). Advances in prion detection: Microbial food contamination, second edition. Edited by C.L.Wilson (Taylor and Francis Group, LLC). pp 256-275.

Morante, S., Gonzalez-Iglesias, R., Potrich, C., Meneghini, C., Meyer-Klaucke, W., Menestrina, G., and Gasset, M. (2004). Inter- and intra-octarepeat Cu(II) site geometries in the prion protein: implications in Cu(II) binding cooperativity and Cu(II)-mediated assemblies. J Biol Chem *279*, 11753-11759.

Morillas, M., Vanik, D.L., and Surewicz, W.K. (2001). On the mechanism of alpha-helix to beta-sheet transition in the recombinant prion protein. Biochemistry *40*, 6982-6987

Movileanu, L. (2008). Squeezing a single polypeptide through a nanopore. Soft Matter *4*, 925-931.

Movileanu, L., Howorka, S., Braha, O., and Bayley, H. (2000). Detecting protein analytes that modulate transmembrane movement of a polymer chain within a single protein pore. Nat Biotechnol *18*, 1091-1095.

Movileanu, L., Schmittschmitt, J.P., Scholtz, J.M., and Bayley, H. (2005). Interactions of peptides with a protein pore. Biophys J *89*, 1030-1045.

Moyle, M., Lee, J.S., Anderson, W.F., and Ingles, C.J. (1989). The C-terminal domain of the largest subunit of RNA polymerase II and transcription initiation. Mol Cell Biol *9*, 5750-5753.

Moynagh, J., and Schimmel, H. (1999). Tests for BSE evaluated. Bovine spongiform encephalopathy. Nature *400*, 105.

Munoz, V., Thompson, P.A., Hofrichter, J., and Eaton, W.A. (1997). Folding dynamics and mechanism of beta-hairpin formation. Nature *390*, 196-199

Nablo, B.J., Halverson, K.M., Robertson, J.W., Nguyen, T.L., Panchal, R.G., Gussio, R., Bavari, S., Krasilnikov, O.V., and Kasianowicz, J.J. (2008). Sizing the Bacillus anthracis PA63 channel with nonelectrolyte poly(ethylene glycols). Biophys J *95*, 1157-1164.

Nagoshi, K., Honda, J., Sakaue, H., Takahagi, T., and Suzuki, H. (2009). Direct fabrication of nanopores in a metal foil using focused ion beam with in situ measurements of the penetrating ion beam current. Rev Sci Instrum *80*, 125102.

Nakane, J., Akeson, M., and Marziali, A. (2002). Evaluation of nanopores as candidates for electronic analyte detection. Electrophoresis *23*, 2592-2601.

Napper, S., Anderson, J.W., Georges, F., Delbaere, L.T.J., and Waygood, E.B. (1996). Mutation of serine-46 to aspartate in the histidine-containing protein of *Escherichia coli* mimics the inactivation by phosphorylation of serine-46 in HPrs from gram-positive bacteria. Biochemistry *35*, 11260-11267.

Narang, H.K., Dagdanova, A., Xie, Z., Yang, Q., and Chen, S.G. (2005). Sensitive detection of prion protein in human urine. Exp Biol Med (Maywood) *230*, 343-349.

Neher, E., and Sakmann, B. (1976). Single-Channel Currents Recorded from Membrane of Denervated Frog Muscle-Fibers. Nature *260*, 799-802.

Neher, E., and Sakmann, B. (1992). The patch clamp technique. Sci Am *266*, 44-51.

Nevin, S., Mc, M.W., Behrman, S., and Jones, D.P. (1960). Subacute spongiform encephalopathy--a subacute form of encephalopathy attributable to vascular dysfunction (spongiform cerebral atrophy). Brain *83*, 519-564.

Nestorovich, E.M., Danelon, C., Winterhalter, M., and Bezrukov, S.M. (2002). Designed to penetrate: time-resolved interaction of single antibiotic molecules with bacterial pores. Proc Natl Acad Sci USA *99*, 9789-9794.

Neuman, K.C., and Nagy, A. (2008). Single-molecule force spectroscopy: optical tweezers, magnetic tweezers and atomic force microscopy. Nature Methods *5*, 491-505.

Niederweis, M. (2003). Mycobacterial porins-new channel proteins in unique outer membranes. Mol Microbiol *49*, 1167-1177.

Niederweis, M., Ehrt, S., Heinz, C., Klocker, U., Karosi, S., Swiderek, K.M., Riley, L.W., and Benz, R. (1999). Cloning of the mspA gene encoding a porin from Mycobacterium smegmatis. Mol Microbiol *33*, 933-945.

Norstrom, E.M., and Mastrianni, J.A. (2006). The charge structure of helix 1 in the prion protein regulates conversion to pathogenic PrPSc. J Virol *80*, 8521-8529.

Nunziante, M., Kehler, C., Maas, E., Kassack, M.U., Groschup, M., and Schatzl, H.M. (2005). Charged bipolar suramin derivatives induce aggregation of the prion protein at the cell surface and inhibit PrPSc replication. J Cell Sci *118*, 4959-4973.

Oddershede, L., Flyvbjerg, H., and Berg-Sorensen, K. (2003). Single-molecule experiment with optical tweezers: improved analysis of the diffusion of the lambda-receptor in E-coli's outer membrane. J Phys-Condens Mat *15*, S1737-S1746.

Oesch, B., Doherr, M., Heim, D., Fischer, K., Egli, S., Bolliger, S., Biffiger, K., Schaller, O., Vandevelde, M., and Moser, M. (2000). Application of Prionics Western blotting procedure to screen for BSE in cattle regularly slaughtered at Swiss abattoirs. Arch Virol Suppl, 189-195.

Orsi, A., and Sitia, R. (2007). Interplays between covalent modifications in the endoplasmic reticulum increase conformational diversity in nascent prion protein. Prion *1*, 236-242.

Oukhaled, G., Mathe, J., Biance, A.L., Bacri, L., Betton, J.M., Lairez, D., Pelta, J., and Auvray, L. (2007). Unfolding of proteins and long transient conformations detected by single nanopore recording. Phys Rev Lett *98*, 158101.

Owen, F., Poulter, M., Lofthouse, R., Collinge,J., Crow, T.J., Risby,D., Baker, H.F., Ridley, R.M., Hsiao,K., and Prusiner,S.B. (1989) Insertion of prion protein genen in familial Creutzfeldt-Jakob disease. Lancet *1*, 51-52.

Palmer, M.S., Dryden, A.J., Hughes, J.T., and Collinge, J. (1991). Homozygous prion protein genotype predisposes to sporadic Creutzfeldt-Jakob disease. Nature *352*, 340-342.

Pan, K.M., Baldwin, M., Nguyen, J., Gasset, M., Serban, A., Groth, D., Mehlhorn, I., Huang, Z., Fletterick, R.J., Cohen, F.E., and et al. (1993). Conversion of alpha-helices into beta-sheets features in the formation of the scrapie prion proteins. Proc Natl Acad Sci USA *90*, 10962-10966.

Pan, K.M., Stahl, N., and Prusiner, S.B. (1992). Purification and properties of the cellular prion protein from Syrian hamster brain. Protein Sci *1*, 1343-1352.

Pan, T., Chang, B., Wong, P., Li, C., Li, R., Kang, S.C., Robinson, J.D., Thompsett, A.R., Tein, P., Yin, S., *et al.* (2005). An aggregation-specific enzyme-linked immunosorbent assay: detection of conformational differences between recombinant PrP protein dimers and PrP(Sc) aggregates. J Virol *79*, 12355-12364.

Pande, V.S., and Rokhsar, D.S. (1999). Molecular dynamics simulations of unfolding and refolding of a beta-hairpin fragment of protein G. Proc Natl Acad Sci USA *96*, 9062-9067.

Paramithiotis, E., Pinard, M., Lawton, T., LaBoissiere, S., Leathers, V.L., Zou, W.Q., Estey, L.A., Lamontagne, J., Lehto, M.T., Kondejewski, L.H., *et al.* (2003). A prion protein epitope selective for the pathologically misfolded conformation. Nat Med *9*, 893-899.

Parker, M.W., Buckley, J.T., Postma, J.P., Tucker, A.D., Leonard, K., Pattus, F., and Tsernoglou, D. (1994). Structure of the Aeromonas toxin proaerolysin in its water-soluble and membrane-channel states. Nature *367*, 292-295.

Pattison, I.H., and Millson, G.C. (1961). Scrapie produced experimentally in goats with special reference to the clinical syndrome. J Comp Pathol *71*, 101-109.

Pauly, P.C., and Harris, D.A. (1998). Copper stimulates endocytosis of the prion protein. J Biol Chem *273*, 33107-33110.
PClamp 9.0 Users Guide(2005) Axon Inxtruments Inc., (Foster City, CA).

Perera, W.S., and Hooper, N.M. (2001). Ablation of the metal ion-induced endocytosis of the prion protein by disease-associated mutation of the octarepeat region. Curr Biol *11*, 519-523.

Peretz, D., Scott, M.R., Groth, D., Williamson, R.A., Burton, D.R., Cohen, F.E., and Prusiner, S.B. (2001a). Strain-specified relative conformational stability of the scrapie prion protein. Protein Sci *10*, 854-863.

Peretz, D., Williamson, R.A., Kaneko, K., Vergara, J., Leclerc, E., Schmitt-Ulms, G., Mehlhorn, I.R., Legname, G., Wormald, M.R., Rudd, P.M., *et al.* (2001b). Antibodies inhibit prion propagation and clear cell cultures of prion infectivity. Nature *412*, 739-743.

Picciotto, A.R., Alreja, M., and Jentsch, Aj. D. (2002). Acetylcholine;
Neuropsychopharmacology: The fifth generation of progress. K.L Davis., *et al* eds. (American College of Neuropsychopharmacology. pp 3-12.

Pocchiari, M., Casaccia, P., and Ladogana, A. (1989). Amphotericin B: a novel class of antiscrapie drugs. J Infect Dis *160*, 795-802.

Pocchiari, M., Schmittinger, S., and Masullo, C. (1987). Amphotericin B delays the incubation period of scrapie in intracerebrally inoculated hamsters. J Gen Virol *68 (Pt 1)*, 219-223.

Poli, G., Martino, P.A., Villa, S., Carcassola, G., Giannino, M.L., Dall'Ara, P., Pollera, C., Iussich, S., Tranquillo, V.M., Bareggi, S., *et al.* (2004). Evaluation of anti-prion activity of congo red and its derivatives in experimentally infected hamsters. Arzneimittelforschung *54*, 406-415.

Polymenidou, M., Moos, R., Scott, M., Sigurdson, C., Shi, Y.Z., Yajima, B., Hafner-Bratkovic, I., Jerala, R., Hornemann, S., Wuthrich, K., *et al.* (2008). The POM monoclonals: a comprehensive set of antibodies to non-overlapping prion protein epitopes. PLoS One *3*, e3872.

Prusiner, S.B. (1982). Novel proteinaceous infectious particles cause scrapie. Science *216*, 136-144.

Prusiner, S.B. (1989). Creutzfeldt-Jakob disease and scrapie prions. Alzheimer Dis Assoc Disord *3*, 52-78.

Prusiner, S.B. (1998). The prion diseases. Brain Pathol *8*, 499-513.

Prusiner, S.B. (2001). Shattuck lecture-neurodegenerative diseases and prions. N Engl J Med *344*, 1516-1526.

Prusiner, S.B., May, B.C.H., and Cohen, F.E. (2004). Therapeutic approaches to prion diseases; Prion biology and diseases, second edition. Edited by S.B. Prusiner. (Cold Spring Harbor Laboratory press, USA). pp 961-1014.

Prusiner, S.B., Scott, M., Foster, D., Pan, K.M., Groth, D., Mirenda, C., Torchia, M., Yang, S.L., Serban, D., Carlson, G.A., and et al. (1990). Transgenetic studies implicate interactions between homologous PrP isoforms in scrapie prion replication. Cell *63*, 673-686.

Qin, K., Yang, Y., Mastrangelo, P., and Westaway, D. (2002). Mapping Cu(II) binding sites in prion proteins by diethyl pyrocarbonate modification and matrix-assisted laser desorption ionization-time of flight (MALDI-TOF) mass spectrometric footprinting. J Biol Chem *277*, 1981-1990.

Quaglio, E., Chiesa, R., and Harris, D.A. (2001). Copper converts the cellular prion protein into a protease-resistant species that is distinct from the scrapie isoform. J Biol Chem *276*, 11432-11438.

Raeber, A.J., Borchelt, D.R., Scott, M., and Prusiner, S.B. (1992). Attempts to convert the cellular prion protein into the scrapie isoform in cell-free systems. J Virol *66*, 6155-6163.

Ralls, K.S., Buhrman, R.A., and Tiberio, R.C. (1989). Fabrication of Thin-Film Metal Nanobridges. Appl Phys Lett *55*, 2459-2461.

Ramon, R., Sawadogo, D., Koko, F.S., Noba, V., Likikouet, R., Gourvellec, G., Viho, I., Mandelbrot, L., Dabis, F., Ekra, C.W., and Msellati, P. (1999). Haematological characteristics and HIV status of pregnant women in Abidjan, Cote d'Ivoire, 1995-96. Trans R Soc Trop Med Hyg *93*, 419-422.

Riek, R., Hornemann, S., Wider, G., Billeter, M., Glockshuber, R., and Wuthrich, K. (1996). NMR structure of the mouse prion protein domain PrP(121-321). Nature *382*, 180-182.

Roos, R., Gajdusek, D.C., and Gibbs, C.J., Jr. (1973). The clinical characteristics of transmissible Creutzfeldt-Jakob disease. Brain *96*, 1-20.

Rossi, D., Cozzio, A., Flechsig, E., Klein, M.A., Rulicke, T., Aguzzi, A., and Weissmann, C. (2001). Onset of ataxia and Purkinje cell loss in PrP null mice inversely correlated with Dpl level in brain. EMBO J *20*, 694-702.

Roy, R., Hohng, S., and Ha, T. (2008). A practical guide to single-molecule FRET. Nature Methods *5*, 507-516.

Ryou, C., and Mays, C.E. (2008). Prion propagation in vitro: are we there yet? Int J Med Sci *5*, 347-353.

Saborio, G.P., Permanne, B., and Soto, C. (2001). Sensitive detection of pathological prion protein by cyclic amplification of protein misfolding. Nature *411*, 810-813.

Sadqi, M., Lapidus, L.J., and Munoz, V. (2003). How fast is protein hydrophobic collapse? Proc Natl Acad Sci USA *100*, 12117-12122.

Safar, J., Roller, P.P., Gajdusek, D.C., and Gibbs, C.J., Jr. (1993). Thermal stability and conformational transitions of scrapie amyloid (prion) protein correlate with infectivity. Protein Sci *2*, 2206-2216.

Safar, J., Wille, H., Itri, V., Groth, D., Serban, H., Torchia, M., Cohen, F.E., and Prusiner, S.B. (1998). Eight prion strains have PrP(Sc) molecules with different conformations. Nat Med *4*, 1157-1165.

Safar, J.G., Scott, M., Monaghan, J., Deering, C., Didorenko, S., Vergara, J., Ball, H., Legname, G., Leclerc, E., Solforosi, L., *et al.* (2002). Measuring prions causing bovine spongiform encephalopathy or chronic wasting disease by immunoassays and transgenic mice. Nat Biotechnol *20*, 1147-1150.

Sage, L. (2006). Detecting prions in blood. Anal Chem *78*, 14.

Sakaguchi, S., Katamine, S., Nishida, N., Moriuchi, R., Shigematsu, K., Sugimoto, T., Nakatani, A., Kataoka, Y., Houtani, T., Shirabe, S., *et al.* (1996). Loss of cerebellar Purkinje cells in aged mice homozygous for a disrupted PrP gene. Nature *380*, 528-531.

Saleh, O.A., and Sohn, L.L. (2003). Direct detection of antibody-antigen binding using an on-chip artificial pore. Proc Natl Acad Sci U S A *100*, 820-824.

Sansom, M.S.P. (1999). Membrane proteins: A tale of barrels and corks. Curr Biol *9*, R254-R257.

Sartor, Marta. "Dynamic Light Scattering" University of California – San Diego. http://physics.ucsd.edu/neurophysics/courses/physics_173_273/dynamic_light_scattering_03.pdf

Schaller, O., Fatzer, R., Stack, M., Clark, J., Cooley, W., Biffiger, K., Egli, S., Doherr, M., Vandevelde, M., Heim, D., *et al.* (1999). Validation of a western immunoblotting procedure for bovine PrP(Sc) detection and its use as a rapid surveillance method for the diagnosis of bovine spongiform encephalopathy (BSE). Acta Neuropathol *98*, 437-443.

Scott, M., Foster, D., Mirenda, C., Serban, D., Coufal, F., Walchli, M., Torchia, M., Groth, D., Carlson, G., DeArmond, S.J., *et al.* (1989). Transgenic mice expressing hamster prion protein produce species-specific scrapie infectivity and amyloid plaques. Cell *59*, 847-857.

Seeger, H., Heikenwalder, M., Zeller, N., Kranich, J., Schwarz, P., Gaspert, A., Seifert, B., Miele, G., and Aguzzi, A. (2005). Coincident scrapie infection and nephritis lead to urinary prion excretion. Science *310*, 324-326.

Selvin, P.R., and Ha, T. (2008). Single-molecule techniques: A laboratory manual. (New York: Cold spring harbor laboratory press), pp. 3-371.

Sexton, L.T., Horne, L.P., Sherrill, S.A., Bishop, G.W., Baker, L.A., and Martin, C.R. (2007). Resistive-pulse studies of proteins and protein/antibody complexes using a conical nanotube sensor. J Am Chem Soc *129*, 13144-13152.

Shaked, G.M., Shaked, Y., Kariv-Inbal, Z., Halimi, M., Avraham, I., and Gabizon, R. (2001). A protease-resistant prion protein isoform is present in urine of animals and humans affected with prion diseases. J Biol Chem *276*, 31479-31482.

Shenoy, D.K., Barger, W.R., Singh, A., Panchal, R.G., Misakian, M., Stanford, V.M., and Kasianowicz, J.J. (2005). Functional reconstitution of protein ion channels into planar polymerizable phospholipid membranes. Nano Lett *5*, 1181-1185.

Shibuya, S., Higuchi, J., Shin, R.-W., Tateishi, J., and Kitamoto,T. (1998). Protective prion protein polymorphisms against sporadic Creutzfeldt-Jakob disease. Lancet *351*, 419.

Sigurdsson, E.M., Brown, D.R., Alim, M.A., Scholtzova, H., Carp, R., Meeker, H.C., Prelli, F., Frangione, B., and Wisniewski, T. (2003). Copper chelation delays the onset of prion disease. J Biol Chem *278*, 46199-46202.

Singer, A., Wanunu, M., Morrison, W., Kuhn, H., Frank-Kamenetskii, M., and Meller, A. (2010). Nanopore Based Sequence Specific Detection of Duplex DNA for Genomic Profiling. Nano Lett *10*, 738-742.

Singh, N., Singh, A., Das, D., and Mohan, M.L. (2010). Redox control of prion and disease pathogenesis. Antioxid Redox Signal *12*, 1271-1294.

Siwy, Z., Apel, P., Dobrev, D., Neumann, R., Spohr, R., Trautmann, C., and Voss, K. (2003). Ion transport through asymmetric nanopores prepared by ion track etching. Nucl Instrum Meth B *208*, 143-148.

Siwy, Z., Trofin, L., Kohli, P., Baker, L.A., Trautmann, C., and Martin, C.R. (2005). Protein biosensors based on biofunctionalized conical gold nanotubes. J Am Chem Soc *127*, 5000-5001.

Smeets, R.M., Kowalczyk, S.W., Hall, A.R., Dekker, N.H., and Dekker, C. (2009). Translocation of RecA-coated double-stranded DNA through solid-state nanopores. Nano Lett *9*, 3089-3096.

Sofia, S.J., and Merrill, E.W. (1998). Grafting of PEO to polymer surfaces using electron beam irradiation. J Biomed Mater Res *40*, 153-163.

Solassol, J., Crozet, C., Perrier, V., Leclaire, J., Beranger, F., Caminade, A.M., Meunier, B., Dormont, D., Majoral, J.P., and Lehmann, S. (2004). Cationic phosphorus-containing dendrimers reduce prion replication both in cell culture and in mice infected with scrapie. J Gen Virol *85*, 1791-1799.

Song, L., Hobaugh, M.R., Shustak, C., Cheley, S., Bayley, H., and Gouaux, J.E. (1996). Structure of staphylococcal alpha-hemolysin, a heptameric transmembrane pore. Science *274*, 1859-1866.

Soto, C. (2004). Diagnosing prion diseases: needs, challenges and hopes. Nat Rev Microbiol *2*, 809-819.

Soto, C., Saborio, G.P., and Anderes, L. (2002). Cyclic amplification of protein misfolding: application to prion-related disorders and beyond. Trends Neurosci *25*, 390-394.

Spencer, M.D., Knight, R.S., and Will, R.G. (2002). First hundred cases of variant Creutzfeldt-Jakob disease: retrospective case note review of early psychiatric and neurological features. BMJ *324*, 1479-1482.

Stahl, C., Kubetzko, S., Kaps, I., Seeber, S., Engelhardt, H., and Niederweis, M. (2001). MspA provides the main hydrophilic pathway through the cell wall of Mycobacterium smegmatis. Mol Microbiol *40*, 451-464.

Stankovic, C.J., Heinemann, S.H., Delfino, J.M., Sigworth, F.J., and Schreiber, S.L. (1989). Transmembrane channels based on tartaric acid-gramicidin A hybrids. Science *244*, 813-817.

Stefureac, R.I. (2006). Thesis:"Analysis of DNA, proteins and peptides with nanopores". Department of Biochemistry. University of Saskatchewan. pp 117.

Stefureac, R., Long, Y.T., Kraatz, H.B., Howard, P., and Lee, J.S. (2006). Transport of alpha-helical peptides through alpha-hemolysin and aerolysin pores. Biochemistry-Us *45*, 9172-9179.

Stefureac, R.I., Madampage, C.A., Andrievskaia, O., and Lee, J.S. (2010). Nanopore analysis of the interaction of metal ions with prion proteins and peptides. Biochem Cell Biol *88*, 347-358.

Stefureac, R., Waldner, L., Howard, P., and Lee, J.S. (2008). Nanopore analysis of a small 86-residue protein. Small *4*, 59-63.

Stefureac, R.I., and Lee, J.S. (2008). Nanopore analysis of the folding of zinc fingers. Small *4*, 1646-1650.

Stockel, J., Safar, J., Wallace, A.C., Cohen, F.E., and Prusiner, S.B. (1998). Prion protein selectively binds copper(II) ions. Biochemistry *37*, 7185-7193.

Stoddart, D., Heron, A.J., Mikhailova, E., Maglia, G., and Bayley, H. (2009). Single-nucleotide discrimination in immobilized DNA oligonucleotides with a biological nanopore. Proc Natl Acad Sci USA *106*, 7702-7707.

Stoddart, D., Maglia, G., Mikhailova, E., Heron, A.J., and Bayley, H. (2010). Multiple base-recognition sites in a biological nanopore: two heads are better than one. Angew Chem Int Ed Engl *49*, 556-559.

Stohr, J., Weinmann, N., Wille, H., Kaimann, T., Nagel-Steger, L., Birkmann, E., Panza, G., Prusiner, S.B., Eigen, M., and Riesner, D. (2008). Mechanisms of prion protein assembly into amyloid. Proc Natl Acad Sci USA *105*, 2409-2414.

Storm, A.J., Chen, J.H., Ling, X.S., Zandbergen, H.W., and Dekker, C. (2003). Fabrication of solid-state nanopores with single-nanometre precision. Nat Mater *2*, 537-540.

Storm, A.J., Chen, J.H., Zandbergen, H.W., and Dekker, C. (2005a). Translocation of double-strand DNA through a silicon oxide nanopore. Phys Rev E *71*, 051903(1-10).

Storm, A.J., Storm, C., Chen, J.H., Zandbergen, H., Joanny, J.F., and Dekker, C. (2005b). Fast DNA translocation through a solid-state nanopore. Nano Lett *5*, 1193-1197.

Strick, T., Allemand, J., Croquette, V., and Bensimon, D. (2000). Twisting and stretching single DNA molecules. Prog Biophys Mol Biol *74*, 115-140.

Subbarao, G.V., and van den Berg, B. (2006). Crystal structure of the monomeric porin OmpG. J Mol Biol *360*, 750-759.

Sun, L., and Crooks, R.M. (1999). Fabrication and characterization of single pores for modeling mass transport across porous membranes. Langmuir *15*, 738-741.

Supattapone, S., Nguyen, H.O., Cohen, F.E., Prusiner, S.B., and Scott, M.R. (1999). Elimination of prions by branched polyamines and implications for therapeutics. Proc Natl Acad Sci USA *96*, 14529-14534.

Supattapone, S., Wille, H., Uyechi, L., Safar, J., Tremblay, P., Szoka, F.C., Cohen, F.E., Prusiner, S.B., and Scott, M.R. (2001). Branched polyamines cure prion-infected neuroblastoma cells. J Virol *75*, 3453-3461.

Sutherland, T.C., Dinsmore, M.J., Kraatz, H.B., and Lee, J.S. (2004a). An analysis of mismatched duplex DNA unzipping through a bacterial nanopore. Biochem Cell Biol *82*, 407-412.

Sutherland, T.C., Long, Y.T., Stefureac, R.I., Bediako-Amoa, I., Kraatz, H.B., and Lee, J.S. (2004b). Structure of peptides investigated by nanopore analysis. Nano Lett *4*, 1273-1277.

Tabard-Cossa, V., Wiggin, M., Trivedi, D., Jetha, N.N., Dwyer, J.R., and Marziali, A. (2009). Single-molecule bonds characterized by solid-state nanopore force spectroscopy. ACS Nano *3*, 3009-3014.

Talaga, D.S., and Li, J. (2009). Single-molecule protein unfolding in solid state nanopores. J Am Chem Soc *131*, 9287-9297.

Tateishi, J., Kitamoto, T., Hoque, M.Z., and Furukawa, H. (1996). Experimental transmission of Creutzfeldt-Jakob disease and related diseases to rodents. Neurology *46*, 532-537.

Telling, G. (2001). Protein-based PCR for prion diseases? Nat Med *7*, 778-779.

Telling, G.C., Parchi, P., DeArmond, S.J., Cortelli, P., Montagna, P., Gabizon, R., Mastrianni, J., Lugaresi, E., Gambetti, P., and Prusiner, S.B. (1996). Evidence for the conformation of the pathologic isoform of the prion protein enciphering and propagating prion diversity. Science *274*, 2079-2082.

Thackray, A.M., Fitzmaurice, T.J., Hopkins, L., and Bujdoso, R. (2006). Ovine plasma prion protein levels show genotypic variation detected by C-terminal epitopes not exposed in cell-surface PrPC. Biochem J *400*, 349-358.

Thadani, V., Penar, P.L., Partington, J., Kalb, R., Janssen, R., Schonberger, L.B., Rabkin, C.S., and Prichard, J.W. (1988). Creutzfeldt-Jakob disease probably acquired from a cadaveric dura mater graft. Case report. J Neurosurg *69*, 766-769.

Thompsett, A.R., Abdelraheim, S.R., Daniels, M., and Brown, D.R. (2005). High affinity binding between copper and full-length prion protein identified by two different techniques. J Biol Chem *280*, 42750-42758.

Thompsett, A.R., and Brown, D.R. (2007). Dual polarisation interferometry analysis of copper binding to the prion protein: evidence for two folding states. Biochim Biophys Acta *1774*, 920-927.

Todorova-Balvay, D., Simon, S., Creminon, C., Grassi, J., Srikrishnan, T., and Vijayalakshmi, M.A. (2005). Copper binding to prion octarepeat peptides, a combined metal chelate affinity and immunochemical approaches. J Chromatogr B Analyt Technol Biomed Life Sci *818*, 75-82.

Trevitt, C.R., and Collinge, J. (2006). A systematic review of prion therapeutics in experimental models. Brain *129*, 2241-2265.

Thompsett, A.R., and Brown, D.R. (2007). Dual polarisation interferometry analysis of copper binding to the prion protein: evidence for two folding states. Biochim Biophys Acta *1774*, 920-927.

Trevitt, C.R., and Collinge, J. (2006). A systematic review of prion therapeutics in experimental models. Brain *129*, 2241-2265.

Trias, J., and Benz, R. (1994). Permeability of the cell wall of Mycobacterium smegmatis. Mol Microbiol *14*, 283-290.

Uchiyama,K., Ishida, C., Yago,s., Kurumaya,H., and Kitamoto, T.(1994). An Autopsy case of Creutzfeldt-Jakob disease associated with corneal transplantation. Dementia *8*, 466-473.

Uversky, V.N., Oldfield, C.J., and Dunker, A.K. (2008). Intrinsically disordered proteins in human diseases: introducing the D2 concept. Annu Rev Biophys *37*, 215-246.

van den Hout, M., Vilfan, I.D., Hage, S., and Dekker, N.H. (2010). Direct force measurements on double-stranded RNA in solid-state nanopores. Nano Lett *10*, 701-707.

van der Goot, F.G., Ausio, J., Wong, K.R., Pattus, F., and Buckley, J.T. (1993). Dimerization stabilizes the pore-forming toxin aerolysin in solution. J Biol Chem *268*, 18272-18279.

van der Goot, F.G., Hardie, K.R., Parker, M.W., and Buckley, J.T. (1994a). The C-terminal peptide produced upon proteolytic activation of the cytolytic toxin aerolysin is not involved in channel formation. J Biol Chem *269*, 30496-30501.

van der Goot, F.G., Lakey, J., Pattus, F., Kay, C.M., Sorokine, O., Van Dorsselaer, A., and Buckley, J.T. (1992). Spectroscopic study of the activation and oligomerization of the channel-forming toxin aerolysin: identification of the site of proteolytic activation. Biochemistry *31*, 8566-8570.

van der Goot, F.G., Pattus, F., Parker, M., and Buckley, J.T. (1994b). The cytolytic toxin aerolysin: from the soluble form to the transmembrane channel. Toxicology *87*, 19-28.

van Holde, K., and Zlatanova, J. (2006). Scanning chromatin: a new paradigm? J Biol Chem *281*, 12197-12200.

Vassallo, N., and Herms, J. (2003). Cellular prion protein function in copper homeostasis and redox signalling at the synapse. J Neurochem *86*, 538-544.

Venkatesan, B.M., Dorvel, B., Yemenicioglu, S., Watkins, N., Petrov, I., and Bashir, R. (2009). Highly Sensitive, Mechanically Stable Nanopore Sensors for DNA Analysis. Adv Mater *21*, 2771.

Venkatesan, B.M., Shah, A.B., Zuo, J.M., and Bashir, R. (2010). DNA Sensing Using Nanocrystalline Surface-Enhanced Al_2O_3 Nanopore Sensors. Adv Funct Mater *20*, 1266-1275.

Vercoutere, W., Winters-Hilt, S., Olsen, H., Deamer, D., Haussler, D., and Akeson, M. (2001). Rapid discrimination among individual DNA hairpin molecules at single-nucleotide resolution using an ion channel. Nat Biotechnol *19*, 248-252.

Viles, J.H., Cohen, F.E., Prusiner, S.B., Goodin, D.B., Wright, P.E., and Dyson, H.J. (1999). Copper binding to the prion protein: structural implications of four identical cooperative binding sites. Proc Natl Acad Sci USA *96*, 2042-2047.

Viles, J.H., Klewpatinond, M., and Nadal, R.C. (2008). Copper and the structural biology of the prion protein. Biochem Soc Trans *36*, 1288-1292.

Walker, B., Kasianowicz, J., Krishnasastry, M., and Bayley, H. (1994). A pore-forming protein with a metal-actuated switch. Protein Eng *7*, 655-662.

Wallace, B.A. (1986). Structure of gramicidin A. Biophys J *49*, 295-306.

Walter, E.D., Chattopadhyay, M., and Millhauser, G.L. (2006). The affinity of copper binding to the prion protein octarepeat domain: evidence for negative cooperativity. Biochemistry *45*, 13083-13092.

Walter, E.D., Stevens, D.J., Visconte, M.P., and Millhauser, G.L. (2007). The prion protein is a combined zinc and copper binding protein: Zn^{2+} alters the distribution of Cu^{2+} coordination modes. J Am Chem Soc *129*, 15440-15441.

Wan, X., Steudle, E., and Hartung, W. (2004). Gating of water channels (aquaporins) in cortical cells of young corn roots by mechanical stimuli (pressure pulses): effects of ABA and of HgCl2. J Exp Bot *55*, 411-422.

Wang, D., Zhao, Q., de Zoysa, R. S., and Guan, X. (2009). Detection of nerve agent hydrolytes in an engineered nanopore. Sens. Actuators B Chem. *139*, 440-446.

Wanunu, M., Sutin, J., McNally, B., Chow, A., and Meller, A. (2008). DNA translocation governed by interactions with solid-state nanopores. Biophys J *95*, 4716-4725.

Wei, R., Pedone, D., Zurner, A., Doblinger, M., and Rant, U. (2010). Fabrication of metallized nanopores in silicon nitride membranes for single-molecule sensing. Small *6*, 1406-1414.

Weiss, S. (2000). Measuring conformational dynamics of biomolecules by single molecule fluorescence spectroscopy. Nat Struct Biol *7*, 724-729.

Weiss, S., Proske, D., Neumann, M., Groschup, M.H., Kretzschmar, H.A., Famulok, M., and Winnacker, E.L. (1997). RNA aptamers specifically interact with the prion protein PrP. J Virol *71*, 8790-8797.

Weissmann, C. (1996). The Ninth Datta Lecture. Molecular biology of transmissible spongiform encephalopathies. FEBS Lett *389*, 3-11.

Wells, G.A.H., Scott, A.C., Johnson, C.T., Gunning, R.F., Hancock, R.D., Jeffrey, M., Dawson, M., and Bradley, R. (1987). A Novel Progressive Spongiform Encephalopathy in Cattle. Veterinary Record *121*, 419-420.

Wells, M.A., Jackson, G.S., Jones, S., Hosszu, L.L., Craven, C.J., Clarke, A.R., Collinge, J., and Waltho, J.P. (2006). A reassessment of copper(II) binding in the full-length prion protein. Biochem J *399*, 435-444.

Westaway, D., Zuliani, V., Cooper, C.M., Dacosta, M., Neuman, S., Jenny, A.L., Detwiler, L., and Prusiner, S.B. (1994). Homozygosity for Prion Protein Alleles Encoding Glutamine-171 Renders Sheep Susceptible to Natural Scrapie. Gene Dev *8*, 959-969.

White, A.R., Enever, P., Tayebi, M., Mushens, R., Linehan, J., Brandner, S., Anstee, D., Collinge, J., and Hawke, S. (2003). Monoclonal antibodies inhibit prion replication and delay the development of prion disease. Nature *422*, 80-83.

White, R.J., Ervin, E.N., Yang, T., Chen, X., Daniel, S., Cremer, P.S., and White, H.S. (2007). Single ion-channel recordings using glass nanopore membranes. J Am Chem Soc *129*, 11766-11775.

Whittal, R.M., Ball, H.L., Cohen, F.E., Burlingame, A.L., Prusiner, S.B., and Baldwin, M.A. (2000). Copper binding to octarepeat peptides of the prion protein monitored by mass spectrometry. Protein Sci *9*, 332-343.

Wild, M.A., Spraker, T.R., Sigurdson, C.J., O'Rourke, K.I., and Miller, M.W. (2002). Preclinical diagnosis of chronic wasting disease in captive mule deer (Odocoileus hemionus) and white-tailed deer (Odocoileus virginianus) using tonsillar biopsy. Journal of General Virology *83*, 2629-2634.

Wilesmith, J.W., Ryan, J.B.M., and Atkinson, M.J. (1991). Bovine Spongiform Encephalopathy - Epidemiologic Studies on the Origin. Veterinary Record *128*, 199-203.

Wille, H., Bian, W., McDonald, M., Kendall, A., Colby, D.W., Bloch, L., Ollesch, J., Borovinskiy, A.L., Cohen, F.E., Prusiner, S.B., and Stubbs, G. (2009). Natural and synthetic prion structure from X-ray fiber diffraction. Proc Natl Acad Sci USA *106*, 16990-16995.

Wille, H., Govaerts, C., Borovinskiy, A., Latawiec, D., Downing, K.H., Cohen, F.E., and Prusiner, S.B. (2007). Electron crystallography of the scrapie prion protein complexed with heavy metals. Arch Biochem Biophys *467*, 239-248.

Wille, H., Michelitsch, M.D., Guenebaut, V., Supattapone, S., Serban, A., Cohen, F.E., Agard, D.A., and Prusiner, S.B. (2002). Structural studies of the scrapie prion protein by electron crystallography. Proc Natl Acad Sci USA *99*, 3563-3568.

Williams, E.S., and Young, S. (1980). Chronic Wasting Disease of Captive Mule Deer - Spongiform Encephalopathy. J Wildlife Dis *16*, 89-98.

Wilmsen, H.U., Buckley, J.T., and Pattus, F. (1991). Site-directed mutagenesis at histidines of aerolysin from Aeromonas hydrophila: a lipid planar bilayer study. Mol Microbiol *5*, 2745-2751.

Wilmsen, H.U., Leonard, K.R., Tichelaar, W., Buckley, J.T., and Pattus, F. (1992). The aerolysin membrane channel is formed by heptamerization of the monomer. EMBO J *11*, 2457-2463.

Wilmsen, H.U., Pattus, F., and Buckley, J.T. (1990). Aerolysin, a hemolysin from Aeromonas hydrophila, forms voltage-gated channels in planar lipid bilayers. J Membr Biol *115*, 71-81.

Winklhofer, K.F., Hartl, F.U., and Tatzelt, J. (2001). A sensitive filter retention assay for the detection of PrP(Sc) and the screening of anti-prion compounds. FEBS Lett *503*, 41-45.

Winklhofer, K.F., and Tatzelt, J. (2000). Cationic lipopolyamines induce degradation of PrPSc in scrapie-infected mouse neuroblastoma cells. Biol Chem *381*, 463-469.

Wolfe, A.J., Mohammad, M.M., Cheley, S., Bayley, H., and Movileanu, L. (2007). Catalyzing the translocation of polypeptides through attractive interactions. J Am Chem Soc *129*, 14034-14041.

Wolfe, L.L., Conner, M.M., Baker, T.H., Dreitz, V.J., Burnham, K.P., Williams, E.S., Hobbs, N.T., and Miller, M.W. (2002). Evaluation of antemortem sampling to estimate chronic wasting disease prevalence in free-ranging mule deer. J Wildlife Manage *66*, 564-573.

Wong, C., Xiong, L.W., Horiuchi, M., Raymond, L., Wehrly, K., Chesebro, B., and Caughey, B. (2001). Sulfated glycans and elevated temperature stimulate PrP(Sc)-dependent cell-free formation of protease-resistant prion protein. EMBO J *20*, 377-386.

Wong, D., Jeon, T.J., and Schmidt, J. (2006). Single molecule measurements of channel proteins incorporated into biomimetic polymer membranes. Nanotechnology *17*, 3710-3717.

Wood, J.L., McGill, I.S., Done, S.H., and Bradley, R. (1997). Neuropathology of scrapie: a study of the distribution patterns of brain lesions in 222 cases of natural scrapie in sheep, 1982-1991. Vet Rec *140*, 167-174.

Woolley, G.A., and Wallace, B.A. (1992). Model ion channels: gramicidin and alamethicin. J Membr Biol *129*, 109-136.

Wopfner, F., Weidenhofer, G., Schneider, R., von Brunn, A., Gilch, S., Schwarz, T.F., Werner, T., and Schatzl, H.M. (1999). Analysis of 27 mammalian and 9 avian PrPs reveals high conservation of flexible regions of the prion protein. J Mol Biol *289*, 1163-1178.

Wu, H.C., Astier, Y., Maglia, G., Mikhailova, E., and Bayley, H. (2007). Protein nanopores with covalently attached molecular adapters. J Am Chem Soc *129*, 16142-16148.

Wu, H.C., and Bayley, H. (2008). Single-molecule detection of nitrogen mustards by covalent reaction within a protein nanopore. J Am Chem Soc *130*, 6813-6819.

Wu, X., and Brooks, B.R. (2004). Beta-hairpin folding mechanism of a nine-residue peptide revealed from molecular dynamics simulations in explicit water. Biophys J *86*, 1946-1958.

Xie, H., Braha, O., Gu, L.Q., Cheley, S., and Bayley, H. (2005). Single-molecule observation of the catalytic subunit of cAMP-dependent protein kinase binding to an inhibitor peptide. Chem Biol *12*, 109-120.

Xu, Y., Oyola, R., and Gai, F. (2003). Infrared study of the stability and folding kinetics of a 15-residue beta-hairpin. J Am Chem Soc *125*, 15388-15394.

Yildiz, O., Vinothkumar, K.R., Goswami, P., and Kuhlbrandt, W. (2006). Structure of the monomeric outer-membrane porin OmpG in the open and closed conformation. EMBO J *25*, 3702-3713.

Ying, Y.L., Li, D.W., Li, Y., Lee, J.S. and Long, Y.T. (2011). Enhanced translocation of single poly(T) through an α-hemolysin nanopore by binding with antibody. Chem.commun, *47*, 5690-5692.

Zahn, R., Liu, A., Luhrs, T., Riek, R., von Schroetter, C., Lopez Garcia, F., Billeter, M., Calzolai, L., Wider, G., and Wuthrich, K. (2000). NMR solution structure of the human prion protein. Proc Natl Acad Sci USA *97*, 145-150.

Zhao, Q., Jayawardhana, D.A., Wang, D., and Guan, X. (2009). Study of peptide transport through engineered protein channels. J Phys Chem B *113*, 3572-3578.

Zhu, F., Davies, P., Thompsett, A.R., Kelly, S.M., Tranter, G.E., Hecht, L., Isaacs, N.W., Brown, D.R., and Barron, L.D. (2008). Raman optical activity and circular dichroism reveal dramatic differences in the influence of divalent copper and manganese ions on prion protein folding. Biochemistry *47*, 2510-2517.

Zhuang, X., Bartley, L.E., Babcock, H.P., Russell, R., Ha, T., Herschlag, D., and Chu, S. (2000). A single-molecule study of RNA catalysis and folding. Science *288*, 2048-2051.

Zlatanova, J., and van Holde, K. (2006). Single-molecule biology: what is it and how does it work? Mol Cell *24*, 317-329.